Regulation of hematopoietic stem cell migration and function

Regulation of Hematopoietic Stem Cell Migration and Function

A dissertation presented

by

Ellen Marie Durand

to

The Division of Medical Sciences

in partial fulfillment of the requirements

for the degree of

Doctor of Philosophy

in the subject of

Human Biology and Translational Medicine

Harvard University

Cambridge, Massachusetts

April 2014

Dissertation Advisor: Dr. Leonard Zon Ellen M. Durand

Regulation of Hematopoietic Stem Cell Migration and Function

Abstract

Hematopoietic stem cell transplantation (HSCT) is an effective treatment for blood disorders and autoimmune diseases. Following HSCT, these cells must successfully migrate to the marrow niche and replenish the blood system of the recipient. This process requires both non-cell and cell-autonomous regulation of hematopoietic stem and progenitor cells (HSPCs). A transgenic reporter line in zebrafish allowed the investigation of factors that regulate HSPC migration and function. To directly observe cells in their endogenous microenvironment, confocal live imaging was used to track runx1:GFP^{+} HSPCs as they arrive and lodge in the niche. A novel cellular interaction was observed that involves triggered remodeling of perivascular endothelial cells during niche formation. A chemical screen identified the TGF-beta pathway as a regulator of HSPC and niche interactions. Chemical manipulation of HSPCs was used to improve engraftment and repopulation capability following transplantation. Runx1:GFP fish treated with prostaglandin E2 (PGE_2) during embryogenesis exhibit increased runx1+ cells in the AGM and CHT, consistent with previous in situ data. This increase in HSPCs is maintained into adulthood, even in the absence of prolonged PGE_2 exposure. Kidney marrow from these treated fish can outcompete control marrow in transplantation assays. The ability of PGE_2 to confer a long-term advantage on sorted mouse marrow populations in competitive transplantation assays was tested. I found that PGE_2-treated

short-term (ST)-HSCs, but not long-term (LT)-HSCs show enhanced transplantability in recipients compared to control animals. My studies demonstrate that the effects of PGE_2 on HSC function persist over substantial time despite transient exposure. A population of short-term HSCs can engraft and give rise to long-term multilineage reconstitution following PGE_2 treatment. Collectively, our studies have led to novel insights regarding the pathways involved in HSC migration, homing, and repopulation.

Table of Contents

Acknowledgements

I thought my acknowledgements would be the easiest part of thesis writing. Instead I found myself avoiding them until the last possible second, literally. Not because I don't have anyone to thank, but quite the opposite. This thesis would not have been possible without many people, and writing this section makes me realize how soon I will be moving on. Joining the Zon lab one of the first, and best, decisions I made in grad school. I started rotating in my 3rd week and by week 4 I knew I would be joining. Len is a great mentor- he is invested in his lab members' scientific growth AND their happiness. The Zon lab is simply a fun place to be year-round: March madness season turns to fantasy baseball season turns to Halloween planning season turns to Halloween season turns to fantasy football season. Repeat.

I will be tremendously sad to leave the lab, but most of all I will miss the friends I have made. My first bay on the 8th floor was like a mini family; Jared and I were the clumsy, newest lab babies and our post doc parents Katie and Owen had to make sure we didn't break anything. I learned and continue to learn so much from all of them, and I am so thankful that I got to spend my first year in the lab as their baymate. After moving down to the coveted 7th floor, I was lucky enough to join the carebear bay…need I say more? Katie, Alison, and Colleen made every day at work more fun. Filmwise, sporcle, and "totally looks like" were routine ways to pass the time. I am so lucky to have remained friends with these girls. When Alison and Colleen graduated, Vera and Ellen (what are the odds?!) joined the bay. I am always thankful for their suggestions and support.

I was fortunate to have fantastic peer mentors in the lab as well. I first rotated with Pulin, who continued to help me in many aspects of my project once I joined the lab. Teresa probably answered more of my questions than anyone. Besides being ridiculously knowledgeable about blood, she is one of the coolest people I know. I want to also thank the technicians I've worked with, Margot and Becca, for preventing me from messing up my own experiments from time to time.

Finally, I need to thank the entire lab, especially my fellow grad students. You all have made this place feel like a second home for the past 5 years.

To my family, I cannot give you all the thanks on paper that you deserve. You have shown me constant support and love throughout my entire life. I can't remember a time in the past few months where I haven't heard my parents ask: "What can we do for you? What do you need to make your life easier?" I don't think I could have made it through grad school without you, I love you all so much and I dedicate this thesis to you.

Chapter 1

Introduction

Attributions

I wrote a review article entitled "Newly emerging roles for prostaglandin E2 regulation of hematopoiesis and hematopoietic stem cell engraftment"[1] (Durand and Zon, Curr Op in Hematol. 2010 17:308–312). Excerpts from this review are updated and included in the introduction chapter. The review in its entirety is included in the appendix.

Review

Hematopoietic stem cells (HSCs) are a rare cell type with the ability to self renew and differentiate. In addition to maintaining hematopoietic homeostasis, HSCs must respond to stress conditions and fluctuate between a quiescent and an actively cycling state. Following HSC transplantation, these cells must successfully migrate to the marrow niche and replenish the blood system of the recipient. Although much is known about the importance and clinical relevance of HSCs, very little is known regarding the mechanisms of HSC function. Utilizing the zebrafish as a model system has allowed us to study novel pathways, identified through chemical screening, involved in HSC migration, homing, and repopulation.

Hematopoietic Stem Cells

HSCs are a rare cell population with the ability to both self-renew and differentiate into all mature blood cells via a life-long process called hematopoiesis[1,2,3]. Vertebrate hematopoiesis occurs in two waves, the primitive wave and the definitive wave. During the primitive wave, erythrocytes and macrophages are produced to help oxygenate and remodel the developing embryo. The definitive wave is marked by the emergence of HSCs, which will support the hematopoietic system for the life of the organism. In the mouse, the first long-term HSCs are detected in the aorta–gonad–mesonephros (AGM) region by embryonic day 10.5 and later colonize the fetal liver, thymus, spleen, and bone marrow[4]. Key transcription factors that play a role in the development of the hematopoietic system include *runx1, scl*, and *c-myb*.

The bone marrow is composed of a diverse set of cell types, including osteoblasts,

endothelial cells, stromal cells, adipocytes, and mature blood cells, which form a regulatory environment called the niche[5]. HSCs must respond to regulatory signals in the marrow niche and either maintain the HSC pool through self-renewal, or produce mature blood cells by dividing into progenitor cells. Through this cellular hierarchy, HSCs are able to maintain hematopoietic homeostasis throughout the lifespan of an organism.

Zebrafish Hematopoiesis

Despite the extensive evolutionary divergence between bony fish and mammals, the teleost *Danio rerio*, more commonly called the zebrafish, remains a robust model for studying hematopoiesis. Genetic pathways regulating hematopoiesis have been conserved from zebrafish to mammals, including two distinct waves of hematopoiesis, outlined in figure 1[6]. Zebrafish undergo primitive hematopoiesis in an intraembryonic region called the intermediate cell mass (ICM), compared with the extraembryonic yolk sac in mammals[7]. The primitive wave produces lineage-committed erythroid and myeloid progenitor cells, which express specific transcription factors such as gata1 and pu.1[8]. Zebrafish definitive hematopoiesis occurs in the ventral wall of the dorsal aorta, the aorta-gonad-mesonephros (AGM) equivalent region in the zebrafish. Definitive hematopoiesis produces all lineages of blood cells and functional HSCs, which express transcription factors such as *runx1*, *cmyb*, *CD41*, and *lmo2*[9]. The zebrafish equivalent of mammalian bone marrow is the kidney, which supports definitive hematopoiesis from 4 days post fertilization (dpf) through adulthood. Whole kidney marrow (WKM) transplanted into lethally irradiated recipient fish has been shown to rescue recipient fish and repopulate all blood lineages.

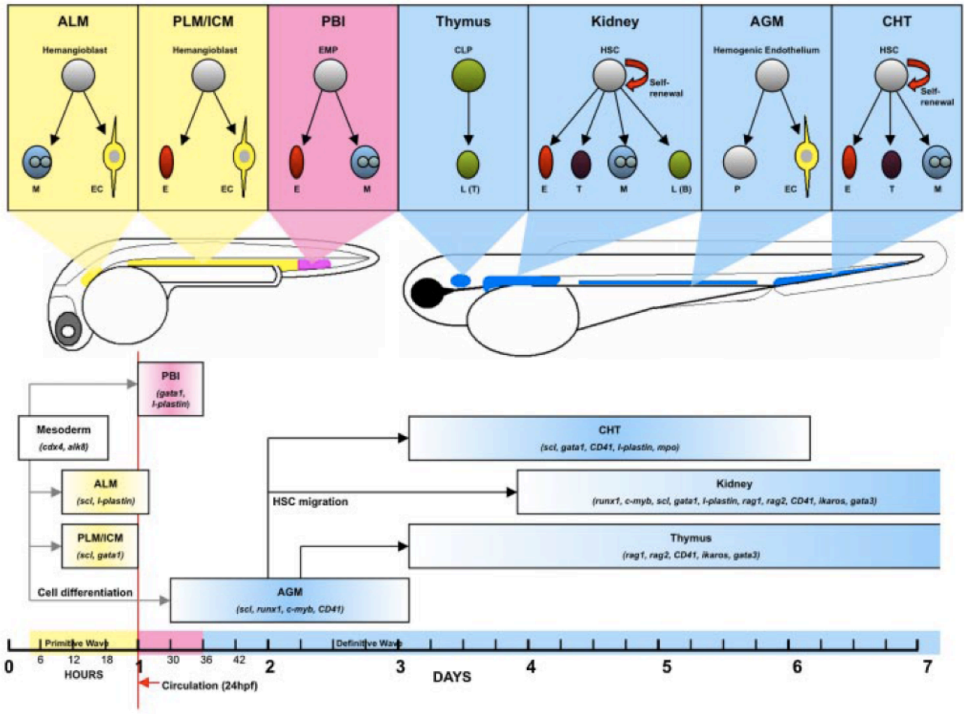

Figure 1. Spatial and temporal representation of hematopoiesis in the zebrafish

The primitive wave of hematopoiesis is depicted in yellow and the definitive wave is depicted in blue. The locations of different sites of hematopoiesis are depicted in a 24hpf embryo (left) and a 72hpf embryo (right). The timline for expression of blood-specific markers at different sites of hematopoiesis is shown in the bottom panel.

FACS analysis of whole kidney marrow can be used to analyze the hematopoietic system and differentiate cell populations[10]. A member of our lab has successfully developed a competitive transplant assay system in which the homing and engraftment of HSCs into irradiated recipient fish can be assessed using fluorescence microscopy and FACS analysis (Figure 2). Using a transparent fish called *Casper*, a double mutant in pigment genes *nacre* and *roy*, allows for easy visualization of the transplanted cell populations using fluorescence microscopy[11]. This competitive transplant assay allows

for analysis of different HSC conditions and their effect on engraftment efficiency during WKM transplant. Aside from genetic similarity, the zebrafish has other advantages for studying hematopoiesis. Unlike mammals, zebrafish red blood cells are nucleated, making it possible to utilize them in certain experiments such as ChIP and DNase hypersensitivity mapping. Zebrafish embryos are also transparent, which makes it possible to view blood circulation with a dissecting microscope[12]. In addition, a pair of zebrafish can produce 100-200 embryos per week, making them a useful system for large-scale chemical and genetic screens.

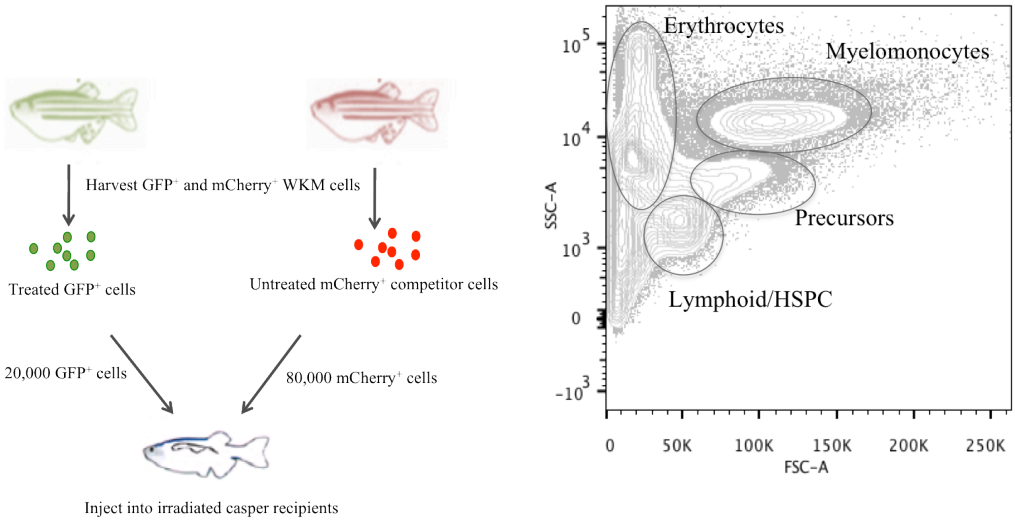

Figure 2. Competitive transplantation and readout schematic

The diagram on the left is a schematic of competitive transplantation in adult zebrafish. Marrow cells are harvested from GFP$^+$ donor fish and treated with chemical or vehicle. 20,000 treated WKM cells are mixed with 80,000 untreated mCherry$^+$ cells and injected into irradiated recipient fish. Several months following transplantation, FACS analysis is performed on WKM of recipient fish. The graph on the right is a representative plot that shows the major blood lineages detectable by FACS.

Hematopoietic Stem Cell Niche

The bone marrow niche for HSCs is a complex microenvironment that regulates hematopoietic stem and progenitor cell (HSPC) function and supports both self-renewal and differentiation processes[13]. Many interacting cell types and signaling networks exist in the niche environment, which have a mixture of direct and indirect effects on HSCs[14]. The niche protects HSCs from cellular stress, particularly by limiting the accumulation of reactive oxygen species. In addition, it is thought that osteoblastic cells help maintain HSCs in a quiescent state, which is necessary to prevent excessive proliferation and exhaustion, although this effect may not be direct[15]. Within the bone marrow, a perivascular niche comprised of a network of sinusoidal vessels provides a connection between circulating cells and the marrow niche. It is common for HSCs to localize to sinusoids, suggesting that the cell types that surround these vessels play a role in HSC maintenance[16]. For example, mesenchymal stem cells (MSCs) are found proximal to niche blood vessels and express fibroblast activation protein (FAP). Knock down of FAP^+ cells results in anemia and hypocellularity in the bone marrow[17–19]. Endothelial cells in the perivascular niche have also been shown to regulate HSC maintenance both *in vitro* and *in vivo*, however it is unknown whether this effect is direct or indirect[20,21].

Although the bone marrow niche is a highly dynamic structure, comprised of numerous cell types and signaling networks and closely linked to circulation, our current methods of studying this environment are lacking. Experimental protocols looking at fixed sections and sorted cells lack information about the dynamic cellular interactions occurring the in the niche space. In addition, our knowledge about HSC migration to and subsequent colonization of the niche remains largely unknown. Understanding these

trafficking and engraftment mechanisms is critically important because they are mimicked during clinical stem cell mobilization and transplantation.

Hematopoietic Stem Cell Transplantation

HSCs are arguably the most studied type of stem cell, and transplantation of HSCs has been used in the clinic for several decades as an effective therapy for leukemia, lymphoma, blood disorders, and autoimmune diseases[1,2]. Hematopoietic stem cell transplantation (HSCT) is achieved through transplantation of bone marrow, mobilized peripheral blood, or umbilical cord blood-derived HSPCs. Preconditioning for HSCT entails ablation of the recipients' bone marrow, leaving patients at risk for infection, anemia, and thrombocytopenia. Transplanted HSCs must efficiently home to the niche, differentiate, and repopulate the host hematopoietic system. Recent studies have focused on the use of chemicals to enhance collection and transplantation efficiency of HSCs and HSPCs in order to shorten engraftment time and diminish risk for myeloablated patients[22,23]. This effort includes improving HSC expansion prior to transplantation, as well as improving the efficacy of HSPC homing and niche interaction following transplantation. One way to test for successful engraftment in patients is to measure neutrophil recovery. Improving this parameter by even a few days could have a dramatic effect on patient outcome.

Phenotypic Characterization of HSCs

Blood cells are an extremely heterogeneous population comprised of stem cells with varying degrees of repopulation activity, multipotent progenitor cells, and fully

differentiated cells. For decades we have been able to study the functionality of these cells using elegant *in vivo* repopulation techniques[24]. The gold standard to identify a bona fide HSC is to perform bone marrow transplantation and observe multilineage reconstitution for at least 6-12 months following transplant. However, true HSCs are very rare amid all blood cells. In mice only about 1 in 10^5 bone marrow cells is a long-term reconstituting stem cell; in humans this number is closer to 1 in 10^6 cells[25]. In the past 25 years or so, a significant number of antibody combinations have been developed for both mouse and human to distinguish between stem and progenitor cells, and differentiated lineages. Murine HSCs were initially identified as lineage$^-$, Sca1$^+$, c-Kit$^+$ (LSK) cells in the bone marrow[26]. The Nakauchi lab demonstrated through single cell transplantation experiments that LSKCD34$^-$ cells give rise to multilineage reconstitution in 40% of recipient mice, demonstrating a tremendous improvement in the purification of HSCs[27]. Similarly, Sean Morrison's lab identified the signaling lymphocyte activation molecule (SLAM) family as a reliable and robust method for isolating HSCs. SLAM family receptors mark a variety of immune cells and are differentially expressed in HSPC populations[28]. They demonstrated 47% of LSKCD48$^-$CD150$^+$ cells can give rise to long-term multilineage reconstitution in recipient mice. Alternatively, progenitor populations have been observed that are LSKCD34$^+$Flk2$^+$, or LSKCD48$^+$CD150$^-$, which remain multipotent, but have only transient reconstitution capabilities[29].

In contrast to surface marker characterizations in mouse, almost all human HSCs reside in the CD34$^+$ fraction. Human HSCs are most commonly defined by a CD34$^+$Thy1$^+$CD38$^-$CD45RA$^-$ phenotype[30–32]. However, these markers alone are not enough to exclusively distinguish cells with long-term repopulation capacity from those

without. Sophisticated marker combinations allow us to study the functionality of more purified populations, as well as the molecular factors that underlie these differences. This is especially useful when studying the heterogeneity of human blood cells, and could have important clinical implications for patients receiving HSCT.

Regulation of HSC Homing and Engraftment

The cytokine stromal-derived factor 1 (SDF-1) is a strong chemo-attractant for $CD34^+$ cells, which express its receptor, CXCR4. The migration potential of HSPCs towards a gradient of SDF-1 has been demonstrated both *in vitro* and *in vivo*. In the bone marrow, SDF-1 –expressing stromal cells keep HSPCs in the niche. Mobilized HSPCs have decreased expression of CXCR4, making it an attractive target to manipulate both migration and homing[33]. During preconditioning for HSCT, SDF-1 levels in bone marrow are increased, allowing for enhanced trafficking of HSCs to the niche. It has recently been reported that complement is also activated upon myeloablation, and that a specific protein component fragment, C3a, increases the responsiveness of HSCs to SDF-1[34]. Mice treated with the small molecule SB290157, a C3a receptor (C3aR) antagonist, displayed enhanced mobilization following granulocyte colony signaling factor (G-CSF) treatment. In addition, these cells exhibit impaired engraftment[35]. Interestingly, this engraftment defect is blocked when C3aR-deficient cells are primed with C3a prior to transplantation.

Following transplantation, cells must home to the bone marrow niche to effectively repopulate the recipient blood system. Improving homing and engraftment efficiency is crucial for the recovery of myeloablated patients. As mentioned previously,

HSCs expressing CXCR4 will migrate towards a gradient of SDF-1 present in bone marrow, whereas mobilized HSCs exhibit reduced CXCR4 expression. This suggests that maintaining a functional interaction between CXCR4 and SDF-1 is essential for proper homing. CD26/DPP4 is a membrane-bound extracellular peptidase found on a subpopulation of $CD34^+$ cells. It is known to cleave SDF-1 at the N-terminus and prevent its interaction with CXCR4, resulting in decreased migration of these cells to the niche[36,37]. Treatment of $CD34^+$ cells with Diprotin A, a small molecule inhibitor of CD26/DPP4, greatly enhances homing and engraftment following transplantation. Similar effects were observed in CD26/DPP4- deficient cells. This effect is dependent on CXCR4, as co-treatment with AMD3100 blocks the effect of Diprotin A treatment on homing[38].

Umbilical Cord Blood Transplantation

Trafficking of HSCs from the bone marrow to peripheral blood, termed mobilization, is an important element of maintaining hematopoietic homeostasis. In addition, mobilized HSCs are generally the preferred source of stem cells for autologous and allogeneic-donor transplantation. However, the frequency of steady-state HSCs present in peripheral blood at any time during homeostasis is not high enough for successful transplantation and engraftment[39]. Therefore, prior to transplantation, autologous patient and allogeneic donor HSCs are mobilized using chemotherapy or cytokines. Efficient mobilization of HSCs is essential in order to yield enough stem cells for HSCT. G-CSF is commonly used to induce mobilization of HSCs to peripheral blood prior to collection. There are several disadvantages to G-CSF, including a lengthy

administration protocol, an unpredictable variable response, and rare but serious side effects[40].

Umbilical cord blood (UCB) has emerged as a promising source of transplantable HSCs for patients without a related or immune-matched donor. Although the stringency for HLA-matching is reduced, there are insufficient numbers of HSCs in a single UCB unit to engraft an adult patient in the United States. To compensate, two UCB units are given as the standard of care during transplantation (Figure 3)[41,42]. The ability to expand HSCs in culture prior to transplantation has important clinical applications. Despite a growing body of research on the mechanisms governing HSC self-renewal, previous attempts at culturing HSCs *in vitro* while maintaining their stem cell properties have failed to generate large numbers in culture. Expansion of UCB HSCs prior to transplantation could potentially reduce the number of UCB units necessary for successful engraftment. Utilizing small molecules to expand HSCs *in vitro* is particularly appealing as chemicals can be removed before cells are introduced to patients.

Prostaglandin E_2

A chemical screen for HSC formation in zebrafish

A small molecule screen in zebrafish identified 16,16-dimethyl-Prostaglandin E_2 (PGE_2) as a mediator of HSC formation during embryonic hematopoiesis[43]. Zebrafish embryos treated with PGE_2 during embryogenesis displayed increased expression of HSC markers *runx1* and *cmyb* in the dorsal aorta. Expressions of these markers were used as a proxy for HSCs as both are expressed in all HSCs and are required for proper HSC generation in the AGM region[44,45]. Endogenous requirement for PGE_2 in HSC formation

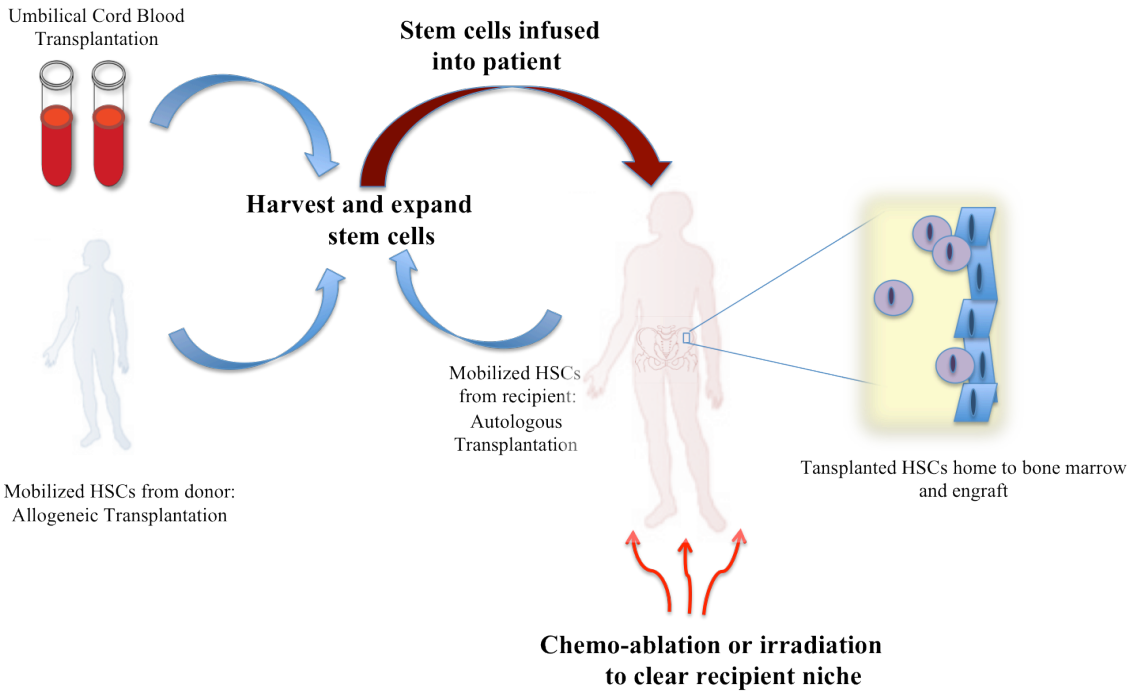

Figure 3. Review of hematopoietic stem cell transplantation

HSCT is achieved through transplantation of cells derived from the patient, as in autologous transplant. Alternatively, a healthy donor marrow or a cord blood unit cells can be used in allogeneic transplant, During cord blood transplantation, two cords are required for an adult patient. HSCs are usually mobilized or eliminated prior to transplant. The transplanted cells must successfully home to and engraft in the niche following transplantation.

was confirmed using morpholino knock out of the PGE_2 biosynthetic enzymes *Cox-1* and *Cox-2*, resulting in decreased HSCs. Irradiation recovery experiments were used as an injury model to demonstrate HSC activation. Treatment with PGE_2 enhanced the rate of kidney marrow recovery in irradiated recipients compared with control treated animals, suggesting PGE_2 treatment as a potential therapy to improve the recovery time of myeloablated patients.

Conservation in mammals

The effects of PGE_2 on HSCs were tested using murine transplantation assays. Bone marrow cells were treated *ex vivo* with PGE_2 and transplanted into irradiated recipients to assess either short-term progenitor potential or long-term-HSC function. Colony forming units (CFU-Spleen) assays demonstrated that PGE_2 enhances HSPC activity. Competitive repopulation with limiting dilution analysis showed that *ex vivo* PGE_2 treatment increased the number of repopulating HSCs without disrupting differentiation.

A study by Hoggatt *et al*.[46] confirmed enhanced murine HSC engraftment following exposure to PGE_2, observing a four-fold increase in HSCs up to 20 weeks following transplantation. Whole bone marrow (WBM) harvested from primary recipients at 20 weeks post transplant maintained PGE_2-induced enhancement of HSC frequency in secondary recipients without additional PGE_2 treatment. These findings suggest that short-term PGE_2 exposure results in a long-term repopulation advantage of transplanted WBM.

The effects of PGE_2 on HSCs could be the result of an increase in HSC number, homing capability, proliferation, survival, or a combination thereof. To evaluate the homing capabilities of PGE_2-treated WBM, labeled cells were transplanted into irradiated recipients. A significant increase in homing of PGE_2-treated LSK cells to recipient marrow was observed compared with control. Consistent with the murine LSK population, PGE_2-treated UCB cells displayed enhanced homing to the marrow. This homing effect is partially attributed to an increase in CXCR4 expression following PGE_2 treatment. PGE_2 treatment of murine LSK and human $CD34^+$ cells increased expression

of CXCR4. In addition to its affect on homing, PGE_2 increased Survivin, an important regulator of HSC survival and proliferation, in LSK and UCB cells following pulse treatment. Further supporting a role in HSC proliferation, SLAM LSK cells treated with PGE_2 displayed a significant increase in the percentage of cycling cells.

Until recently there existed no data for *in vivo* treatment of PGE_2 in the murine system. Frisch *et al*.[47] utilized a continuous *in vivo* treatment regimen to study the effects of PGE_2 in mice. Consistent with previous *in vitro* data, it was observed that *in vivo* $dmPGE_2$ treatment significantly increased the LSK population without disrupting hematopoietic differentiation. To determine which subpopulation(s) in LSK cells are directly affected by PGE_2, SLAM receptors were used to distinguish the long-term-HSC subset from short-term-HSCs and multipotent progenitors (MPPs). *In vivo* PGE_2 treatment preferentially increased the short term (ST)-HSC/MPP subpopulation without changing the frequency of long term (LT)-HSCs. Consistent with *ex vivo* treatment transplantation assays, transplanted cells from mice treated with PGE_2 *in vivo* demonstrated increased engraftment and hematopoietic reconstitution of host animals; however, this competitive advantage was eventually lost, most likely due to exhaustion.

PGE_2 in clinical trials

Human $CD34^+$ cells treated with PGE_2 and transplanted into immunodeficient mice demonstrate enhanced transplantation abilities. The number of human $CD45^+$ cells detected in the peripheral blood and bone marrow of recipient mice was ~2-fold higher in PGE_2-treated groups compared to control[48]. This data suggested that PGE_2 could be used to expand UCB cells prior to transplantation. A phase 1 trial was recently completed to

test expansion and subsequent transplantation of UCB HSCs following *ex vivo* PGE_2 exposure, which included 12 patients and optimized treatment conditions[49]. Each patient received two cord blood units (CBUs) infused in succession; the first CBU was treated with PGE_2, the second CBU was untreated. Neutrophil engraftment was observed in 100% of patients in the trial, compared to 90% of historic control. The median time to engraftment was 17.5 days versus 21 days, respectively. PGE_2-treated CBU displayed enhanced engraftment by outcompeting the untreated CBU in 10 out of 12 patients. Initial results demonstrate that this PGE_2 treatment regimen is clinically well tolerated. It may be possible in the future to achieve engraftment in patients receiving only a single CBU that is expanded with PGE_2. Collectively, these studies have clearly defined a role for PGE_2 in the function of HSPCs, yet the mechanisms behind its effects remain largely unknown.

Synthesis and mechanism of action

Prostaglandins are lipid compounds of the eicosanoid family that play a major role in inflammatory and immune response as well as various other tissue responses[50,51]. They are found in a majority of tissues and are produced by a number of cell types. When synthesized, prostaglandins function locally as autocrine or paracrine lipid mediators. Prostaglandins are derived from arachidonic acid, which is oxidized by Cox-1 and Cox-2 to form PGG_2. PGG_2 is subsequently reduced to PGH_2, from which all three classes of prostaglandins originate. Prostaglandin E synthase acts on PGH_2 to produce PGE_2[52]. Cox-1 is constitutively expressed in most tissues, whereas Cox-2 is silenced in normal physiological conditions but can rapidly activate downstream targets during times

of stress.

PGE_2 acts via four G-protein coupled E-prostanoid receptors PTGER1-4 (EP1-4), resulting in various and sometimes opposing downstream effects[53]. PGE_2 has been shown to be both a vasodilator (in arterial and venous beds) and a vasoconstrictor (in the trachea and intestine), supporting evidence of multiple functional E-prostanoid receptors[54]. These receptors are loosely classified based on their function as relaxants or constrictors of smooth muscle cells. EP2 and EP4 are relaxant receptors and result in production of cAMP upon binding of PGE_2. Despite this common pathway, additional unique functions have been shown for each receptor. PGE_2 bound to EP2 but not EP4 can result in activation of the EGF receptor leading to increased invasion of colon cancer cells. EP1 receptors are constrictors, where binding of PGE_2 increases intracellular calcium levels in smooth muscle cells. The diverse effects of PGE_2 signaling are further demonstrated through EP3 receptor activity. Different splice variants of EP3 receptors have been implicated in cAMP induction and inhibition, as well as generation of IP_3. In addition, PGE_2 binds E-prostanoid receptors with different affinities, with a higher affinity for EP3 and EP4, and a lower affinity for EP1 and EP2[55].

In zebrafish, the PGE_2 receptors expressed on HSCs are Ptger2 and Ptger4. Knock down of *ptger2* or *ptger4* results in a decrease of *runx/cmyb* expression in the AGM that is not rescued with PGE_2 treatment[43]. This suggests that PGE_2 signals through Ptger2 and Ptger4 to regulate HSC formation in zebrafish embryos. Interestingly, binding of PGE_2 to EP2 or EP4 can lead to activation of GSK-3/β-catenin signaling pathway via protein kinase A and phosphoinositide 3-kinase, respectively[56]. Furthermore, a recent study demonstrated an *in vivo* conserved genetic interaction

between PGE_2 and Wnt at the level of the β-catenin stabilization in the zebrafish[57]. PGE_2 treatment significantly increases expression of a β-catenin responsive GFP reporter in the AGM region, while treatment with indomethacin, a non-selective COX inhibitor, decreased expression. Co-localization of the GFP reporter and *lmo2* indicated Wnt activity was present in HSCs and endothelial cells of the dorsal aorta. Induction of Wnt signaling during embryogenesis increased *runx1*$^+$ cells in the AGM, however treatment with indomethacin blocked this increase, suggesting PGE_2 is required for this effect. A zebrafish *cmyb*:GFP reporter line was used to demonstrate that PGE_2 and Wnt signaling synergize to increase HSC number in the AGM. Combined treatment of PGE_2 and Wnt activation enhanced the effect of Wnt activation alone. These results suggest that PGE_2 is required for Wnt-mediated effects on HSC development and can enhance Wnt activity *in vivo*.

PGE_2 and Wnt interaction was tested in the adult zebrafish using a kidney marrow recovery assay. FACS analysis of recovering marrow indicates that Wnt activation significantly increased HSPC population and this was blocked by indomethacin. These results support interplay of PGE_2 and Wnt signaling in the adult zebrafish. To determine whether this interaction is conserved in mammals, purified LSK cells were transplanted into irradiated mice. Recipients were treated with 6-bromoindirubin-3'-oxime (BIO), a GSK3β inhibitor, indomethacin, or both. CFU-S assays following treatment demonstrated an increase in progenitor cells after BIO treatment; this effect was reduced to baseline levels upon treatment of indomethacin, demonstrating that PGE_2 mediates Wnt activity on mammalian hematopoietic progenitor cells.

All 4 EP receptors are expressed on murine progenitor populations (LSK) as well as more purified stem cell populations ($LSKCD48^{-}CD150^{+}$). EP1-EP4 receptors are also found on human $CD34^{+}CD38^{-}$ cells[46]. This data, combined with the observed genetic interaction between PGE_2 and Wnt, suggests the EP2 and EP4 receptors in particular might play an important role in the regulation of HSCs.

Knockdown of EP4 in LSK cells results in decreased repopulation ability following transplantation, as well as a skewing towards T cell and myeloid lineages during differentiation[58]. In contrast, EP2 knockout mice exhibit normal hematopoiesis, reconstitution capabilities, and differentiation. In addition, treatment of LSK cells with an EP4 agonist, but not an EP2 agonist, lead to an increase in phosphorylation of GSK3β and β-catenin. Co-treatment of a PKA inhibitor with PGE_2 blocked the activation of GSK3β. This data suggests that PGE_2 acts through EP4 to activate the cAMP/PKA pathway in HSPCs.

Thesis Review

In this thesis we have used zebrafish and mouse models to study the endogenous microenvironment and trafficking of HSPCs in the niche. We have also studied the long-term repopulating capabilities of PGE_2-treated HSPCs following transplantation. To accomplish this, we developed a novel zebrafish transgenic reporter line that enabled us to visualize and purify zebrafish HSPCs. We demonstrate that the *runx1*:GFP labels a population of stem and progenitor cells in zebrafish close to that of LSK in mice. We used this line to observe a novel and essential cellular behavior that involves triggered remodeling of perivascular endothelial cells upon arrival of an HSPC in a new site of hematopoiesis. A chemical screen during zebrafish embryogenesis revealed novel compounds that regulate cellular behaviors, such as adhesion and division, in the CHT. Imaging of fetal liver explants revealed that our observed endothelial niche remodeling is conserved in mammals.

Runx1:GFP fish treated with PGE_2 during embryogenesis exhibit increased runx1+ cells in the AGM and CHT, consistent with previous *in situ* data. This increase in HSPCs is maintained into adulthood, even in the absence of prolonged PGE_2 exposure. Kidney marrow from these treated fish can outcompete control marrow in transplantation assays. This advantage appears to be due to an effect on the HSPC pool as a whole, rather than an individual cell basis. The long-term effect of PGE_2 on HSCT is conserved in mammals; WBM cells treated with PGE_2 maintain increased chimerism levels in recipient mice over 1-year post transplantation. These cells display enhanced transplantability in competitive secondary transplantations without additional PGE_2 treatment.

Further purification of murine HSPCs using cell surface marker antibody combinations demonstrated that PGE_2 affects a specific population of HSCs that are phenotypically LSKCD48$^-$CD34$^+$CD150$^+$. Historically thought to only have transient multilineage potential, we show that following PGE_2 treatment these cells display long-term multilineage reconstitution that persists at least 1-year post primary transplant. Gene expression data and ChIP-seq analysis in human CD34$^+$ cells suggests that PGE_2 may play a role in the quiescent state of these cells.

Our studies provide a glimpse into the dynamic interactions between HSPCs and their endogenous niche. In addition, we show that a population of short-term HSCs can engraft and give rise to long-term multilineage reconstitution following PGE_2 treatment. Collectively, we have gained novel insights in the pathways involved in HSC migration, homing, and repopulation.

Chapter 2

Live imaging of hematopoietic stem cell lodgement reveals dynamic endothelial niche remodeling

Attributions

This chapter is to be submitted as a co-first author paper with Owen Tamplin, a post-doctoral fellow in the lab. Owen established the *Runx1*:GFP and *Runx1*:mCherry transgenic zebrafish lines. I characterized these lines by designing and performing all FACS experiments to detect Runx1$^+$ cells in embryonic and adult zebrafish and compared the new *Runx1* lines to previously used HSPC zebrafish lines. I also designed and performed the limit dilution transplantations in adult fish and performed FACS analysis on embryonic transplants. Owen performed all confocal microscopy and time-lapse movies using the *Runx1* transgenic lines. EM microscopy was done by Sarah Childs at Alberta Children's Hospital Research Institute, University of Calgary. Owen performed the chemical screen in zebrafish embryos. I established a FACS protocol to study the effect of Lycorine on Runx1$^+$ cells and designed and performed the experiments for microarray on Lycorine-treated cells. We both designed experiments for studying murine fetal liver HSCs. Owen performed microscopy for fetal liver explants, and I characterized these cells and performed the FACS analysis/sorts.

The addendum to this chapter includes work done in the mouse system to further study the interactions between the CXCR4 and S1P signaling pathways during mobilization and homing that is not included in the publication. Owen designed and performed the chemical screen in zebrafish that identified a role for the S1P pathway in CHT engraftment, as well as optimized dose response and interactions with CXCR4 in the zebrafish. I designed and performed all mouse experiments, including treating cells and FACS analysis, mobilization, and homing experiments.

Abstract

Hematopoietic stem and progenitor cells (HSPCs) are able to reconstitute and sustain the entire blood system, making them critical for clinical transplantation as a treatment for leukemia and blood disease. To directly observe HSPCs in their endogenous microenvironment, we established a highly specific transgenic reporter in the zebrafish. Using confocal live imaging to track an HSPC as it arrives and lodges in the perivascular niche, we observed a novel cellular interaction—a small group of endothelial cells remodel around a single HSPC to form a surrounding pocket. To resolve the ultrastructure of this niche, we correlated live imaging of these rare cellular events with high-resolution 3D scanning electron microscopy data. Endothelial niche formation triggered by HSPC arrival is evolutionarily conserved in the mouse fetal liver. A chemical screen identified small molecule regulators of HSPC niche colonization. Our work establishes a new dynamic model of niche formation during stem cell engraftment.

Introduction

Hematopoietic stem and progenitor cells (HSPCs) self-renew and give rise to all blood cell types. During development and throughout adulthood, HSPCs will undergo many migration events. Definitive HSPCs arise from the hemogenic endothelium of the dorsal aorta (DA)[59–61] are released into circulation, and then seed an intermediate hematopoietic niche before colonizing the adult marrow. In mammals, this intermediate tissue is the fetal liver (FL), and in zebrafish it is the caudal hematopoietic tissue (CHT), a vascular plexus in the ventral tail of the embryo[62,63]. After rapid expansion in the intermediate niche, HSPCs will leave and go on to seed the adult marrow, which in

mammals is bone and in zebrafish is kidney[64]. During life the changing requirements for HSPCs in the marrow and other tissues of the body dictate that stem cells continue migrating between different locations[65]. HSPC trafficking during development and in the adult is highly regulated, enabling release of stem cells into circulation, followed by homing and engraftment into a niche. Understanding these trafficking mechanisms is critically important because they are mimicked during clinical stem cell mobilization and transplantation.

The HSPC niche is a complex microenvironment that maintains the stem cell pool throughout life, while balancing the production of multilineage progenitors. It has been thought that the endosteum of the bone marrow and its osteoblastic cells create a unique region that favors HSPC quiescence[15]. The bone marrow also contains a complex network of sinusoidal vessels that act as an interface between circulation and the niche. In fact, most HSPCs are proximal to these vessels and are therefore considered to be in a perivascular niche[28,66,67]. Studies have shown that endothelial cells (EC) have distinct properties that enable them to support and expand associated HSPCs[68,69]. However, there are many different cell types, such as perivascular mesenchymal cells, stromal cells, and arterioles that also play a role in the niche[67,70,71]. Together these studies build a model of the many interacting cell types and signals that make up the HSPC niche microenvironment. Yet the static images we have acquired from fixed samples do not give us a dynamic view of the interactions between endogenous cell types in the niche.

Live imaging of the adult HSPC niche is a challenging task. Homing of circulating HSPCs to the adult bone marrow has been observed in a number of elegant studies[72–76]. These studies have been technically limited to multiphoton intravital microscopy of surgically accessed bone, such as the skull, or bone explants such as the femur. There has been the caveat that labeled, sorted and transplanted HSPCs could differ physiologically from endogenous HSPCs. Also, in the case of myelosuppressed recipients there can be significant damage to the perivascular niche[69]. In the embryo, confocal time-lapse microscopy has been used to capture the emergence of HSPCs from the hemogenic endothelium of the DA in both mouse explants and live zebrafish embryos[59–61], but the immigration of HSPCs into secondary sites of colonization has not been extensively studied.

The zebrafish embryo is particularly amenable to live imaging studies. Here we sought to develop a novel transgenic zebrafish that we could use to follow HSPCs during migration. Definitive hematopoiesis progresses quickly in the zebrafish: HSPC birth in the DA, migration to the CHT, seeding of the thymus, and colonization of the kidney marrow takes only five days[62]. Conserved hematopoietic regulatory genes have led to the development of HSPC transgenic reporter lines, although none of these are entirely specific (e.g. *cmyb*:EGFP, *cd41*:EGFP[77], and *runx1P2*:EGFP[78]). To establish a more specific HSPC line, we utilized a regulatory element from the first intron of the mouse *Runx1* locus that is +23 kb downstream of the ATG in the first promoter to drive expression of a reporter[79]. In mouse, the *Runx1*+23 enhancer drives early expression in the primitive wave of hematopoiesis, then in the definitive wave from HSPC birth in the

DA to long-term repopulating hematopoietic stem cells (LTR-HSC) in adult bone marrow. We used the *Runx1*+23 enhancer from mouse to establish a novel HSPC-specific transgenic line in zebrafish. The ability to track endogenous HSPC in the live embryo allowed us to observe dynamic interactions with other cell types in the niche. We have discovered a novel and essential cellular behavior that involves triggered remodeling of perivascular EC upon arrival of an HSPC in a new site of hematopoiesis. Using 3D reconstruction of high resolution serial section electron microscopy scans, we have an accurate view of the stem cell and the adjacent cells in the niche. Furthermore, we have shown that a similar event occurs in the mouse FL, suggesting this is a highly conserved step during lodgement of an HSPC in its niche.

Materials and Methods

Zebrafish maintenance and lines

Zebrafish and mice were maintained in accordance with Animal Research Guidelines at Children's Hospital Boston. Transgenic zebrafish lines were crossed and selected by fluorescent microscopy. Time-lapse live imaging was performed using a spinning disk confocal with an incubated chamber and moving XY stage. Zebrafish embryos and mouse embryo explants were mounted and imaged as previously described[59,80]. We screened a chemical library of ~2400 known bioactive compounds at concentrations optimized for whole embryo treatments. After treatment, we checked for secondary defects (e.g. stopped circulation, toxicity, developmental delay). Next, we performed WISH with HSPC markers *cmyb* and *runx1* as previously described[81].

Imaging

Staged transgenic zebrafish embryos were selected and mounted for imaging in 1% LMP agarose with E3 media and tricaine as described. Some zebrafish embryos had 0.003% PTU (1-Phenyl-2-thiourea) added to the media to block melanogenesis. Zebrafish embryos and FL explants were imaged in MatTek glass bottom dishes or multi-well plates (No. 1.5 cover slip). Zebrafish live imaging was performed in an incubated chamber at 28°C. Mouse embryo explant live imaging was performed in an incubated chamber at 37°C with humidified CO_2 with culture media (DMEM, 20% FCS, glutamine, sodium pyruvate, 2-mercaptoethanol, 1% penicillin-streptomycin, recombinant mouse IL-3 (R&D Systems; final concentration 50 ng/ml)). Confocal microscopy was performed using a Yokogawa spinning disk and Nikon inverted Ti microscope. Our microscope configuration allowed imaging of multiple embryos within a 2-5 minute interval using a moving XY stage, as well as acquisition of z-stacks through the entire CHT (1-2 μm optical slices) in multiple fluorescent channels. Objectives lenses (Nikon): 20x Plan-Apo DIC N.A. 0.75; 40x Plan-Apo phase N.A. 0.95 dry; 40x Apo LWD WI NA 1.15 lambda S. Image acquisition was done with a single Andor iXon DU-897 EM-CCD camera (512x512 pixels) or dual Andor iXon x3 EM-CCD cameras (512x512 pixels) and Andor iQ or NIS-elements computer software. Fixed transgenic zebrafish embryos were scanned using a Nikon C2si confocal system and NiE upright microscope. These embryos were briefly fixed for 10 minutes with PEM fixation buffer (dH_20, EGTA 10 mM, MgSO4 1 mM, PIPES 100 mM, Triton X-100 0.1%, PFA 4%; Cold Spring Harbor Protocols, 2009, doi:10.1101/pdb.rec11730), then washed and mounted with DRAQ5 (1:500) for staining of nuclei.

Imaging analysis

Image processing and rendering was done using Fluorender, Imaris (Bitplane), NIS-elements (Nikon), Volocity (PerkinElmer) and ImageJ/Fiji. The MTrackJ plugin was used for manual cell tracking. Lineage trees were created using Endro. Point-to-point measurements were made with Imaris. Manual tracing, segmentation, and surface rendering of objects was performed using Imaris. Confocal z-stack images are presented as single slices, maximum projections, or 3D rendered projections. In some cases, background subtraction was performed, and brightness and contrast was adjusted in one or more channels of a multi-channel image.

Immunohistochemistry of adult WKM

Adult zebrafish were fixed with 4% paraformaldehyde, paraffin-embedded, sectioned, and stained with hematoxylin and eosin (H&E). Immunohistochemistry was performed using anti-GFP monoclonal antibody (clone JL-8). The Dako Mouse Envision kit with EDTA antigen retrieval was used for visualization. Incubation in the primary antibody was 60 minutes, and 30 minutes in the secondary, followed by DAB development for 5 minutes and counterstained with hematoxilyn.

Adult-to-Adult HSPC Transplantation

WKM cells from 3-month *Runx1*:mCherry;ubi:GFP fish were isolated and sorted by FACS. Double-positive cells were transplanted into irradiated *casper* recipients (n=20-48 recipients per cell dose) along with untreated helper marrow at the following ratios: 1:20,000; 5:20,000; 10:20,000; 25:20,000; 50:20,000. Transplantation procedures

were performed as previously described[82]. At 3 months post-transplant, WKM from recipient fish was collected and analyzed by FACS to detect chimerism levels of mCherry and GFP-positive cells in the marrow. We confirmed multi-lineage reconstitution by observing differentiated GFP-positive cells in multiple cell populations, as determined by forward and side scatter profiles. Stem cell frequency was determined using ELDA software (confidence interval=0.95).

Embryo-to-Embryo HSPC Transplantation

Adapted from previously published protocols[10,83]. *Runx1*:mCherry;ubi:EGFP or *Runx1*:GFP;ubi:mCherry 3 dpf embryos were collected and chopped finely with a razor blade. Embryos were dissociated in a 1:65 dilution of Liberase TM (Roche) in PBS, incubated at 37°C for 20 minutes before addition of PBS/5% FCS to stop the reaction. Dissociated cells were passed through a 45 μM filter, spun, and resuspended in PBS/5% FCS. mCherry+/GFP+ cells were collected using a FACSAria cell sorter (BD Biosciences). Collected cells were resuspended in PBS at an estimated concentration of 400 cells/microliter with 0.5% rhodamine-dextran(10k) as a marker for injection. A microinjection needle (without filament) was back-filled with the cell suspension. The drop volume was calibrated to 1 nanoliter and each embryo was injected with 1, 2, or 4 drops. This gave an estimated cell dose of 0.4, 0.8 or 1.6 cells per embryo. Drops were injected into the sinus venosus (i.e. duct of Cuvier) of 48 hpf wild-type AB embryo recipients. Embryos were held in place using agarose injection ramps. Approximately 30 embryos were injected per dose and 12-26 embryos per group survived to adulthood (3-5 months). WKM was then analyzed for percentage of engrafted Runx+ cells using a LSR

II flow cytometer (BD Biosciences). Any recipients with positive cells detected above background were scored as engrafted. Flow cytometry data was analyzed using FACSDiva and FlowJo software.

Serial block face scanning electron microscopy and 3D reconstructions

Immediately at the end of live imaging time-lapse acquisition 60 hpf embryos were fixed in 2.5% glutaraldehyde and 4% paraformaldehyde in a 0.1 M sodium cacodylate buffer. Embryos were embedded in 5% low melting point agarose in 0.1M sodium cacodylate buffer for orientation. Samples were submitted to Renovo Neural Inc (Cleveland, USA) for further processing. Samples were stained with heavy metals following the protocol from the National Center for Microscopy and Imaging Research; http://ncmir.ucsd.edu/sbfsem-protocol.pdf. Samples were embedded in Epon resin, and mounted onto pins (detailed protocol available from Renovo Neural). Serial blockface images (analogous to serial sectioning) were obtained using a Zeiss Sigma VP scanning electron microscope equipped with a Gatan 3View in-chamber ultramicrotome. A series of 500-1000 images were acquired at 2 kV using at 15,000 magnification from the region of interest. Image and stack resolution was 10 nm/pixel with 100 nm slices. Images were registered and resized as necessary using ImageJ/Fiji software. Images were imported into the program IMOD 4.5 then aligned and reconstructed using dual-axis tomography. Cells were manually outlined and 3D reconstructions were generated. Movies were rendered using IMOD and Fiji.

Microarrays

Runx1:GFP;*kdrl*:RFP embryos were collected and raised in E3 media at 28.5C. Embryos were treated from 2-3 dpf with E3/1% DMSO or E3/1%DMOS/75 uM Lycorine (~100-150 embryos per group). Embryos were dissociated and sorted as above. Three populations were collected: GFP+ HSPC (~1-2k cells/experiment), RFP+ EC (~10-20k cells/experiment), and negative cells (~100k cells/experiment; total embryo as a comparator population). In total, 18 samples were collected: 3 biological replicates x 2 treatment conditions x 3 cell populations. Cells were sorted directly in Trizol LS. Trizol extraction was performed as per the manufacturer's instructions, with the addition of GenElute LPA (Sigma, Cat.#56575). Total RNA was amplified and labeled using the NuGEN Ovation Pico WTA System V2 and Encore Biotin Module kits, respectively. Affymetrix ZebGene-1_0-st microarrays were hybridized, washed, and stained using Ambion kits. Microarrays were scanned using the Genechip Scanner 3000 7G.

Fetal liver preparations

Live fetal liver explants: Pregnant wild-type *C57/BL6* and *Ly6a*-GFP mice were dissected at E11-11.5 (vaginal plug observation was E0). Embryos were removed from the uterus in PBS with 10% FCS and penicillin-streptomycin. Embryos were staged as E11-E11.5 by counting >42 somite pairs. FLs were removed from the embryo and treated as described by Boisset and colleagues (“protocol b”). Conjugated antibodies used for detection were CD31-FITC (PECAM-1, BD Biosciences, Rat anti-mouse, clone MEC 13.3) and c-kit-APC (CD117, BD Biosciences, Rat anti-mouse, clone 2B8).

Fixed fetal livers: Embryos were dissected as above and fixed in 2% PFA on ice for 20 minutes. Embryos were then rinsed and dehydrated in methanol. FLs were removed, mounted, cleared and imaged using the method by Yokomizo et al. Livers from E11.5 *Ly6a*-GFP mice were stained with rat anti-CD144, rabbit anti-RUNX1, and chicken anti-GFP. Primary and secondary antibody details are below. Specimens were scanned using a Zeiss LSM 710 confocal microscope with a 25x oil objective. Images were acquired using multi-track sequential mode and Zeiss Zen software. Pinhole was set at 1 Airy unit, steps were 1.14 μm per z-section. 3D projections were made using Volocity software.

Results

Establishment of a highly specific HSPC transgenic zebrafish line

To observe and study endogenous HSPC, we established a transgenic zebrafish line with the mouse Runx1+23 enhancer driving either cytoplasmic EGFP (*Runx*:GFP) or nuclear localized mCherry (*Runx*:mCherry). These two lines were crossed to demonstrate that the green and red fluorescent proteins marked the same cell populations (Figure S1A). Time-lapse live imaging showed that Runx+ cells emerge from the hemogenic endothelium of the DA (Figure S1B and Movie S1). Intercrossing the *Runx*:mCherry line with *cmyb*:EGFP and *cd41*:EGFP lines showed that Runx+ cells marked an overlapping population of HSPC in all major hematopoietic sites of the embryo, including the DA, CHT, thymus and kidney (Figure S1C-L and data not shown). We detected Runx:GFP+ cells in the adult kidney marrow using anti-GFP immunohistochemistry and fluorescence-activated cell sorting (FACS; Figure S1M-P).

Next, we followed HSPCs after their emergence, when they travel through circulation to arrive in and seed the CHT niche. At the early stages of FL colonization in mouse at embryonic day (E) 11 it is estimated there is only about one transplantable HSPC[84], predicting that the number of Runx+ cells in the CHT would be rare. We quantified the number of Runx:GFP+ cells in the CHT at different developmental stages. We found there were only an average of 1, 2, or 5 Runx:GFP+ high cells (and 2, 6, or 10 Runx:GFP+ low cells) in the CHT at 48, 58, and 80 hpf, respectively (Figure 4A-F). Cell numbers in the *Runx*:mCherry line were comparable, except from 72 hpf there was a greater number of Runx:mCherry+ low cells that are likely progeny (Figure S1G-L). Looking at Runx:GFP+ cells in the CHT together with a vascular transgenic reporter

(*kdrl*:RFP[85] or *kdrl*:Hsa.hras-mCherry) we found that HSPC were closely associated with the EC of the caudal vein plexus (Figure 4A-C).

To further understand the association of Runx+ cells with the CHT niche, we crossed the *Runx*:GFP and *cxcl12a*:DsRed2 transgenic lines to observe HSPC together with stromal cells[86]. To quantify the proximity of these two cell types within 3D confocal z-stacks, we measured the distance between a Runx+ HSPC and its nearest cxcl12a+ stromal cell (Figure 4G-I). This analysis showed that 60% of HSPC are in contact with a cxcl12a+ cell and 85% are ≤3 microns distance away. We performed time-lapse live imaging of CHT colonization in these double transgenic embryos and found that arrival and expansion of most HSPC occurred in close proximity to stromal cells (data not shown). This provided further support that cxcl12a+ cells are an important component of the CHT microenvironment. We confirmed that endothelial and stromal cells are closely associated in the CHT[62], similar to the perivascular niche in fetal and adult bone marrow[67,87], and showed that cxcl12a+ cells are distributed in abluminal spaces that underlie kdrl+ EC (Figure 4J). The HSPC-specific transgenic line, together with endothelial and stromal markers, has allowed us to demarcate HSPCs and their niche in the developing zebrafish embryo.

The functional stem cell characteristics of Runx+ HSPC in the zebrafish

To assess the functional characteristics of cells in the Runx+ pool, we performed limiting dilution transplantation as a standard assay to determine hematopoietic stem cell content. We purified Runx:mCherry+ cells from the kidney marrow of adult transgenic donors. These donors also carried the ubiquitous ubi:GFP transgene[88] so that

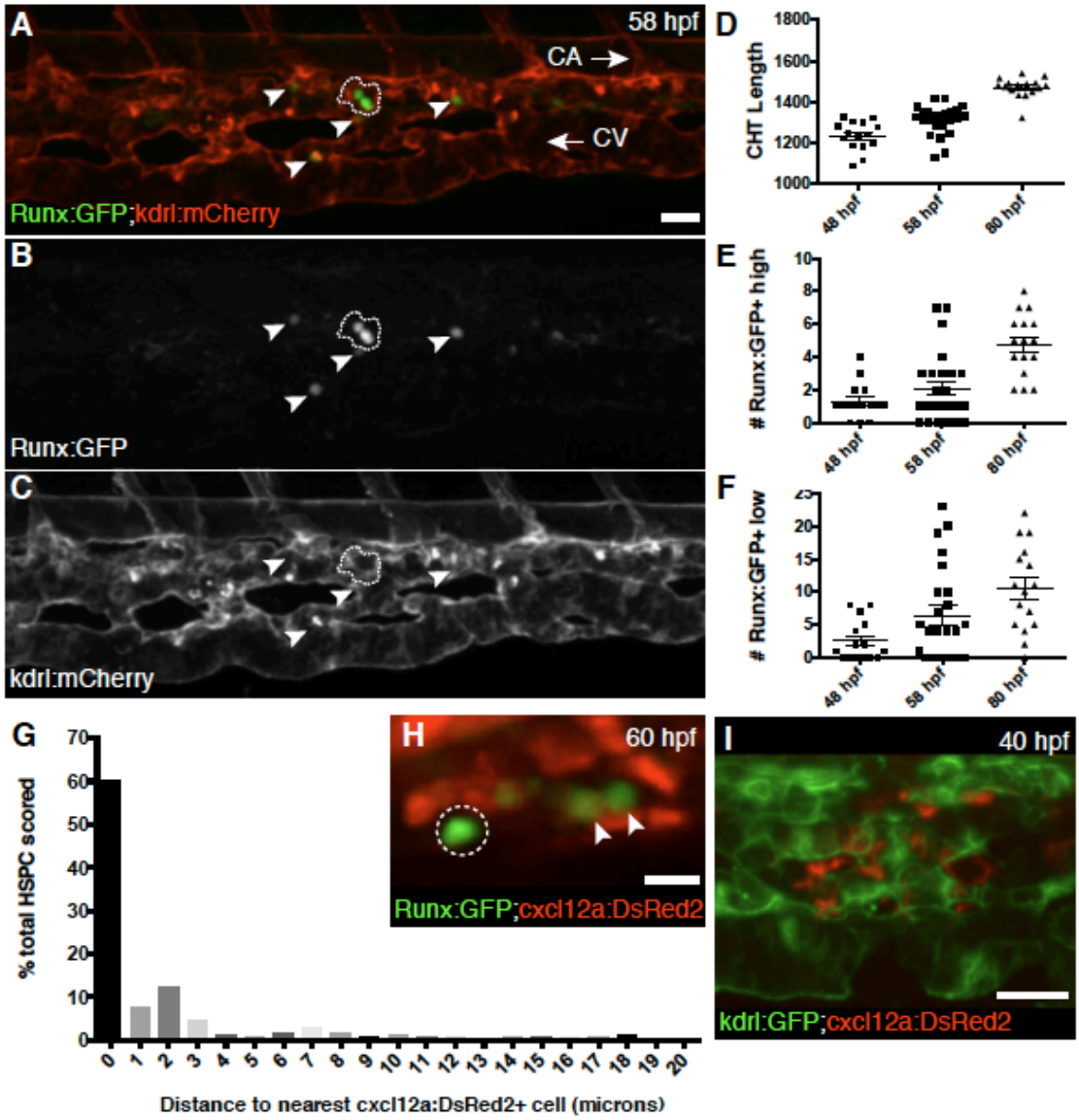

Figure 4. A novel transgenic zebrafish line specifically marks HSPC in the CHT niche

(A-C) The CHT is colonized by Runx:GFP+ HSPC (green) that are closely associated with kdrl:mCherry+ EC (red). The caudal artery (CA) is dorsal to the CHT, and the caudal vein (CV) is ventral, with circulation running posterior (arrow right) and anterior (arrow left), respectively. A cluster of 3 Runx:GFP+ high cells are outlined with a dashed line and 4 Runx:GFP+ low cells are indicated with arrowheads. 58 hpf embryo. (D-F) The number of Runx:GFP+ high and low cells are quantified, together with the length of the CHT as an indicator of stage. (G) Percentage of HSPCs in the CHT scored by distance to the nearest stromal cell (n=168 total cells from 25 embryos). (H) Detail of Runx:GFP+ HSPCs (green) in proximity to cxcl12a:DsRed2+ stromal cells (red). Arrowheads mark HSPCs in contact with stromal cell. Circle marks HSPC with a 2 µm gap between it and the stromal cell. 60 hpf embryo. (I) cxcl12a:DsRed2+ stromal cells (red) underlie kdrl:GFP+ EC (green). 40 hpf embryo. Note: Confocal images are 3D rendered depth projections of 20-30 µm z-stacks. Scale bars: (A,I) 25 µm; (H) 10 µm. See also Figure S1.

multilineage contribution could be assessed if the *Runx*:mCherry HSPC enhancer was down-regulated upon differentiation. Sorted double positive cells were diluted in a range between 1 and 50 then transplanted into irradiated recipients. Survival rates improved in recipients that received a greater number of donor HSPCs, and at 3 months post-transplantation the kidney marrow of recipients was dissected for FACS analysis. Runx:mCherry+ cells were present in the kidney marrow and had contributed ubi:GFP+ progeny to all lineages (Figure S2A). Statistical analysis of engraftment over a range of cell doses estimated a stem cell frequency of approximately 1/35 (Figure 5). We consider this to be an underestimate because the donors and recipients are non-isogenic, and are therefore not immune matched, leading us to assume that some donor cells would be rejected. The Runx+ HSPC pool can be sorted with a single transgenic marker, and no additional labeling of cell surface markers, to a purity that is within the range of the well-characterized KSL (c-Kit+ Sca-1+ Lin-) population in mouse[89]. Based on the ability of a small number of adult Runx+ cells to engraft long-term, self-renew, and produce all lineages, we have demonstrated there is substantial stem cell content within this pool of cells. However, there are no antibodies available in zebrafish to further purify this population, or to distinguish between a stem cell and a progenitor. Therefore we will continue to use the term HSPC to describe the Runx+ cells in this study.

We also wanted to evaluate the stem cell characteristics of the Runx+ population in the embryo. A number of studies have shown that hematopoietic stem cells isolated from different tissues of the mouse embryo have the capacity to reconstitute hematopoiesis in the adult[84,90,91]. However, technical limitations in mouse have made it difficult to assess the stem cell potential of an HSPC transplanted from one

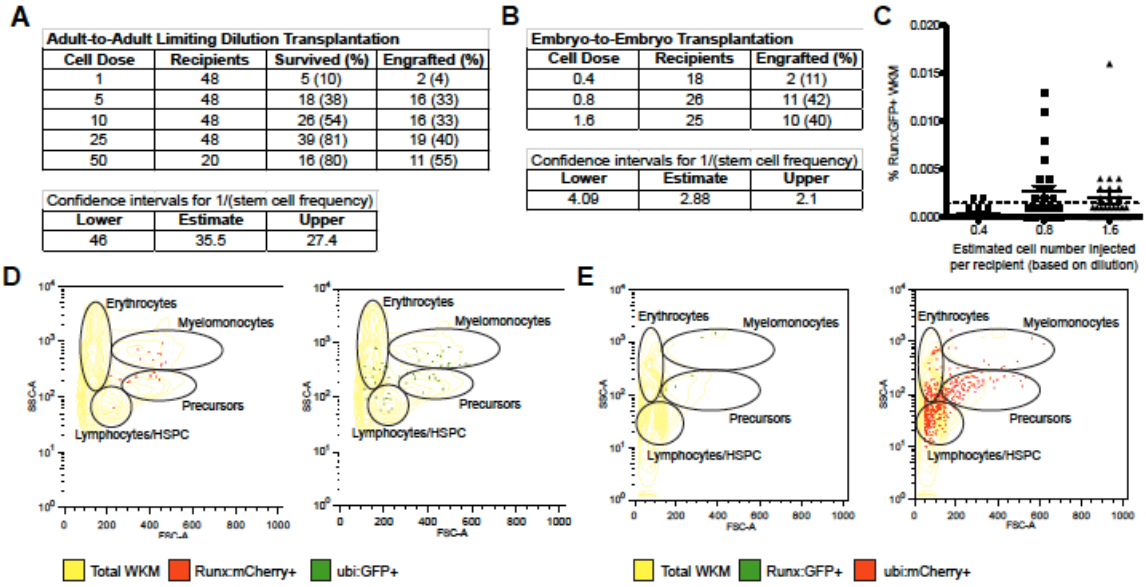

Figure 5. Runx+ cells in the adult and embryo are functional HSPC

Summary of results from (A) adult-to-adult and (B) embryo-to-embryo limiting dilution transplantation experiments. (C) Embryo-to-embryo transplantation recipients with engraftment of Runx:GFP+ cells in the kidney marrow at 3 months (above background; >0.001%). Representative kidney marrow FACS plots of (D) an adult-to-adult transplantation recipient with Runx:mCherry+ HSPC and ubi:GFP+ lineages, and (E) embryo-to-embryo transplantation recipient with Runx:GFP+ HSPC and ubi:mCherry+ lineages. See also Figure S2.

embryo to another. Based on a previous approach[83] we have further developed an HSPC transplantation assay that is unique to zebrafish. HSPCs are sorted from a pool of double transgenic Runx+ and ubi+ donor embryos that were 3 dpf. Only 1-2 cells were injected into the circulation of a wild-type recipient embryo at 2 dpf. A dilution series established the number of cells injected for each experiment.

At 2 dpf the CHT is being colonized by endogenous HSPCs but the thymus has not formed, allowing introduction of exogenous cells without the possibility of immune rejection. Recipient embryos are then raised to adulthood and their kidney marrow is

FACS analyzed for engraftment at 3-5 months. We scored engraftment as any detectable Runx+ cells above background (Figure 5 and Figure S2). This rationale was chosen because approximately one donor HSPC will be competing with endogenous stem cells in an unconditioned wild-type recipient embryo, and there is no precedent to predict chimerism in this scenario. The transplanted cells must seed the CHT, migrate to the kidney, and persist into adulthood where they will self-renew and contribute to all lineages. We identified recipients with Runx+ HSPCs and ubi+ progeny in the kidney marrow, as well as some that had ubi+ cells in the peripheral blood (Figure S2 and data not shown). Statistical analysis estimated the stem cell frequency of the Runx+ population in the 3 dpf embryo to be approximately 1/2.88 cells (Figure 5 and Figure S2).

These results were representative of three independent experiments—two with *Runx*:GFP;*ubi*:mCherry double transgenic lines and a third with the opposite *Runx*:mCherry;*ubi*:GFP transgenic combination. Together, our limiting dilution transplantation in adults, as well as our novel embryo transplantation assay, demonstrates that Runx+ cells mark a highly purified HSPC population with functional stem cell characteristics.

Dynamic visualization of stem cell colonization of the CHT niche

To directly observe the interaction of HSPCs with surrounding EC during CHT colonization, we performed time-lapse live imaging with spinning-disk confocal microscopy. We were able to routinely acquire image series with high temporal resolution (1-2 minutes per 2-channel confocal z-stack) for up to 16 continuous hours. A widefield image was acquired using a 20x objective because the rare lodgement of a

single HSPC could occur anywhere in the length of the CHT (Figure 4A). We observed HSPC arrival in the CHT via circulation, followed by adherence to endothelial walls (Figure S3A and Movie S2). Next, cells underwent rapid extravasation to the abluminal side of the endothelial wall (<5 minutes; Figure S3A). Once HSPCs lodged in the CHT, we made a striking and novel observation: a small group of EC actually remodeled around a single HSPC to form a stem cell pocket, which we call "endothelial cuddling" (Figure 6A and S3B). Within the 12-16 hour limit of time-lapse acquisition, an HSPC would make one of three cell division decisions: symmetric, asymmetric, or no division. In this example the division is asymmetrical, with one daughter cell crawling out of the endothelial niche and the other remaining (Figure S3C).

After HSPC lodgement in the CHT, we used higher magnification (40-60x) to better detail the close association and contact of surrounding ECs (Figure 6B). To quantify the number of surrounding ECs, we briefly fixed and stained embryos with a nuclear dye, then imaged using scanning confocal microscopy (Figure 6C). The ECs in contact with a single HSPC were outlined with membrane-bound mCherry and their nuclei were counted. In each pocket we typically observed 5-6 ECs surrounding a single HSPC. Time-lapse live imaging of endogenous Runx+ HSPCs in the embryo using our novel transgene has revealed striking interactions with perivascular ECs in the niche microenvironment.

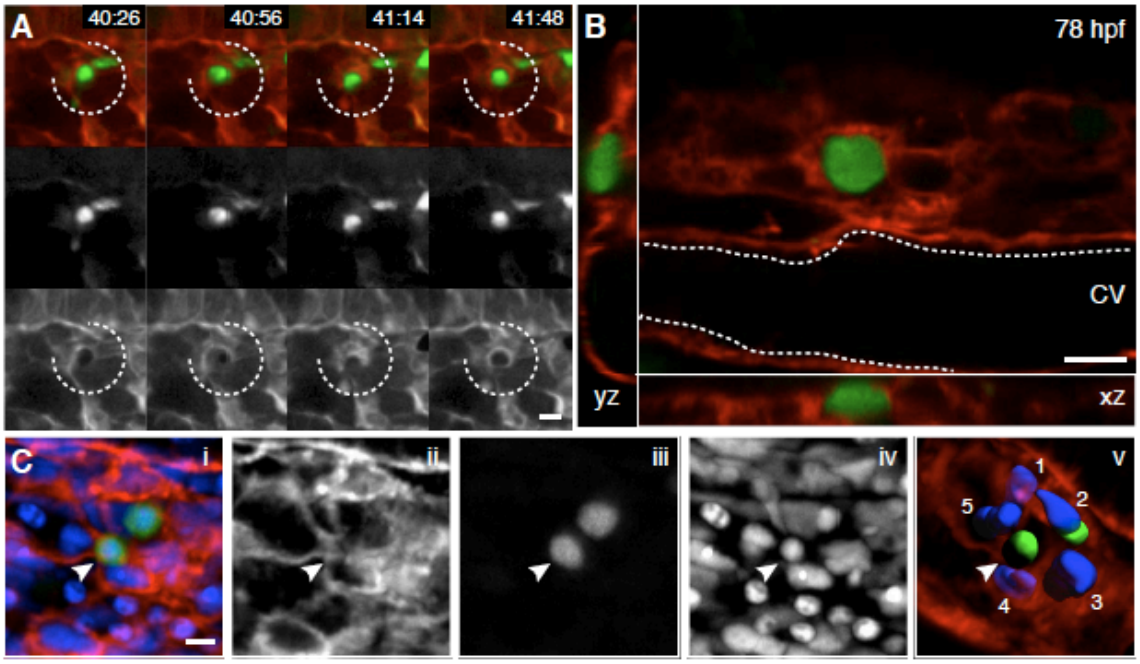

Figure 6. Remodeling of the perivascular niche after HSPC arrival in the CHT

(A) 4 frames selected from time-lapse Movie S2 between 40-42 hpf (hours:minutes). Upper row is a merge of Runx:GFP+ HSPC (green, middle row) and kdrl:RFP EC (red, lower row). A group of surrounding EC (broken circle) remodel around a single HSPC soon after its arrival. (B) Higher magnification (60x) live image of a single Runx:GFP+ HSPC surrounded by kdrl:mCherry at 78 hpf (orthogonal views). CV: caudal vein. (C) 3D rendered projection of scanning confocal image from fixed 80 hpf embryo. (i) merge, (ii) kdrl:mCherry EC, (iii) Runx:GFP+ HSPC, (iv) DRAQ5 nuclei, (v) kdrl:mCherry projection with modeled green HSPC and 5 blue surrounding EC nuclei (arrowhead indicates HSPC in EC surround). All views: dorsal up, ventral down. Scale bars: 10 μm. See also Figure S3.

High-resolution ultrastructure of the perivascular niche surrounding an HSPC

We sought to better reveal the cellular interactions between an HSPC and its perivascular niche that would not otherwise be visible with confocal light microscopy. To do this we used correlative light and electron microscopy[92]. First, to confirm that an HSPC was lodged in the CHT, we performed time-lapse live imaging of *Runx*:GFP;*kdrl*:mCherry embryos as above (Figure 6A). Imaging multiple stage-matched

embryos in parallel, we confirmed that 1-2 HSPCs per embryo had not only migrated to the CHT, but had also lodged and triggered an EC remodeling event that was stable for more than 6 hours (Figure 7A-B). Embryos were then fixed and embedded for electron microscopy (EM). Serial block face scanning EM captured large sections of the CHT at high resolution (Figure 7C; XY: 10 nm/pixel, Z: 100 nm/slice). Based on a number of cellular and anatomical markers (e.g. melanocytes, somites, vessels), the position of the lodged HSPC in time-lapse could be correlated with EM serial sections (Figure S4).

3D reconstruction of EM scans shows that the HSPC lodges in a region just below the ventral endothelial surface of the dorsal aorta. As predicted from our confocal microscopy analysis (Figure 6C), the HSPC is surrounded by at least 5 ECs. There are two stromal cells in proximity to the HSPC, but only one is in contact in a narrow region near the mid-point of the cell (Figure 7D). This is also consistent with our confocal microscopy of Runx+ HSPC and cxcl12a+ stromal transgenic lines (Figure 4G-I). An observation that could not have been made with confocal microscopy was that a fourth cell type (i.e. mesenchymal-like cells with melanophore inclusions), was found together with the HSPC, ECs, and stromal cells (Figure 7D,F and Movie S3). These two cells wrap the HSPC tightly and intertwine with each other. We found another example of an HSPC that is not associated with mesenchymal-like cells, or in proximity to stromal cells, but is surrounded by approximately 5 ECs, showing there are different configurations of this HSPC-EC niche (Figure S4). We were also able to identify Runx+ HSPC in time-lapse movies that were transiently migrating through the CHT and had not lodged in the perivascular niche. These HSPC had only adhered to the vessel walls and in EM sections

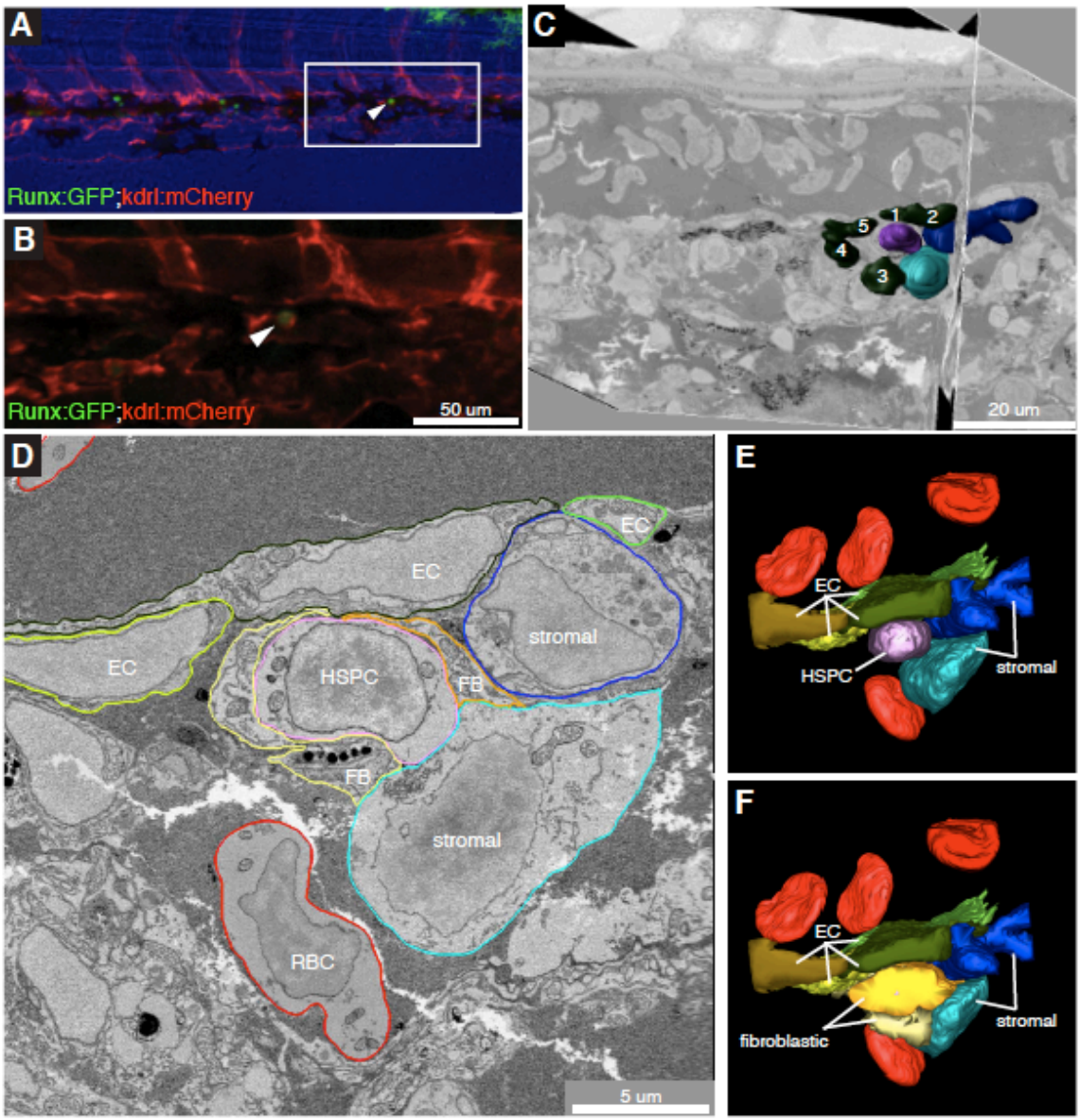

Figure 7. Serial block face scanning EM of CHT after time-lapse

(A) Last frame of CHT time-lapse (60 hpf). Arrowhead marks HSPC lodged >6 hours. Runx:GFP (green), kdrl:mCherry (red), brightfield (blue). Anterior left, posterior right, dorsal top, ventral bottom.
(B) Detail of region in (A) marked by box. (C) Single section and orthogonal slice from serial block face EM scans. Lodged HSPC is purple, surrounding EC nuclei are green and numbered, stromal cells are blue. (D) High resolution EM of HSPC lodged in perivascular niche just ventral to the dorsal aorta (circulating RBC visible). The HSPC (outlined in pink) is in direct contact with one stromal cell (light blue), is wrapped in 2 fibroblastic cells with melanophore inclusions (yellow and orange), and is surrounded by EC (3 of 6+ shown in green shades). (E,F) 3D rendered models of HSPC and niche in the same view as (D). Fibroblastic cells are not shown in (E) but are shown in (F). See also Figure S4 and Movie S3.

did not have the characteristic EC surround structure (data not shown). This further emphasized that the HSPC-EC niche formation event is rare and distinct.

A chemical genetic screen to discover small molecule regulators of CHT niche colonization

Having tracked HSPC lodgement in the CHT niche, we wanted to identify the signaling mechanisms that regulate these cellular events. We performed a chemical genetic screen by introducing individual small molecules to embryos during the peak window of HSPC migration to the CHT (48-72 hpf; Figure 8). Hits were scored if they increased or decreased hematopoietic progenitor markers *cmyb* and *runx1* with similar activities to control compounds (±)11,12-epoxyeicosatrienoic acid (EET; P.L. and L.I.Z., unpublished) or the CXCR4 antagonist, AMD3100, respectively. We chose AMD3100 as a positive control in the embryo because: 1) the duplicated homologs for CXCR4 and CXCL12 are expressed in the DA and CHT (*cxcr4a/b* and *cxcl12a/b*; Figure S5A); 2) the *cxcl12a* transgenic reporter[93] is expressed in CHT stromal cells (Figure 4G-J); 6) AMD3100 blocks CXCL12-dependent migration of kidney marrow cells[93]. After treating embryos with a range of AMD3100 doses, we observed dose-dependent reduction of HSPC markers in the CHT (Figures 8B,E and S5B). Following these results, we screened ~2400 known bioactive compounds, and identified 40 individual compounds that increased and 107 that decreased CHT hematopoiesis.

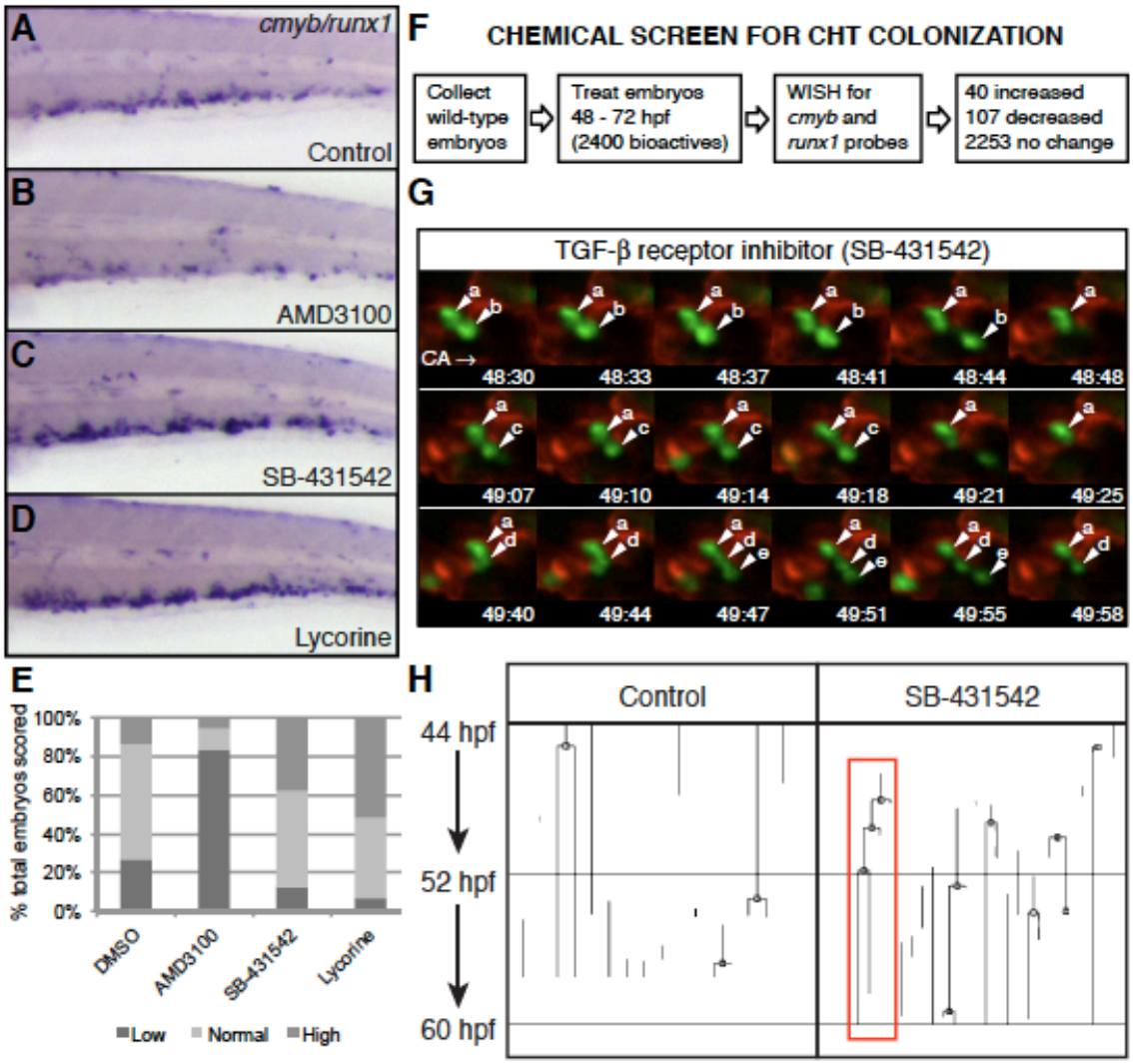

Figure 8. Chemical genetic screen to identify small molecule regulators of CHT niche colonization

(A-D) WISH of *cmyb/runx1* probes in the CHT of 72 hpf embryos. Treatments from 48 hpf as indicated. (A) DMSO control with normal expression. (B) Low expression after 25 μM AMD3100 treatment. High expression after treatment with 40 μM SB-431542 (C) or 25 μM lycorine (D). (E) Percentage of total embryos scored with *cmyb/runx1* expression levels as shown in (A-D). (F) Overview of chemical screen. (G) Selected frames from time-lapse movie of a Runx:GFP (green) x kdrl:RFP (red) double transgenic embryo treated with TGF-β inhibitor, SB-431542. In <90 minutes, an HSPC (a) undergoes rounds of division and releases daughter cells (b,c,e) into circulation (caudal artery, CA; circulation to posterior, right). (H) Lineage tree analysis of HSPC tracked in parallel time-lapse movies, with and without SB-431542 treatment, from 44-60 hpf. One line is one continuously tracked HSPC from the time it enters the CHT field of view until it exits. Branch points mark cell divisions. The red box marks the lineage of the cells shown in (G). See also Figure S5.

Live imaging with small molecule regulators reveals distinct cellular behaviors within the CHT

We tested a subset of our chemical screen hits by adding individual compounds to the media of *Runx*:GFP+;*kdrl*:mCherry+ embryos during time-lapse imaging to directly observe the behavior of HSPC as they colonize the CHT. One of the hits in our screen that increased CHT hematopoiesis was SB-431542 (Figure 8C), a selective inhibitor of transforming growth factor (TGF)-β type I receptors, and most potently ALK5/TGFBR1. When added during time-lapse imaging, we observed normal HSPC arrival in the CHT and adherence to vessel walls. However, soon after arrival HSPCs began to undergo frequent rounds of asymmetric division (Figure 8G,H and Movie S4). One daughter cell would bud off into circulation, while the other remained adhered to the vessel wall. To quantify this difference, we performed lineage tree analysis of HSPCs during parallel time-lapse movies (i.e. control and treated stage-matched embryos imaged side-by-side; Figure 8H). Scoring cell divisions between 44 and 60 hpf, more HSPCs divided in SB-431542 treated CHT movies (n=8-10 versus n=3-4 in DMSO treated controls). These data illustrate that inhibition of TGF-β receptor signaling using the chemical SB-431542 expands HSPC populations by increasing the frequency of cell divisions. This is consistent with previously published *in vitro* and *in vivo* data that showed TGF-β signaling negatively regulates HSPC proliferation[94–99]. Directly visualizing the effect of SB-431542 on HSPCs has demonstrated that we can rapidly identify cellular response to a specific signal in the endogenous niche.

A second compound we identified in our screen was lycorine, a natural alkaloid extracted from the Amaryllidaceae plant family that dose-dependently increased *cmyb* and *runx1* in the CHT (Figure 8D and 9A). This drug does not have a defined target or mechanism of action, but is a candidate anti-inflammatory and anti-cancer drug (Kang et al., 2012; Lamoral-Theys et al., 2010; Yamazaki and Kawano, 2011). Running parallel time-lapse movies, we observed more HSPCs nestled in the CHT in lycorine-treated embryos compared to controls (Figure 9B,C). Over time, lycorine treatment dramatically increased HSPC number in the CHT (Figure 9D). We also scored the total amount of time each HSPC was resident in the CHT during the time-lapse, and found lycorine treatment produced a significant shift towards longer durations spent in the niche (Figure 9E; median difference 1.67 hours; Wilcoxon signed rank test, $p=0.01$). Lycorine treatment during the peak of CHT colonization also had a sustained effect on the total number of HSPC in the embryo. A pool of Runx:GFP+ embryos that were treated with lycorine from 2-3 dpf then washed off, had a significantly higher number of GFP+ HSPCs at 7 dpf compared to DMSO controls (Figure 9F). To obtain a better understanding of the molecular effects of lycorine on HSPC, we treated Runx:GFP;kdrl:RFP embryos from 2-3 dpf, then sorted Runx+ HSPCs and kdrl+ ECs for whole genome microarray analysis. (Figure S6). Lycorine treatment induces significant changes in both HSPC and EC that promotes the interaction of HSPC with the perivascular CHT niche.

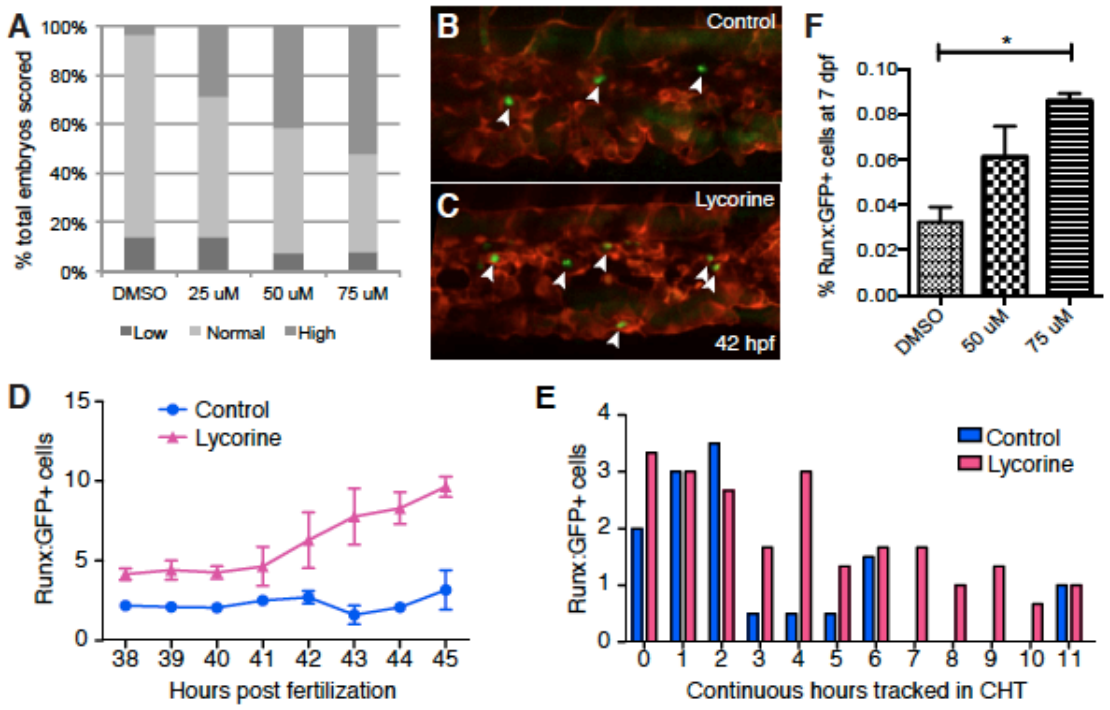

Figure 9. Lycorine modulates HSPC-EC interactions in the CHT

(A) Lycorine treatment dose-dependently increases the percentage of embryos with high *cmyb/runx1* expression levels, as shown in Figure 5D. (B-C) Stage-matched frames at 42 hpf from parallel time-lapse movies of Runx:GFP;kdrl:RFP double transgenic embryos. There are more HSPCs (marked with arrowheads) in lycorine-treated (25 μM) embryos (C) compared to DMSO-treated controls (B). (D) HSPCs are counted in each frame of a time-lapse movie and then averaged each hour. 5 movies imaged in parallel: n=2 controls and n=3 lycorine-treated (25 μM). (E) Same movies as in (D) were scored for continuous hours an HSPC was tracked in the CHT. There was a significant difference in the median time HSPC spent in the CHT between controls and lycorine-treated embryos (1.67 hours; Wilcoxon signed-rank test, p=0.01; HSPC counts were normalized because the lycorine group had 3 embryos and the control group had only 2). (F) Pools of Runx:GFP+ embryos treated with lycorine from 2-3 dpf have significantly increased HSPC at 7 dpf (p=0.0004; FACS of 4 independent pools per dose). Error bars show mean ± s.e.m. See also Table S1.

Endothelial niche remodeling is conserved in mammalian fetal liver

It was important to establish if the distinct endothelial niche structure we identified in the zebrafish CHT was also found in mammals. The equivalent tissue is the FL as it is the first tissue colonized by definitive HSPC from the dorsal aorta. The FL is an intermediate site of hematopoiesis where HSPC expand before leaving to colonize the

adult marrow and it produces the majority of blood during development[90,100,101]. To examine the earliest stages of FL colonization, we dissected E11.5 FL from *Ly6a*-GFP (Sca-1) mice, which have GFP+ HSPC[102,103]. Together with HSPC marker Runx1, and EC marker VE-cadherin (Cdh5), we found Ly6a-GFP+/Runx1+ HSPC in one of 3 compartments in the FL: 1) an abluminal space with no EC contact (Figure 10A); 2) adherent to EC on one side (Figure 10B); 3) inside an EC pocket (Figure 10C and Movie S5). The similarity of a single HSPC surrounded by a small group of EC in both the mouse FL and zebrafish CHT (compare Figure 6B and 10C), suggests that this cellular structure is important for stem cell lodgement in hematopoietic niches.

The identification of a potentially conserved HSPC-endothelial niche structure raised the possibility that HSPC also trigger a dynamic remodeling of EC during colonization of the FL. The FL tissue in mouse is not directly accessible to confocal microscopy, so we instead applied a protocol for live imaging of embryo explants. We dissected wild-type and *Ly6a*-GFP E11.5 FL, soaked the explant FL in fluorescently conjugated antibodies to detect c-kit+ HSPC and CD31+ (Pecam1+) EC, and immediately performed live imaging for up to 4 hours. We observed c-kit+ hematopoietic cells adhered to the sinusoidal network of CD31+ EC (Figure 10D-E and S7). We followed a c-kit+ HSPC attached to the sinusoid as it migrated into a small group of EC (Figure 10D and Movie S6). Next, EC tightly surrounded the HSPC in what looked strikingly similar to endothelial niche remodeling in the zebrafish CHT (compare Figure 6A and 10D). Tracking a Ly6a-GFP+/c-kit+ HSPC in another explant, we observed one cell division (Figure 10E). Intriguingly, the daughter cell proximal to the sinusoid remained surrounded by EC, while the daughter cell distal to the sinusoid migrated away

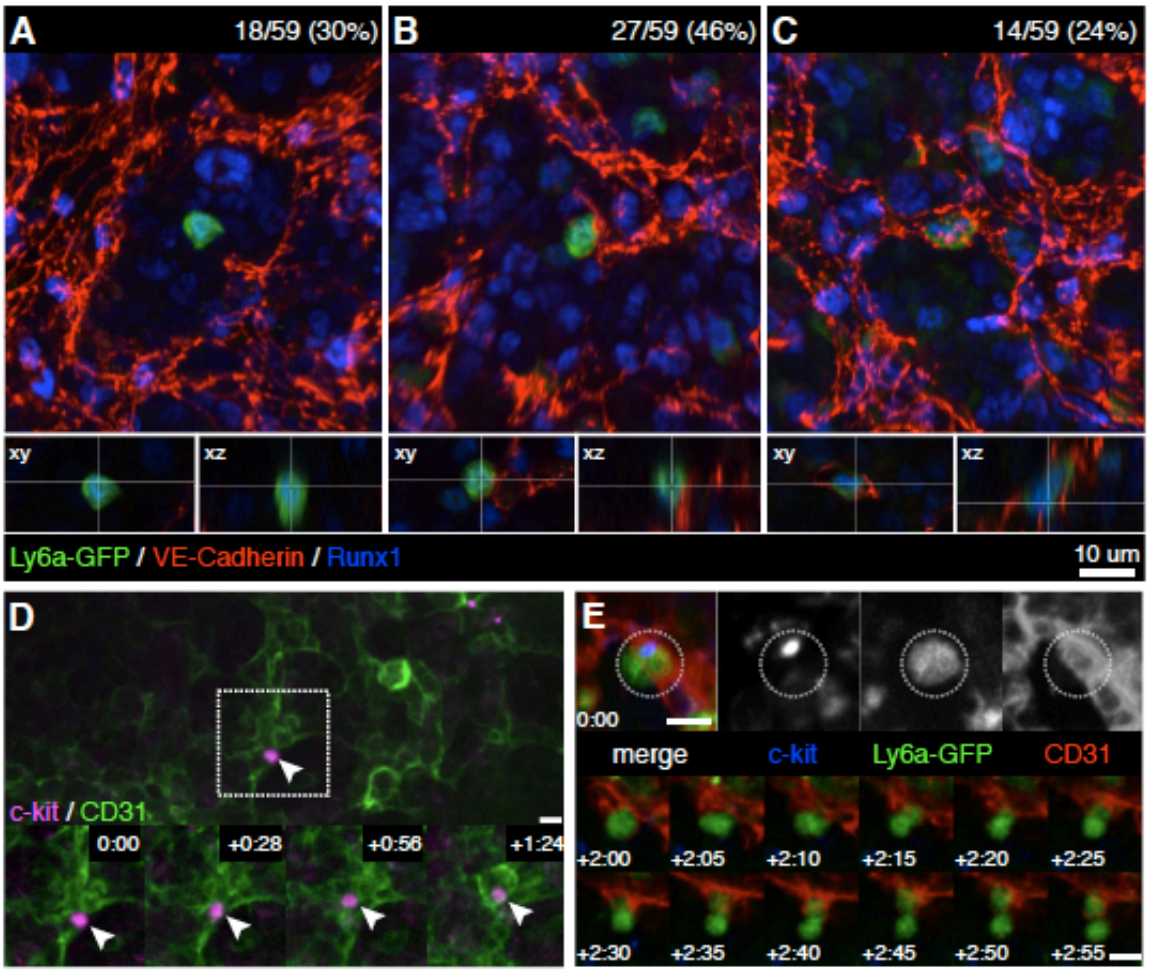

Figure 10. Conserved remodeling of ECs around HSPCs in the mouse fetal liver

(A-C) Fetal livers from E11.5 Ly6a-GFP mice were fixed and stained for immunofluorescence with anti-VE-Cadherin (red), anti-Runx (blue), and anti-GFP (green) antibodies. We scored 59 Ly6a-GFP+/Runx1+ cells from 3 fetal livers and identified three different HSPC-EC configurations: (A) abluminal with no contact between HSPC and EC; (B) EC contact on one side of the HSPC; (C) HSPC surrounded on all sides with EC. See Movie S5. (D) An HSPC with c-kit+ accumulation (magenta) is shown adhered to CD31+ endothelial sinusoid (green) in one lobe of an E11.5 FL (arrowhead). The white box marks details below. Key time-lapse frames show in <90 minutes the HSPC migrates into a field of SEC. Soon after the SEC surround the HSPC to form a niche. See Movie S6. (E) Ly6a-GFP+ HSPC (green) is adhered to the abluminal side of a CD31+ sinusoid (red), with a c-kit+ contact point (blue). Following this same cell for >2 hours (1 frame/5 minutes), shows the cell divides, with one cell remaining in the endothelial niche and the other migrating away. See Movie S7. Confocal images are 3D rendered depth projections (A,B,C,E), orthogonal views (A,B,C below) or maximum projections (A) of z-stacks. Scale bars: 10 μm. See also Figure S6.

into the abluminal space (Figure 10E and Movie S7). In another time-lapse sequence, a c-kit+ HSPC was observed undergoing discrete steps towards lodgement: adherence, extravasation, abluminal migration, and endothelial niche remodeling (Figure S7A-C). We also identified an accumulation of c-kit at the contact point between the HSPC and EC (Figure 10E and S7C). This observation is similar to data that showed c-kit condenses with clustering lipid rafts in cytokine-induced HSPC[104,105]. Even with the caveat that FL explants have been removed from circulation and are imaged *ex vivo*, our live imaging data strongly suggest an evolutionary conserved process of dynamic EC remodeling around a single HSPC in a hematopoietic niche.

Discussion

The ability to follow endogenous HSPCs in the live zebrafish as they lodge in a niche has allowed us to capture never before seen cellular behaviors during this important event in the life of a stem cell. This high-resolution view of the zebrafish CHT has shown events that have not been visible in the mammalian bone marrow. We watched as HSPCs attached to the endothelial wall of a vessel, underwent extravasation, migrated into the abluminal space, then triggered a striking endothelial remodeling event to form a niche (summarized in Figure S3D). Live imaging of mouse FL explants revealed that these steps towards HSPC lodgement are highly conserved. This high resolution tracking of HSPC interaction with the perivascular niche opens many possibilities to further dissect the mechanisms of hematopoietic colonization.

The combination of time-lapse live imaging and chemical genetics in the zebrafish has enabled us to rapidly screen compounds that have an effect on endogenous

HSPCs in their microenvironment. We have validated this approach by showing that signaling pathways with well-established roles in HSPC trafficking and proliferation, CXCR4-CXCL12 and TGF-β, respectively also regulate HSPCs in the zebrafish embryo. We found that treatment of the embryo during CHT colonization with the compound lycorine dose-dependently increased the number of hematopoietic progenitors. Analysis of live imaging data suggested that HSPCs accumulated in the CHT because of longer interaction times with the perivascular niche. The additional finding that the increase in HSPC number was sustained long after lycorine was removed raises the possibility that HSPC-niche interactions during development could have a role in determining the long-term size of the stem cell pool. We are currently testing this hypothesis at later time-points and into adulthood. To reveal clues to the mechanism of lycorine action, we isolated HSPC and EC from lycorine-treated embryos. We found there was cell type-specific variations in gene expression that point to changes in the migratory and adhesive properties of HSPC and EC. Our results show there is a functional role for interactions between HSPC and EC during development, and this may be important for setting aside the long-term hematopoietic stem cells that will colonize the adult marrow.

Our finding that HSPC arrival triggers cellular changes in the local perivascular niche raises interesting questions about what constitutes a hematopoietic stem cell niche. Rather than a static number of niches that can be either cleared or filled (Schofield, 1978), our results are suggestive of basic niche components that create a permissive environment for an arriving stem cell. Once attracted to these general locations in the marrow, the stem cell will move out of circulation and lodge in its new surroundings. The rapid remodeling of endothelial cells around a stem cell may provide a mechanism to

retain and protect these new arrivals. It will be important to determine how much plasticity there is in the number and locations that a stem cell can reside. We focused our study on the hematopoietic microenvironment in the zebrafish CHT and mouse fetal liver. These are intermediate niches are required to rapidly expand the stem cell pool. With continual advancements in imaging technology we will soon be able to resolve similar cellular dynamics in the adult marrow.

Prior to HSPC transplantation, myelosuppression by chemotherapy or irradiation is used to condition a recipient and prepare their bone marrow to receive donor stem cells. Conceptually, this has been thought to "clear" or "open" the niche. However, studies have shown that myelosuppression causes significant damage to the bone marrow vascular epithelium that must be repaired for hematopoiesis to recover (Hooper et al., 2009). This has presented a dynamic model of the vascular niche that requires angiogenesis, together with engraftment of incoming HSPC, to rebuild a functional hematopoietic bone marrow. The ability to modulate these HSPC-EC interactions, as we and others have started to demonstrate, will likely have an important impact on clinical stem cell transplantation.

Addendum

A chemical screen for CHT colonization in zebrafish embryos demonstrated that signaling pathways with well-established roles in HSPC trafficking and proliferation also regulate HSPCs in zebrafish. AMD3100, a CXCR4 antagonist, dose-dependently decreased the numbers of HSPCs that localized to the CHT during embryogenesis. In addition, we identified a number of small molecules that regulate the sphingosine-1-phosphate (S1P) pathway, which has previously been shown to play a role in chemotaxis and cell migration. Out of the 5 G-protein coupled receptors for S1P, S1PR1 is considered to be the one that is critical for blood cell migration. We looked at the expression pattern of S1PR1 receptor during the key stages of CHT colonization and found that it's expressed in both the dorsal aorta and the CHT.

To test if there was an interaction between CXCR4 and S1PR1 signaling, two important pathways that reduce CHT hematopoiesis, we used a chemical genetic interaction matrix, taking advantage of two clinically relevant small molecule regulators of these receptors: AMD3100 and FTY720 (Figure 11). This matrix demonstrated that there were combined doses of the two drugs that increased CHT hematopoiesis at concentrations where one drug alone had no effect. This result is highly suggestive of an interaction between these pathways in colonization of the CHT.

This result suggested a potential for modulating both homing and engraftment in mammals. SDF-1, the ligand for CXCR4, and S1P, the ligand for S1PR1, are both powerful chemoattractants for murine HSCs, which express both receptor types. However, whereas SDF-1 levels are high in the bone marrow and cause HSCs to home to the niche via CXCR4, S1P levels are quite low in tissues, and are most highly expressed

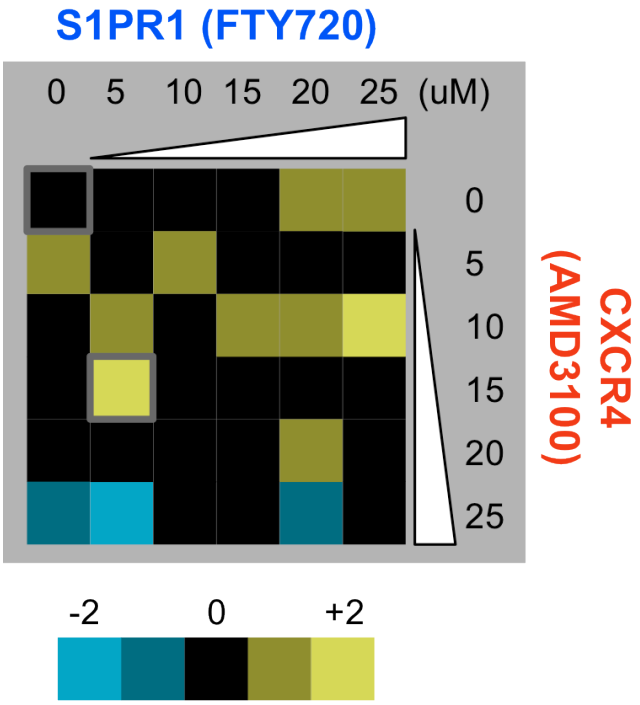

Figure 11: Chemical interaction matrix of FTY720 and AMD3100

Zebrafish embryos were treated from 48hpf-72hpf with the doses of chemical indicated on the matrix. In situ hybridization was performed for runx1/cmyb^{+} cells. "0" score indicates no change in cell number from control, +2 indicates an increase of runx1/cmyb^{+} in the CHT, -2 indicates a decrease.

in the blood. The S1P agonist SEW2781 enhances HSC mobilization from the bone marrow following CXCR4 inhibition by AMD3100. This suggests an intricate connection between the CXCR4/SDF-1 and S1PR1/S1P signaling pathways to control HSC migration in and out of the bone marrow. Based on our chemical matrix and previous data, we hypothesized that during niche colonization HSCs respond and migrate towards high levels of S1P in the blood. Once in circulation, HSCs internalize S1PR1 and CXCR4 emerges on the surface of these cells. This allows HSCs to home to the

CHT, where CXCR4 internalizes and S1PR1 resurfaces once again, to enable cells to migrate to the next site.

To examine the effect of these two drugs on CXCR4 and S1PR1 expression in mice, we treated whole bone marrow cells with varying doses of AMD3100 and FTY750 and performed FACS analysis to look at surface receptor expression. We found that treatment with either of the drugs alone, or in combination, resulted in dynamic changes in receptor expression (Figure 12). Treatment with higher doses of AMD3100 alone decreased CXCR4 expression while S1PR1 expression was increased. Conversely, treatment with FTY750 alone increased S1PR1 and decreased CXCR4 expression. Interestingly, combination treatments showed both increases and decreases in receptor expression dependent on dose.

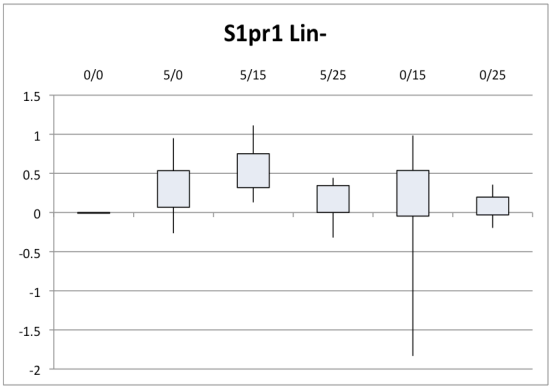

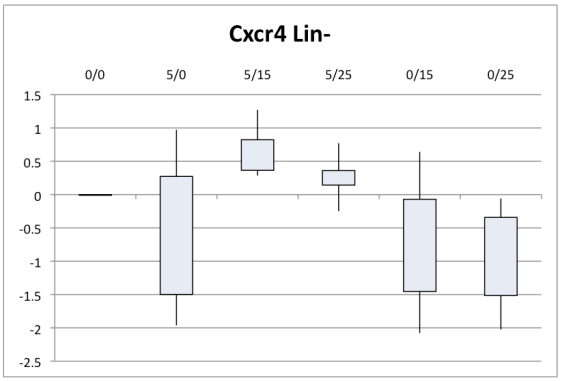

FTY720 (uM)	0	5	5	5	0	0
AMD3100 (uM)	0	0	15	25	15	25

Figure 12: S1PR1 and CXCR4 receptor expression data in WBM cells

WBM was treated for 60 min at 37°C (n=8 total from 2 experiments), cells were sorted for lineage negative population and analyzed by FACS for receptor expression. The graph shows the change in number of WBM cells expressing receptor (log_2, relative to control).

We next wanted to check if these changes in receptor expression level were correlated with changes in HSC homing and mobilization. We performed homing transplants using 4 x10^6 CD45.1 WBM cells treated with PBS, FTY750 alone, AMD 3100 alone, or a combination, for 1 hour. Cells were mixed with equal numbers of CD45.1.2 WBM cells and injected into CD45.2 recipient mice. 16 hours following transplantation, the marrow of recipient mice was harvested and stained for CD45 markers. As expected, we found a slight decrease in the homing capabilities of cells treated with AMD3100 alone (Figure 13). Interestingly, we found that the combination treatment resulted in a slight increase of homing potential, however these results must be repeated with optimized conditions.

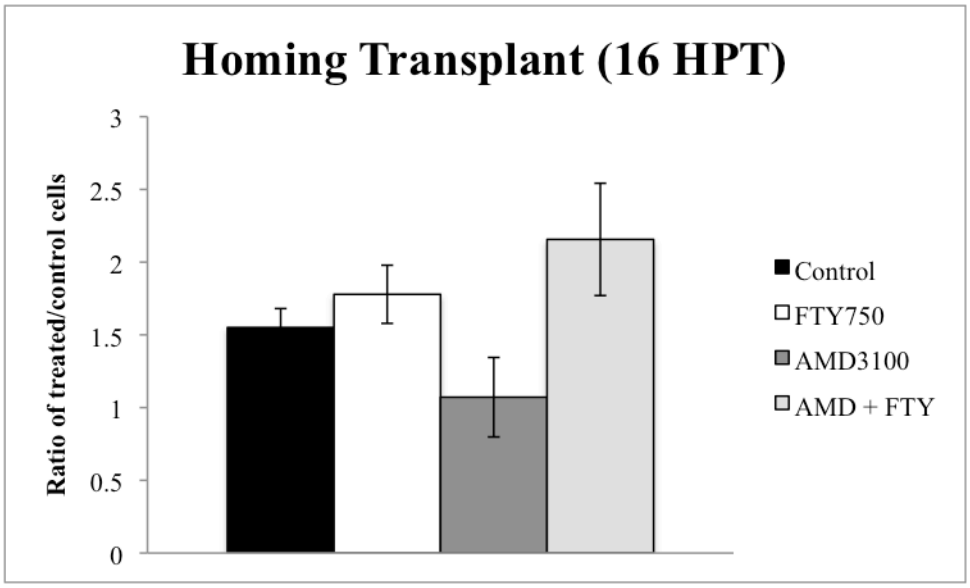

Figure 13: Effect of AMD3100 and FTY720 treatment on homing of WBM cells

WBM cells were treated with AMD3100, FTY720, or both for 1 hour. The graph indicates the ratio of treated cells: competitor cells in the marrow of recipient mice. These results were obtained 16 hours post transplantation. N=5 mice/group.

We also wanted to observe the combinatorial effects of these drugs on the mobilization of HSCs from the bone marrow to peripheral blood. *In vivo* treatment of mice with AMD3100 results in a dramatic increase of HSCs in circulation that peaks at 1-hour post injection and steadily decreases thereafter. We injected mice with PBS, AMD3100 alone, or AMD3100+FTY750 at multiple doses. At 1-hour post injection, we bled the treated mice and performed colony-forming assays to confirm the presence of HSCs in the peripheral blood. As expected, mice treated with PBS had essentially no circulating HSCs, evidenced by the absence of colonies at day 7, whereas mice treated with AMD3100 alone had high levels of circulating HSCs (Figure 14). The addition of FTY750 did not enhance mobilization over AMD3100 alone. However a low dose of FTY750 (0.01mg/kg) resulted in significantly more colonies than a high dose (1.0mg/kg).

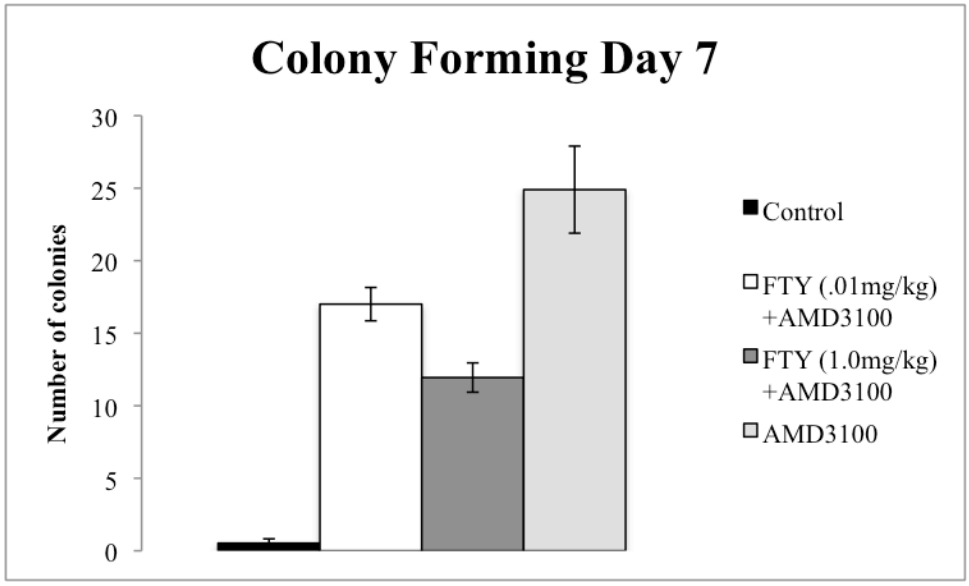

Figure 14: Effect of AMD3100 and FTY720 treatment on mobilization of HSCs

Graph shows the number of colonies on day 7 from peripheral blood that was isolated from mice 1 hour-post treatment with various drugs (as indicated in figure legend).

Our results suggest that we can modulate the processes of homing and mobilization using small molecule regulators of migration pathways and are consistent with recently published studies[106,107]. Further characterization of the CXCR4 and S1PR1 receptor dynamics in response to chemical modulation will be necessary to take advantage of this interaction. In the future, it should be possible to identify combinatorial doses of AMD3100 and FTY750 that favor either mobilization or homing. These treatment regimens could have useful clinical applications.

Chapter 3

Prostaglandin E_2 regulates long-term repopulation activity of ST-HSCs

Attributions

I designed and completed all zebrafish and mouse transplantation experiments. I analyzed transplant recipients with help from technicians Margot Brandt and Rebecca Maher. I performed all zebrafish and mouse FACS experiments, which included analysis of *runx1*:GFP fish, *ex vivo* treated cells, and sorted cells for transplantation. Owen Tamplin performed the confocal microscopy on dmPGE$_2$-treated zebrafish. I performed cell sorts and treatments for the microarray and ChIP-seq experiments. Yi Zhou, Song Yang, and Eva Fast performed bioinformatics and data analysis for microarray and ChIP-seq experiments.

Abstract

16,16- dimethyl prostaglandinE2 ($dmPGE_2$) increases the number of embryonic HSCs in zebrafish and improves long-term engraftment of bone marrow and cord blood transplantation. The mechanism of signaling has been shown to involve CXCR4 upregulation and wnt activation, but the cellular activity of dmPGE2 remains to be determined. To investigate the long-term effects of $dmPGE_2$, we transiently treated zebrafish embryos from gastrulation to 36 hours post fertilization (hpf), and grew up these animals to 3-4 months of age. Kidney marrow (KM) cells from adult zebrafish pulse-treated with $dmPGE_2$ during embryogenesis were studied in a competitive transplantation experiment using GFP^+ treated KM and untreated DsRed KM. The ratio of GFP^+ cells present in KM 3 months post-transplant was higher in $dmPGE_2$-treated groups compared to control (1.25 vs. 0.68, $p<.001$). We tested the ability of $dmPGE_2$ to confer a long-term advantage on sorted marrow populations in competitive transplantation assays in the mouse. ST-HSCs, but not LT-HSCs or MPPs, showed enhanced reconstitution in recipient animals a full 12 months after $dmPGE_2$ exposure, compared to control animals. The effects of $dmPGE_2$ on HSC function persist over substantial time despite transient exposure, and suggest the long-term effects of $dmPGE_2$ are due to a stimulatory effect on the ST-HSC population to acquire long-term activity. Gene expression data and ChIP-seq analysis in human $CD34^+$ cells suggests that $dmPGE_2$ may play a role in the quiescent state of these cells. Our studies are the first to demonstrate that a small molecule can prevent exhaustion of ST-HSCs, which facilitates long-term reconstitution following transplant.

Introduction

Hematopoietic stem cell transplantation (HSCT) is an effective treatment for blood disorders and autoimmune diseases. Enhancing hematopoietic stem and progenitor cell (HSPC) frequency and function will shorten engraftment time and lower risk factors in myeloablated patients. 16,16- dimethyl prostaglandinE2 ($dmPGE_2$) was previously identified in a chemical screen and found to regulate HSC development during zebrafish embryogenesis[43]. The effect of $dmPGE_2$ on hematopoiesis is conserved in mammals. Several groups have demonstrated that *ex vivo* treatment of $dmPGE_2$ confers an advantage on mouse marrow cells in competitive repopulation studies[43,46]. Treatment of human $CD34^+$ cells with $dmPGE_2$ prior to transplantation into immunodeficient mice results in increased chimerism in the peripheral blood and bone marrow of recipients[48]. Long-term transplantation studies have been carried out to analyze the repopulation kinetics of marrow cells following pulse exposure to $dmPGE_2$. Recipient mice have normal blood counts and bone marrow histology through quinary transplants, with an absence of lineage bias; demonstrating that pulse treatment of $dmPGE_2$ does not lead to a cancerous phenotype[108]. In addition, bone marrow cells pre-treated with $dmPGE_2$ are protected from hematopoietic injury when exposed to chemotherapy reagents. Treated mice display accelerated recovery of hematopoiesis following total body irradiation[109]. These data suggest *ex vivo* treatment with $dmPGE_2$ as a potential clinical therapy to enhance HSPC engraftment following transplantation.

A recent phase 1 trial assessed the potential of $dmPGE_2$ treatment to increase the effective dose of HSCs for umbilical cord blood (UCB) transplantation[49]. Although transplanting cord blood reduces the stringency for HLA matching, the concentration of

HSPCs per cord blood unit (CBU) is too low for successful engraftment in adult recipients. The current standard for UCB transplantation is to infuse a patient with 2 CBU. To determine whether $dmPGE_2$ treatment improves engraftment of cells following UCB transplantation, patients were infused with one $dmPGE_2$-treated CBU and one untreated CBU. *Ex vivo* pulse with $dmPGE_2$ enhances the engraftment of CBU in patients as determined by the median time to neutrophil engraftment (17.5 days vs. 21 days). Chimerism analysis demonstrated that the $dmPGE_2$-treated cord preferentially engrafted in >80% of patients. Historically, there is a 50% chance for either cord unit to reconstitute a patients' hematopoietic system. These preliminary results have exciting therapeutic implications. It may be possible to eliminate the need for a second CBU, which would reduce strain on current resources. Shortening engraftment time will also reduce the risk of infection to myeloablated patients.

Although UCB has emerged as a valuable source of HSPCs for transplantation, there are limitations for its use in adult patients. Recently, studies have aimed to chemically manipulate these cells *ex vivo* with the goal of expanding HSPCs prior to transplant, or to enhance homing and engraftment of these cells following transplantation. Improving either of these aspects would allow more patients to benefit from the advantages of cord blood transplantation. Using small molecules to treat entire CBUs can be somewhat complex; cord blood cells are a heterogeneous population that contains not only HSPCs but also mesenchymal stem cells, endothelial progenitors, and naïve immune cells[110]. In addition to its effects on HSPCs, $dmPGE_2$ has immunomodulatory effects and promotes the survival of naïve UCB T cells through the Wnt/β-catenin pathway[111]. This protective effect could enhance recipient T-cell chimerism following

transplant. This has important clinical implications since delayed immunological reconstitution is a huge risk factor for transplant patients.

The initial chemical screen in zebrafish that identified PGE_2 as a regulator of HSPCs showed an increase in *runx1* and *cmyb* positive cells, a heterogeneous population that includes HSCs, progenitors, and differentiated myeloid cells[43]. Follow-up studies in mice demonstrated that $dmPGE_2$ enhances the homing and transplantation of murine LSK cells and human $CD34^+$ cells, both heterogeneous populations[46,48]. Serial transplants in mice suggest that PGE_2 is acting on a long-term repopulating cell, yet treated LT-HSCs do not demonstrate enhanced repopulation compared to control cells[108]. Consistent with these results, mice treated *in vivo* with $dmPGE_2$ show no change in LT-HSC frequency, but display an increase of ST-HSCs/MPPs. These results suggest that a population of cells distinct from LT-HSCs mediate the effects of PGE2.

ST-HSCs/MPPs are functionally defined by their multipotent but transient repopulation capacity[27]. Transplantation of ST-HSCs/MPPs from mice that are continuously treated with $dmPGE_2$ into irradiated recipients results in enhanced short-term, but not long-term reconstitution, most likely due to exhaustion. In contrast, we have found that ST-HSCs treated with an *ex vivo* pulse of $dmPGE_2$ enhance long-term reconstitution for up to 1-year post transplant compared to control cells. Treated ST-HSCs maintain improved function in secondary transplants without additional exposure to $dmPGE_2$. We have found through microarray and ChIP-seq analysis in human $CD34^+$ cells that dmPGE2 induces gene expression that is associated with quiescence. Stimulation of this gene signature may prevent exhaustion of ST-HSCs. Our results show that $dmPGE_2$ enhances the long-term potency of ST-HSCs, which were previously

thought to have transient reconstitution capabilities. Identifying the subpopulation of HSPCs that is responsive to dmPGE$_2$ has important therapeutic implications and may help to improve pre-transplantation expansion protocols.

Materials and Methods

Zebrafish maintenance and lines

Zebrafish and mice were maintained in accordance with Animal Research Guidelines at Children's Hospital Boston. Embryo chemical treatments were performed in 1XE3 fish water.

HSPC population FACS sorting

HSPC populations were sorted from freshly isolated WBM cells using a FACS ARIA (BD Biosystems) using the following antibodies: Lineage- Ter119, CD4, CD8, B220, Mac1, Gr-1 (PE-cy5) Sca1 (PE) cKit (APC) CD48 (Pacific Blue) CD34 (FITC) CD150 (PE-cy7). The following marker combinations were used to differentiate LT-HSCs (LSKCD48$^-$CD34$^-$CD150$^+$), ST-HSCs (LSKCD48$^-$CD34$^+$CD150$^+$), and MPPs (LSKCD48$^-$CD34$^+$CD150$^-$)

Adult zebrafish repopulation assays

WKM cells from 3-month donor fish were isolated and sorted by FACS (Runx1$^+$ cell transplants) or counted using a hemocytometer (WKM transplants). Donor cells were transplanted into irradiated *casper* recipients (30gy, split dose) along with untreated

helper marrow. Transplantation procedures were performed as previously described[82]. At 3 months post-transplant, WKM from recipient fish was collected and analyzed by FACS to detect chimerism levels of mCherry and GFP-positive cells in the marrow or by fluorescence microscopy.

WBM repopulation assays

Recipient mice (*C57bl/6* CD45.2) are irradiated with 8Gy the day before transplantation. Bone marrow cells are freshly isolated from donor mice (SJL CD45.1). Spin down harvested marrow cells and resuspend cells in DMEM +2%FBS for treatment. Marrow cells are treated with 10uM $dmPGE_2$ or DMSO for 2 hours on ice. Treated cells are competed against freshly isolated CD45.2 cells. For sorted transplants, HSPC populations are FACS-sorted as described above. Individual populations are then treated with 10uM $dmPGE_2$ or DMSO for 2 hours on ice and transplanted along with helper marrow (200K or 400K). For 5-FU transplants, donor mice were treated with 5 FU or PBS as previously described[112]. Marrow was harvested two days later and treated with 10uM $dmPGE_2$ or DMSO for 2 hours on ice and transplanted along with 200K helper marrow cells.

PB chimerism analysis

Peripheral blood was isolated from recipient mice by RO bleed every 4 weeks following transplantation. Red blood cells were lysed and white blood cells were analyzed using the following antibody combinations for multilineage engraftment: Ter119 (PE-cy5) Mac1 (Alexa680) Gr-1 (PE-cy7) B220 (Pacific blue) CD3 (APC) CD45.1(PE) and CD45.2 (FITC).

pCREB ChIP-sequence

Human $CD34^+$ isolated cord blood cells were treated with 10uM $dmPGE_2$ or DMSO for 2 hours at 37°C. ChIP was performed with a pCREB antibody from Santa Cruz (sc-7978) as previously described[113].

Results

PGE_2 increases $runx1^+$ HSPCs in embryo and adult zebrafish

Treatment with $dmPGE_2$ was previously shown to increase the number of runx1/$cmyb^+$ cells in zebrafish embryos by in situ hybridization. We tested the effect of $dmPGE_2$ on a *runx1*:GFP transgenic line that labels HSPCs. Embryos were treated from 3 somite stage (ss) to 36 hpf with 50μM $dmPGE_2$ or DMSO as control. The chemical was washed off at 36 hpf and embryos were imaged using confocal microscopy at 60 hpf. Consistent with previous results, we observed an increase of $runx1^+$ GFP cells in the caudal hematopoietic tissue (CHT) of $dmPGE_2$-treated embryos compared to controls (Figure 15). Given that the increase of $runx1^+$ cells was still present a full day after $dmPGE_2$ was removed, we next looked at these cells in the whole kidney marrow (WKM) of adult fish. *Runx1*:GFP fish were treated with $dmPGE_2$ or DMSO from 3ss-36hpf, at which point chemical was removed and embryos were grown to adulthood. FACS

analysis of WKM at 3 months revealed the number of runx1^{+} HSPCs was increased in fish previously treated with dmPGE$_2$ (Figure 16). This indicates that the enhancement of HSPCs by dmPGE$_2$ during embryogenesis is maintained through development to adulthood.

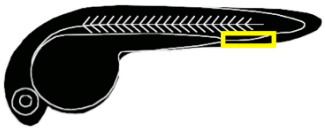

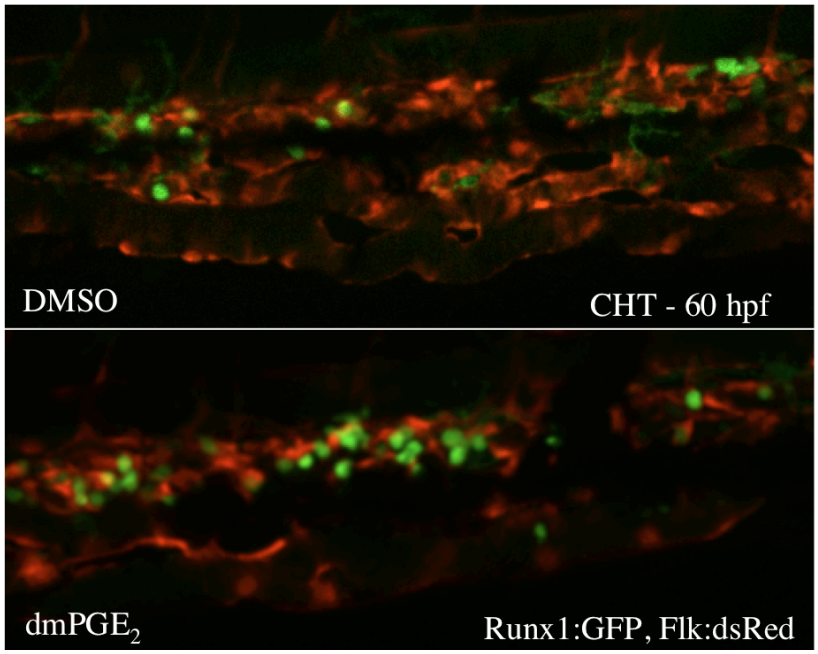

Figure 15: dmPGE$_2$ increases Runx1^{+} cells in the CHT

Zebrafish embryos were treated from 3ss-36hpf with 50uM dmPGE$_2$ (bottom panel) or DMSO (top panel). The cartoon image demonstrates the region of the CHT depicted in the confocal image at 60hpf. HSPCs are labeled with GFP, endothelial cells are labeled with dsRed.

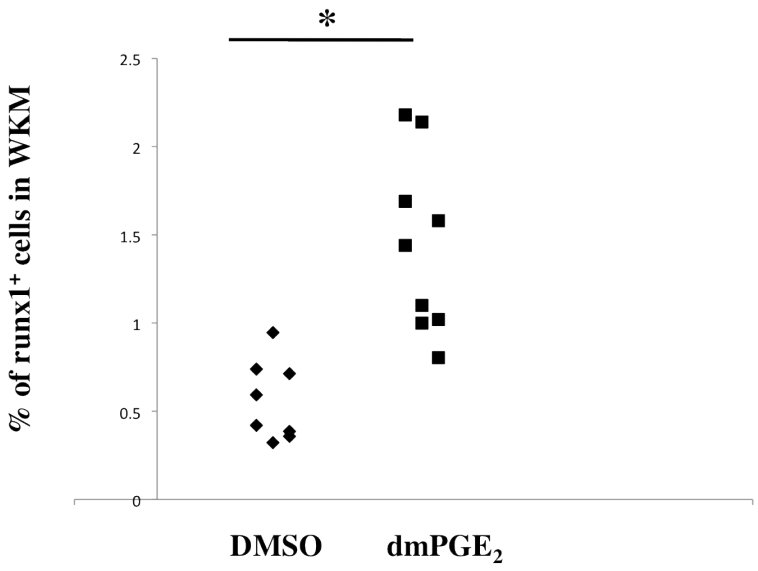

Figure 16: dmPGE$_2$ increases Runx1$^+$ cells in the adult kidney marrow

Zebrafish embryos were treated from 3ss-36hpf with 50uM dmPGE$_2$ or DMSO and then chemical was removed. Fish were grown up to adulthood and kidney marrow was dissected and FACS-analyzed for Runx1$^+$:GFP cells.

Short-term exposure of PGE$_2$ enhances long-term repopulation of the HSPC pool

Our initial data from zebrafish and previous work by others in the murine system demonstrated that a short pulse of dmPGE$_2$ leads to long-term effects on HSPCs[43,46,108]. We confirmed this in the mouse using competitive transplantation assays. Primary competitive transplants were performed using freshly isolated CD45.1 cells treated with dmPGE$_2$ or DMSO. Treated cells were competed against fresh CD45.2 competitor marrow. FACS analysis on peripheral blood (PB) demonstrated robust chimerism in mice that received dmPGE$_2$-treated cells compared to mice receiving cells treated with

DMSO. Recipients in the $dmPGE_2$ group at 1-year post transplant maintain increased PB chimerism without lineage skewing (Figure 17). To test the robustness of treatment with $dmPGE_2$ on repopulation capability, we performed competitive secondary transplants. WBM from primary recipient mice in each group was harvested at 1-year post transplant and FACS-sorted to isolate CD45.1 positive cells. These cells were transplanted in the presence of fresh CD45.2 competitor cells without additional $dmPGE_2$ or DMSO treatment. PB chimerism analysis at 24 weeks post transplant indicates that $dmPGE_2$-treated cells were still able to out-compete control cells in secondary transplantation assays without disrupting differentiation status (Figure 18).

Collectively, our results demonstrate that just a brief (2-hour) *ex vivo* exposure of WBM cells to $dmPGE_2$ confers long-term repopulation advantage that is maintained through multiple rounds of transplantation. We next wanted to examine if $dmPGE_2$ treatment months prior to transplantation would enhance the repopulation capacity of HSPCs. Since this type of experiment would be technically challenging in mice, we utilized the zebrafish to treat embryos during HSPC specification. We tested the ability of pulse treatment with $dmPGE_2$ during zebrafish embryogenesis to confer a transplantation advantage on adult WKM cells. *β-actin*:GFP embryos were treated with $dmPGE_2$ or DMSO. Following this treatment, the chemical was washed off and fish were left to grow to adulthood. After 3 months, WKM was harvested and prepared for transplantation into irradiated recipient fish. 20,000 WKM cells from each treated fish were competitively transplanted against 80,000 cells from untreated *RedGlo* fish into *casper* recipients (Figure 19a).

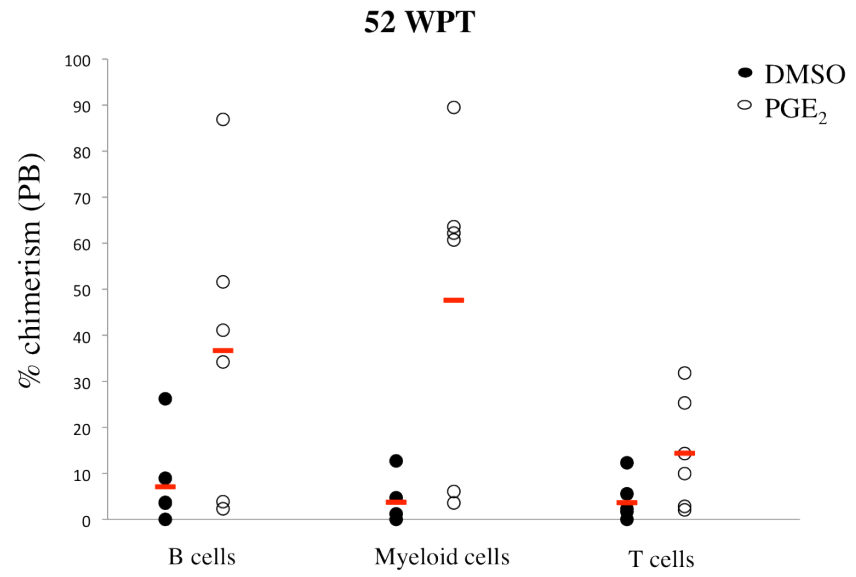

Figure 17: dmPGE$_2$ increases long-term repopulation in primary recipients

Analysis of PB chimerism was performed 1-year post transplantation in mice that received DMSO-treated cells (filled circles) or dmPGE$_2$-treated cells (open circles). Multilineage reconstitution was determined by assessing B cells, myeloid cells, and T cells. Each circle represents an individual recipient.

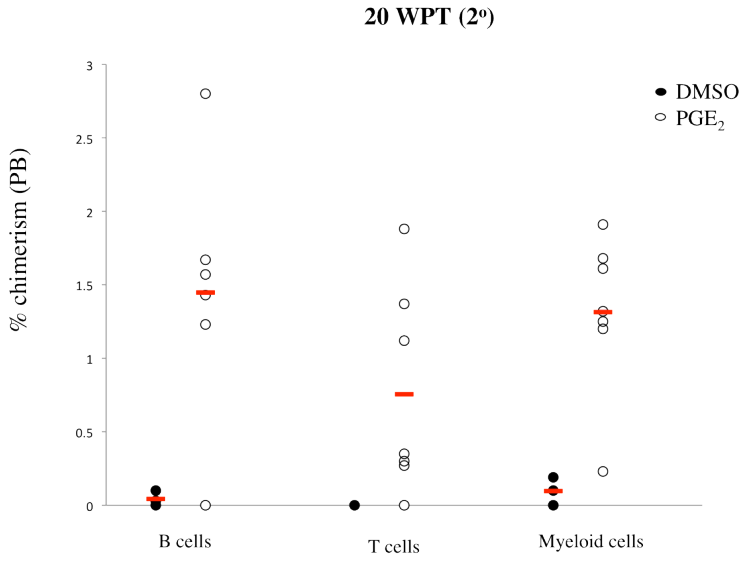

Figure 18: dmPGE$_2$ increases long-term repopulation in secondary recipients

Analysis of PB chimerism was performed 20 weeks post secondary transplantation in mice that received DMSO-treated cells (filled circles) or dmPGE$_2$-treated cells (open circles). Multilineage reconstitution was determined by assessing B cells, myeloid cells, and T cells. Each circle represents an individual recipient.

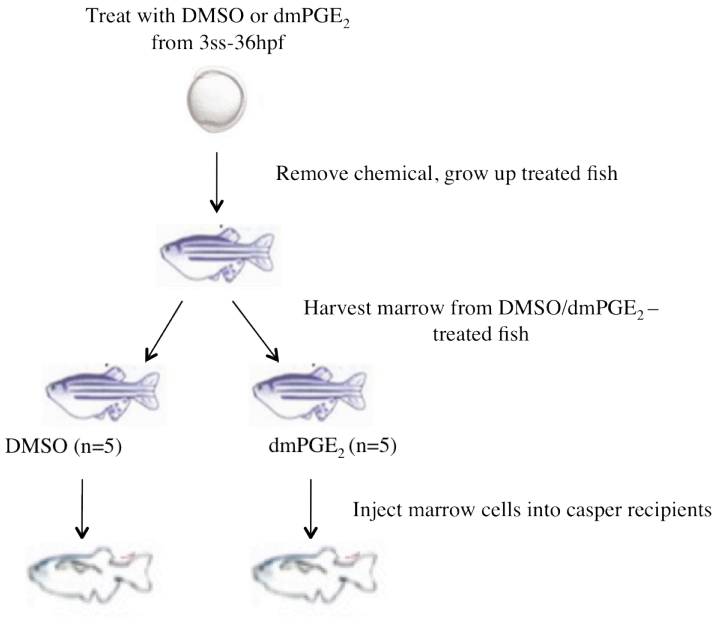

Figure 19a: Schematic of adult WKM transplant

Zebrafish embryos were treated with DMSO or $dmPGE_2$ from 3ss-36hpf. Chemical was removed and fish were grown to adulthood. Marrow from treated fish was transplanted into *casper* recipients.

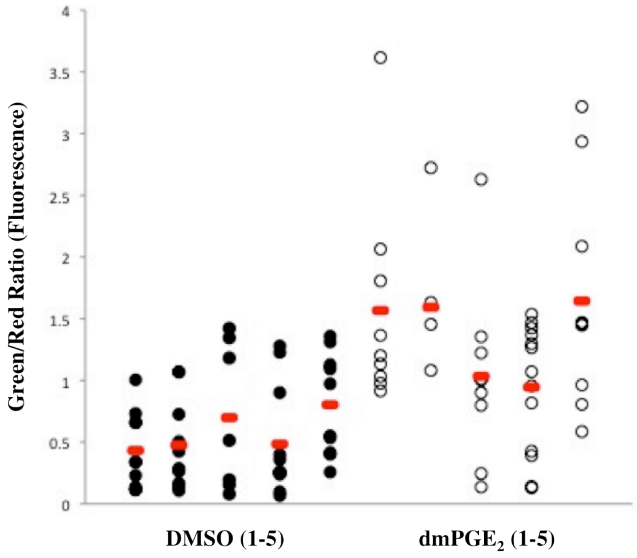

Figure 19b: $dmPGE_2$ treatment during embryogenesis enhances adult transplantation

Each column represents recipients that received marrow from a single donor fish previously treated with DMSO (filled circles) or $dmPGE_2$ (open circles). Each dot represents an individual recipient fish. The Y axis represents the ratio of green (treated) cells versus red (competitor) cells in recipient kidney marrow.

Four months following transplantation, recipient fish were imaged using a fluorescent microscope and the ratio of green to red cells (treated: untreated) in each kidney analyzed using ImageJ software. We observed that transient treatment with $dmPGE_2$ during embryogenesis resulted in increased transplantation potential in adults (Figure 19b). We next tested this transplantation assay using *runx1*:GFP fish to examine at the effect of $dmPGE_2$ on HSPCs specifically. Interestingly, when equal numbers of $runx1^+$ cells were competitively transplanted into recipient fish, the advantage of $dmPGE_2$ treatment was lost. This suggests that *in vivo* treatment of zebrafish with $dmPGE_2$ results in a long-term repopulation advantage due to an increase in the $runx1^+$ pool, rather than a change in inherent cell competitiveness. These results are consistent with murine transplantation experiments in which equal numbers of LSK SLAM cells from primary recipients mice did not demonstrate an advantage of $dmPGE_2$ treatment in secondary transplants.

PGE_2 preferentially affects ST-HSCs

Previous transplantation studies using $dmPGE_2$ have been performed on fairly heterogeneous cells populations, including $runx1^+$ cells in zebrafish, WBM or LSK cells in mice, and $CD34^+$ human cells. To differentiate the effects of $dmPGE_2$ treatment on the repopulation potential of individual stem and progenitor cell populations, we performed competitive transplants using sorted mouse marrow. WBM was FACS-sorted into three populations that we will refer to as MPPs ($LSKCD150^-CD34^+$), ST-HSCs ($LSKCD150^+CD34^+$), and LT-HSCs ($LSKCD150^+CD34^-$). Cells were treated with $dmPGE_2$ or DMSO and transplanted in various doses against competitor cells (outlined in Figure 20). Interestingly, sorted LT-HSCs or MPPs treated with $dmPGE_2$ lost their

competitive advantage in transplantation assays. However, ST HSCs treated with $dmPGE_2$ displayed increased PB chimerism in recipients that was stable 1-year post transplantation (Figure 21). In addition, when we further purify this population by selecting against CD48, the effect of $dmPGE_2$ on repopulation is enhanced (Figure 22). Together, these data suggest that the long-term transplantation effects of $dmPGE_2$ are mediated through the ST-HSC compartment.

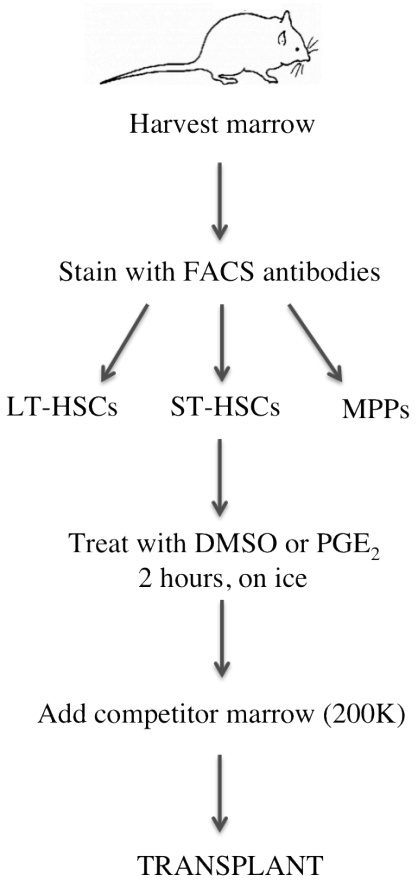

Figure 20: Schematic of HSPC-sorted population transplants

Whole bone marrow is harvested from donor mice and stained with FACS antibodies. Cells are sorted into LT-HSCs, ST-HSCs, or MPPs. Cells are treated ex vivo with DMSO or $dmPGE_2$ before transplantation along with competitor marrow.

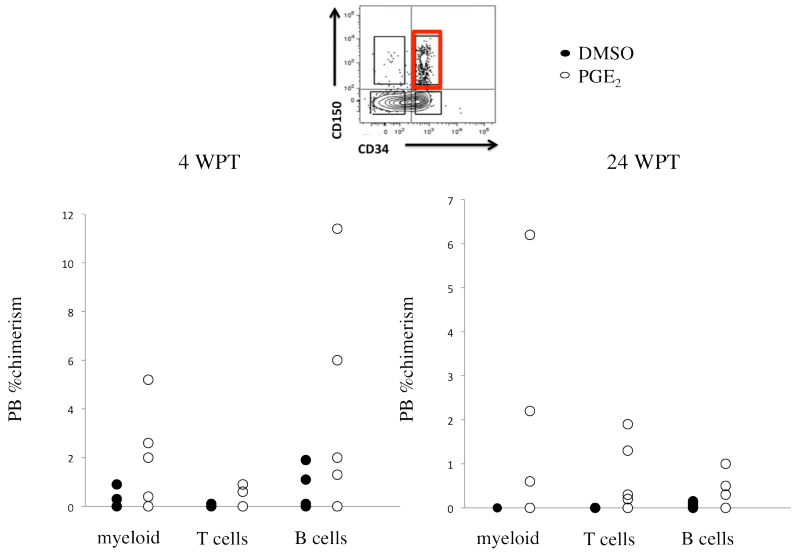

Figure 21: dmPGE$_2$ treatment enhances long-term repopulation of ST-HSCs

LSK cells were further purified for ST-HSCs using CD150 and CD34 (red box). Analysis of PB chimerism was performed at 4 weeks (left graph) and 24 weeks (right graph) post transplantation in mice that received DMSO-treated ST-HSCs (filled circles) or dmPGE$_2$-treated ST-HSCs (open circles). Multilineage reconstitution was determined by assessing B cells, myeloid cells, and T cells. Each circle represents an individual recipient.

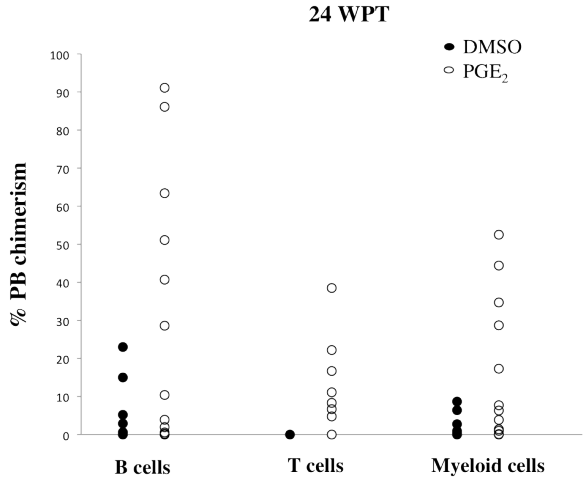

Figure 22: The effect of dmPGE$_2$ is enhanced in a subset of ST-HSCs

ST-HSCs were further purified by negative selection of CD48 (LSKCD48$^-$CD34$^+$CD150$^+$). Analysis of PB chimerism was performed at 24 weeks post transplantation in mice that received DMSO-treated ST-HSCs (filled circles) or dmPGE$_2$-treated ST-HSCs (open circles). Multilineage reconstitution was determined by assessing B cells, myeloid cells, and T cells. Each circle represents an individual recipient.

PGE_2 may protect cycling cells from exhausting

ST-HSCs are functionally distinguished from LT-HSCs by their transient ability to repopulate all lineages of the blood. This behavior reflects a key distinction in cycling status between LT-HSCs and ST-HSCs; it is thought that quiescence prevents depletion of LT-HSCs, thereby preserving long-term repopulation activity. $dmPGE_2$ treatment has been shown to increase the percentage of cycling cells *in vitro* in all HSC populations, but the use of varying culture conditions and reporters of cell cycle status could be confounding factors. It is unclear how PGE_2 affects cell cycle kinetics *in vivo,* or whether it preferentially acts on cells that are proliferating or quiescent. Given that $dmPGE_2$-treated ST-HSCs rapidly proliferate and give rise to long-term multilineage reconstitution in competitive repopulation assays, we wondered if PGE_2 protects these cells from exhaustion. To test the effect of $dmPGE_2$ on cycling cells, we performed transplants using mice treated with 5-fluorouracil (5-FU) as donors. Donor mice were injected with PBS or 5-FU such that HSCs will be forced into cycle[112]. WBM cells were harvested and treated with DMSO or $dmPGE_2$ before being transplanted with competitor marrow into recipients (Figure 23). Consistent with previous results, mice that received cells from 5-FU-treated donors displayed decreased chimerism compared to PBS controls at 4 weeks post transplant[114] (Figure 24). Cells treated with $dmPGE_2$ performed better in both experimental groups. Interestingly, by 12 weeks post transplant, recipient mice in the 5-FU/$dmPGE_2$ group had chimerism levels greater than PBS controls (Figure 24). These data suggest that cycling HSCs treated with $dmPGE_2$ are able to contribute to hematopoiesis for at least 3 months following transplantation, long after control cells have depleted.

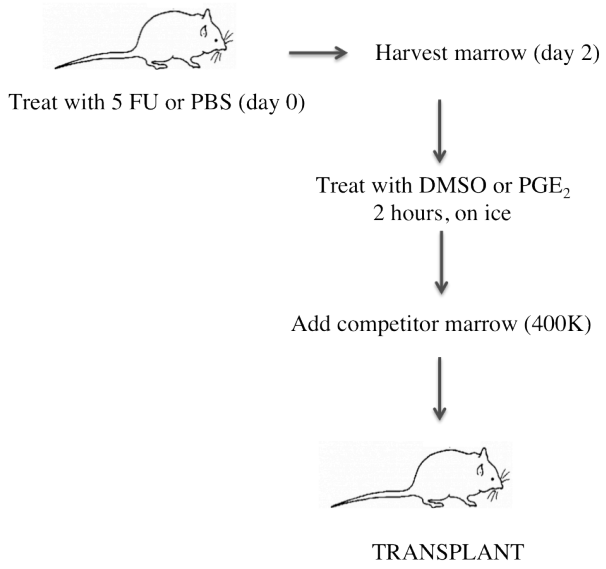

Figure 23: Schematic of 5-FU-treated donor transplants

Whole bone marrow is harvested from donor mice that were treated with either 5-FU or PBS 2 days before transplant. Cells are treated ex vivo with DMSO or $dmPGE_2$ before transplantation along with competitor marrow.

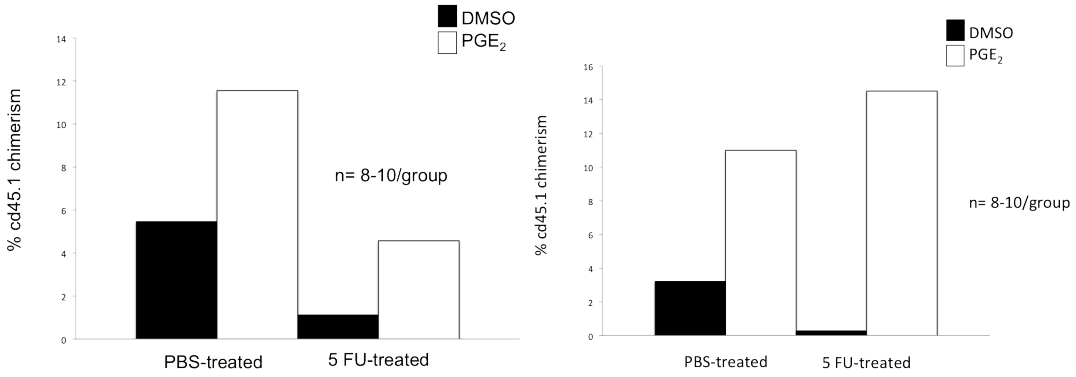

Figure 24: dmPGE2 enhances repopulation following 5-FU treatment

Total donor marrow chimerism was analyzed in recipients of mice 4 weeks (left graph) and 12 weeks (right graph) post transplant. Donor cells were treated with DMSO (filled bars) or $dmPGE_2$ (open bars). The x axis illustrates if donor mice were treated with PBS or 5-FU prior to transplant.

PGE_2 induces a quiescent gene signature in human $CD34^+$ cells

Microarray analysis of human UCB $CD34^+$ cells treated with $dmPGE_2$ revealed differentially regulated genes that play a role in cell surface receptor signal transduction, cell proliferation and migration[49]. This gene signature was confirmed using RNA sequencing on $CD34^+$ cells (V. Binder, unpublished data). PGE_2 robustly activates cAMP signaling in $CD34^+$ cells through EP2 and EP4 receptors. We therefore performed ChIP-sequence analysis for activated *cAMP response element-binding* protein (pCREB) in human $CD34^+$ cells. CREB is a transcription factor that binds cAMP response elements (CRE) on DNA. Using gene set enrichment analysis (GSEA), we compared genes that are up-regulated by PGE_2 and bound by pCREB to published gene lists known to be involved in quiescence. Human $CD34^+$ cells were mobilized and FACS-sorted for microarray analysis of quiescent and cycling cells[115]. We found a strong correlation between the genes that are up-regulated in quiescent cells and genes that are up-regulated by $dmPGE_2$ treatment (Figure 25). In addition, close to half of the up-regulated genes in quiescent $CD34^+$ cells are bound by pCREB after $dmPGE_2$ treatment. A recent study in mice identified a set of genes that is down regulated in HSCs after just one cell division, which correlates with diminished repopulation potential[116]. GSEA shows genes that are specifically down following cell division are up-regulated when treated with PGE_2 (Figure 25).

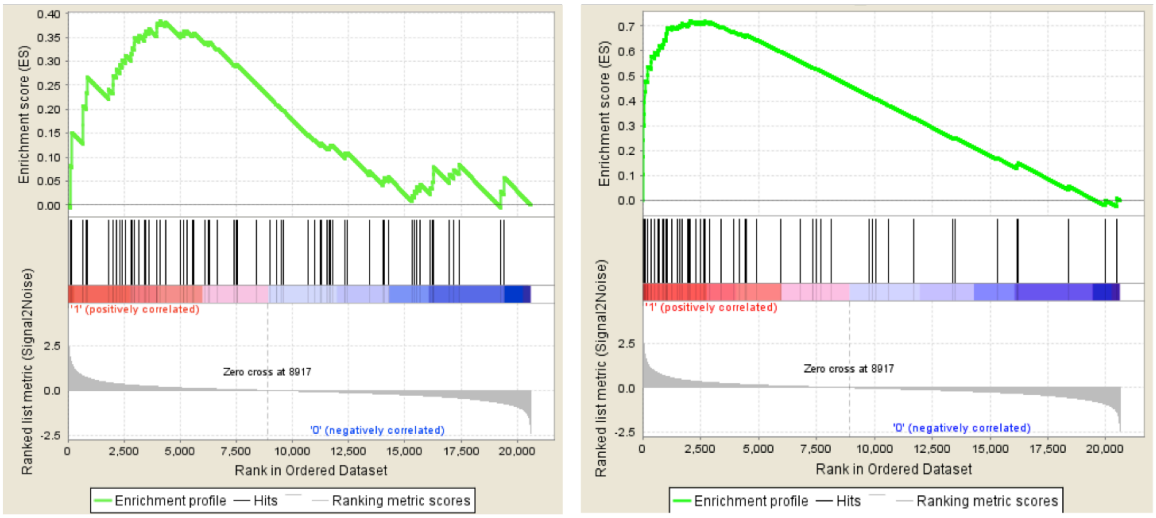

Figure 25: GSEA shows significant enrichment of quiescent gene expression by dmPGE$_2$

Enrichment plots for mouse (left) and human (right) gene sets that have been previously associated with HSPC quiescence. FDR and p-value are all <0.05 and Normalized Enrichment Score (NES) = 1.4 (left) and 2.6 (right). ChIP-seq analysis shows that 33% (left) and 46% (right) of the genes in the leading edge are bound by pCREB in the presence of dmPGE$_2$.

Discussion

Our studies demonstrate that pulse exposure of $dmPGE_2$ enhances long-term repopulation of HSPCs. Using a *runx1*:GFP zebrafish transgenic line, we have shown that treatment with $dmPGE_2$ during development increases the number of embryonic HSPCs; an effect that is maintained through adulthood. This HSPC pool has improved engraftment and reconstitution in competitive transplantation assays, suggesting $dmPGE_2$ increases functional HSPCs. However, this advantage is most likely attributed to an overall increase in cell number, rather than cell intrinsic memory from a signal. In contrast, mouse studies indicate that PGE_2 preferentially enhances the function of ST-HSCs, without affecting cell number. PGE_2 may induce a quiescent gene signature in this population that is normally found in more potent LT-HSCs.

Variations in experimental systems could account for the different effects of $dmPGE_2$ treatment on HSPCs. Zebrafish whole embryos are treated *in vivo* for a 24-hour developmental window, during which HSCs are being specified. In contrast, adult mouse marrow cells are treated *ex vivo* for 2 hours. Our methods of identifying HSPCs in zebrafish and mouse also differ greatly. Currently in the zebrafish, the runx1:GFP transgenic line is the most specific tool for isolating HSCs; however this population of cells most closely resembles that of LSK in the mouse. It is possible that PGE_2 does preferentially affect a subset of $runx1^+$ HSPCs that resembles the ST-HSC pool in mice, however we cannot distinguish this population with our current system.

There is a distinction between *ex vivo* and *in vivo* treatment of $dmPGE_2$ in mice. Prolonged *in vivo* exposure to $dmPGE_2$ leads to increased proliferation and repopulation capacity of ST-HSCs/MPPs, followed by subsequent exhaustion and loss of

differentiation potential. Continuous exposure to $dmPGE_2$ may induce multiple rounds of excessive proliferation from which cells cannot recover. Patients with mutations in the prostaglandin transporter gene, *SLCO2A1*, have elevated levels of circulating PGE_2, which eventually leads to pancytopenia with bone marrow hypocellularity[117]. In addition, EP receptors have been shown to internalize upon constant stimulation, which would alter the response to PGE_2. In contrast, ST-HSCs treated *ex vivo* with a brief pulse of $dmPGE_2$ exhibit enhanced, long-term repopulation and do not deplete up to 1-year post transplant. These results have important clinical implications, as the latter treatment protocol is more amenable for human transplantation studies.

Transplant recipients are at high risk for infection until they have a fully reconstituted hematopoietic system. PGE_2 improves the homing and repopulation capacity of UCB donor cells, making it a valuable clinical resource. ST-HSCs/MPPs that are proliferative and actively cycling are the first cells to contribute to hematopoiesis following transplantation and are therefore critical for the initial recovery of myeloablated patients. Clonal analysis suggests that contribution from this progenitor-like pool is transient; once these cells exhaust, LT-HSCs provide long-term reconstitution (J. Sun, unpublished). PGE_2 has a protective effect on cycling cells, specifically ST-HSCs, which may delay or prevent exhaustion and enable long-term contribution. Our studies show that PGE_2 treatment improves transplantation by conferring the advantages of ST-HSCs and LT-HSCs—rapid contribution to hematopoiesis and long-term reconstitution—on ST-HSCs alone.

GSEA demonstrates that genes which are up-regulated by PGE_2 are enriched for genes associated with HSPC quiescence in human and mice. In addition, many of these

genes are targets of CREB, and are bound by pCREB following $dmPGE_2$ treatment. Interestingly, about 60% of pCREB- bound sequences contain Runx1 binding motifs. We also observed that Runx1 target genes appear to be enriched in PGE_2- up regulated gene lists. Runx1 plays a critical role in adult hematopoiesis[44] and is required for HSC specification during embryogenesis[43]. Although not required for adult HSC self-renewal, Runx1-deficient HSCs display dysregulated cell cycle and cell survival pathways[118]. It will be interesting to compare the overlap of pCREB target genes with those of other transcription factors regulating HSC self-renewal and function. PGE_2 may prevent exhaustion of cycling cells that are contributing to hematopoiesis by inducing a quiescent gene signature.

Clonal tracking of HSCs in mice and non-human primates demonstrates that short-term clones repopulate the majority of mature blood immediately following transplantation[119]. After time, these short-term clones exhaust and are replaced by long-term clones that provide multi-lineage reconstitution for the duration of the organism's life. We hypothesize that treatment with $dmPGE_2$ extends the period of time post-transplantation that short-term clones can effectively contribute to the blood pool. A model to explain the enhanced transplantation potential of cells treated with dmPGE2 is summarized in figure 26. The improved repopulation effect of $dmPGE_2$ on short-term HSCs may be enhanced by the additional support of long-term clones, however this has yet to be tested. Treatment of human cord blood cells with $dmPGE_2$ induces a gene signature that is enriched in quiescent cells, presumably through activation of intracellular cAMP and associated transcription factors such as CREB and CREM. Induction of genes that are important for quiescence may support the maintenance of

short-term clones post-transplantation by improving engraftment potential, or preventing exhaustion of contributing cells. Additional experimentation should identify the specific genes required for this effect.

Identifying a population of human cord blood cells that is specifically affected by $dmPGE_2$ treatment will have important clinical implications. Improving expansion protocols prior to transplantation may decrease the number of required units and increase the availability of donor cords. In addition, further characterization of the specific genes induced by $dmPGE_2$ treatment may give us additional insights into fundamental mechanisms regulating HSC self-renewal and function.

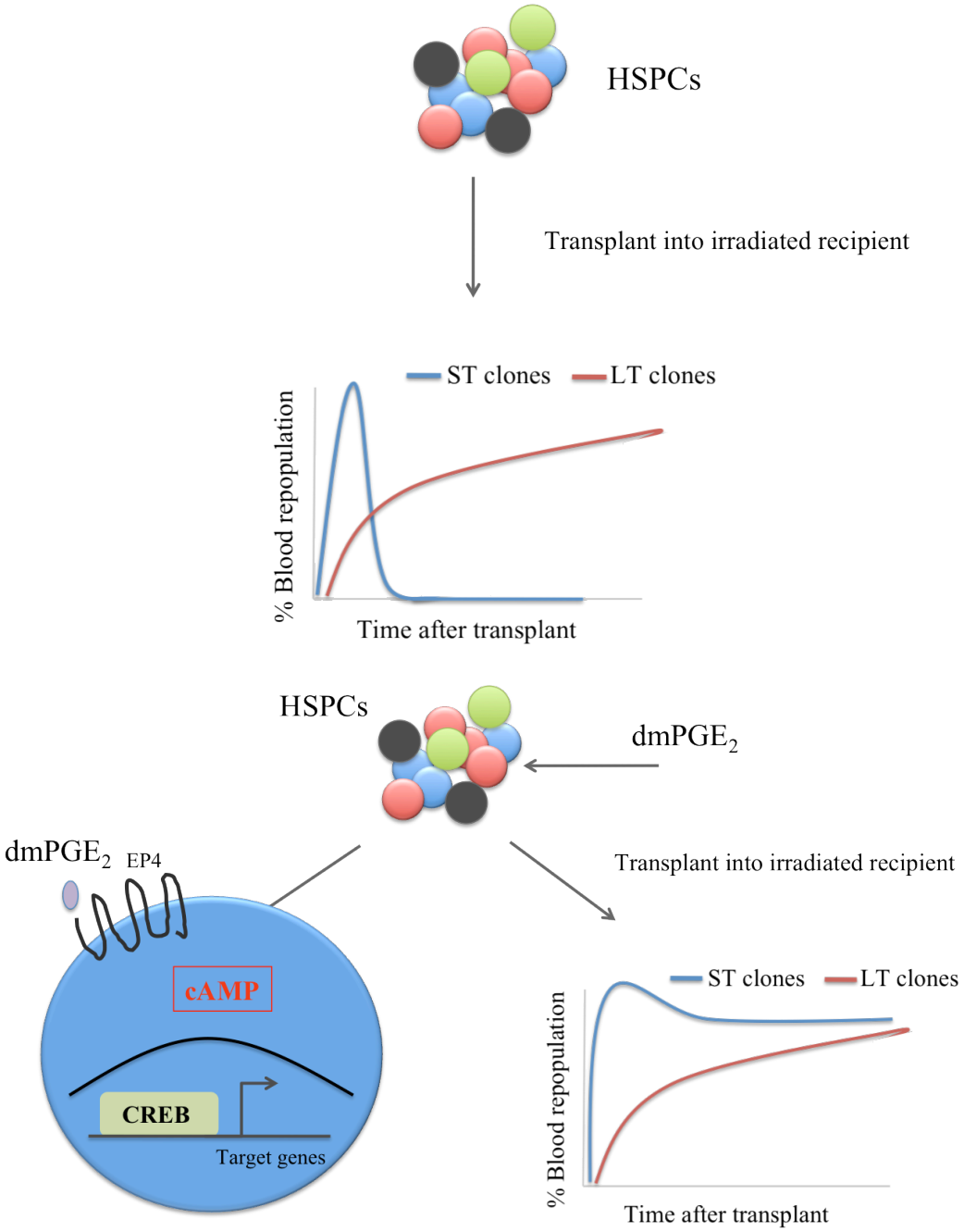

Figure 26: Summary model of dmPGE$_2$ effect on HSC repopulation

The top panel represents a normal transplantation setting after HSPCs are transplanted into irradiated recipients. Initially, short-term clones give rise to all mature blood cells in the peripheral blood. Once these clones exhaust, long-term clones take over and reconstitute the hematopoietic system. The bottom panel shows that when HSPCs are treated with dmPGE$_2$, short-term clones give rise to multilineage reconstitution for an extended time post-transplantation. This effect is potentially due to an induction of genes associated with quiescence in these ST cells.

Chapter 4

Concluding discussion and future directions

Concluding Discussion:

Generation of a specific HSPC transgenic zebrafish line

We have developed a novel HSPC-specific transgenic zebrafish using a regulatory element that is +23 kb downstream of the ATG in the first promoter of mouse *Runx1* to drive expression of a reporter[79]. Time-lapse live imaging showed that Runx1$^+$ cells emerge from the hemogenic endothelium of the dorsal aorta, enter circulation, and seed the CHT, where definitive hematopoiesis first occurs. FACS analysis and cytospins confirmed that these cells are spherical with a high nucleus to cytoplasmic ratio, which is consistent with the morphology of murine HSCs. We developed an embryonic transplantation assay to calculate the frequency of HSCs in Runx1:GFP embryos. Embryonic limit dilution analysis estimated the stem cell frequency of the Runx1$^+$ population in the 3 dpf embryo to be approximately 1/2.88 cells. A number of studies have shown that hematopoietic stem cells isolated from different tissues of the mouse embryo have the capacity to reconstitute hematopoiesis in the adult[84,90,91]. However, technical limitations in mouse have made it difficult to assess the stem cell potential of an HSPC transplanted from one embryo to another. Our studies are the first to document the functional capacity of embryonic HSPCs in an embryo transplant.

FACS analysis of adult kidney marrow confirmed that Runx1$^+$ cells go on to seed the adult niche. These cells give rise to long-term multilineage reconstitution when transplanted into irradiated recipients. This is consistent with studies in mice that demonstrate Runx1$^+$ fetal liver cells successfully transplant into adult mice. Through adult limit dilution analysis of Runx1$^+$ cells, we calculated a stem cell frequency of approximately 1/35. This is most likely an underestimate as zebrafish donors and

recipients are non-isogenic and are therefore not immune matched, which leads to immune rejection of some donor cells. Currently there are no antibodies available in zebrafish to further purify this population, or to distinguish between a stem cell and a progenitor. Our results demonstrate that the HSPC pool in zebrafish can be sorted with a single transgenic marker to a purity that is within the range of the well-characterized LSK ($Lin^-Sca1^+cKit^+$) population in mouse[89]. Our characterization of the *Runx1* transgenic line, including a novel embryo transplantation assay and limiting dilution transplantation in adults, demonstrates that $Runx1^+$ cells mark a highly purified HSPC population with functional stem cell characteristics.

Live imaging reveals a novel endothelial cell behavior during stem cell colonization

We performed time-lapse live imaging of *Runx1*:GFP embryos and directly observed distinct steps of HSPC engraftment, including a novel cellular behavior of remodeling endothelial cells. Upon entering circulation from the dorsal aorta, $Runx1^+$ cells adhered to endothelial vessel walls in the CHT and underwent rapid extravasation to the abluminal side of the endothelial wall. Once an HSPC lodged in the CHT, a small group of endothelial cells remodeled around the stem cell to form a closely associated niche. This niche formation event was typically completed in 30-60 minutes and was marked by a single HSPC surrounded by a group of 5-6 endothelial cells. Through live imaging, we found that endothelial cell niche remodeling is conserved in fetal liver explants. *Ly6a*-GFP^+/c-kit^+ HSPCs underwent discrete steps towards lodgement: adherence, extravasation, abluminal migration, and endothelial niche remodeling.

3D reconstruction of high-resolution serial section electron microscopy scans

confirmed that HSPCs lodged in the CHT are surrounded by 5-6 endothelial cells. There are also stromal cells in proximity to the HSPC, which is consistent with our confocal microscopy of Runx1^{+} HSPC and cxcl12a^{+} stromal transgenic lines. Cell types not observed by confocal microscopy, including a fibroblastic mesenchymal cell with melanophore inclusions, were found together with the HSPC, endothelial cells and stromal cells. Melanophore inclusions are indicative of neural crest origin, and such cells have been found in the adult marrow[71,120,121]. HSPC-endothelial cell niches were heterogeneous, but the formation of niches was specific to more primitive HSCs. Our high-resolution reconstruction of a zebrafish HSPC niche recapitulates many features of the perivascular niche in mice, which contains a diverse set of cell types including mesenchymal stem and progenitor cells, endothelial cells, and nerves. An advantage of our system is the ability to observe dynamic interactions of these cell types *in vivo*.

After remodeling of endothelial cells, HSPCs made one of three cell fate decisions: it remained quiescent, underwent symmetrical division, or it divided asymmetrically where one daughter cell exited the endothelial niche. Similarly, we observed in fetal liver explants that Ly6a-GFP+/c-kit+ HSPCs underwent cell divisions where the daughter cell proximal to the sinusoid remained surrounded by endothelial cells, while the daughter cell distal to the sinusoid migrated away into the abluminal space. Zebrafish CHT endothelial cells do not directly differentiate into budding HSPCs, as is seen in the hemogenic endothelium of the dorsal aorta. This is consistent with the model that the CHT is equivalent to fetal liver and is not a site of de novo stem cell production[122] but instead must be seeded by HSPC arriving through circulation[123]. Our

studies provide dynamic observations of HSPC niche interactions during development that reveal a novel endothelial cell remodeling.

Chemical genetics reveals small molecule regulators of CHT niche colonization

Treatment of zebrafish embryos with AMD3100 reduced the number of HSPCs in the CHT. This is consistent with the role of CXCR4-CXCL12 signaling during adult homing and engraftment and served as a proof-of-principle for the screen. A chemical screen identified 147 compounds that regulate CHT hematopoiesis. We combined selected chemical hits together with our live imaging assay to associate specific signals with the distinct engraftment steps we previously described. One screen hit, a selective inhibitor of TGF-β type I receptors, SB-431542, increased CHT hematopoiesis via increased frequency of HSPC cell divisions. HSPCs arrived normally in the CHT and adhered to the vessel wall, but before each cell engrafted, they underwent excessive rounds of division. These data illustrate that inhibition of TGF-β receptor signaling expands the HSPC population by causing extra cell divisions. This is consistent with previous studies for the role of TGF-β in quiescence that show knock down of *TGF-β* in mice results in excessive HSC proliferation[95].

Another hit from the screen DMOG, which stabilizes HIF-1α under normoxic conditions[124], increased the number of runx1^{+} cells in the CHT by altering HSPC localization. HSPCs in DMOG-treated embryos extended protrusions into the abluminal space and preferentially migrated to those regions. The HIF-1α inhibitor YC-1 also increased HSPCs in the CHT, but these cells were retained in the vessel lumen. Our data suggest HIF-1α stability and a hypoxic state promotes HSPC migration into abluminal

spaces within the niche. HIF-1α is expressed in the zebrafish CHT (Rojas et al., 2007). Consistent with our results, HIF-1α is an important HSPC maintenance factor in mammals. HIF-1α-deficient HSCs exhibit excessive proliferation, and overstabilization of HIF-1α reduces the transplantation potential of HSCs[125].

We identified lycorine, a natural alkaloid extracted from the Amaryllidaceae plant family, as a novel regulator of hematopoiesis. Treatment with lycorine increased CHT hematopoiesis by retaining HSPCs in the niche. Time-lapse imaging confirmed that lycorine treatment increased the number of HSPCs that resided in endothelial cell niches, as well as the total duration each HSPC spent in the CHT. The increased number of HSPCs observed in the CHT is maintained after treatment. Together, these results demonstrate that lycorine treatment modulates the number of endothelial niches that are triggered upon HSPC arrival in the CHT, and also the time that HSPC stay within these niches.

Several chemicals that regulate the sphingosine-1-phosphate (S1P) pathway induced alterations in the migration pattern of HSPCs. Consistent with our results, S1P is an important signal in adult HSPC and lymphocyte trafficking[126]. Embryos injected with *s1pr1* morpholino had reduced numbers of HSPCs in the CHT. S1PR1-deficient HSPCs were unable to extravasate into the CHT after adherence to the endothelial wall. These experiments support a cell autonomous role for s1pr1 in HSPC extravasation during colonization of the CHT. We and others[106,107] have demonstrated that combination of S1P agonists and CXCR4 antagonists facilitates HSC mobilization from the niche in a G-CSF-independent manner. These results suggest that the current standard of G-CSF mobilization in patients could be improved by manipulation of the

S1P/CXCR4 signaling axis. Our chemical screen demonstrates the ability to modulate HSPC- endothelial cell interactions, at several key steps, and will likely have an important impact on clinical stem cell transplantation.

Short-term exposure of PGE_2 enhances long-term repopulation of the HSPC pool

A similar chemical screen identified PGE_2 as a regulator of HSPCs in the AGM. Zebrafish embryos treated with $dmPGE_2$ during embryogenesis displayed an increase of $Runx1^+$ cells in the AGM, CHT, and adult kidney marrow, without additional treatment. Whole kidney marrow from treated fish demonstrated improved repopulation compared to control cells in competitive transplantation assays. However, $Runx1^+$ cells did not demonstrate an advantage during transplantation on a cell-by-cell basis. These results are consistent with murine transplantation experiments in which equal numbers of LSK SLAM cells from primary recipients mice did not demonstrate an advantage of $dmPGE_2$ treatment in secondary transplants[108]. Our data suggest that zebrafish treated *in vivo* with $dmPGE_2$ results in a long-term repopulation advantage due to an increase in the $Runx1^+$ pool, rather than a change in inherent cell competitiveness. Mouse marrow cells treated *ex vivo* with a short pulse of $dmPGE_2$ displayed improved repopulation capabilities compared to control cells in primary transplants. Increased peripheral blood chimerism levels were maintained in recipients up to 1-year post transplant. Treated cells continued to demonstrate a transplantation advantage in secondary recipients without additional $dmPGE_2$ treatment. This is consistent with previous transplantation studies that show a single pulse with $dmPGE_2$ improves the repopulation capacity of HSPCs through quinary transplants[46,108]. Collectively, our results demonstrate that just a brief (2-hour) *ex vivo*

exposure of WBM cells to $dmPGE_2$ confers long-term repopulation advantage that is maintained through multiple rounds of transplantation, however this is not due to improvement in inherent cell function of LT-HSCs.

PGE_2 preferentially affects ST-HSCs and prevents exhaustion of cycling cells

We found that treatment with $dmPGE_2$ enhanced long-term repopulation by modulating a population of ST-HSCs that are phenotypically $LSKCD34^+CD150^+$. FACS-sorted ST-HSCs treated with $dmPGE_2$ displayed improved reconstitution in recipients that was stable 1-year post transplantation, and was maintained through secondary transplantation. This advantage was specific to the ST-HSC compartment; there was no improvement in repopulation of $dmPGE_2$-treated LT-HSCs or MPPs. The effect of $dmPGE_2$ on the repopulation capacity of ST-HSCs was significantly enhanced following negative selection of CD48 expression. $CD48^+$ cells account for close to 30% of $LSKCD34^+CD150^+$ cells. This illustrates the heterogeneity of purified HSPCs and suggests that PGE_2 affects a small subset of the ST-HSC population.

A study by the Calvi lab demonstrated that mice continuously treated *in vivo* with $dmPGE_2$ displayed specific expansion of the ST-HSC/MPP pool[47]. Sorted ST-HSCs/MPPs from treated mice quickly lost repopulation potential following transplantation, suggesting these cells exhausted. It has been previously described that $LSKCD34^+$ cells have only transient multilineage potential that is lost by ~12 weeks-post transplant[27]. In contrast, we demonstrate that *ex vivo* pulse treatment with $dmPGE_2$ confers long-term repopulation capabilities on ST-HSCs that are maintained through serial transplantation.

We performed transplants with mice treated with 5-FU as donors to test the effect of $dmPGE_2$ on cycling cells. Previous work showed that $dmPGE_2$ treatment increased the percentage of cycling cells *in vitro* in all HSC populations[46]. It is not known how PGE_2 affects cell cycle kinetics *in vivo*, or whether it preferentially acts on cells that are proliferating or quiescent. Cells treated with $dmPGE_2$ performed better in both experimental groups (5-FU or PBS). Mice that received cells from 5-FU-treated donors displayed decreased chimerism levels, irrespective of treatment group, compared to PBS controls at 4 weeks-post transplant. This is consistent with previous studies that demonstrate the impaired repopulation potential of 5-FU-treated cells[114]. Recipient mice in the 5-FU/$dmPGE_2$ group showed higher chimerism levels than PBS controls at 12 weeks-post transplant. These data suggest that cycling HSCs treated with $dmPGE_2$ robustly contribute to hematopoiesis for at least 3 months following transplantation, long after control cells have depleted. Collectively, our data suggest that *ex vivo* pulse treatment with $dmPGE_2$ prevents exhaustion of ST-HSCs and facilitates long-term reconstitution following transplant.

PGE_2 induces a quiescent gene signature in human $CD34^+$cells

We found a strong correlation between genes that are up-regulated in quiescent HSCs and genes that are up-regulated by $dmPGE_2$ in human $CD34^+$ cells. RNA sequencing of human $CD34^+$ cells treated with $dmPGE_2$ revealed an induction of genes involved in cell surface receptor signal transduction (FOS, PTGER4, S1PR1), cell proliferation (TGFB2, PTGS2), and migration (CXCR4, S1PR1). We find a high degree of overlap with published microarray gene lists of $dmPGE_2$-treated human $CD34^+$ cells.

PGE_2 robustly activates cAMP signaling in $CD34^+$ cells through EP2 and EP4 receptors[48]. We identified a subset of genes that are bound by activated cAMP response element-binding protein (pCREB) following $dmPGE_2$ treatment in human $CD34^+$ cells. GSEA demonstrated a strong correlation between previously defined genes that are up-regulated in quiescent cells, and genes that are differentially expressed and bound by pCREB following $dmPGE_2$ treatment.

A recent study developed a novel label retention Tet-off system in mice to monitor the cell division history of HSPCs[116]. In their system, HSPCs take up H2B:GFP until Dox is administered. Following Dox chase, label retention is assessed to determine the cycle history of HSPCs. HSCs that have previously undergone cell division have greatly impaired repopulation capabilities compared to cells that were previously quiescent. The authors identified a set of genes that are significantly down regulated following HSC division. GSEA demonstrated these genes are enriched in the gene signature induced by $dmPGE_2$ treatment in human $CD34^+$ cells. Our data suggest that PGE_2 induces a gene signature associated with quiescent cells that have high repopulation potential. This is a potential mechanism by which PGE_2 prevents exhaustion in cycling cells, such as the ST-HSC population.

Concluding Remarks

In this thesis, we have studied and characterized the endogenous microenvironment and trafficking of zebrafish HSPCs in the niche. We developed a novel zebrafish transgenic reporter line that enabled us to visualize and purify HSPCs. This line was used to observe a novel and essential cellular behavior that involves triggered remodeling of perivascular endothelial cells upon arrival of an HSPC in a new site of hematopoiesis. Live imaging of fetal liver explants confirmed that this endothelial remodeling effect is conserved in mammals.

Using runx1:GFP zebrafish, we observed a long-term effect of PGE_2 on hematopoiesis that is conserved in mammals; WBM cells treated with PGE_2 maintain increased chimerism levels in recipient mice over 1-year post transplantation and display enhanced transplantability in competitive secondary transplantations without additional PGE_2 treatment. We demonstrate that PGE_2 affects a population of HSPCs that was not previously thought to have long-term repopulation potential. Gene expression data and ChIP-seq analysis in human $CD34^+$ cells suggests that PGE_2 may protect cycling cells from exhaustion by inducing a quiescent gene signature in these cells.

Our studies provide a glimpse into the dynamic interactions between HSPCs and their endogenous niche. In addition, we show that a population of short-term HSCs can engraft and give rise to long-term multilineage reconstitution following $dmPGE_2$ treatment. Collectively, we have gained novel insights in the pathways involved in HSC migration, homing, and repopulation.

Future Directions

Improving HSC purification in zebrafish

We described a novel transgenic zebrafish that we could use to follow HSPCs during migration. Adult limit dilution analysis estimated a stem cell frequency of approximately 1/35. This is a dramatic enhancement of purity over previously identified markers of zebrafish HSPCs such as cmyb and CD41. However, this level of purity could most likely be improved upon, especially considering that murine HSCs can be isolated at a frequency closer to 1/2. CD41 marks two populations of zebrafish blood cells; $CD41^{hi}$ expressing cells are thrombocytes and $CD41^{lo}$ expressing cells are transplantable HSPCs[127]. In addition to HSPCs, Runx1 also marks a population of thrombocytes. This suggests CD41 as a potential secondary marker for further purifying zebrafish HSCs. HSPCs from Runx1:mCherry/CD41:GFP double transgenic fish could be sorted out to compare the transplantation efficiency of $Runx1^{+}CD41^{lo}$ and $Runx1^{+}CD41^{-}$ cells to $Runx1^{+}$ cells alone. Limit dilution analysis of each population would confirm if CD41 further purifies the stem cell frequency of the $Runx1^{+}$ HSPC pool. I would expect that a population of $Runx1^{+}/CD41^{lo}$ cells would have a higher stem cell frequency than $Runx1^{+}$ cells alone. However, it is unlikely that these two markers alone will demonstrate purity close to that of LT-HSCs in mice.

We have performed microarrays on sorted embryonic $Runx1^{+}$ HSPCs and $Flk1^{+}$ endothelial cells, which may implicate other genes that distinguish HSCs from other cell types in the embryo. We also looked at gene expression of $Runx1^{+}$ cells at different stages of development. Since we know that adult $Runx1^{+}$ cells retain HSPC function, genes that are common across all time-points will be of particular interest. HSPC-

specific genes can first be tested in co-expression studies with Runx1^{+} cells, and eventually transplantation assays. Currently there are no antibodies available in zebrafish to further purify HSPCs, or to distinguish between a stem cell and a progenitor. Improved purification of HSCs combined with the strengths of the zebrafish system would be beneficial to the field, and is especially important for our niche studies, as we may uncover unique niche dynamics that are specific to different HSPC subpopulations.

Finally, it will be interesting to identify the developmental stage at which definitive HSPCs are mature enough to repopulate adult recipients. Runx1^{+} cells could be sorted at different developmental stages and transplanted into adult recipients. This will determine whether maturation in the CHT is sufficient for HSPCs to maintain adult hematopoiesis. If HSPCs in the CHT cannot repopulate adult recipients, it is likely that further maturation is required in the kidney marrow, the next site of hematopoiesis.

Testing downstream functional consequences of niche perturbations

We identified several compounds that affect endogenous HSPCs in their interaction with the niche microenvironment. However, we do not know what subsequent functional consequences these perturbations may have on HSPCs. An important follow-up study would be to elucidate the downstream effects of altering HSPC-niche interactions. Zebrafish embryos can be treated with chemicals that we previously described to affect distinct stages of engraftment, such as: SB-431542, DMOG, lycorine, and S1P agonists. During treatment, embryos could be imaged using confocal microscopy to confirm the affected phenotype. Following CHT colonization, chemical would be washed off and fish would be grown to adulthood. HSPC migration

and colonization of the kidney marrow could be assayed using FACS analysis for Runx1$^+$ cells. In this assay, it is possible to observe the presence or absence of Runx1$^+$ cells, as well as determine the number of HSPCs. To test the functionality of these cells, Runx1$^+$ cells could be sorted out and transplanted into irradiated recipients.

I would expect that a TGF-β inhibitor, like SB-431542, might lead to increased numbers of Runx1+ cells in the kidney marrow due to excessive proliferation, but that these cells would not perform as well in a functional transplantation assay. If DMOG also affects the localization of Runx1$^+$ cells in the kidney marrow, the total number of HSPCs will be increased. Similarly, I expect that these cells will have decreased repopulation capacity since stabilization of HIF-1α in the mouse reduces transplantation potential of HSCs. Lycorine demonstrates a similar effect to PGE_2; a pulse treatment results in increased numbers of Runx1$^+$ cells long after the chemical is washed off. Based on our PGE_2 results, I would expect that lycorine-treated embryos would have higher numbers of HSPCs in kidney marrow, but would not have altered repopulation potential on a cell-by-cell basis.

It is also possible that chemical treatment during CHT colonization will not affect later stages of adult hematopoiesis. Instead, we can treat adult fish with these chemicals to determine if they directly play a role in mediating adult HSPC-niche interactions. In this experiment, we can also look at peripheral blood of treated fish. If any chemicals induce mobilization of HSPCs, we would detect Runx1$^+$ cells in circulation. The combination of time-lapse live imaging and chemical genetics in zebrafish embryos allowed us to identify novel chemicals that affect different and distinct aspects of HSPC

migration and colonization. We can now test these chemicals on endogenous adult HSPCs and their microenvironment.

Characterizing additional cell types that interact with HSPCs in the niche

Confocal microscopy of *Runx1*:GFP; *cxcl12a*:DsRed double transgenic lines demonstrated that Runx1^{+} HSCPs are in close proximity to stromal cells in the CHT. Therefore, it would be interesting to repeat live imaging studies with our previously identified chemicals using *Runx1*:GFP; *cxcl12a*:DsRed fish. In particular, chemicals that mediate the localization of HSPCs may modify the architecture of HSPC-stromal interactions. Future studies should also focus on visualizing how Runx1^{+} HSPCs interact with multiple niche cells at once. Additional transgenic lines for *Flk1*, *cxcl12a*, and *nestin* should be generated driving CFP or far red expression so that more cell types can be visualized. Chemical treatments of these embryos would give a more complete picture of HSPC niche dynamics.

We used high-resolution serial section electron microscopy (EM) scans to better reveal cellular interactions between HSPCs and the niche. As predicted from our confocal microscopy analysis, the HSPC is surrounded by at least 5 endothelial cells with stromal cells in close proximity to the HSPC. EM revealed an additional cell type that was not detected by confocal microscopy. A fibroblastic mesenchymal cell, with what appears to be melanophore inclusions, was found together with the HSPC, endothelial cells, and stromal cells. An important future experiment is to repeat EM scans on embryos that have been treated with chemical. The benefit of this experiment is two-fold: treated embryos that display the expected CHT phenotype can be pre-selected

before EM scanning, which will give high resolution detail of the perturbed endothelial cell remodeling event. Secondly, EM scans will provide a more complete picture of additional cell types in the niche that cannot be visualized using confocal microscopy. Lastly, analysis of more EM scans will determine whether this remodeling event is specific to Runx1^{+} HSPCs in the CHT. There is dynamic cellular migration and trafficking in the CHT during this stage of development. I expect that our observed endothelial remodeling event is specific to HSPCs that are lodged in the CHT, as opposed to more mature hematopoietic cells. The combination of these two microscopy tools will be a powerful assay for piecing together the endogenous microenvironment of HSPCs.

Identifying genes that are targets of PGE_2 in ST-HSCs

GSEA on data from RNA sequencing, microarray, and ChIP sequencing analysis identified a correlation between genes that are up-regulated and bound by pCREB in the presence of $dmPGE_2$, and genes that are up-regulated in quiescent cells. The majority of this data is from human CD34^{+} cells, and therefore future work should focus on discovering specific gene targets of PGE_2 in the ST-HSC population. Previous microarray experiments on sorted LT-HSCs, ST-HSCs, and MPPs treated with or without $dmPGE_2$ were inconclusive in identifying a PGE_2-induced gene signature. Microarray experiments should be repeated, with minor changes to the previous protocol. Cells were harvested, stained and sorted for different HSPC populations (LT/ST/MPP), and treated with $dmPGE_2$ or DMSO for 2 hours on ice before RNA collection. It is possible that a 2-hour treatment on ice is not conducive to observe differential gene expression. In

addition, cells may need a "rest" period between sorting and chemical treatment, as they might already be in an activated stress state.

It is possible that our population of ST-HSCs (LSKCD48$^-$CD34$^+$CD150$^+$) remains heterogeneous. If PGE_2 only affects a small subset of these cells, we might not detect expression changes on whole genome microarray. Single-cell PCR experiments could be performed using a successful protocol that was developed by the Orkin lab. This would enable us to test the heterogeneity of response of sorted cell populations to $dmPGE_2$ treatment at the single cell level. PGE_2-regulated genes identified from human CD34$^+$ cells should be tested, as well as known mouse lineage genes. Although we did not identify a $dmPGE_2$ signature specific to ST-HSCs in microarray experiments, we discovered genes that are differentially regulated between LT-HSCs, ST-HSCs, and MPPs. It will be important to test genes from this list, as we are using a unique antibody combination to most published expression analyses.

Once genes have been identified that are regulated by PGE_2 in ST-HSCs, they should be tested in functional assays. If the gene list is large, morpholino knock-downs or CRISPR in fish could serve as a mini screen to test target genes. *Runx1*:GFP zebrafish embryos would be injected with morpholino to the gene of interest, and treated with $dmPGE_2$. Runx1$^+$ cells would be assayed in the AGM of 36hpf zebrafish. If a particular gene is necessary for PGE_2-mediated increase of Runx1$^+$ cells, Runx1 expression will resemble control embryos, or might be decreased. Genes that are found to inhibit the effect of $dmPGE_2$ treatment on Runx1$^+$ cells in the fish (or the initial gene list if it is small) should be tested in mouse transplantation assays. Sorted ST-HSCs would be infected with a single shRNA designed to target the candidate gene list. Following

infection, cells would be treated with $dmPGE_2$ or DMSO and transplanted into irradiated recipients. After 24 weeks, long-term reconstitution will be assessed by PB chimerism. If a gene is specifically required for enhanced repopulation by PGE_2, those recipients will display chimerism levels similar to control cells. It is possible that certain genes may be required for normal reconstitution; knockdown of these genes would show an effect in transplant of DMSO-treated cells. These experiments will identify genes that are regulated by PGE_2 in ST-HSCs, and are required for its effect on HSC function.

Investigating epigenetic regulation of HSCs by PGE_2

The long-term transplantation effects of a brief pulse of $dmPGE_2$ could, in part, be mediated by epigenetic changes. It is possible that PGE_2 induces a stable change in epigenetic state that enables long-term repopulation by ST-HSCs. PGE_2 has been shown to affect DNA methylation patterns in the intestine and increases global DNA methylation via induction of DNMT3a in fibroblasts[128]. To test the effect of $dmPGE_2$ on DNA methylation in zebrafish, $Runx1^+$ cells from treated embryos would be sorted out at different stages following treatment. Whole-genome bisulfite sequencing could be used to identify changes in DNA methylation. Alternatively, methylation analysis could be performed solely on the previously identified gene list. It would be interesting to follow methylation patterns at different times post-treatment. $Runx1^+$ cells would most likely acquire changes in DNA methylation on some HSC maintenance or survival genes induced by $dmPGE_2$ treatment. This methylation pattern would still be observed in adult $Runx1^+$ cells. In addition, DNA methylation analysis can be performed on sorted mouse marrow populations as well as human $CD34^+$ cells. It would be interesting to compare

methylation changes in zebrafish, induced by *in vivo* treatment during embryogenesis, and mouse or human cells, which are pulse-treated *ex vivo*. DNMT3a regulates HSC differentiation in mice, and is highly enriched in primitive HSC populations[129]. Based on data from other systems, it is likely that $dmPGE_2$ will affect the methylation status of these cells. Epigenetic mechanisms are the most likely candidate to explain the long-term effects of PGE_2 on HSPC function.

Investigating PGE_2 and cycling cells

$dmPGE_2$ treatment increases the percentage of cycling cells *in vitro* in all HSC populations, but it is not known how PGE_2 affects cell cycle kinetics *in vivo,* or whether it preferentially acts on cells that are proliferating or quiescent. A recent study by Qui et al demonstrates that current methods of analyzing cell cycle, such as Ki67, Hoescht, and Draq5 staining only provide a snapshot of the quiescent state of a cell that is not always indicative of a cell's cycling history[116]. Using an inducible, GFP label-retention transgenic mouse, the authors tracked cell division history of HSPCs. This system enables cells to be analyzed based on current quiescent state, as well as cell cycle history. Our initial transplantation experiments showed a modest effect of $dmPGE_2$ treatment on $LSKCD34^+CD150^+$ cells that was significantly enhanced when the population was further purified using CD48 expression. Interestingly, Qui et al found that negative selection of CD48 enriches for a more dormant HSC population (0.19% of $LSKCD48^+CD150^-$ cells are highly quiescent, compared to 3.37% of $LSKCD48^-CD150^-$ cells).

Future experiments should test if PGE_2 preferentially affects quiescent or cycling cells. Using this transgenic mouse system, $LSKCD48^-CD34^+CD150^+$ ST-HSCs can be

split into highly dormant and more active HSCs based on their levels of GFP retention. Each population would be treated with $dmPGE_2$ or DMSO and compared in repopulation assays. Chimerism analysis would reveal if PGE_2 preferentially acts on one of these cell populations, as they are phenotypically identical. To determine if PGE_2 acts preferentially on cells that are actively cycling, $LSKCD48^-CD34^+CD150^+$ ST-HSCs stained with Draq5 can be sorted into different cycling populations based on DNA content. These experiments will provide insight into the cell population that is affected by PGE_2. Identifying a population of HSPCs that is specifically affected by $dmPGE_2$ treatment will have important clinical implications. A phase 1 trial was recently completed to test expansion and subsequent transplantation of cord blood HSCs following *ex vivo* $dmPGE_2$ exposure. Improving expansion protocols prior to transplantation may decrease the number of required units and increase the availability of donor cords.

Exploring additional expansion protocols for UCB cells

Although UCB has emerged as a valuable source of HSPCs for transplantation, there are limitations for its use in adult patients. Delayed neutrophil and platelet recovery in adult recipients is attributed to low HSPC numbers in a single cord unit[130]. Double cord transplantation improves the overall survival and recovery time in adult patients, but has an increased risk of acute GVHD[131]. Recent studies have focused on developing expansion protocols, including chemical manipulation of UCB *ex vivo*, to expand HSPCs prior to transplant or enhance homing and engraftment of these cells following transplantation- reviewed in[22]. Improving either of these aspects would allow more

patients to benefit from the advantages of cord blood transplantation. In the future it will be important to investigate *ex vivo* expansion of UCB through chemical manipulation of signaling pathways, in addition to prostaglandin, that regulate HSC function. The Notch signaling pathway has previously been implicated in hematopoiesis; *Notch1* is expressed in human $CD34^+$ cells[132] and overexpression of Notch1 improves the repopulation potential of these cells[133]. *Ex vivo* treatment of UCB with the notch ligand Delta1 led to expansion of HSPCs and shortened time to neutrophil engraftment in patients, although this effect was only transient[134]. Future work should focus on optimizing expansion protocols that manipulate notch signaling in UCB. The Wnt pathway has also been identified as an important regulator of HSPC function. Treatment of UCB with 6-bromoindirubin 3'-oxime (BIO), an inhibitor of GSK-3β, expands HSPCs *ex vivo*, and improves the engraftment and repopulation potential of these cells in immunodeficient mice[135]. Interestingly, treatment with BIO leads to activation of notch in UCB cells, and may promote notch signaling during *ex vivo* expansion[135]. In addition, prostaglandin and Wnt signaling pathways interact to regulate HSC function[57], suggesting that targeting multiple pathways may enhance *ex vivo* expansion of UCB.

References

1. Shizuru, J. a, Negrin, R. S. & Weissman, I. L. Hematopoietic stem and progenitor cells: clinical and preclinical regeneration of the hematolymphoid system. *Annu. Rev. Med.* **56,** 509–38 (2005).

2. Kondo, M. *et al.* Biology of hematopoietic stem cells and progenitors: implications for clinical application. *Annu. Rev. Immunol.* **21,** 759–806 (2003).

3. Reya, T. Regulation of hematopoietic stem cell self-renewal. *Recent Prog. Horm. Res.* **58,** 283–95 (2003).

4. Orkin, S. H. & Zon, L. I. Hematopoiesis: an evolving paradigm for stem cell biology. *Cell* **132,** 631–44 (2008).

5. Zhang, J. *et al.* Identification of the haematopoietic stem cell niche and control of the niche size. *Nature* **425,** 0–5 (2003).

6. Chen, A. T. & Zon, L. I. Zebrafish blood stem cells. *J. Cell. Biochem.* **108,** 35–42 (2009).

7. Davidson, A. J. & Zon, L. I. The "definitive" (and "primitive") guide to zebrafish hematopoiesis. *Oncogene* **23,** 7233–46 (2004).

8. Davidson, A. J. *et al.* Cdx4 Mutants Fail To Specify Blood Progenitors and Can Be Rescued By Multiple Hox Genes. *Nature* **425,** 300–6 (2003).

9. De Jong, J. L. O. & Zon, L. I. Use of the zebrafish system to study primitive and definitive hematopoiesis. *Annu. Rev. Genet.* **39,** 481–501 (2005).

10. Traver, D. *et al.* Transplantation and in vivo imaging of multilineage engraftment in zebrafish bloodless mutants. *Nat. Immunol.* **4,** 1238–46 (2003).

11. White, R., Sessa, A., Burke, C. & Bowman, T. Transparent adult zebrafish as a tool for in vivo transplantation analysis. *Cell Stem Cell* **2,** 183–189 (2008).

12. Berman, J. N., Kanki, J. P. & Look, a T. Zebrafish as a model for myelopoiesis during embryogenesis. *Exp. Hematol.* **33,** 997–1006 (2005).

13. Scadden, D. T. The stem-cell niche as an entity of action. *Nature* **441,** 1075–9 (2006).

14. Morrison, S. J. & Spradling, A. C. Stem cells and niches: mechanisms that promote stem cell maintenance throughout life. *Cell* **132,** 598–611 (2008).

15. Calvi, L. M. *et al.* Osteoblastic cells regulate the haematopoietic stem cell niche. 841–846 (2003). doi:10.1038/nature02041.1.

16. Kiel, M. J. *et al.* SLAM family receptors distinguish hematopoietic stem and progenitor cells and reveal endothelial niches for stem cells. *Cell* **121,** 1109–21 (2005).

17. Morikawa, S. *et al.* Prospective identification, isolation, and systemic transplantation of multipotent mesenchymal stem cells in murine bone marrow. *J. Exp. Med.* **206,** 2483–96 (2009).

18. Tran, E. *et al.* Immune targeting of fibroblast activation protein triggers recognition of multipotent bone marrow stromal cells and cachexia. *J. Exp. Med.* **210,** 1125–35 (2013).

19. Roberts, E. W. *et al*. Depletion of stromal cells expressing fibroblast activation protein-α from skeletal muscle and bone marrow results in cachexia and anemia. *J. Exp. Med*. **210,** 1137–51 (2013).

20. Yao, L., Yokota, T., Xia, L., Kincade, P. W. & McEver, R. P. Bone marrow dysfunction in mice lacking the cytokine receptor gp130 in endothelial cells. *Blood* **106,** 4093–101 (2005).

21. Li, W., Johnson, S. a, Shelley, W. C. & Yoder, M. C. Hematopoietic stem cell repopulating ability can be maintained in vitro by some primary endothelial cells. *Exp. Hematol*. **32,** 1226–37 (2004).

22. Cutler, C. & Ballen, K. K. Improving outcomes in umbilical cord blood transplantation: state of the art. *Blood Rev*. **26,** 241–6 (2012).

23. Horn, B. & Cowan, M. J. Unresolved issues in hematopoietic stem cell transplantation for severe combined immunodeficiency: need for safer conditioning and reduced late effects. *J. Allergy Clin. Immunol*. **131,** 1306–11 (2013).

24. Till, J. E. & McCulloch, E. a. A direct measurement of the radiation sensitivity of normal mouse bone marrow cells. 1961. *Radiat. Res*. **178,** AV3–7 (2012).

25. Repopulating, H. *et al*. Quantitative Analysis Reveals Expansion of Human. **186,** 619–624 (1997).

26. Ikuta, K. & Weissman, I. Evidence that hematopoietic stem cells express mouse c-kit but do not depend on steel factor for their generation. *PNAS* **89**, 1502-1506 (1992).

27. Osawa, M., Hanada, K., Hamada, H. & Nakauchi, H. Long-term lymphohematopoietic reconstitution by a single CD34-low/negative hematopoietic stem cell. *Science* **273,** 242–5 (1996).

28. Kiel, M. J. *et al*. SLAM family receptors distinguish hematopoietic stem and progenitor cells and reveal endothelial niches for stem cells. *Cell* **121,** 1109–1121 (2005).

29. Kiel, M. J., Yilmaz, O. H. & Morrison, S. J. CD150- cells are transiently reconstituting multipotent progenitors with little or no stem cell activity. *Blood* **111,** 4413–4; author reply 4414–5 (2008).

30. Cells, H., Marrow, B., Lansdorp, B. P. M., Sutherland, H. & Eaves, C. Selective Expression of CD45 Isoforms on Functional Subpopulations of CD34 + Hemopoietic Cells from Human Bone Marrow By P.M. Lansdorp, Hj. Sutherland, and Cj. Eaves. **172,** (1990).

31. Conneally, E., Cashman, J., Petzer, a & Eaves, C. Expansion in vitro of transplantable human cord blood stem cells demonstrated using a quantitative assay of their lympho-myeloid repopulating activity in nonobese diabetic-scid/scid mice. *Proc. Natl. Acad. Sci. U. S. A.* **94,** 9836–41 (1997).

32. Bhatia, M., Wang, J. C., Kapp, U., Bonnet, D. & Dick, J. E. Purification of primitive human hematopoietic cells capable of repopulating immune-deficient mice. *Proc. Natl. Acad. Sci. U. S. A.* **94,** 5320–5 (1997).

33. Aiuti, B. A., Webb, I. J., Bleul, C. & Springer, T. New Mechanism to Explain the Mobilization of CD34 ♀ Progenitors to Peripheral Blood. **185,** (1997).

34. Ratajczak, J. *et al*. Mobilization studies in mice deficient in either C3 or C3a receptor (C3aR) reveal a novel role for complement in retention of hematopoietic stem/progenitor cells in bone marrow. *Blood* **103,** 2071–8 (2004).

35. Wysoczynski, M. *et al*. Defective engraftment of C3aR-/- hematopoietic stem progenitor cells shows a novel role of the C3a-C3aR axis in bone marrow homing. *Leukemia* **23,** 1455–61 (2009).

36. Factor-, C. S. C., Ii, K. W. C., Hangoc, G. & Hal, E. Cell surface peptidase CD26/Dipeptidylpeptidase IV regulates CXCL12/Stromal cell-derived factor-1 alpha- mediated chemotaxis of human cord blood CD34+ progenitor cells. *J. Immunol.* **169,** 7000–7008 (2014).

37. Ii, K. W. C., Cooper, S. & Broxmeyer, H. E. Cell surface peptidase CD26 / DPPIV mediates G-CSF mobilization of mouse progenitor cells. **101,** 4680–4686 (2003).

38. Christopherson, K. W., Hangoc, G., Mantel, C. R. & Broxmeyer, H. E. Modulation of hematopoietic stem cell homing and engraftment by CD26. *Science* **305,** 1000–3 (2004).

39. Abkowitz, J. L., Robinson, A. E., Kale, S., Long, M. W. & Chen, J. Mobilization of hematopoietic stem cells during homeostasis and after cytokine exposure. *Blood* **102,** 1249–53 (2003).

40. Thomas, J., Liu, F. & Link, D. C. Mechanisms of mobilization of hematopoietic progenitors with granulocyte colony-stimulating factor. *Curr. Opin. Hematol.* **9,** 183–9 (2002).

41. Schoemans, H. *et al*. Adult umbilical cord blood transplantation: a comprehensive review. *Bone Marrow Transplant.* **38,** 83–93 (2006).

42. Rocha, V. & Gluckman, E. Clinical use of umbilical cord blood hematopoietic stem cells. *Biol. Blood Marrow Transplant.* **12,** 34–41 (2006).

43. North, T. E. *et al*. Prostaglandin E2 regulates vertebrate haematopoietic stem cell homeostasis. *Nature* **447,** 1007–11 (2007).

44. North, T. E. *et al*. Runx1 expression marks long-term repopulating hematopoietic stem cells in the midgestation mouse embryo. *Immunity* **16,** 661–72 (2002).

45. Mukouyama, Y. S. *et al*. Hematopoietic cells in cultures of the murine embryonic aorta-gonad-mesonephros region are induced by c-Myb. *Curr. Biol.* **9,** 833–6 (2002).

46. Hoggatt, J., Singh, P., Sampath, J. & Pelus, L. M. Prostaglandin E2 enhances hematopoietic stem cell homing, survival, and proliferation. *Blood* **113,** 5444–55 (2009).

47. Frisch, B. J. *et al*. In vivo prostaglandin E2 treatment alters the bone marrow microenvironment and preferentially expands short-term hematopoietic stem cells. *Blood* **114,** 4054–63 (2009).

48. Goessling, W. *et al*. Prostaglandin E2 enhances human cord blood stem cell xenotransplants and shows long-term safety in preclinical nonhuman primate transplant models. *Cell Stem Cell* **8,** 445–58 (2011).

49. Cutler, C. *et al*. Prostaglandin-modulated umbilical cord blood hematopoietic stem cell transplantation. *Blood* **122,** 3074–81 (2013).

50. Smyth, E. M., Grosser, T., Wang, M., Yu, Y. & FitzGerald, G. a. Prostanoids in health and disease. *J. Lipid Res.* **50 Suppl,** S423–8 (2009).

51. Nathan, C. Points of control in inflammation. *Nature* **420,** 846–52 (2002).

52. Smith, W. L., DeWitt, D. L. & Garavito, R. M. Cyclooxygenases: structural, cellular, and molecular biology. *Annu. Rev. Biochem.* **69,** 145–82 (2000).

53. Regan, J. W. EP2 and EP4 prostanoid receptor signaling. *Life Sci.* **74,** 143–153 (2003).

54. Breyer, R. M., Bagdassarian, C. K., Scott, A. & Breyer, M. D. P ROSTANOID R ECEPTORS : Subtypes. (2001).

55. Hata, A. N. & Breyer, R. M. Pharmacology and signaling of prostaglandin receptors: multiple roles in inflammation and immune modulation. *Pharmacol. Ther.* **103,** 147–66 (2004).

56. Fujino, H., West, K. a & Regan, J. W. Phosphorylation of glycogen synthase kinase-3 and stimulation of T-cell factor signaling following activation of EP2 and EP4 prostanoid receptors by prostaglandin E2. *J. Biol. Chem.* **277,** 2614–9 (2002).

57. Goessling, W. *et al*. Genetic interaction of PGE2 and Wnt signaling regulates developmental specification of stem cells and regeneration. *Cell* **136,** 1136–47 (2009).

58. Ikushima, Y. M. *et al*. Prostaglandin E(2) regulates murine hematopoietic stem/progenitor cells directly via EP4 receptor and indirectly through mesenchymal progenitor cells. *Blood* **121,** 1995–2007 (2013).

59. Bertrand, J. Y. *et al*. Haematopoietic stem cells derive directly from aortic endothelium during development. *Nature* **464,** 108–11 (2010).

60. Boisset, J.-C. *et al*. In vivo imaging of haematopoietic cells emerging from the mouse aortic endothelium. *Nature* **464,** 116–120 (2010).

61. Kissa, K. & Herbomel, P. Blood stem cells emerge from aortic endothelium by a novel type of cell transition. *Nature* **464,** 112–5 (2010).

62. Murayama, E. *et al*. Tracing Hematopoietic Precursor Migration to Successive Hematopoietic Organs during Zebrafish Development. *Immunity* **25,** 963–975 (2006).

63. Orkin, S. H. & Zon, L. I. Hematopoiesis: an evolving paradigm for stem cell biology. *Cell* **132,** 631–644 (2008).

64. Traver, D. *et al*. Transplantation and in vivo imaging of multilineage engraftment in zebrafish bloodless mutants. *Nat. Immunol.* **4,** 1238–1246 (2003).

65. Laird, D. J., von Andrian, U. H. & Wagers, A. J. Stem cell trafficking in tissue development, growth, and disease. *Cell* **132,** 612–630 (2008).

66. Nombela-Arrieta, C. *et al*. Quantitative imaging of haematopoietic stem and progenitor cell localization and hypoxic status in the bone marrow microenvironment. *Nat. Cell Biol.* (2013). doi:10.1038/ncb2730

67. Sugiyama, T., Kohara, H., Noda, M. & Nagasawa, T. Maintenance of the Hematopoietic Stem Cell Pool by CXCL12-CXCR4 Chemokine Signaling in Bone Marrow Stromal Cell Niches. *Immunity* **25,** 977–988 (2006).

68. Butler, J. M. *et al*. Endothelial cells are essential for the self-renewal and repopulation of Notch-dependent hematopoietic stem cells. *Cell Stem Cell* **6,** 251–264 (2010).

69. Hooper, A. T. *et al*. Engraftment and reconstitution of hematopoiesis is dependent on VEGFR2-mediated regeneration of sinusoidal endothelial cells. *Cell Stem Cell* **4,** 263–274 (2009).

70. Oguro, H., Ding, L. & Morrison, S. J. SLAM family markers resolve functionally distinct subpopulations of hematopoietic stem cells and multipotent progenitors. *Cell Stem Cell* **13,** 102–16 (2013).

71. Méndez-Ferrer, S. *et al*. Mesenchymal and haematopoietic stem cells form a unique bone marrow niche. *Nature* **466,** 829–834 (2010).

72. Köhler, A. *et al*. Altered cellular dynamics and endosteal location of aged early hematopoietic progenitor cells revealed by time-lapse intravital imaging in long bones. *Blood* **114,** 290–298 (2009).

73. Lewandowski, D. *et al*. In vivo cellular imaging pinpoints the role of reactive oxygen species in the early steps of adult hematopoietic reconstitution. *Blood* **115,** 443–452 (2010).

74. Lo Celso, C. *et al*. Live-animal tracking of individual haematopoietic stem/progenitor cells in their niche. *Nature* **457,** 92–6 (2009).

75. Takaku, T. *et al*. Hematopoiesis in three dimensions: human and murine bone marrow architecture visualized by confocal microscopy. *Blood* (2010). doi:10.1182/blood-2010-02-268466

76. Xie, Y. *et al*. Detection of functional haematopoietic stem cell niche using real-time imaging. *Nature* **457,** 97–101 (2009).

77. Lin, H.-F. *et al*. Analysis of thrombocyte development in CD41-GFP transgenic zebrafish. *Blood* **106,** 3803–3810 (2005).

78. Lam, E. Y. N. *et al*. Zebrafish runx1 promoter-EGFP transgenics mark discrete sites of definitive blood progenitors. *Blood* **113,** 1241–1249 (2009).

79. Nottingham, W. T. *et al*. Runx1-mediated hematopoietic stem-cell emergence is controlled by a Gata/Ets/SCL-regulated enhancer. *Blood* **110,** 4188–4197 (2007).

80. Boisset, J.-C. *et al*. In vivo imaging of haematopoietic cells emerging from the mouse aortic endothelium. *Nature* **464,** 116–20 (2010).

81. Thisse, C. & Thisse, B. High-resolution in situ hybridization to whole-mount zebrafish embryos. *Nat. Protoc.* **3,** 59–69 (2008).

82. Pugach, E. K., Li, P., White, R. & Zon, L. Retro-orbital injection in adult zebrafish. *J. Vis. Exp.* 4–6 (2009). doi:10.3791/1645

83. Stachura, D. L. & Traver, D. Cellular dissection of zebrafish hematopoiesis. *Methods Cell Biol* **101,** 75–110 (2011).

84. Kumaravelu, P. *et al*. Quantitative developmental anatomy of definitive haematopoietic stem cells/long-term repopulating units (HSC/RUs): role of the aorta-gonad-mesonephros (AGM) region and the yolk sac in colonisation of the mouse embryonic liver. *Development* **129,** 4891–4899 (2002).

85. Huang, H., Zhang, B., Hartenstein, P. A., Chen, J. N. & Lin, S. NXT2 is required for embryonic heart development in zebrafish. *BMC Dev Biol* **5,** 7 (2005).

86. Glass, T. J. *et al*. Stromal cell-derived factor-1 and hematopoietic cell homing in an adult zebrafish model of hematopoietic cell transplantation. *Blood* **118,** 766–774 (2011).

87. Ara, T. *et al*. Long-term hematopoietic stem cells require stromal cell-derived factor-1 for colonizing bone marrow during ontogeny. *Immunity* **19,** 257–267 (2003).

88. Mosimann, C. *et al*. Ubiquitous transgene expression and Cre-based recombination driven by the ubiquitin promoter in zebrafish. *Development* **138,** 169–177 (2011).

89. Osawa, M. *et al*. In vivo self-renewal of c-Kit+ Sca-1+ Lin(low/-) hemopoietic stem cells. *J. Immunol. (Baltimore, Md 1950)* **156,** 3207–3214 (1996).

90. Medvinsky, A. & Dzierzak, E. Definitive hematopoiesis is autonomously initiated by the AGM region. *Cell* **86,** 897–906 (1996).

91. Müller, A. M., Medvinsky, A., Strouboulis, J., Grosveld, F. & Dzierzak, E. Development of hematopoietic stem cell activity in the mouse embryo. *Immunity* **1,** 291–301 (1994).

92. Mironov, A. A. & Beznoussenko, G. V. Correlative microscopy: a potent tool for the study of rare or unique cellular and tissue events. *J Microsc* **235,** 308–321 (2009).

93. Glass, T. J. *et al*. Stromal cell-derived factor-1 and hematopoietic cell homing in an adult zebrafish model of hematopoietic cell transplantation. *Blood* **118,** 766–74 (2011).

94. Batard, P. *et al*. TGF-(beta)1 maintains hematopoietic immaturity by a reversible negative control of cell cycle and induces CD34 antigen up-modulation. *J. Cell Sci.* **113 (Pt 3,** 383–390 (2000).

95. Larsson, J. *et al*. TGF-beta signaling-deficient hematopoietic stem cells have normal self-renewal and regenerative ability in vivo despite increased proliferative capacity in vitro. *Blood* **102,** 3129–35 (2003).

96. Sitnicka, E., Ruscetti, F. W., Priestley, G. V, Wolf, N. S. & Bartelmez, S. H. Transforming growth factor beta 1 directly and reversibly inhibits the initial cell divisions of long-term repopulating hematopoietic stem cells. *Blood* **88,** 82–88 (1996).

97. Soma, T., Yu, J. M. & Dunbar, C. E. Maintenance of murine long-term repopulating stem cells in ex vivo culture is affected by modulation of transforming growth factor-beta but not macrophage inflammatory protein-1 alpha activities. *Blood* **87,** 4561–4567 (1996).

98. Yamazaki, Y. & Kawano, Y. Inhibitory effects of herbal alkaloids on the tumor necrosis factor-alpha and nitric oxide production in lipopolysaccharide-stimulated RAW264 macrophages. *Chem Pharm Bull* **59,** 388–391 (2011).

99. Yamazaki, S. *et al*. TGF-beta as a candidate bone marrow niche signal to induce hematopoietic stem cell hibernation. *Blood* **113,** 1250–1256 (2009).

100. Morrison, S. J., Hemmati, H. D., Wandycz, A. M. & Weissman, I. L. The purification and characterization of fetal liver hematopoietic stem cells. *Proc. Natl. Acad. Sci. U. S. A.* **92,** 10302–10306 (1995).

101. Sánchez, M. J., Holmes, A., Miles, C. & Dzierzak, E. Characterization of the first definitive hematopoietic stem cells in the AGM and liver of the mouse embryo. *Immunity* **5,** 513–525 (1996).

102. Ma, X. *et al*. Expression of the Ly-6A (Sca-1) lacZ transgene in mouse haematopoietic stem cells and embryos. *Br J Haematol* **116,** 401–408 (2002).

103. Ma, X., Robin, C., Ottersbach, K. & Dzierzak, E. The Ly-6A (Sca-1) GFP transgene is expressed in all adult mouse hematopoietic stem cells. *Stem Cells* **20,** 514–521 (2002).

104. Jahn, T., Leifheit, E., Gooch, S., Sindhu, S. & Weinberg, K. Lipid rafts are required for Kit survival and proliferation signals. *Blood* **110,** 1739–1747 (2007).

105. Yamazaki, S. *et al*. Cytokine signals modulated via lipid rafts mimic niche signals and induce hibernation in hematopoietic stem cells. *EMBO J*. **25,** 3515–3523 (2006).

106. Golan, K., Kollet, O. & Lapidot, T. Dynamic Cross Talk between S1P and CXCL12 Regulates Hematopoietic Stem Cells Migration, Development and Bone Remodeling. *Pharmaceuticals (Basel)*. **6,** 1145–69 (2013).

107. Juarez, J. G. *et al*. Sphingosine-1-phosphate facilitates trafficking of hematopoietic stem cells and their mobilization by CXCR4 antagonists in mice. *Blood* **119,** 707–16 (2012).

108. Hoggatt, J., Mohammad, K. S., Singh, P. & Pelus, L. M. Prostaglandin E2 enhances long-term repopulation but does not permanently alter inherent stem cell competitiveness. *Blood* **122,** 2997–3000 (2013).

109. Porter, R. L. *et al*. Prostaglandin E2 increases hematopoietic stem cell survival and accelerates hematopoietic recovery after radiation injury. *Stem Cells* **31,** 372–83 (2013).

110. Yu, X., Gu, Z., Wang, Y. & Wang, H. New strategies in cord blood cells transplantation. *Cell Biol. Int*. **37,** 865–74 (2013).

111. Li, L. *et al*. Prostaglandin E2 promotes survival of naive UCB T cells via the Wnt/β-catenin pathway and alters immune reconstitution after UCBT. *Blood Cancer J*. **4,** e178 (2014).

112. Wilson, A. *et al*. Hematopoietic stem cells reversibly switch from dormancy to self-renewal during homeostasis and repair. *Cell* **135,** 1118–29 (2008).

113. Lee, T., Johnstone, S. & Young, R. Chromatin immunprecipitation and microarray-based analysis of protein location. *Nat. Protoc*. **1,** 729–748 (2006).

114. Harrison, D. E. & Lerner, C. P. Most primitive hematopoietic stem cells are stimulated to cycle rapidly after treatment with 5-fluorouracil. *Blood* **78,** 1237–40 (1991).

115. Graham, S. M., Vass, J. K., Holyoake, T. L. & Graham, G. J. Transcriptional analysis of quiescent and proliferating CD34+ human hemopoietic cells from normal and chronic myeloid leukemia sources. *Stem Cells* **25,** 3111–20 (2007).

116. Qiu, J., Papatsenko, D., Niu, X., Schaniel, C. & Moore, K. Divisional History and Hematopoietic Stem Cell Function during Homeostasis. *Stem Cell Reports* **2,** 1–18 (2014).

117. Diggle, C. P. *et al*. Prostaglandin transporter mutations cause pachydermoperiostosis with myelofibrosis. *Hum. Mutat*. **33,** 1175–81 (2012).

118. Cai, X. *et al*. Runx1 loss minimally impacts long-term hematopoietic stem cells. *PLoS One* **6,** e28430 (2011).

119. Kim, S. *et al*. Dynamics of HSPC Repopulation in Nonhuman Primates Revealed by a Decade-Long Clonal-Tracking Study. *Cell Stem Cell* **14,** 473–485 (2014).

120. Nagoshi, N. *et al*. Ontogeny and multipotency of neural crest-derived stem cells in mouse bone marrow, dorsal root ganglia, and whisker pad. *Cell Stem Cell* **2,** 392–403 (2008).

121. Yamazaki, S. *et al*. Nonmyelinating Schwann cells maintain hematopoietic stem cell hibernation in the bone marrow niche. *Cell* **147,** 1146–1158 (2011).

122. Murayama, E. *et al*. Tracing hematopoietic precursor migration to successive hematopoietic organs during zebrafish development. *Immunity* **25,** 963–75 (2006).

123. JOHNSON, G. R. & MOORE, M. A. S. Role of stem cell migration in initiation of mouse foetal liver haemopoiesis. *Nature* **258,** 726–728 (1975).

124. Jaakkola, P. *et al*. Targeting of HIF-alpha to the von Hippel-Lindau ubiquitylation complex by O2-regulated prolyl hydroxylation. *Science* **292,** 468–72 (2001).

125. Takubo, K. *et al*. Regulation of the HIF-1alpha level is essential for hematopoietic stem cells. *Cell Stem Cell* **7,** 391–402 (2010).

126. Rivera, J., Proia, R. L. & Olivera, A. The alliance of sphingosine-1-phosphate and its receptors in immunity. *Nat. Rev. Immunol.* **8,** 753–63 (2008).

127. Ma, D., Zhang, J., Lin, H., Italiano, J. & Handin, R. I. The identification and characterization of zebrafish hematopoietic stem cells. *Blood* **118,** 289–97 (2011).

128. Huang, S. K. *et al*. Prostaglandin E_2 increases fibroblast gene-specific and global DNA methylation via increased DNA methyltransferase expression. *FASEB J.* **26,** 3703–14 (2012).

129. Challen, G. A. *et al*. Dnmt3a is essential for hematopoietic stem cell differentiation. *Nat. Genet.* **44,** 23–31 (2012).

130. Laughlin, M. J. *et al*. Outcomes after transplantation of cord blood or bone marrow from unrelated donors in adults with leukemia. *N. Engl. J. Med.* **351,** 2265–75 (2004).

131. Ballen, K. K. *et al*. Double unrelated reduced-intensity umbilical cord blood transplantation in adults. *Biol. Blood Marrow Transplant.* **13,** 82–9 (2007).

132. Milner, B. L. A., Kopan, R., Martin, D. I. K. & Bernstein, I. D. A Human Homologue of the Drosophila Developmental Gene,. 2057–2062 (1994).

133. Varnum-Finney, B. et al. Pluripotent, cytokine-dependent, hematopoietic stem cells are immortalized by constitutive Notch1 signaling. *Nat. Med.* **6**, 1278–1281 (2000).

134. Delaney, C. *et al*. Notch-mediated expansion of human cord blood progenitor cells capable of rapid myeloid reconstitution. *Nat Med.* **16**, 232-6 (2010).

135. Ko, K.H. *et al*. GSK-3b Inhibition Promotes Engraftment of Ex Vivo-Expanded Hematopoietic Stem Cells and Modulates Gene Expression. *Stem Cells.* **29**, 108-118 (2010).

Appendix

Supplemental Information (Tamplin, Durand et al., 2014)

Supplemental Figure, Table and Movie Legends

Figure S1. Characterization of stable Runx:GFP and Runx:mCherry transgenic zebrafish lines.

(A) Intercross of Runx:GFP and Runx:mCherry lines to show overlapping expression in the CHT (arrowheads). dpf: days post fertilization

(B) Emergence of Runx:mCherry+ HSPC (red nuclei; arrowheads) in the kdrl:GFP+ endothelial cells (ECs) of the ventral wall of the dorsal aorta (DA; green). See Movie S1. hpf: hours post fertilization

(C,E,G,I,K) Cross of Runx:mCherry and cd41:EGFP lines. (D,F,H,J,L) Cross of Runx:mCherry and cmyb:EGFP lines. Co-expression at stages and in embryonic sites of hematopoiesis as marked (i.e. thymus and CHT). We predict the larger number of Runx:mCherry+ cells in 3 and 5 dpf embryos are HSPC progeny.

(M) Section of Runx:GFP zebrafish kidney stained with hematoxylin and eosin (H&E).

(N) Immunohistochemistry of adjacent section to (M). Anti-GFP shows rare GFP+ cells in the kidney marrow (brown; arrowheads; counterstained with hematoxilyn).

(O) Fluorescence-activated cell sorting (FACS) of whole kidney marrow (WKM) from adult Runx:GFP transgenic zebrafish. Runx:GFP+ cells represent on average 0.133% of the total WKM.

(P) Forward scatter (FSC) and side scatter (SSC) were used to distinguish characteristic WKM populations (Traver et al., 2003). Runx:GFP+ cells were found predominately in the lymphoid/HSPC gate.

Figure S2. Runx:mCherry positive cells in the embryo are functional HSPC.

(A) Summary of results from embryo-to-embryo limiting dilution transplantation experiments.

(B) Embryo-to-embryo transplantation recipients with engraftment of Runx:mCherry+ cells in the kidney marrow at 3 months (scored if above background; >0.001%).

(C) Representative WKM FACS plots of an embryo-to-embryo transplantation recipient with Runx:mCherry+ HSPC and ubi:GFP+ lineages.

Figure S3. Time-lapse live imaging sequence of CHT colonization.

See Movie S2. Selected frames of time-lapse are shown (1 frame/2 minutes). First row frames are a merge of Runx:GFP+ HSPC (green; second row) and kdrl:RFP+ ECs (red; third row in B). Times are hours:minutes post fertilization.

(A) HSPC (arrowhead) extravasates by squeezing through endothelial wall.

(B) ECs remodel around HSPC to form niche (broken circle).

(C) After HSPC division the daughter cells undergo a 90º rotation (arrowheads). The upper cell becomes migratory and crawls out of niche.

(D) A diagram summarizing the steps of HSPC lodgement in the perivascular niche. The times shown correspond to the time-lapse frames shown above. Other possible cell division decisions are shown.

Figure S4. Serial block face scanning EM of CHT after time-lapse.

(A,B) Embryo 1 (same embryo as shown in Figure 4). Comparison of 3D projections from (A) confocal z-stack data and (B) serial EM scans to confirm the position of the lodged HSPC. (A) 3D rendered projection of z-stack (Imaris software) showing one lodged Runx:GFP+ HSPC (green; arrowhead) and kdrl:mCherry+ ECs (red). Scale bar: 20 microns. (B) Vessel lumen manually outlined, surface rendered, and shown in red (Imaris software). 3D projection overlaid on a single EM section. Rotation performed to match orientation of image in (A). Orientation: D (dorsal), V (ventral), A (anterior), P (posterior). CA (caudal artery). Circulation is towards the posterior (left; arrow). Major vessels outlined.

(C-G) Embryo 2. A second independent example of serial block face EM sections on a lodged HSPC after time-lapse. (C) Last frame of CHT time-lapse (60 hpf). Arrowhead marks HSPC lodged >6 hours. Runx:GFP green; kdrl:mCherry red; brightfield blue. Anterior left, posterior right, dorsal top, ventral bottom. (D) Detail of region in (C) marked by box. The brightness of the GFP channel was adjusted independently of the mCherry channel to clearly show the position of the Runx:GFP+ HSPC. Scale bar 50 microns. (E) Single section and orthogonal slice from serial block face EM scans. Lodged HSPC is purple, surrounding EC nuclei are green and numbered. Part of the HSPC is missing because it was not captured in serial EM sections. (F,G) High resolution EM sections with cells of interest outlined as follows: EC (dark green, bright green, blue, light blue, yellow, orange); HSPC (purple); FB (fibroblastic mesenchymal cell; white); RBC (red blood cell; red). (F) Direct contact between the midsection of the pink HSPC

and dark green EC is visible. (G) Gaps are visible between the HSPC and surrounding cells. There are some contacts with the fibroblastic mesenchymal cell (FB; white). This FB cell does not have the melanophore inclusions observed in Embryo 1 (Figure S4G and data not shown; compare to Figure 4D). There are no stromal cells visible in this example. For 3D reconstruction see Movie S4. Scale bars: 5 microns.

Figure S5. Embryonic expression patterns of CXCR4-CXCL12 homologs in zebrafish and dose-dependency of CXCR4 antagonist AMD3100.

(A) Whole mount *in situ* expression patterns of *cxcr4a*, *cxcr4b*, *cxcl12a*, and *cxcl12b* between 34-38 hpf. For each example a detail of the trunk and tail is shown, with the DA and caudal hematopoietic tissue (CHT), respectively, marked with dashed white boxes. All genes are expressed in the head and lateral line. *cxcr4b* but not *cxcr4a* is expressed in the CHT. *cxcl12a* and *cxcl12b* are expressed in the DA and CHT.

(B) Dose-dependent decrease in *cmyb/runx1* expression levels with increasing concentrations of CXCR4 antagonist AMD3100. Wild-type AB embryos were treated from 48-72 hpf and scored as those in Figure 5A,B. The percentage of total is shown.

Figure S6. Time-lapse live imaging of E11.5 fetal liver (FL) explant with labeled HSPC and ECs.

(A) A time-lapse sequence from a FL lobe showing a c-kit+ HSPC (magenta) adhered to a CD31+ sinusoid (green). In ~30 minutes, the anterior of the cell protrudes (arrowhead) and extravasates to the abluminal side of the sinusoid (division marked by dotted line). Luminal versus abluminal sides of the sinusoid were confirmed in single z slices of

confocal stacks (data not shown). Scale bar: 10 microns. Times are hours:minutes after start of explant imaging.

(B) After extravasation, the HSPC migrates on the abluminal side of the sinusoid.

(C) ECs surround the HSPC as a rosette (dotted line). There is an accumulation of c-kit at the contact point between the HSPC and the ECs (compare to similar c-kit accumulation in Figure 7D,E).

(D) A diagram summarizing the steps of HSPC lodgement in the FL. The times shown correspond to the time-lapse frames shown above. A morphologically symmetric division is observed in Figure 7D. Other possible cell division decisions are shown.

Table S1. Ingenuity Pathway Analysis (IPA) of microarray data from Lycorine-treated embryos.

Double transgenic Runx:GFP;kdrl:RFP embryos were treated with DMSO (1%) or Lycorine (75 μM) from 48-72 hpf. Embryos from each pool were dissociated and sorted into three populations: 1) GFP+ HSPC; 2) RFP+ EC; 3) negative whole embryo. Three biological replicates were collected and analyzed. Lycorine-treated versus DMSO were compared for both HSPC and EC populations. Availabe Entrez Gene IDs were used for IPA analysis. (A) The Lycorine-treated EC population was enriched for genes associated with adhesion and extravasation. (B) The Lycorine-treated HSPC population was enriched for genes associated with adhesion and activation.

Movie S1. Emergence of Runx:mCherry+ HSPC from the hemogenic endothelium of the DA. Corresponds to Figure S1B. Runx:mCherry+ nuclei (red) are seen in the kdrl:GFP+ DA (green) at ~28 hpf. The cells round up and protrude on the ventral side of the DA. Time-lapse live imaging captured at 2 minutes/frame and rendered at 6 frames/second.

Movie S2. HSPC niche colonization in the zebrafish CHT reveals novel steps to engraftment. Corresponds to Figure 3A and S3. A double transgenic embryo with kdrl:RFP+ ECs (red) and Runx:GFP+ HSPC (green) imaged during colonization of the CHT (~38-43 hpf). An arriving HSPC attaches to the endothelial wall, undergoes extravasation and migration to the abluminal side, followed by endothelial remodeling into a pocket, cell division, a 90º turn, and migration of one daughter cell out of the niche. Time-lapse live imaging captured at 2 minutes/frame and rendered at 6 frames/second.

Movie S3. Reconstructed cells from TEM tomography are shown in relationship to each other in a 3D model. Corresponds to Figure 4D-F. A lodged hematopoietic progenitor stem cell (HSPC; purple), is closely associated with two putative stromal cells (light and dark blue), one of which directly contacts the HSPC. These three cells are nestled close to the endothelial cell wall of the dorsal aorta (individual cells outlined in different shades of green). Erythrocytes (red) are seen both within the dorsal aorta (as in Figure 4E,F upper), and in the sinusoids of the CHT in proximity to one of the stromal

cells (as in Figure 4E,F lower). Two additional fibroblastic mesenchymal cells with melanophore inclusions wrap the HSPC tightly (white and yellow).

Movie S4. Reconstructed cells from TEM tomography from a second embryo are shown in relationship to each other in a 3D model. Corresponds to Figure S4F,G (Embryo 2). A lodged HSPC (purple) is closely associated with EC (dark green, bright green, dark blue, light blue). One EC (dark green) directly contacts the HSPC. Part of an RBC (red) is seen on the luminal side of an EC. Gaps are visible between the HSPC and surrounding cells. There are some contacts with the fibroblastic mesenchymal cell (FB; white) that tightly wraps the HSPC. There are no stromal cells visible in this example.

Movie S5. 3D reconstruction of an HSPC surrounded by EC in an E11.5 FL. Corresponds to Figure 7C. A 3D rendered projection of a confocal z-stack using Volocity software. This example shows a Ly6a-GFP+/Runx1+ HSPC surrounded by VE-Cadherin+ EC. Contacts with EC are visible on all sides of the HSPC.

Movie S6. Time-lapse live imaging detail of an E11.5 FL explant showing EC remodeling around an HSPC. Corresponds to Figure 7D. A c-kit+ HSPC (magenta) migrates into a field of CD31+ sinusoidal ECs (green). The ECs then remodel around the HSPC. Maximum projection of confocal z-stack. ImageJ used for bleach correction over time. Time-lapse live imaging captured at 2 minutes/frame and rendered at 6 frames/second. Times are hours:minutes after start of explant imaging.

Movie S7. Time-lapse live imaging detail of an E11.5 FL explant showing HSPC division. Corresponds to Figure 7E. A white arrowhead tracks the movement of a Ly6a-GFP+ (green)/c-kit+(blue) HSPC that is adhered to CD31+ sinusoidal ECs (red). The HSPC undergoes division, with one daughter remaining surrounded by EC and the other migrating away. Note: Ly6a-GFP also marks some ECs and macrophages in the FL. Times are hours:minutes after start of explant imaging. Scale bar is 10 microns.

Supplemental Experimental Procedures

All animals were handled according to approved Institutional Animal Care and Use Committee (IACUC) of Boston Children's Hospital protocols.

Vectors and transgenesis

All PCR was performed using the High Fidelity Advantage 2 PCR Kit (Clontech). The Runx1 +23 enhancer (Nottingham et al., 2007) was PCR amplified from C57/BL6 mouse genomic DNA using the following primers: Forward (underlined XhoI and BamHI sites added) 5'-GGCTCGAGGGATCCGGGGTGGGAGGTGTAAGTTC-3' 5'-GGGGTGGGAGGTGTAAGTTC-3' and Reverse (underlined BglII and NotI sites added) 5'- GGGCGGCCGCAGATCTCAGGTGTCAGCAACCCATC -3'. The PCR fragment was gel purified, XhoI/BglII digested, ligated into XhoI/BamHI digested Tol2kit (Kwan et al., 2007) #228 p5E-MCS vector and sequence verified. The mouse β-globin minimal promoter was PCR amplified from C57/BL6 mouse genomic DNA using the following primers: Forward (underlined SpeI site added) 5'-GGACTAGTCCAATCTGCTCAGAGAGGACA-3' and Reverse (underlined SacII site added) 5'-GGCCGCGGGATGTCTGTTTCTGAGGTTGC-3'. The β-globin minimal promoter and Runx1+23 5' entry vector were SpeI/SacII digested and ligated together. Multisite Gateway reactions were performed according to the Invitrogen protocol. The Runx1+23 5' entry enhancer/minimal promoter construct was assembled with middle

entry vectors Tol2kit #383 pME-EGFP or Tol2kit #233 pME-NLS-mCherry, 3' entry vector Tol2kit #302 p3E-polyA, and destination vector Tol2kit #394 pDestTol2pA2. Transgenic lines were established as previously described (Mosimann et al., 2011). At least two independent lines with 50% transmission from the F2 generation were established for each construct (Runx:GFP and Runx:mCherry).

Transgenic zebrafish lines

We are grateful to those who generously shared the following lines for this study: kdrl(flk1):GFP (specifically kdrl(flk1):GRCFP (Cross et al., 2003)); kdrl(flk1):RFP (Huang et al., 2005); cxcl12a(sdf-1a):DsRed2 (Glass et al., 2011); cmyb:EGFP (North et al., 2007); cd41:EGFP (Lin et al., 2005); ubi:EGFP and ubi:mCherry (Mosimann et al., 2011).

Imaging

Staged transgenic zebrafish embryos were selected and mounted for imaging in 1% LMP agarose with E3 media and tricaine as described (Bertrand et al., 2010). Some zebrafish embryos had 0.003% PTU (1-Phenyl-2-thiourea) added to the media to block melanogenesis. Zebrafish embryos and FL explants were imaged in MatTek glass bottom dishes or multi-well plates (No. 1.5 cover slip). Zebrafish live imaging was performed in an incubated chamber at 28°C. Mouse embryo explant live imaging was performed in an incubated chamber at 37°C with humidified CO_2 with culture media (DMEM, 20% FCS,

glutamine, sodium pyruvate, 2-mercaptoethanol, 1% penicillin-streptomycin, recombinant mouse IL-3 (R&D Systems; final concentration 50 ng/ml)). Confocal microscopy was performed using a Yokogawa spinning disk and Nikon inverted Ti microscope. Our microscope configuration allowed imaging of multiple embryos within a 2-5 minute interval using a moving XY stage, as well as acquisition of z-stacks through the entire CHT (1-2 μm optical slices) in multiple fluorescent channels. Objectives lenses (Nikon): 20x Plan-Apo DIC N.A. 0.75; 40x Plan-Apo phase N.A. 0.95 dry; 40x Apo LWD WI NA 1.15 lambda S. Image acquisition was done with a single Andor iXon DU-897 EM-CCD camera (512x512 pixels) or dual Andor iXon x3 EM-CCD cameras (512x512 pixels) and Andor iQ or NIS-elements computer software. Fixed transgenic zebrafish embryos were scanned using a Nikon C2si confocal system and NiE upright microscope. These embryos were briefly fixed for 10 minutes with PEM fixation buffer (dH_20, EGTA 10 mM, MgSO4 1 mM, PIPES 100 mM, Triton X-100 0.1%, PFA 4%; Cold Spring Harbor Protocols, 2009, doi:10.1101/pdb.rec11730), then washed and mounted with DRAQ5 (1:500) for staining of nuclei.

Imaging analysis

Image processing and rendering was done using Fluorender (Wan et al., 2009), Imaris (Bitplane), NIS-elements (Nikon), Volocity (PerkinElmer) and ImageJ/Fiji (Schindelin et al., 2012). The MTrackJ plugin was used for manual cell tracking (Meijering et al., 2012). Lineage trees were created using Endrov (Henriksson et al., 2012). Point-to-point measurements were made with Imaris. Manual tracing, segmentation, and surface

rendering of objects was performed using Imaris. Confocal z-stack images are presented as single slices, maximum projections, or 3D rendered projections. In some cases, background subtraction was performed, and brightness and contrast was adjusted in one or more channels of a multi-channel image.

Immunohistochemistry of adult WKM

Adult zebrafish were fixed with 4% paraformaldehyde, paraffin-embedded, sectioned, and stained with hematoxylin and eosin (H&E). Immunohistochemistry was performed using anti-GFP monoclonal antibody (clone JL-8). The Dako Mouse Envision kit with EDTA antigen retrieval was used for visualization. Incubation in the primary antibody was 60 minutes, and 30 minutes in the secondary, followed by DAB development for 5 minutes and counterstained with hematoxilyn.

Adult-to-Adult HSPC Transplantation

WKM cells from 3-month Runx:mCherry;ubi:GFP fish were isolated and sorted by FACS. Double-positive cells were transplanted into irradiated casper recipients (n=20-48 recipients per cell dose) along with untreated helper marrow at the following ratios: 1:20,000; 5:20,000; 10:20,000; 25:20,000; 50:20,000. Transplantation procedures were performed as previously described (Pugach et al., 2009). At 3 months post-transplant, WKM from recipient fish was collected and analyzed by FACS to detect chimerism levels of mCherry and GFP-positive cells in the marrow. We confirmed multi-lineage

reconstitution by observing differentiated GFP-positive cells in multiple cell populations, as determined by forward and side scatter profiles (Traver et al., 2003). Stem cell frequency was determined using ELDA software (confidence interval=0.95; (Hu and Smyth, 2009)).

Embryo-to-Embryo HSPC Transplantation

Adapted from previously published protocols (Stachura and Traver, 2011; Traver et al., 2003). Runx:mCherry;ubi:EGFP or Runx:GFP;ubi:mCherry 3 dpf embryos were collected and chopped finely with a razor blade. Embryos were dissociated in a 1:65 dilution of Liberase TM (Roche) in PBS, incubated at 37°C for 20 minutes before addition of PBS/5% FCS to stop the reaction. Dissociated cells were passed through a 45 μM filter, spun, and resuspended in PBS/5% FCS. mCherry+/GFP+ cells were collected using a FACSAria cell sorter (BD Biosciences). Collected cells were resuspended in PBS at an estimated concentration of 400 cells/microliter with 0.5% rhodamine-dextran(10k) as a marker for injection. A microinjection needle (without filament) was back-filled with the cell suspension. The drop volume was calibrated to 1 nanoliter and each embryo was injected with 1, 2, or 4 drops. This gave an estimated cell dose of 0.4, 0.8 or 1.6 cells per embryo. Drops were injected into the sinus venosus (i.e. duct of Cuvier) of 48 hpf wild-type AB embryo recipients. Embryos were held in place using agarose injection ramps. Approximately 30 embryos were injected per dose and 12-26 embryos per group survived to adulthood (3-5 months). WKM was then analyzed for percentage of engrafted Runx+ cells using a LSR II flow cytometer (BD Biosciences). Any recipients with positive cells

detected above background were scored as engrafted. Flow cytometry data was analyzed using FACSDiva and FlowJo software.

Serial block face scanning electron microscopy and 3D reconstructions

Immediately at the end of live imaging time-lapse acquisition 60 hpf embryos were fixed in 2.5% glutaraldehyde and 4% paraformaldehyde in a 0.1 M sodium cacodylate buffer. Embryos were embedded in 5% low melting point agarose in 0.1M sodium cacodylate buffer for orientation. Samples were submitted to Renovo Neural Inc (Cleveland, USA) for further processing. Samples were stained with heavy metals following the protocol by Deerinck et al., 2010 (available from the National Center for Microscopy and Imaging Research; http://ncmir.ucsd.edu/sbfsem-protocol.pdf). Samples were embedded in Epon resin, and mounted onto pins (detailed protocol available from Renovo Neural). Serial blockface images (analogous to serial sectioning) were obtained using a Zeiss Sigma VP scanning electron microscope equipped with a Gatan 3View in-chamber ultramicrotome. A series of 500-1000 images were acquired at 2 kV using at 15,000 magnification from the region of interest. Image and stack resolution was 10 nm/pixel with 100 nm slices. Images were registered and resized as necessary using ImageJ/Fiji software (Schindelin et al., 2012). Images were imported into the program IMOD 4.5 (Kremer et al., 1996) then aligned and reconstructed using dual-axis tomography (Mastronarde, 1997). Cells were manually outlined and 3D reconstructions were generated. Movies were rendered using IMOD and Fiji.

Chemicals

Chemical screening was adapted from previously published methods in our lab (Kaufman et al., 2009; North et al., 2007; White et al., 2011). For chemical screening, stage-matched AB embryos were dechorionated and arrayed 8-10/well in 96-well mesh-bottomed plates (Millipore). Embryos were treated with individual library chemicals (~2400 bioactives) from 48-72 hpf by placement directly in 96-well receiver plates containing small molecules diluted in E3 media + 1% DMSO (typical concentration 30 μM). After treatment and before fixation, we checked for secondary defects (e.g. stopped circulation, toxicity, developmental delay). WISH was performed as previously described (Thisse and Thisse, 2008), except 0.2% glutaraldehyde was added to 4% formaldehyde at the post-fixation step. Chemicals used in the study were as follows: AMD3100 (Sigma #A5602, optimal concentration 25 μM in dH_2O, (Schols et al., 1997)); SB-431542 (Sigma #S4317, optimal concentration 40 μM in DMSO, (Inman et al., 2002)); Lycorine (Sigma #L5139, concentration between 25-75 μM in DMSO).

Microarrays

Runx:GFP;kdrl:RFP embryos were collected and raised in E3 media at 28.5C. Embryos were treated from 2-3 dpf with E3/1% DMSO or E3/1%DMOS/75 uM Lycorine (~100-150 embryos per group). Embryos were dissociated and sorted as above. Three populations were collected: GFP+ HSPC (~1-2k cells/experiment), RFP+ EC (~10-20k cells/experiment), and negative cells (~100k cells/experiment; total embryo as a

comparator population). In total, 18 samples were collected: 3 biological replicates x 2 treatment conditions x 3 cell populations. Cells were sorted directly in Trizol LS. Trizol extraction was performed as per the manufacturer's instructions, with the addition of GenElute LPA (Sigma, Cat.#56575). Total RNA was amplified and labeled using the NuGEN Ovation Pico WTA System V2 and Encore Biotin Module kits, respectively. Affymetrix ZebGene-1_0-st microarrays were hybridized, washed, and stained using Ambion kits. Microarrays were scanned using the Genechip Scanner 3000 7G.

All ZebGene-1_0-st array data was processed using the BioConductor (Gentleman et al., 2004) package oligo (Carvalho and Irizarry, 2010). Arrays were assessed for quality with arrayQualityMetrics (Kauffmann et al., 2009) and normalized using the Robust Multichip Average (RMA, (Bolstad et al., 2003)) method at the probe level, collapsing probes into "core" transcripts based on the pd.zebgene.1.0.db annotation package (Benilton Carvalho. pd.zebgene.1.0.st: Platform Design Info for Affymetrix ZebGene-1_0-st. R package version 3.8.0.). Batch correction was performed with the sva (Leek et al., 2012) package and the ComBat method (Johnson et al., 2007). Control probes and those with either mean log transformed intensity values of less than 2.5 or standard deviations of less than 0.1 among all samples were removed. Probes were assigned to genes using Netaffx (Liu et al., 2003) annotations (ZebGene-1_0-st-v1.na33.3.zv9.transcript.csv); probes were not combined at the gene level, but were treated as independent assays. Differential expression statistics for pairwise and three-way (interaction terms) comparisons were generated by linear model for microarray data analysis (limma) (Smyth, 2004) using empirical Bayes shrinkage methods. Differentially expressed genes were assessed as

those with least a log fold expression change of 1 and an FDR (Benjamini and Hochberg, 1995) based adjusted p-value of less than 0.25. Genes annotated with a zebrafish Entrez Gene ID were used for "Ingenuity Pathway Analysis" (IPA; QIAGEN, www.qiagen.com/ingenuity).

Fetal liver preparations

Live fetal liver explants: Pregnant wild-type C57/BL6 and Ly6a-GFP mice were dissected at E11-11.5 (vaginal plug observation was E0). Embryos were removed from the uterus in PBS with 10% FCS and penicillin-streptomycin. Embryos were staged as E11-E11.5 by counting >42 somite pairs. FLs were removed from the embryo and treated as described by Boisset and colleagues ("protocol b") (Boisset et al., 2010). Conjugated antibodies used for detection were CD31-FITC (PECAM-1, BD Biosciences, Rat anti-mouse, clone MEC 13.3) and c-kit-APC (CD117, BD Biosciences, Rat anti-mouse, clone 2B8).

Fixed fetal livers: Embryos were dissected as above and fixed in 2% PFA on ice for 20 minutes. Embryos were then rinsed and dehydrated in methanol. FLs were removed, mounted, cleared and imaged using the method by Yokomizo et al. (Yokomizo et al., 2012). Livers from E11.5 Ly6a-GFP mice were stained with rat anti-CD144, rabbit anti-RUNX1, and chicken anti-GFP. Primary and secondary antibody details are below. Specimens were scanned using a Zeiss LSM 710 confocal microscope with a 25x oil objective. Images were acquired using multi-track sequential mode and Zeiss Zen

software. Pinhole was set at 1 Airy unit, steps were 1.14 μm per z-section. 3D projections were made using Volocity software.

Primary antibodies: anti-CD144 (VE-cadherin) (BD Pharmingen, Catalog# 550548, Clone: 11D4.1, Isotype: Rat IgG2a, κ); anti-RUNX1 rabbit (Abcam, Catalog# ab92336, Clone # EPR3099); anti-GFP Chicken IgY (Invitrogen/Life technologies, Catalog# A10262).

Secondary antibodies: Goat Anti-Rabbit IgG (H+L) Alexa Fluor® 488 (Invitrogen/Life technologies, Catalog# A-11034); Goat Anti-Rabbit IgG (H+L) Alexa Fluor® 647 (Abcam, Catalog# 150079); Goat Anti-Chicken IgY (IgG) (H+L) Alexa Fluor® 647 (Jackson, Catalog# 103-605-155); Goat Anti-Rat IgG (H+L) Alexa Fluor® 555 (Abcam, Catalog# ab150158); Goat anti-chicken IgG (H+L) Alexa Fluor® 488 (Invitrogen/ Life Technologies, Catalog# A11039).

Supplemental References

Benjamini, Y., and Hochberg, Y. (1995). Controlling the false discovery rate: a practical and powerful approach to multiple testing. Journal of the Royal Statistical Society Series B (Methodological), 289-300.

Bertrand, J.Y., Chi, N.C., Santoso, B., Teng, S., Stainier, D.Y.R., and Traver, D. (2010). Haematopoietic stem cells derive directly from aortic endothelium during development. Nature *464*, 108-111.

Boisset, J.-C., Van Cappellen, W., Andrieu-Soler, C., Galjart, N., Dzierzak, E., and Robin, C. (2010). In vivo imaging of haematopoietic cells emerging from the mouse aortic endothelium. Nature *464*, 116-120.

Bolstad, B.M., Irizarry, R.A., Astrand, M., and Speed, T.P. (2003). A comparison of normalization methods for high density oligonucleotide array data based on variance and bias. Bioinformatics *19*, 185-193.

Carvalho, B.S., and Irizarry, R.A. (2010). A framework for oligonucleotide microarray preprocessing. Bioinformatics *26*, 2363-2367.

Cross, L.M., Cook, M.A., Lin, S., Chen, J.N., and Rubinstein, A.L. (2003). Rapid analysis of angiogenesis drugs in a live fluorescent zebrafish assay. Arterioscler Thromb Vasc Biol *23*, 911-912.

Gentleman, R.C., Carey, V.J., Bates, D.M., Bolstad, B., Dettling, M., Dudoit, S., Ellis, B., Gautier, L., Ge, Y., Gentry, J.*, et al.* (2004). Bioconductor: open software development for computational biology and bioinformatics. Genome Biol *5*, R80.

Glass, T.J., Lund, T.C., Patrinostro, X., Tolar, J., Bowman, T.V., Zon, L.I., and Blazar, B.R. (2011). Stromal cell-derived factor-1 and hematopoietic cell homing in an adult zebrafish model of hematopoietic cell transplantation. Blood *118*, 766-774.

Henriksson, J., Hench, J., Abou-Zied, A., Lüppert, M., Dethlefsen, J., Tong, Y.-G., Tang, L., Baillie, D., and Bürglin, T. (2012). Endrov – An integrated platform for image analysis and systems biology. Manuscript in preparation.

Hu, Y., and Smyth, G.K. (2009). ELDA: extreme limiting dilution analysis for comparing depleted and enriched populations in stem cell and other assays. Journal of Immunological Methods *347*, 70-78.

Huang, H., Zhang, B., Hartenstein, P.A., Chen, J.N., and Lin, S. (2005). NXT2 is required for embryonic heart development in zebrafish. BMC Dev Biol *5*, 7.

Inman, G.J., Nicolas, F.J., Callahan, J.F., Harling, J.D., Gaster, L.M., Reith, A.D., Laping, N.J., and Hill, C.S. (2002). SB-431542 is a potent and specific inhibitor of transforming growth factor-beta superfamily type I activin receptor-like kinase (ALK) receptors ALK4, ALK5, and ALK7. Mol Pharmacol *62*, 65-74.

Johnson, W.E., Li, C., and Rabinovic, A. (2007). Adjusting batch effects in microarray expression data using empirical Bayes methods. Biostatistics *8*, 118-127.

Kauffmann, A., Gentleman, R., and Huber, W. (2009). arrayQualityMetrics--a bioconductor package for quality assessment of microarray data. Bioinformatics *25*, 415-416.

Kaufman, C.K., White, R.M., and Zon, L. (2009). Chemical genetic screening in the zebrafish embryo. Nature Protocols *4*, 1422-1432.
Kremer, J.R., Mastronarde, D.N., and McIntosh, J.R. (1996). Computer visualization of three-dimensional image data using IMOD. Journal of structural biology *116*, 71-76.
Kwan, K.M., Fujimoto, E., Grabher, C., Mangum, B.D., Hardy, M.E., Campbell, D.S., Parant, J.M., Yost, H.J., Kanki, J.P., and Chien, C.-B. (2007). The Tol2kit: a multisite gateway-based construction kit for Tol2 transposon transgenesis constructs. Developmental dynamics : an official publication of the American Association of Anatomists *236*, 3088-3099.
Leek, J.T., Johnson, W.E., Parker, H.S., Jaffe, A.E., and Storey, J.D. (2012). The sva package for removing batch effects and other unwanted variation in high-throughput experiments. Bioinformatics *28*, 882-883.
Lin, H.-F., Traver, D., Zhu, H., Dooley, K., Paw, B.H., Zon, L.I., and Handin, R.I. (2005). Analysis of thrombocyte development in CD41-GFP transgenic zebrafish. Blood *106*, 3803-3810.
Liu, G., Loraine, A.E., Shigeta, R., Cline, M., Cheng, J., Valmeekam, V., Sun, S., Kulp, D., and Siani-Rose, M.A. (2003). NetAffx: Affymetrix probesets and annotations. Nucleic Acids Res *31*, 82-86.
Mastronarde, D.N. (1997). Dual-axis tomography: an approach with alignment methods that preserve resolution. Journal of structural biology *120*, 343-352.
Meijering, E., Dzyubachyk, O., and Smal, I. (2012). Methods for cell and particle tracking. Methods Enzymol *504*, 183-200.
Mosimann, C., Kaufman, C.K., Li, P., Pugach, E.K., Tamplin, O.J., and Zon, L.I. (2011). Ubiquitous transgene expression and Cre-based recombination driven by the ubiquitin promoter in zebrafish. Development (Cambridge, England) *138*, 169-177.
North, T.E., Goessling, W., Walkley, C.R., Lengerke, C., Kopani, K.R., Lord, A.M., Weber, G.J., Bowman, T.V., Jang, I.-H., Grosser, T.*, et al.* (2007). Prostaglandin E2 regulates vertebrate haematopoietic stem cell homeostasis. Nature *447*, 1007-1011.
Nottingham, W.T., Jarratt, A., Burgess, M., Speck, C.L., Cheng, J.-F., Prabhakar, S., Rubin, E.M., Li, P.-S., Sloane-Stanley, J., Kong-A-San, J.*, et al.* (2007). Runx1-mediated hematopoietic stem-cell emergence is controlled by a Gata/Ets/SCL-regulated enhancer. Blood *110*, 4188-4197.
Pugach, E.K., Li, P., White, R., and Zon, L. (2009). Retro-orbital injection in adult zebrafish. Journal of visualized experiments : JoVE.
Schindelin, J., Arganda-Carreras, I., Frise, E., Kaynig, V., Longair, M., Pietzsch, T., Preibisch, S., Rueden, C., Saalfeld, S., Schmid, B.*, et al.* (2012). Fiji: an open-source platform for biological-image analysis. Nat Methods *9*, 676-682.
Schols, D., Struyf, S., Van Damme, J., Este, J.A., Henson, G., and De Clercq, E. (1997). Inhibition of T-tropic HIV strains by selective antagonization of the chemokine receptor CXCR4. J Exp Med *186*, 1383-1388.
Smyth, G.K. (2004). Linear models and empirical bayes methods for assessing differential expression in microarray experiments. Statistical applications in genetics and molecular biology *3*, Article3.
Stachura, D.L., and Traver, D. (2011). Cellular dissection of zebrafish hematopoiesis. Methods in cell biology *101*, 75-110.

Thisse, C., and Thisse, B. (2008). High-resolution in situ hybridization to whole-mount zebrafish embryos. Nature Protocols *3*, 59-69.
Traver, D., Paw, B.H., Poss, K.D., Penberthy, W.T., Lin, S., and Zon, L.I. (2003). Transplantation and in vivo imaging of multilineage engraftment in zebrafish bloodless mutants. Nature Immunology *4*, 1238-1246.
Wan, Y., Otsuna, H., Chien, C.B., and Hansen, C. (2009). An interactive visualization tool for multi-channel confocal microscopy data in neurobiology research. IEEE Trans Vis Comput Graph *15*, 1489-1496.
White, R.M., Cech, J., Ratanasirintrawoot, S., Lin, C.Y., Rahl, P.B., Burke, C.J., Langdon, E., Tomlinson, M.L., Mosher, J., Kaufman, C*., et al.* (2011). DHODH modulates transcriptional elongation in the neural crest and melanoma. Nature *471*, 518-522.
Yokomizo, T., Yamada-Inagawa, T., Yzaguirre, A.D., Chen, M.J., Speck, N.A., and Dzierzak, E. (2012). Whole-mount three-dimensional imaging of internally localized immunostained cells within mouse embryos. Nat Protoc *7*, 421-431.

Figure S1 - further characterization of the Runx lines

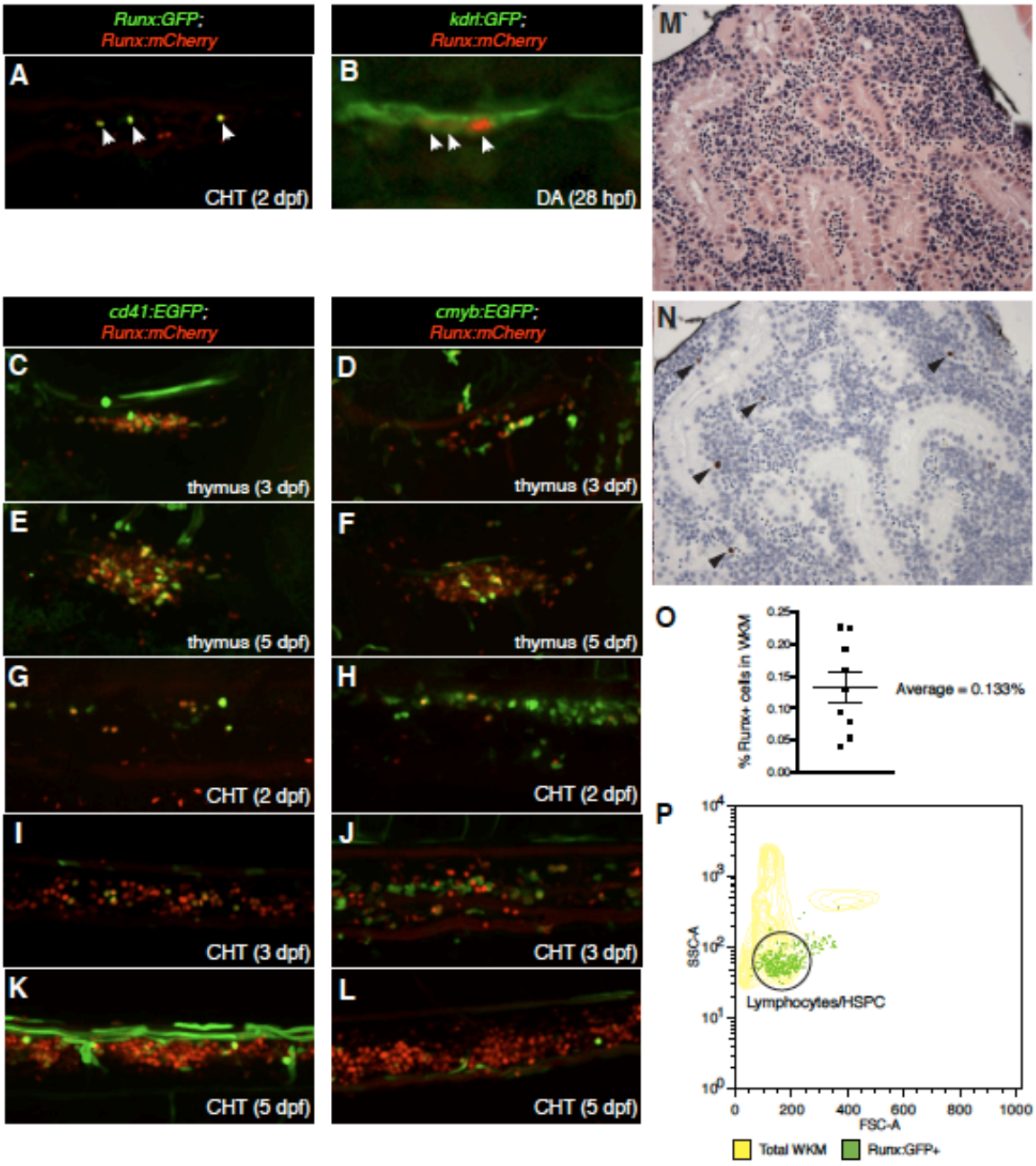

Figure S2. Runx:mCherry/ubi:GFP transplantation, cutoff for scored engraftment 0.001%

A

Embryo-to-embryo transplantation

Cell Dose	Recipients	Engrafted (%)
0.4	15	9 (60)
0.8	12	6 (50)
1.6	18	16 (89)

Confidence intervals for 1/(stem cell frequency)

Lower	Estimate	Upper
1.55	1.34	1.15

B

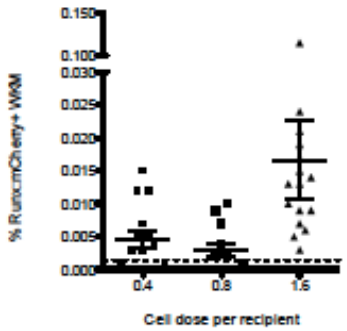

C

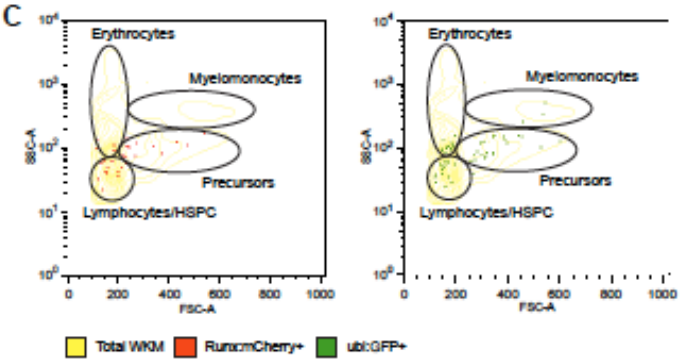

Figure S3. Cuddling time-lapse details

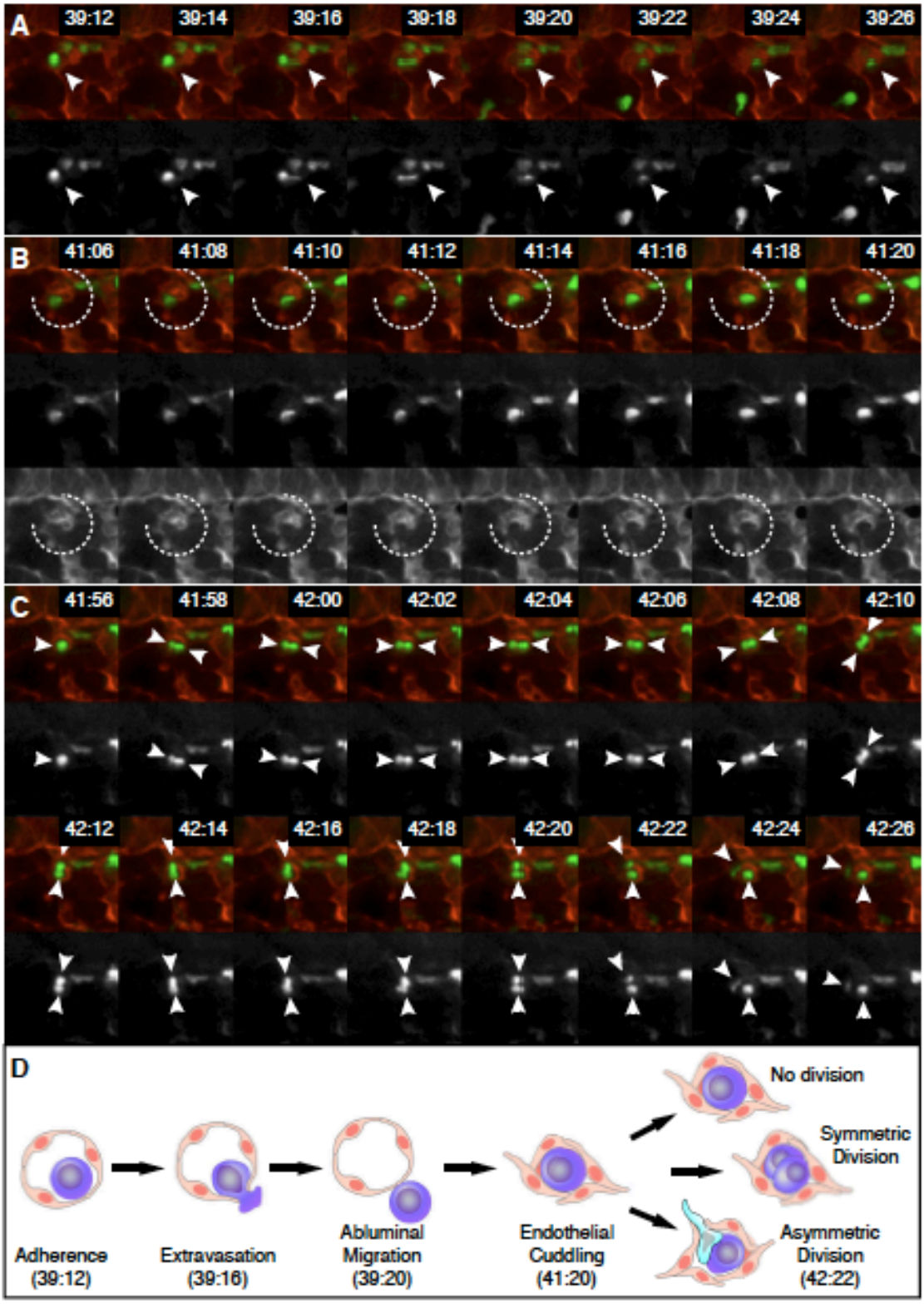

Figure S4. Serial block face scanning EM of CHT after time-lapse

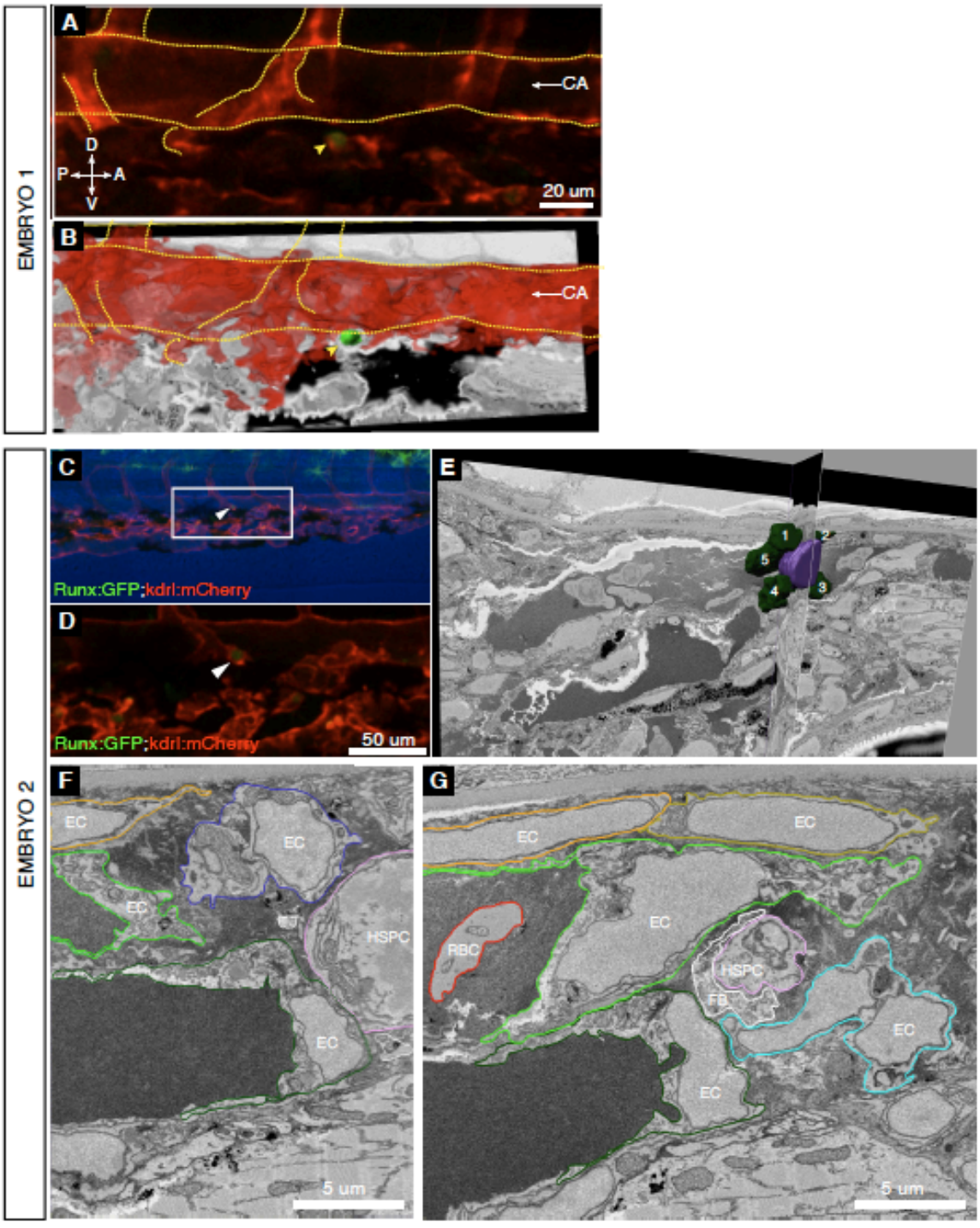

Figure S5. cxcr4/cxcl12 expression patterns - dose-dependent AMD3100 treatments

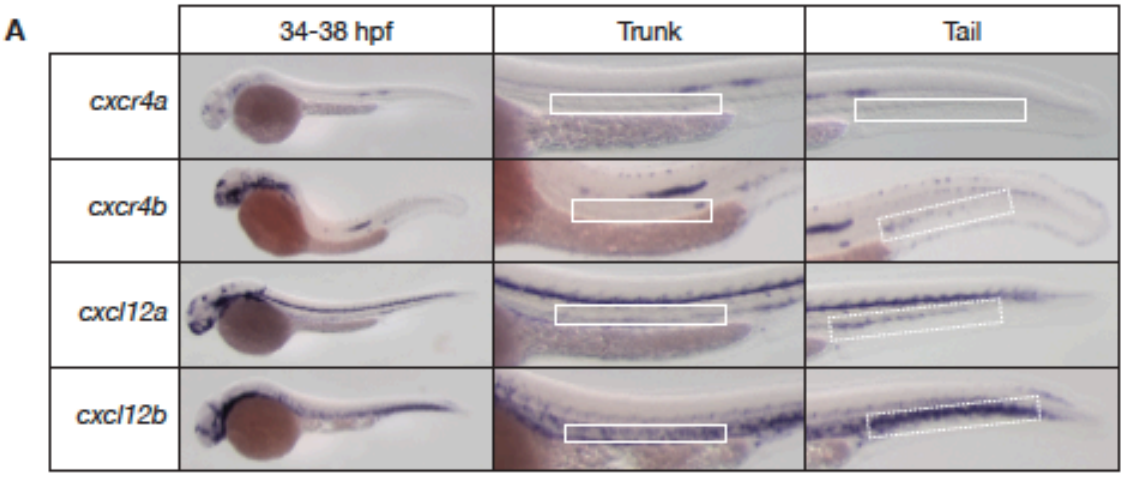

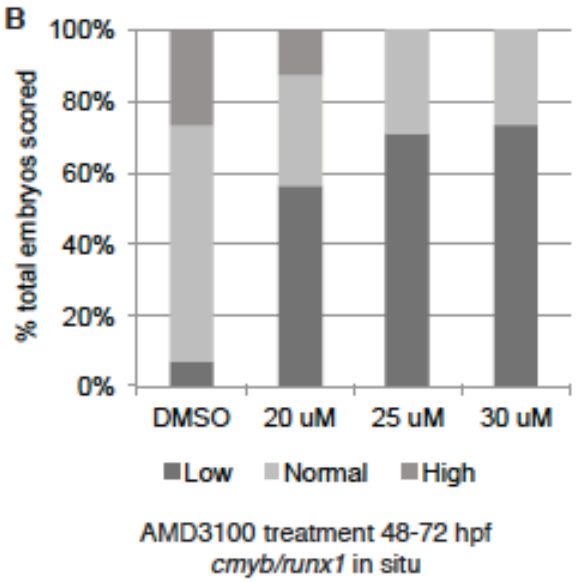

Figure S6. Second example of time-lapse FL explant

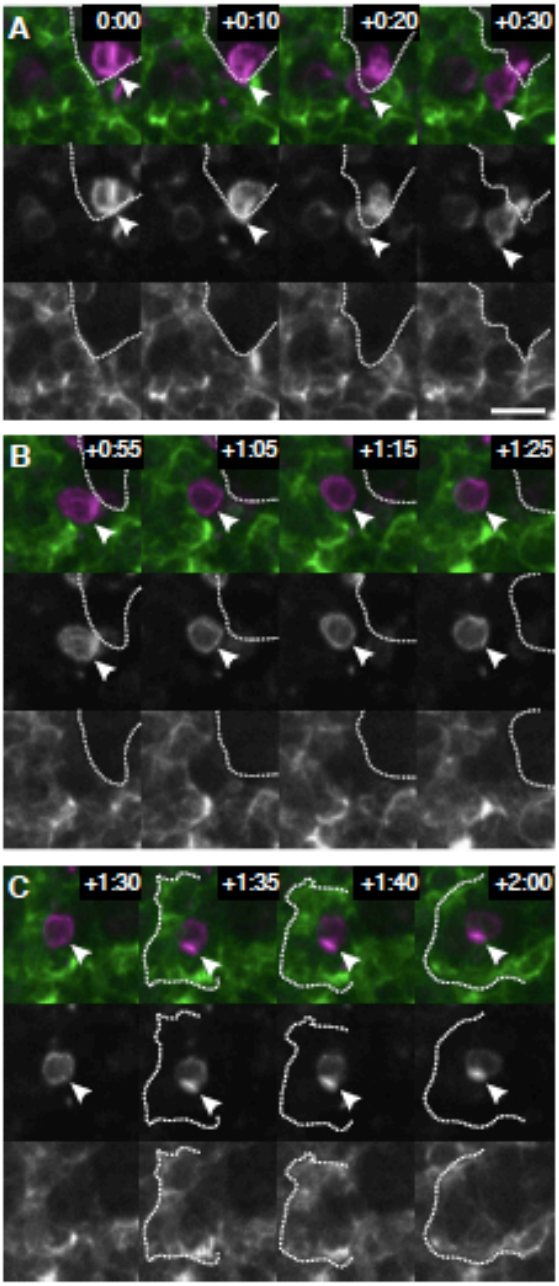

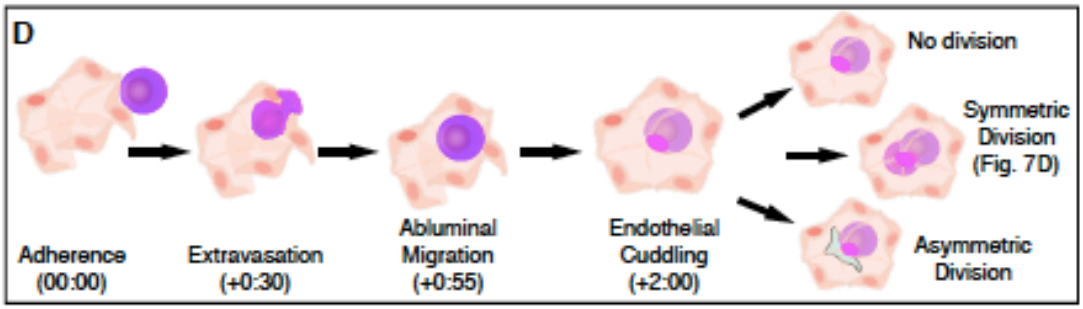

Table S1A. Ingenuity Pathway Analysis (IPA) of EC in Lycorine-treated embryos

Category	*Diseases or Functions Annotation*	*p-Value*	*Activation z-score*	*Molecules*	*# Molecules*
Cell-To-Cell Signaling and Interaction	adhesion of immune cells	5.60E-03	-1.917	BDKRB1, CXCR4, ERG, F10, FLT1, FUT7, MYADM, PODXL, SPON2, VTN	10
Cell-To-Cell Signaling and Interaction	attachment of cells	2.52E-03	-1.408	FBLN5, FUT7, LOX, MBL2, PODXL, VTN	6
Cell-To-Cell Signaling and Interaction	adhesion of endothelial cells	8.09E-05	-1.195	BDKRB1, CXCR4, EDIL3, F10, FBLN5, FLT1, MYADM, VTN	8
Cellular Movement	extravasation	9.36E-03	-1.982	CXCR4, FUT7, MIA, MMP10	4

Table S1B. Ingenuity Pathway Analysis (IPA) of HSPC in Lycorine-treated embryos

Category	*Diseases or Functions Annotation*	*p-Value*	*Activation z-score*	*Molecules*	*# Molecules*
Cell-To-Cell Signaling and Interaction	activation of cells	2.21E-03	-1.382	ADORA2A, ADRB3, CD63, CD74, CORO1A, DCT, EPX, F10, GABRA1, Gh, GP2, HOXA9, IRAK3, MAP3K14, MMP9, NFATC2, NFKB2, PMP2, RAB27A, SERPINE2, SOCS1, SQSTM1, TLR5, TNFAIP8L2, VTN	25
Cell-To-Cell Signaling and Interaction	activation of blood cells	6.47E-03	-1.039	ADORA2A, CD63, CD74, CORO1A, DCT, EPX, F10, Gh, GP2, MMP9, NFATC2, NFKB2, PMP2, RAB27A, SERPINE2, SOCS1, TLR5, TNFAIP8L2, VTN	19
Cell-To-Cell Signaling and Interaction	activation of leukocytes	8.66E-03	-1.665	ADORA2A, CD63, CD74, CORO1A, DCT, EPX, F10, Gh, GP2, MMP9, NFATC2, NFKB2, PMP2, RAB27A, SOCS1, TLR5, TNFAIP8L2	17
Cell-To-Cell Signaling and Interaction	adhesion of blood cells	1.06E-02	-2.174	A2M, ADORA2A, ADRB2, BDKRB1, CD74, CORO1A, F10, MAP3K14, NFKB2, PIP5K1C, VTN	11

Newly emerging roles for prostaglandin E_2 regulation of hematopoiesis and hematopoietic stem cell engraftment

Ellen M. Durand and Leonard I. Zon

Children's Hospital, Boston, Massachusetts, USA

Correspondence to Leonard I. Zon, Stem Cell Program and Division of Hematology/Oncology, Children's Hospital Boston and Dana-Farber Cancer Institute, Howard Hughes Medical Institute, Harvard Stem Cell Institute, Harvard Medical School, Boston, MA 02115, USA
Tel: +1 617 919 2069; fax: +1 617 730 0222; e-mail: zon@enders.tch.harvard.edu

Current Opinion in Hematology 2010, 17:308–312

Purpose of review

Hematopoietic stem cell (HSC) transplantation is an effective treatment for leukemia, lymphoma, blood disorders, and autoimmune diseases. Successful transplantation is dependent upon efficient homing and engraftment of HSCs. Recently, prostaglandin E_2 (PGE_2) exposure, either *in vivo* or *ex vivo*, has been shown to increase engraftment. These results establish PGE_2 as a regulator of hematopoietic development.

Recent findings

The underlying mechanisms of PGE_2 regulation of HSC development were poorly understood until recently. Ex-vivo exposure of LSK cells to PGE_2 results in increased homing efficiency of HSCs to the murine bone marrow compartment. In addition, in-vivo treatment with PGE_2 preferentially expands short-term HSCs without affecting long-term HSC number and engraftment in murine bone marrow. PGE_2 acts through EP4 receptors to mediate lymphoid precursor development in the zebrafish. An in-vivo interaction between PGE_2 and the Wnt signaling pathways controls HSC engraftment.

Summary

PGE_2 has a new role in HSC homing and survival, as well as short-term-HSC engraftment. PGE_2 is currently being tested in clinical trials as a potential therapy to enhance HSC engraftment following a transplantation procedure.

Keywords

engraftment, homing, hematopoietic stem cells, prostaglandin E_2

Curr Opin Hematol 17:308–312

1065-6251

Introduction

Hematopoietic cell transplantation (HCT) is achieved through transplantation of bone marrow, peripheral blood, or umbilical cord blood-derived hematopoietic stem cells (HSCs) and progenitor cells (HSPCs). Patients requiring bone marrow transplantation (BMT) face many possible complications due to myeloablation including infection, anemia and thrombocytopenia. Proper migration of HSCs to marrow niches and repopulation of the hematopoietic system is essential for engraftment, and thus recovery, following HSCT. Enhancing HSPC frequency will shorten the time to engraftment and thus diminish these risk factors in myeloablated patients. Recent studies have shown that prostaglandin E_2 (PGE_2) increases HSC number as well as short-term engraftment in the murine system. This review will address recent findings regarding PGE_2 as a regulator of hematopoiesis and HSC self-renewal and differentiation. Additionally, the use of PGE_2 as a potential therapeutic agent for patients undergoing hematopoietic cell transplantation will be explored.

Hematopoietic development

Hematopoiesis is a life-long process in which HSCs differentiate into all mature blood cells through the production of progenitor cells [1,2]. HSCs are a rare cell population with the ability to both self-renew and differentiate [3]. The first long-term HSCs are detected in the murine aorta–gonad–mesonephros (AGM) region by embryonic day 10.5 and continue to colonize the fetal liver, thymus, spleen, and bone marrow [4].

HSCs are valuable in a clinical setting for patients requiring hematopoietic repair. Preconditioning for HSCT entails ablation of the recipients' bone marrow, resulting in diminished hematopoietic output. Transplanted HSCs must efficiently home to the niche, differentiate, and repopulate the host hematopoietic system. It is important to understand signals that regulate HSC development as they may provide insight for potential therapeutics regarding HSCT [5]. In addition to therapeutic applications, transplantation assays provide a method by which the self-renewal capabilities of HSCs can be assessed.

1065-6251 © 2010 Wolters Kluwer Health | Lippincott Williams & Wilkins DOI:10.1097/MOH.0b013e32833a888c

A single transplanted HSC has the ability to reconstitute the entire hematopoietic system of an irradiated recipient [6]. Cell populations enriched for HSCs can be isolated by FACS using antibodies against certain cell surface proteins. Murine HSCs express stem cell antigen 1 (Sca1) and c-Kit, but lack lineage-specific surface markers. A $Lin^-Sca1^+Kit^+$ (LSK) population enriched for HSCs can be further separated for HSCs with differing self-renewal potential using additional markers such as CD34, CD38, and CD150 [7].

Prostaglandin E_2

Prostaglandins are lipid compounds of the eicosanoid family that play a major role in inflammatory and immune response as well as various other tissue responses [8,9]. Prostaglandins are found in a majority of tissues and are produced by a number of cell types. When synthesized, prostaglandins function locally as autocrine or paracrine lipid mediators.

Synthesis and roles of prostaglandin E *in vivo*

PGE_2 has established roles in platelet aggregation in response to stimulus, smooth muscle relaxation, bronchodilation, and gastric-acid production [10]. In addition, prostaglandins are key players of inflammation, pain, and fever. PGE_2 has also been shown to play a role in T helper cell differentiation and function [11,12•]. PGE_2 synthesis can be abrogated using nonsteroidal anti-inflammatory drugs (NSAIDs), such as indomethacin, designed to block cyclooxygenase (Cox)1/2 [13]. Prostaglandins are derived from arachidonic acid, which is oxidized by Cox-1 and Cox-2 to form PGG_2. PGG_2 is subsequently reduced to PGH_2, from which all three classes of prostaglandins originate. Prostaglandin E synthase acts on PGH_2 to produce PGE_2 [14]. Cox-1 is constitutively expressed in most tissues, whereas Cox-2 is silenced during normal physiological conditions but can rapidly activate downstream targets during times of stress.

Prostaglandin E_2 receptors

PGE_2 acts via four G-protein coupled E-prostanoid receptors (EP1–4), resulting in various and sometimes opposing downstream effects [15]. PGE_2 has been shown to be both a vasodilator (in arterial and venous beds) and a vasoconstrictor (in the trachea and intestine), supporting evidence of multiple functional E-prostanoid receptors [16]. These receptors are loosely classified based on their function as relaxants or constrictors of smooth muscle cells. EP2 and EP4 are 'relaxant' receptors and result in production of 3′-5′-cyclic adenosine monophosphate (cAMP) upon binding of PGE_2. Despite this common pathway, additional unique functions have been shown for each receptor. PGE_2 bound to EP2 but not EP4 can result in activation of the EGF receptor leading to increased invasion of colon cancer cells. In addition, binding of PGE_2 to EP4 but not EP2 can lead to activation of the glycogen synthase kinase-3 (GSK-3)/β-catenin signaling pathway via phosphoinositide 3-kinase. In contrast, EP1 receptors are 'constrictors' as binding of PGE_2 increases intracellular calcium levels in smooth muscle cells. The diverse effects of PGE_2 signaling are furthered demonstrated through EP3 receptor activity. Different splice variants of EP3 receptors have been implicated in cAMP induction and inhibition, as well as generation of IP_3. In addition, PGE_2 binds E-prostanoid receptors with different affinities, with a higher affinity for EP3 and EP4, and a lower affinity for EP1 and EP2 [17].

Prostaglandin E_2 in hematopoietic stem cell regulation

PGE2 has been implicated as a regulator of hematopoietic homeostasis for many years. An example is the defined role of Cox-2 and PGE2 in lymphoid progenitor development, reviewed in [5]. From previous in-vitro and in-vivo studies on PGE2 and hematopoietic progenitors, PGE2 appeared to block differentiation of myeloid progenitors and enhance erythroid progenitors. In addition, there was a lack of a clear understanding of the mechanism of PGE2 action on hematopoietic cells.

Hematopoietic stem cell effects

A recent study by North *et al.* [18] provided evidence of PGE_2 as a regulator of HSC specification in the zebrafish. A chemical screen was performed to identify mediators of HSC formation during embryogenesis. Zebrafish embryos treated with a long-acting derivative of PGE_2, 16,16-dimethyl-PGE_2 ($dmPGE_2$) from 3-somite stage (ss) until 36 h postfertilization (hpf) displayed an increase in *runx1/cmyb* expression in the dorsal aorta. Expressions of these markers were used as a proxy for HSCs as both are expressed in all HSCs and are required for proper HSC generation in the AGM region [19,20]. Treatment with $dmPGE_2$ led to an increase in HSC numbers as seen by *runx1/cmyb* in-situ staining at 36 hpf. In addition, drugs that activated the PGE_2 pathway resulted in increased HSCs, whereas drugs inhibiting the pathway decreased HSC number. Endogenous requirement for PGE_2 was confirmed using morpholino knock out of Cox-1 and Cox-2, resulting in decreased HSCs in the AGM region. Irradiation recovery experiments were used as an injury model to demonstrate HSPC activation. Treatment with $dmPGE_2$ enhanced the rate of kidney marrow recovery in irradiated recipients compared with control treated animals, suggesting PGE_2 as a potential therapy to improve the recovery time of myeloablated patients.

The conservation of the PGE_2 effect was tested using murine transplantation assays. Bone marrow cells were

treated *ex vivo* with PGE_2 and transplanted into irradiated recipients to assess either short-term progenitor potential or long-term-HSC function. Colony forming units (CFU-S) assays demonstrated that PGE_2 enhances HSPC activity. Limiting dilution competitive repopulation analysis showed that *ex vivo* PGE_2 treatment increased the number of repopulating HSCs without disrupting differentiation.

Hematopoietic stem cell homing and survival

These studies defined a role for PGE_2 in HSCs; however, the mechanism remained largely unknown. A recent study by Hoggatt *et al.* [21••] examined HSC homing, survival, and proliferation as possible mechanisms underlying PGE_2 effects on HSCs in the murine system. The authors confirmed enhanced murine HSC engraftment following exposure to PGE_2, observing a four-fold increase in HSCs up to 20 weeks following transplantation. PGE_2-induced increased chimerism was still present in recipient animals at 32 weeks post transplant. Whole bone marrow (WBM) harvested from primary recipients at 20 weeks post transplant maintained PGE_2-induced enhancement of HSC frequency in secondary recipients without additional PGE_2 treatment. These findings suggest that short-term PGE_2 exposure results in a long-term repopulation advantage of transplanted WBM.

The effects of PGE_2 on HSCs could be the result of an increase in HSC number, homing capability, proliferation, survival, or a combination thereof. To evaluate the homing capabilities of PGE_2-treated WBM and the LSK cell population, CFSE-labeled cells were transplanted into irradiated recipients. Consistent with results reported by North *et al.* [18], no significant difference in the percentage of $CFSE^+$ cells were seen in PGE_2 treated WBM compared with control. In contrast to previous studies using WBM, a significant increase in homing of PGE_2-treated LSK cells to recipient marrow was observed compared with control (Fig. 1). To determine whether this effect also occurs in human HSCs, PGE_2-treated umbilical cord blood (UCB) cells were transplanted into NOD/SCID mice [22]. Consistent with the LSK results, PGE_2-treated UCB cells displayed enhanced homing to the marrow. This homing effect is partially attributed to an increase in CXCR4 expression following PGE_2 treatment. CXCR4 is a receptor specific for stromal cell-derived factor-1α (SDF-1α) and has been shown to play a role in HSPC homing to the bone marrow [23]. PGE_2 treatment of LSK and $CD34^+$ cells increased expression of CXCR4.

Figure 1 Bone marrow cells from CD45.1 mice treated with PBS, vehicle, or dmPGE_2 and transplanted into lethally irradiated CD45.2 mice

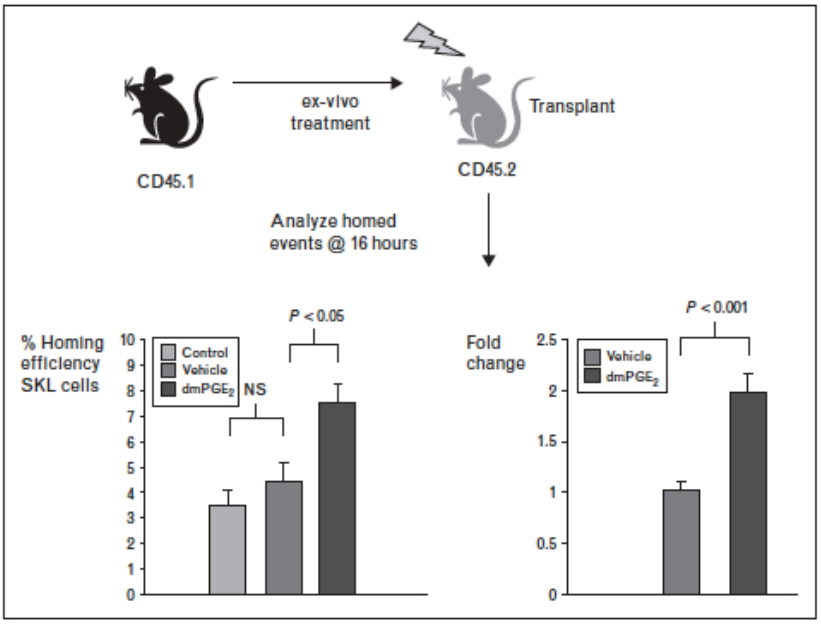

Bone marrow was analyzed for homed SKL cells after 16 h. Reproduced with permission from [21••].

In addition to homing effects, a role of PGE_2 in survival and proliferation was tested. Survivin, an important regulator of HSC survival and proliferation, was increased in LSK and UCB cells following pulse treatment with PGE_2. Supporting a role in long-term-HSC proliferation, SLAM LSK cells treated with PGE_2 displayed a significant increase in the percentage of cycling cells.

Effects of in-vivo prostaglandin E_2 treatment

Until recently there existed no data for in-vivo treatment of PGE_2 in the murine system [24]. Frisch *et al.* [25••] adapted a PGE_2 treatment regimen previously shown in rats. Mice were treated using intraperitoneal injection twice a day (6 mg/kg) for 16 days. Consistent with previous in-vitro data, it was observed that in-vivo PGE_2 treatment significantly increased the LSK population without disrupting hematopoietic differentiation. To determine which subpopulation(s) in LSK cells are directly affected by PGE_2, SLAM receptors were used to distinguish the long-term-HSC subset from short-term-HSCs and multipotent progenitors (MPPs). In-vivo PGE_2 treatment preferentially increased the short-term-HSC/MPP subpopulation without changing the frequency of long-term-HSCs. Consistent with ex-vivo treatment transplant assays, transplanted cells from mice treated with PGE_2 *in vivo* demonstrated increased engraftment and hematopoietic reconstitution of host animals. Also, this competitive advantage was eventually lost, in this case at 6 weeks posttransplant.

In contrast with ex-vivo data, the advantage of PGE_2-mediated reconstitution was lost first in the myeloid lineage. Secondary transplants were performed at 36 weeks following primary transplant (compared with 20 weeks in ex-vivo experiments). No significant difference in hematopoietic reconstitution of PGE_2 treated cells versus control cells was observed in secondary recipients. This data suggests that long-term in-vivo exposure to PGE_2 has no adverse effects on long-term repopulation but may instead selectively impact HSPCs with limited self-renewal capabilities. The disparities between ex-vivo and in-vivo secondary transplant data may be the result of long-term exposure of mice to PGE_2 (twice daily for 16 days) compared with a short-term pulse (2 h). It has previously been shown that long-term treatment of Chinese hamster ovary (CHO) cells with PGE_2 resulted in downregulation of EP2 and EP4 receptors [26,27]. It is possible that receptor internalization or desensitization in response to prolonged exposure to PGE_2 prevents the long-term advantages observed in the ex-vivo system.

Prostaglandin E_2 and Wnt signaling interactions

Biochemical data suggested that PGE_2 signaling cross talks with the Wnt signaling pathway [28]. A recent study by Goessling *et al.* [29••] demonstrated an in-vivo conserved genetic interaction between PGE_2 and Wnt at the level of the β-catenin stabilization in the zebrafish.

Prostaglandin E_2/Wnt regulation of hematopoietic stem cell development

The authors showed that treatment with PGE_2 significantly increased expression of a β-catenin responsive GFP reporter in the AGM region, whereas indomethacin treatment decreased activity. Colocalization of the GFP reporter and *lmo2* indicated Wnt activity was present in HSCs and endothelial cells of the dorsal aorta. Induction of Wnt signaling during embryogenesis increased the *runx1*$^+$ population in the AGM; however, PGE_2 appears to be required for this effect as treatment with indomethacin blocked this increase. A zebrafish *cmyb*:GFP reporter line was used to demonstrate that PGE_2 and Wnt signaling synergize to increase HSC number in the AGM. Combined treatment of PGE_2 and Wnt activation enhanced the effect of Wnt activation alone. These results suggest that PGE_2 is required for Wnt-mediated effects on HSC development and can enhance Wnt activity in-vivo.

PGE_2 treatment or activation of Wnt signaling decreased TUNEL$^+$ cells in the AGM whereas indomethacin treatment increased TUNEL$^+$ cells. BrdU incorporation of cells in the AGM was significantly enhanced by both Wnt activation and PGE_2 treatment, but was inhibited by indomethacin treatment. These results suggest that PGE_2 may mediate the effects of Wnt signaling on HSCs through apoptosis and proliferation during embryonic development. PGE_2/Wnt interaction was tested in the adult zebrafish using a kidney marrow recovery assay. FACS analysis of recovering marrow indicated that Wnt activation significantly increased the HSPC population and this was blocked by indomethacin. These results support interplay of PGE_2 and Wnt signaling in the adult zebrafish.

To determine whether this interaction is conserved in mammals, purified LSK cells were transplanted into irradiated mice. Recipients were treated with 6-bromoindirubin-3′-oxime (BIO), a GSK-3β inhibitor, indomethacin, or both. CFU-S assays following treatment demonstrated an increase in progenitor cells after BIO treatment; this effect was reduced to baseline levels upon treatment of indomethacin, demonstrating that PGE_2 mediates Wnt activity on mammalian hematopoietic progenitor cells.

Moving to the clinic

Clinical trials are currently underway to test PGE_2 as a potential therapy to enhance HSC engraftment following cord blood transplantation. This is for patients with leukemia or lymphoma who are receiving two cord blood

units for hematopoietic reconstitution. One of the cord blood samples is treated with dmPGE_2, and relative blood cell engraftment over time is being monitored.

Conclusion

Recent findings regarding the role of PGE_2 in HSC formation, regulation, and engraftment potential following transplantation have important clinical applications. HSCT is a necessary treatment for patients with hematologic cancers and disorders but has many associated complications. These results implicate PGE_2 as a possible treatment to facilitate HSC engraftment and hematopoietic reconstitution following HSCT.

Acknowledgements

We thank Teresa Bowman and Pulin Li for their critical reading of this manuscript.

L.I.Z. is a founder and stockholder of FATE inc. and a scientific advisor for Stemgent.

References and recommended reading

Papers of particular interest, published within the annual period of review, have been highlighted as:

- • of special interest
- •• of outstanding interest

Additional references related to this topic can also be found in the Current World Literature section in this issue (pp. 377–379).

1 Shizuru JA, Negrin RS, Weissman IL. Hematopoietic stem and progenitor cells: clinical and preclinical regeneration of the hematolymphoid system. Annu Rev Med 2005; 56:509–538.

2 Kondo M, Wagers AJ, Manz MG, *et al.* Biology of hematopoietic stem cells and progenitors: implications for clinical applications. Annu Rev Immunol 2003; 21:759–806.

3 Reya T. Regulation of hematopoietic stem cell self-renewal. Recent Prog Horm Res 2003; 58:283–295.

4 Orkin SH, Zon LI. Hematopoiesis: an evolving paradigm for stem cell biology. Cell 2008; 132:631–644.

5 Lord AM, North TE, Zon LI. Prostaglandin E2: making more of your marrow. Cell Cycle 2007; 24:3054–3057.

6 Zon LI. Intrinsic and extrinsic control of haematopoietic stem-cell self-renewal. Nature 2008; 453:306–313.

7 Chen J, Ellison FM, Keyvanfar K, *et al.* Enrichment of hematopoietic stem cells with SLAM and LSK markers for the detection of hematopoietic stem cell function in normal and Trp53 null mice. Exp Hematol 2008; 36:1236–1243.

8 Gross S, Tilly P, Hentsch D, *et al.* Vascular wall-produced prostaglandin E2 exacerbates arterial thrombosis and atherothrombosis through platelet EP3 receptors. J Exp Med 2007; 204:311–320.

9 Miller SB. Prostaglandins in health and disease: an overview. Semin Arthritis Rheum 2006; 36:37–49.

10 Funk CD. Prostaglandins and leukotrienes: advances in eicosanoid biology. Science 2001; 294:1871–1875.

11 Chizzolini C, Chicheportiche R, Alvarez M, *et al.* Prostaglandin E2 synergistically with interleukin-23 favors human Th17 expansion. Blood 2008; 112:3696–3702.

12 • Boniface K, Bak-Jensen KS, Li Y, *et al.* Prostaglandin E2 regulates Th17 cell differentiation and function through cyclic AMP and EP2/EP4 receptor signaling. J Exp Med 2009; 206:535–547.
The authors demonstrate that PGE_2 promotes differentiation of murine and human T helper cells through cAMP signaling.

13 Jones RL, Giembycz MA, Woodward DF. Prostanoid receptor antagonists: development strategies and therapeutic applications. Br J Pharmacol 2009; 158:104–145.

14 Golan DE. Principles of pharmacology: the pathophysiologic basis of drug therapy. Lippincott Williams & Wilkins; 2008.

15 Regan JW. EP2 and EP4 prostanoid receptor signaling. Life Sciences 2003; 74:143–153.

16 Breyer RM, Bagdassarian CK, Myers SA, *et al.* Prostanoid receptors: subtypes and signaling. Annu Rev Toxicol 2001; 41:661–690.

17 Hata AN, Breyer RM. Pharmacology and signaling of prostaglandin receptors: multiple roles in inflammation and immune modulation. Pharmacol Ther 2004; 103:147–166.

18 North TE, Goessling W, Walkley CR, *et al.* Prostaglandin E2 regulates vertebrate haematopoietic stem cell homeostasis. Nature 2007; 447:1007–1012.

19 North TE, de Bruijn M, Stacy T, *et al.* Runx1 expression marks long-term repopulation hematopoietic stem cells in the midgestation mouse embryo. Immunity 2002; 16:661–672.

20 Mukouyama Y, Chiba N, Mucenski ML, *et al.* Hematopoietic cells in cultures of the murine embryonic aorta-gonad-mesonephros region are induced by c-Myb. Curr Biol 1999; 9:833–836.

21 •• Hoggatt J, Singh P, Sampath J, *et al.* Prostaglandin E2 enhances hematopoietic stem cell homing, survival and proliferation. Blood 2009; 113:5444–5455.
This paper examines homing, survival, and proliferation as possible mechanisms underlying PGE_2 effects on HSCs in the murine system. The authors report enhanced HSC engraftment following treatment with PGE_2. This is potentially due to an increase in homing capabilities and CXCR4 upregulation. An increase in the percentage of cycling cells following PGE_2 treatment was also observed.

22 Jetmore A, Plett PA, Tong X, *et al.* Homing efficiency, cell cycle kinetics, and survival of quiescent and cycling human CD34+ cells transplanted into conditioned NOD/SCID recipients. Blood 2001; 99:1585–1593.

23 Lapidot T, Dar A, Kollet O. How do stem cells find their way home? Blood 2005; 106:1901–1910.

24 Mori S, Jee WS, Li XJ, *et al.* Effects of prostaglandin E2 on production of new cancellous bone in the axial skeleton of ovariectimized rats. Bone 1990; 2:103–113.

25 •• Frisch BJ, Porter RL, Gigliotti BJ, *et al.* In vivo prostaglandin E2 treatment alters the bone marrow microenvironment and preferentially expands short-term hematopoietic stem cells. Blood 2009; 114:4054–4063.
The authors used an in-vivo treatment regimen to examine the effects of PGE_2 in the murine system. Long-term PGE_2 treatment increased the short-term-HSC/MPP subpopulation without affecting long-term-HSCs. In addition the competitive advantage of PGE_2 was eventually lost in long-term transplantation assays.

26 Nishigaki N, Negishi M, Ichikawa A. Two G-coupled prostaglandin E receptor subtypes, EP2 and EP4, differ in desensitization and sensitivity to the metabolic inactivation of the agonist. Mol Pharmacol 1996; 50:1031–1037.

27 Desai S, April H, Nwaneshiudu C, *et al.* Comparison of agonist-induced internalization of the human EP2 and EP4 prostaglandin receptors: role of the carboxyl terminus in EP4 receptor sequestration. Mol Pharmacol 2000; 58:1279–1286.

28 Fujino H, West KA, Regan JW. Phosphorylation of glycogen synthase kinase-3 and stimulation of T-cell factor signaling following activation of EP2 and EP4 prostanoid receptors by prostaglandin E2. J Biol Chem 2002; 277:2614–2619.

29 •• Goessling W, North TE, Loewer S, *et al.* Genetic interaction of PGE2 and Wnt signaling regulates developmental specification of stem cells and regeneration. Cell 2009; 136:1136–1147.
This paper demonstrates an in-vivo genetic interaction between PGE_2 and Wnt signaling pathway in zebrafish. Activation of Wnt signaling during embryogenesis resulted in increased HSCs in the AGM region; however, this effect appears to be dependent upon PGE_2. The effect of PGE_2 was also seen in the murine system using CFU-S assays demonstrating that PGE_2 mediates Wnt activity in murine HSPCs.

© 2013. Published by The Company of Biologists Ltd | Development (2013) 140, 4988-4997 doi:10.1242/dev.102053

RESEARCH ARTICLE

TECHNIQUES AND RESOURCES

zebraflash transgenic lines for *in vivo* bioluminescence imaging of stem cells and regeneration in adult zebrafish

Chen-Hui Chen[1], Ellen Durand[2], Jinhu Wang[1], Leonard I. Zon[2] and Kenneth D. Poss[1,*]

ABSTRACT

The zebrafish has become a standard model system for stem cell and tissue regeneration research, based on powerful genetics, high tissue regenerative capacity and low maintenance costs. Yet, these studies can be challenged by current limitations of tissue visualization techniques in adult animals. Here we describe new imaging methodology and present several ubiquitous and tissue-specific luciferase-based transgenic lines, which we have termed *zebraflash*, that facilitate the assessment of regeneration and engraftment in freely moving adult zebrafish. We show that luciferase-based live imaging reliably estimates muscle quantity in an internal organ, the heart, and can longitudinally follow cardiac regeneration in individual animals after major injury. Furthermore, luciferase-based detection enables visualization and quantification of engraftment in live recipients of transplanted hematopoietic stem cell progeny, with advantages in sensitivity and gross spatial resolution over fluorescence detection. Our findings present a versatile resource for monitoring and dissecting vertebrate stem cell and regeneration biology.

KEY WORDS: Zebrafish, Live imaging, Luciferase, Stem cells, Regeneration, Heart regeneration

INTRODUCTION

Zebrafish have been a valuable model system for vertebrate embryologists for nearly three decades, and the past decade has also seen their widespread use in stem cell and regeneration studies. Zebrafish are highly regenerative as adults, being equipped to regrow tissues such as amputated fins, injured retinae, transected optic nerves and spinal cord, lost heart muscle, brain, hair cells, pancreas, liver, skeletal muscle and kidney (Johnson and Weston, 1995; Bernhardt et al., 1996; Becker et al., 1997; Vihtelic and Hyde, 2000; Poss et al., 2002; Sadler et al., 2007; Ma et al., 2008; Jacoby et al., 2009; Moss et al., 2009; Diep et al., 2011; Andersson et al., 2012; Goldshmit et al., 2012; Kizil et al., 2012). Adult zebrafish present advantages for mechanistic studies as they are small, easy to raise in large numbers and accessible to cell transplantation and molecular genetic manipulations.

Zebrafish lose transparency during larval development. Thus, although fluorescent reporter proteins provide excellent optical tools for phenotyping and real-time imaging in zebrafish embryos, adult zebrafish only have marginal advantages over adult mice in visualizing stem cell and regenerative events by fluorescence detection. *casper* fish, with homozygous mutations in two pigmentation loci, were developed to assist imaging of fluorescent stem cells or melanoma cells after transplantation (White et al., 2008). Although this resource has enhanced the study of transplanted fluorescent cells *in vivo*, detection in these semi-transparent animals is semi-quantitative, can show a low signal-to-noise ratio, and is mainly limited to the labeled cells that are close to the body surface.

Luciferase-based imaging has been widely used in mice for monitoring gene expression, cell proliferation and migration, and bacterial and viral infections (Contag and Bachmann, 2002; Luker and Luker, 2008; Liu et al., 2011; Tinkum et al., 2011; Martínez-Corral et al., 2012; Maguire et al., 2013). Detection of bioluminescent signals generated from the luciferase-luciferin reaction is sensitive, virtually free of background noise, and can reveal biological information even from deep tissues. To date, reports on luciferase imaging in zebrafish have been few and limited to embryos (Mayerhofer et al., 1995; Liang et al., 2000; Weger et al., 2013).

Here, we describe a suitable methodology and several new transgenic lines to facilitate luciferase-based imaging in zebrafish. We find that luciferase activity in adult zebrafish can be reproducibly monitored in various settings, including deep tissues of freely swimming animals. We have applied this technique to monitor the progress of heart regeneration in individual zebrafish with cardiac injuries, removing the need to sacrifice animals for histological analysis. Moreover, stem cell transplantation experiments using transgenic donors enabled noninvasive quantitative assessment of engraftment in live animals, and unambiguously identified colonization and proliferation sites for these cells. We expect luciferase-based imaging in adult zebrafish to have multiple applications in stem cell and regeneration research.

RESULTS

Ubiquitous and tissue-specific luciferase-based transgenic zebrafish lines

To directly compare fluorescence-based and luciferase-based detection in adult zebrafish, we generated several transgenic lines that enable expression of both mCherry and firefly luciferase (Fluc) from a single transcript. Regulatory sequences for these lines were: (1) a 3.5 kb *ubiquitin* (*ubi*) promoter that drives constitutive transgene expression during all developmental stages (Fig. 1A) (Mosimann et al., 2011); (2) a 5.8 kb *β-actin2* promoter that drives widespread transgene expression (supplementary material Fig. S1A) (Higashijima et al., 1997); (3) a 600 bp *cryaa* promoter that drives transgene expression specifically in the lens (Fig. 1B) (Kurita et al., 2003); and (4) a 1.6 kb *cmlc2* (*myl7*) promoter that drives transgene expression in zebrafish cardiomyocytes (Fig. 1C) (Huang et al., 2003). A *cmlc2*-driven luciferase line with EGFP replacing mCherry was also generated (supplementary material Fig. S1B). As expected, fluorescent protein expression was easily visualized at the surface

[1]Department of Cell Biology and Howard Hughes Medical Institute, Duke University Medical Center, Durham, NC 27710, USA. [2]Howard Hughes Medical Institute, Division of Hematology/Oncology, Children's Hospital Boston, Harvard Stem Cell Institute, and Harvard Medical School, Boston, MA 02145, USA.

*Author for correspondence (kenneth.poss@duke.edu)

Received 31 July 2013; Accepted 19 September 2013

Development (2013) doi:10.1242/dev.102053

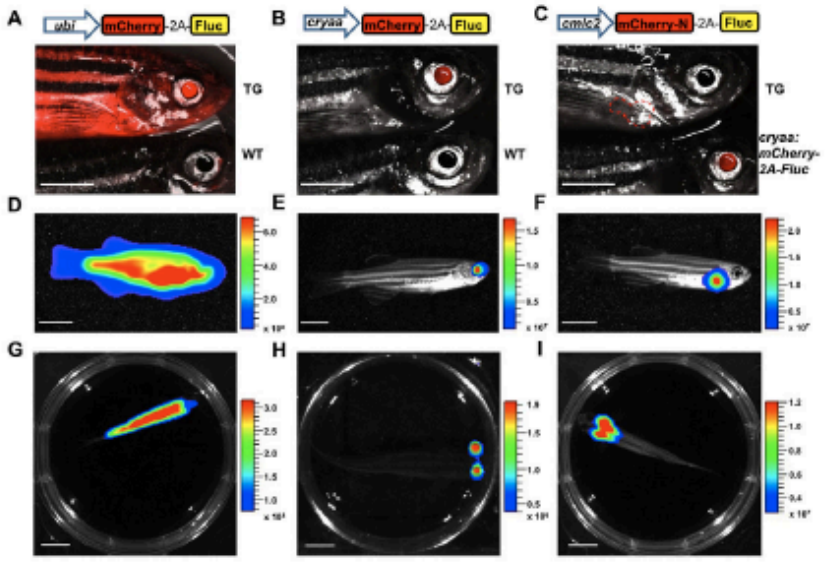

Fig. 1. Ubiquitous and tissue-specific luciferase-based transgenic zebrafish lines. (A-C) Constructs and representative fluorescence images of *ubi:mCherry-2A-Fluc* (A), *cryaa:mCherry-2A-Fluc* (B) and *cmlc2:mCherry-N-2A-Fluc* (C) transgenic (TG) fish. The red dashed line indicates the approximate location of the heart. Control fish are shown at the bottom of the images to indicate wild-type (WT; A,B) or *cryaa:mCherry-2A-Fluc* (C) fluorescence. (D-F) Representative bioluminescence images showing lateral view of *ubi:mCherry-2A-Fluc* (D), *cryaa:mCherry-2A-Fluc* (E) and *cmlc2:mCherry-N-2A-Fluc* (F) fish. (G-I) Representative bioluminescence images from overhead as in D-F. Brightfield and bioluminescence images were captured after luciferin delivery and images were overlaid. Luminescence signals are reported as radiance (p/sec/cm^2/sr) with a color bar. Scale bars: 5 mm.

of the fish (Fig. 1A,B), but was difficult to detect in an internal organ such as the heart (Fig. 1C). By contrast, we readily detected strong bioluminescence from both external and internal sources of expression upon luciferin delivery (Fig. 1D-F). Notably, although melanin absorbs light, the photons emitted from internal heart tissue do not show signs of signal attenuation by the longitudinal stripes of black melanophores, presumably owing to the short distance through which the emitted light has to travel (Fig. 1F; supplementary material Fig. S1B). Using a high-speed imaging camera, we were able to reliably localize cardiac and lens bioluminescence in adult zebrafish to specific structures at low magnification from overhead (Fig. 1G-I). Thus, bioluminescence in these transgenic zebrafish lines, which we have named *zebraflash* for their capacity to produce light, readily penetrates through adult tissues.

Quantitative and multiplex luciferase imaging in freely moving adult zebrafish

To optimize protocols for luciferase-based imaging in adult zebrafish, we used the cardiac *zebraflash* line *cmlc2:mCherry-N-2A-Fluc* (Fig. 1C). We tested two different routes to deliver luciferin: bathing and intraperitoneal injection (Fig. 2A). In both cases, *cmlc2:mCherry-N-2A-Fluc* produced a steady bioluminescent signal lasting for more than an hour (supplementary material Fig. S2A-C). Next, we determined the kinetics of bioluminescence and the optimal concentration of luciferin. To monitor the kinetic curve of the signal, we bathed adults in luciferin and immediately started imaging. Bioluminescence began to peak and reach a steady state ~8-10 minutes after initiating treatment (Fig. 2B; supplementary material Fig. S2D). 100 mM luciferin consistently produced more light than 50 mM luciferin (~2.5 fold increase; Fig. 2C) and was employed for most experiments presented here.

In bioluminescence assays of adult mice, animals are fully sedated during imaging. The plateau phase of the signal usually occurs 15 minutes after luciferin injection and endures for another 20 minutes (Zinn et al., 2008). Sequential measurements are recorded during the plateau phase and averaged for comparisons across different mice. We found that it was challenging to keep fish anesthetized for 20 minutes after luciferin delivery without affecting survival. To image conscious zebrafish, we acquired data from the entire region of interest (ROI) from animals maintained in tissue culture wells. Animal movement during the plateau phase did not affect measurements of bioluminescence (Fig. 2D). We routinely imaged six to nine adult fish at a time (Fig. 2E) or more for juvenile fish (Fig. 2F). Twenty sequential measurements were recorded from individual animals during the plateau phase (Fig. 3A,B). We measured bioluminescence among several fish in these experiments and found that, although the relative signal strength could vary between animals, it was consistent within each animal over 5 days of daily independent measurements (Fig. 3C,D). The posture of the animals during imaging could affect the measured bioluminescence up to 2-fold, and thus required monitoring (Fig. 3E,F). Because of the high bioluminescent output of *zebraflash* tissues, we were able to capture a series of real-time movies with 30 to 50 msecond exposure per frame from freely swimming 4-week-old juveniles (supplementary material Movie 1) or 3-month-old adults

Development (2013) doi:10.1242/dev.102053

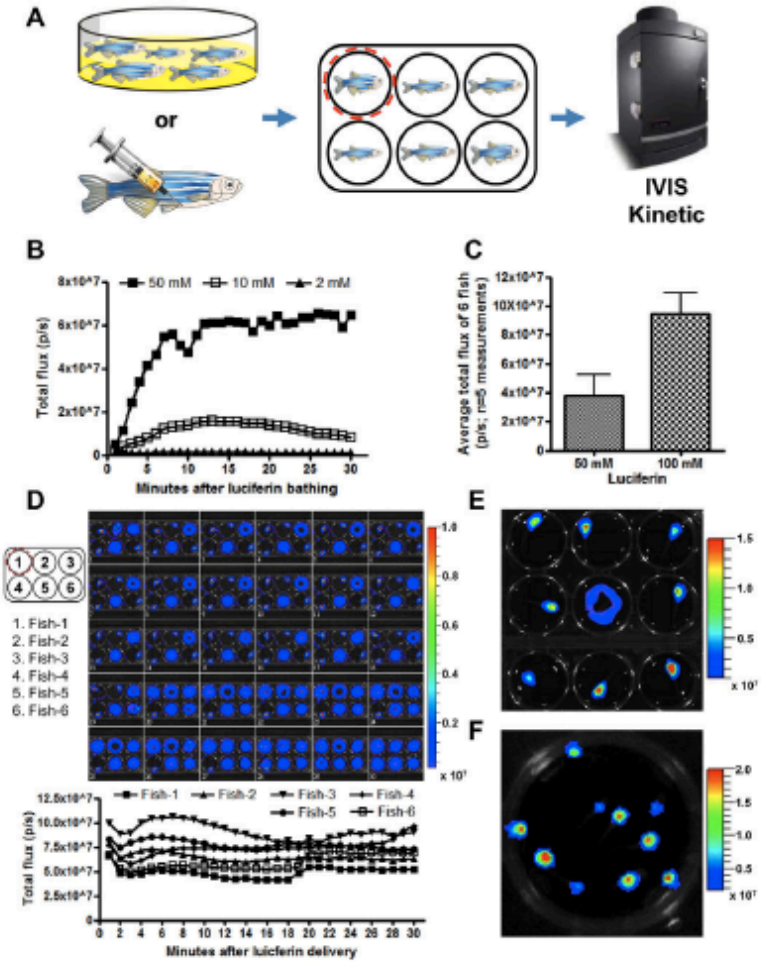

Fig. 2. Quantitative luciferase imaging in freely moving adult zebrafish. (A) Scheme of luciferin delivery and imaging. Bioluminescence from the region of interest (ROI; red dashed line) was measured over 20 minutes and expressed as p/sec. (B) Kinetics of bioluminescence recorded immediately after luciferin delivery. Luciferin (2 mM, 10 mM and 50 mM) was delivered to fish by bath incubation. (C) Comparison of average bioluminescence after delivery of 50 mM or 100 mM luciferin. Luciferin was delivered to the same set of fish (n=6) over five rounds of independent measurements (mean ± s.d.). (D) Bioluminescence recorded during the plateau phase from six freely moving fish over 30 minutes (1 minute/frame ×30) after luciferin delivery. (Top) Trace of bioluminescence in multi-well plates indicating the activity level of the animal during imaging. (Bottom) Bioluminescence recorded from individual animals. (E) Representative bioluminescence images of nine freely moving adult *cmlc2:mCherry-N-2A-Fluc* animals inside an imaging chamber. (F) Snapshot of a movie of ten swimming 4-week-old juvenile *cmlc2:mCherry-N-2A-Fluc* animals, indicating cardiac bioluminescence. Luminescence signals are reported as radiance (p/sec/cm^2/sr) with a color bar.

(supplementary material Movies 2, 3). These results indicated that it is practical to reliably capture and quantify bioluminescence from the internal organs of several fish swimming together.

Longitudinal monitoring of heart regeneration by luciferase-based imaging

Currently, it is possible to estimate readouts of regeneration of internal tissues in individual zebrafish by assessing organ function. For example, glucose levels provide a surrogate readout for islet cell number or function (although this assay requires a cardiac stab injury) (Moss et al., 2009), and swimming endurance recovers concomitant with regeneration of heart muscle (Wang et al., 2011). However, it is not possible to directly monitor the recovery of new internal tissue after injury. Heart regeneration occurs robustly in adult zebrafish after surgical resection, cryoinjury or induced cell death by activating the proliferation of spared cardiomyocytes (Poss et al., 2002; Jopling et al., 2010; Kikuchi et al., 2010; González-Rosa et al., 2011; Wang et al., 2011). Studies of heart regeneration typically employ a large number of animals for each experiment, all of which are sacrificed for tissue collection at various time points to approximate the progression of regeneration. To test whether bioluminescence is capable of interpreting regenerative progress, we first examined its correlation with cardiac size in adult *cmlc2:mCherry-N-2A-Fluc* fish. Quantification of signals in several animals, followed by histological assessment of Myosin heavy chain-positive tissue in ventricular sections, indicated that bioluminescence intensity is a reliable predictor of the amount of cardiac muscle (Fig. 4A). Similarly, bioluminescence quantification correlated positively with *in vitro* luciferase assay readings (supplementary material Fig. S3A).

We then examined whether cardiac injuries that removed ~50% of cardiac muscle cells were detectable by luciferase measurements.

Development (2013) doi:10.1242/dev.102053

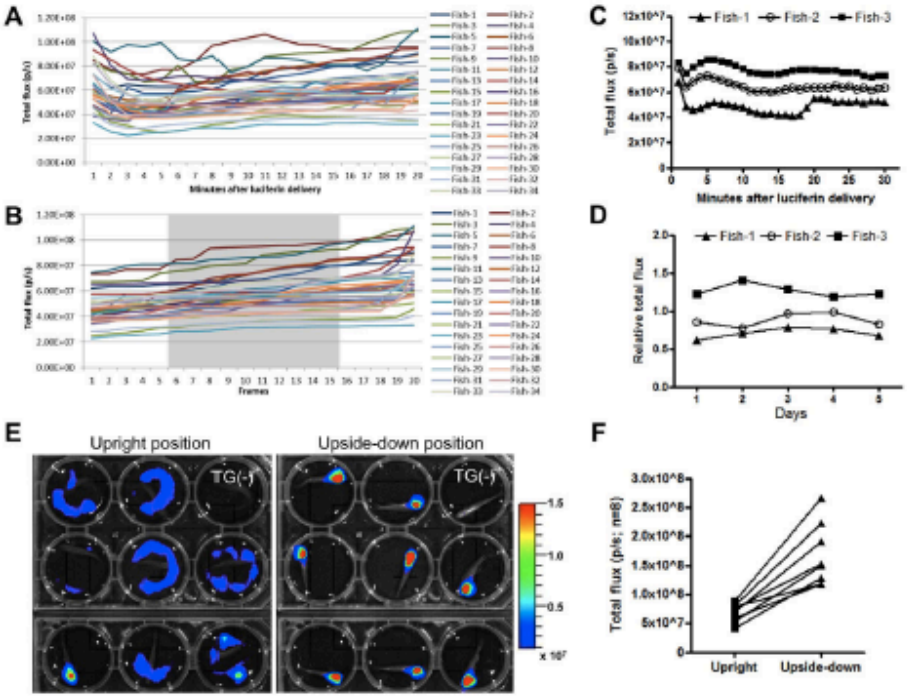

Fig. 3. Multiplex imaging of adult zebrafish. (A,B) Bioluminescence recorded during the plateau phase from 34 freely moving adult *cmlc2:mCherry-N-2A-Fluc* zebrafish over 20 minutes (1 minute/frame ×20) (A). Recorded data were sorted from lowest to highest initial readings. Ten median values from a total of 20 recorded values were averaged (gray areas) and then used for comparison across different animals (B). (C) Representative bioluminescence recorded during the plateau phase from three adult zebrafish after luciferin delivery, indicating that relative signal strength could vary between animals. (D) Relative total flux over 5 days of daily independent measurements, indicating consistency within individual animals. (E) Representative bioluminescence images of animals in either an upright or upside-down position. (Top) Brightfield only; (bottom) brightfield and bioluminescence images overlaid. TG(-), a transgene-negative control animal. Luminescence signals are reported as radiance (p/sec/cm^2/sr) with a color bar. (F) Bioluminescence recorded from the same animals in different positions, indicating that the posture of the animals during imaging affects the measured bioluminescence up to 2-fold (n=9).

For these experiments, we crossed *cmlc2:mCherry-N-2A-Fluc* into a strain that enables inducible diphtheria toxin A-mediated ablation of cardiomyocytes (Wang et al., 2011) (Fig. 4B). We found that the addition of tamoxifen, to induce cardiomyocyte ablation throughout both chambers, significantly reduced cardiac bioluminescence by 10 days post-treatment in most animals (Fig. 4C). Loss of cardiac bioluminescence was visually apparent in movies of swimming vehicle- and tamoxifen-treated zebrafish (Fig. 4D; supplementary material Movie 4). The quantified bioluminescence intensity at this time point was predictive of the extent of cardiomyocyte ablation, as determined by histology and muscle quantification (supplementary material Fig. S3B-D). Next, we examined whether luciferase-based imaging could monitor the progress of heart regeneration within a single animal. To increase the throughput of the imaging, we first tagged individual animals with commercially available p-Chips (supplementary material Fig. S4; see Materials and methods for details). We then induced cardiomyocyte ablation and chose, for longitudinal monitoring, those animals with at least a 25% reduction in bioluminescence at 12 days post-injury. Notably, bioluminescence gradually recovered and reached the approximate pre-ablation level by ~35 days post-injury (n=17; Fig. 4E), consistent with the published kinetics of heart regeneration in this injury model (Wang et al., 2011). Both males and females recovered similarly (Fig. 4F). We also performed a second ablation injury in a portion of these animals, and found that they recovered similar bioluminescence levels as prior to the initial injury, although after a longer period of 100 days (n=6; supplementary material Fig. S3E,F). Thus, luciferase-based imaging can be applied to monitor the level of injury and progression of regeneration *in vivo* in a noninvasive and relatively high-throughput manner.

Luciferase-based live imaging after hematopoietic stem cell transplantation

Current methodology to assess stem cell engraftment involves the transplantation of cells from a transgenic donor strain expressing a fluorescent reporter protein in a tissue-specific or ubiquitous manner, often into the semi-transparent host strain *casper* (Traver et al., 2003; White et al., 2008; Stachura et al., 2011). To examine whether *zebraflash* lines offer broad-spectrum labeling for various blood lineages, we first examined mCherry expression in whole kidney

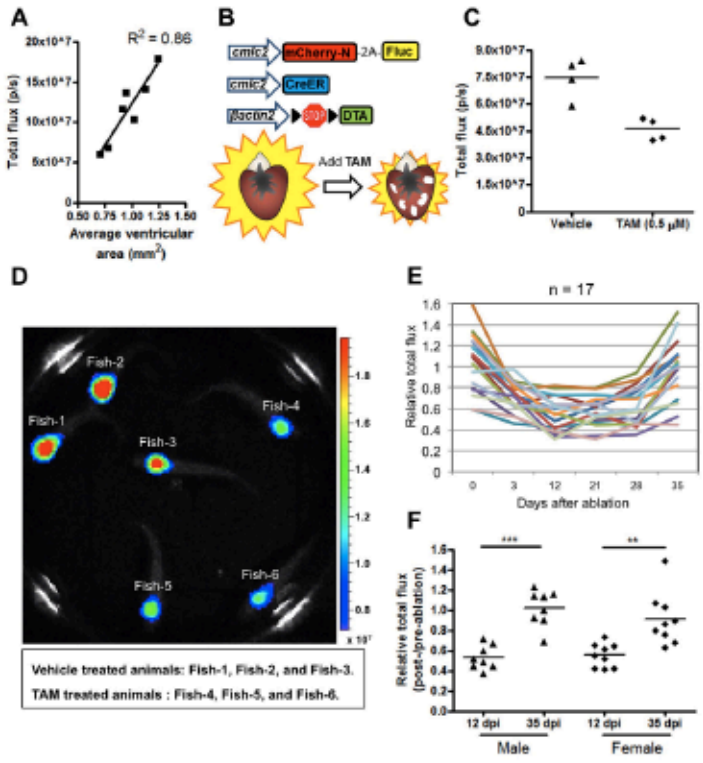

Fig. 4. Longitudinal monitoring of heart regeneration by luciferase imaging. (A) Correlation between bioluminescence (p/sec) and the surface area of tissue sections from adult ventricles. One representative experiment is shown here from two experiments. (B) Cardiac ablation/detection constructs and injury. TAM, tamoxifen. (C) Bioluminescence recorded 10 days after induced genetic cardiomyocyte ablation. One representative experiment is shown here from three replicate experiments. (D) Snapshot of a movie of six swimming adult triple-transgenic animals from these experiments, at 10 days post-treatment. Three have received tamoxifen and have lower bioluminescence signals (Fish-4, Fish-5 and Fish-6) than vehicle-treated animals (Fish-1, Fish-2 and Fish-3). Luminescence signals are reported as radiance (p/sec/cm²/sr) with a color bar. (E) Relative total flux indicating changes in bioluminescence in 17 animals during the course of injury and regeneration. (F) Relative total flux showing increases in bioluminescence between 12 days and 35 days after tamoxifen treatment. Animals are grouped here by sex. ***P<0.001, **P<0.01, paired Student's t-test. dpi, days post-injury.

marrow (WKM) cells isolated from *ubi:mCherry-2A-Fluc* lines and subjected to flow cytometric analysis (Mosimann et al., 2011). One line [*Tg(ubi:mCherry-2A-Fluc)*^{pd75}] displayed particularly robust and ubiquitous labeling (~87.8%) of most WKM cells (Fig. 5A,B), including erythroid (~71.1%), myeloid (~98.6%) and lymphoid (~96%) lineages and precursor cell populations (~97.1%) (Fig. 5C). Then, WKM cells isolated from this line were mixed with wild-type WKM cells in different ratios and injected into irradiated *casper* recipients (Fig. 6A) (Traver et al., 2003; Pugach et al., 2009). After 1 month, we quantified bioluminescence in freely swimming cell recipients. We found a high positive correlation between the intensity of whole animal bioluminescence and the input number of *ubi:mCherry-2A-Fluc* WKM cells (n=6-9 per group; Fig. 6B,C). The variation seen in Fig. 6C most likely reflects the variable number of successfully engrafted WKM cells after transplantation in adult zebrafish, which has been documented by FACS analysis (de Jong et al., 2011). Although we estimated the detection limit in this experiment to be ~500 cells (0.5%), we could not detect bioluminescence above background from most animals with the lowest (5-10%) dilution of transgenic cells (Fig. 6D). This sharp decline in the engraftment ratio at 5000-10,000 transgenic WKM cells closely resembles that reported previously for limiting dilution transplantation experiments (de Jong et al., 2011; Hess et al., 2013). Thus, luciferase imaging offers high sensitivity and a new opportunity for detecting the progeny of engrafted stem cells in freely moving recipient animals.

We next performed higher magnification imaging of anesthetized recipients to visualize sites of stem cell colonization/proliferation. Bioluminescence was strong throughout the entire animal (Fig. 6E,F), ostensibly owing to the proliferation and circulation of multiple WKM-derived blood lineages. By increasing the detection cut-off, we could unambiguously identify signal hotspots in the trunk kidney, the head kidney and the thymus, which are three recognized sites for stem cell colonization in adult zebrafish (Fig.

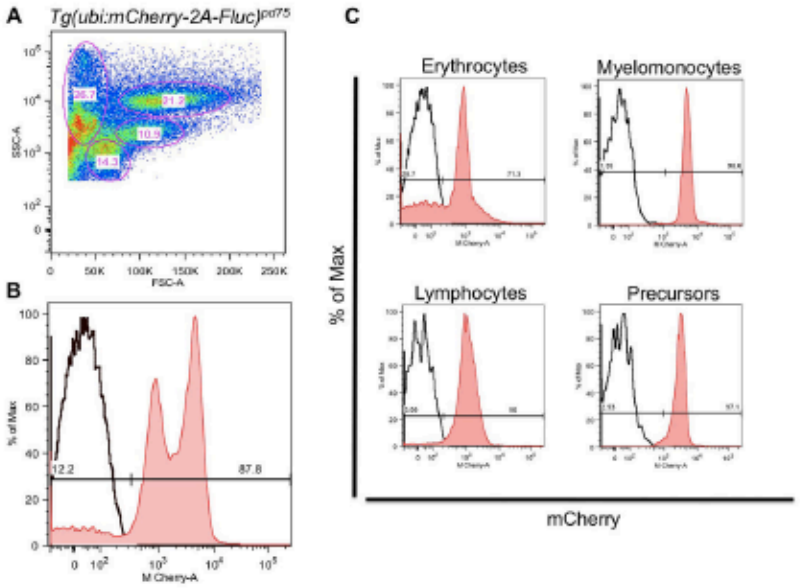

Fig. 5. FACS analysis of labeled WKM cells. Flow cytometry analysis of adult whole kidney marrow (WKM) cells from the transgenic line *Tg(ubi:mCherry-2A-Fluc)*^{pd75}. mCherry-positive cells were resolved by forward scatter and side scatter (A). The majority of isolated WKM cells express mCherry fluorescent protein (B), including the erythroid, myeloid and lymphoid lineages and precursor cell populations (C).

6G) (Murayama et al., 2006). Comparisons of bioluminescence with fluorescence imaging within the same fish indicated that bioluminescence was not only qualitatively better for the detection of transplanted cells in intact animals but also improved the spatial resolution of donor-derived tissues (Fig. 6H). For instance, fluorescent signals from the thymus were completely obstructed (Fig. 6I), whereas thymic bioluminescence was strong and clear (Fig. 6G).

DISCUSSION

By applying the properties of luciferase-based imaging to adult zebrafish, we have established a methodology and new transgenic resources for the study of stem cells and organ regeneration. Bioluminescence is quantitative and highly sensitive, and marries well with small, thin adult zebrafish, which have no body hair to attenuate light (Sadikot and Blackwell, 2008; Curtis et al., 2011). Such a combination is ideal for whole animal imaging to monitor cell loss, migration, expansion and regeneration in internal tissues.

Although luciferase-based imaging requires administration of substrate and relies on the availability of a more sensitive camera and a light-sealed imaging chamber, there are multiple advantages over fluorescence detection for tissue regeneration research that we can identify from this study. First, bioluminescence is more sensitive for deep tissues, enabling clear visualization of signals in freely moving animals. Second, luciferase-based imaging is quantitative, allowing assessment of the amount of tissue that is removed by injury and the amount that is replaced during regenerative events in an individual animal. This allows immediate confirmation of the extent of the injury, and removes the requirement for qualitative histological analysis of fixed tissues to determine the extent of regeneration. Consequently, the ability to follow individual animals throughout the regeneration process without sacrificing them for tissue collection should considerably reduce the number of animals required for experiments. This will also help to detect subtle changes despite variation among individuals. When combined with an inducible genetic injury system, as we have shown here for the heart, the tedium of resection surgery plus that of histological detection is circumvented. These improvements in efficiency and sensitivity should lay the groundwork for discovery approaches such as chemical or genetic screens for effectors of heart regeneration.

By swapping regulatory sequences, the imaging system described here can be readily applied to study the regeneration of other organs in adult zebrafish. Luciferase activity formally reflects gene expression and not tissue amounts. Thus, for quantitative *in vivo* bioluminescence assays of tissue regeneration, it is necessary to identify a tissue-specific promoter that remains largely stable during regeneration. In alternative strategies, injury-responsive or regeneration-responsive regulatory sequences can be used to drive luciferase in transgenic lines. Such tools are predicted to detect sharp changes in expression in response to injury and should be optimal for screening approaches.

The resources that we report here provide similar advantages over fluorescence detection for stem cell transplantation studies. Engraftment can be assessed rapidly, quantitatively and with higher sensitivity in individual animals, and does not require sacrificing animals for end-point flow cytometric analysis. These advantages should enable more efficient experiments with wild-type and mutant donors or recipients, which can include: (1) single-cell transplants,

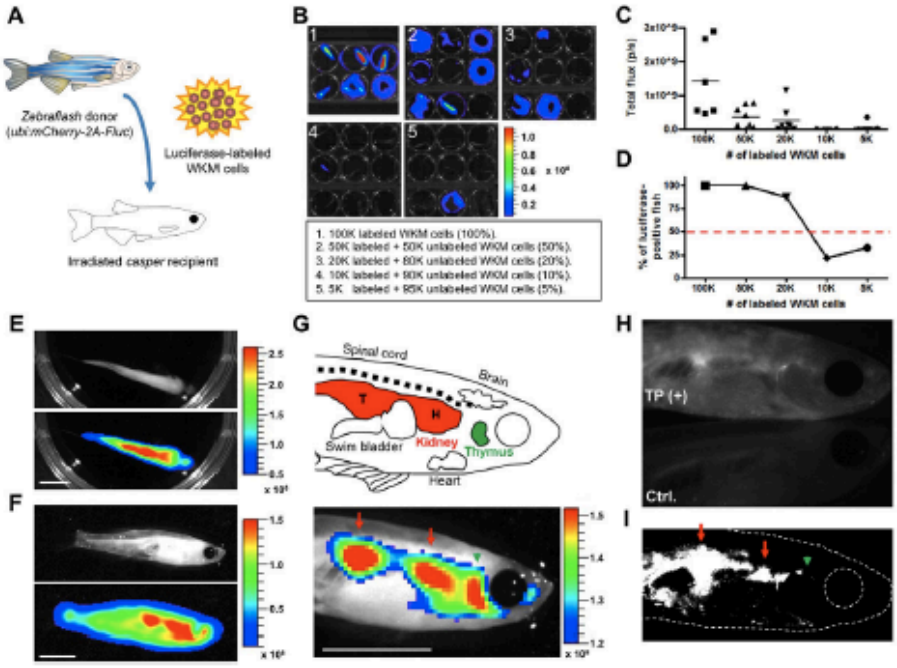

Fig. 6. Luciferase-based live imaging after hematopoietic stem cell transplantation. (A) Scheme of marrow transplantation experiments. (B) Representative bioluminescence images of swimming recipient fish transplanted with different ratios of *ubi:mCherry-2A-Fluc* WKM cells. (C) Bioluminescence reading from recipient fish at 30 days post-transplant (n=6-9 per group). (D) Percentage of recipients with any above-background bioluminescence at 30 days post-transplant. (E,F) Representative bioluminescence images of a freely moving recipient fish, viewed overhead (E) or laterally (F) under anesthesia. (G) (Top) Depiction of the internal anatomy of an adult zebrafish. (Bottom) Representative bioluminescence image of a recipient fish, at high magnification and a higher threshold setting, indicating signals from key hematopoietic stem cell colonization sites. Red arrows indicate the location of trunk kidney (T) and head kidney (H); the green arrowhead points to the thymus. (H,I) Fluorescence images (H) were acquired from the same recipient fish shown in G, along with a non-recipient animal (Ctrl.). Background fluorescence signal was subtracted by ImageJ with a higher threshold setting to reveal signals from key hematopoietic stem cell colonization sites (I). Luminescence signals are reported as radiance (p/sec/cm^2/sr) with a color bar. Scale bars: 5 mm.

as performed to identify self-renewing stem cells that contribute to murine skeletal muscle regeneration or hematopoietic stem cell reconstitution in mice (Wagers et al., 2002; Sacco et al., 2008); (2) stem cell competition assays (Harrison et al., 1993); and (3) whole animal metastasis assays (Ceol et al., 2011).

Although luciferase-based imaging provides certain advantages over fluorescence imaging, it also has limitations. *In vivo* bioluminescence data provide relative quantification rather than absolute measurements of the luciferase expression from a target site. Bioluminescence signals could be attenuated to variable degrees in different anatomical sites or in different animals, such that quantitative analyses are most reliable when the data are collected from equivalent anatomical sites and compared within the same animal over time. Also, unlike fluorescence detection, luciferase-based imaging is typically only a two-dimensional modality with a limited, typically 1-3 mm spatial resolution due to photon scattering. As the output of luciferase-based imaging is simply the number of photons emitted per second from a defined area, it is not possible to visualize/distinguish the structural differences between two nearby, discrete light sources (e.g. a small injury area versus uninjured tissue). In transplantation experiments, it can also be challenging to distinguish the absolute signal from specific organs, such as the kidney, from adjacent anatomical sites, such as blood vessels with circulating luciferase-labeled cells. Recently, technologies have been developed to localize the three-dimensional distribution of the underlying bioluminescent source and generate cross-sectional imaging with enhanced resolution (Chaudhari et al., 2005; Cronin et al., 2012; Collins et al., 2013). The reagents we describe should be amenable to these evolving bioluminescence tools and should also be useful for other applications to visualize and dissect *in vivo* protein-protein interactions (Paulmurugan et al., 2002), apoptosis (Niers et al., 2011; Scabini et al., 2011), inflammation (Van de Bittner et al., 2010), hypoxia responses (Lehmann et al., 2009) and bacterial and viral infections (Phelan et al., 2005; Rawls et al., 2006).

MATERIALS AND METHODS

Zebrafish

Adult zebrafish of 3-5 months of age were used for most experiments. Animal density was maintained at 3-4 per liter in all experiments. All transgenic lines were analyzed as hemizygotes. To induce cardiomyocyte

Development (2013) doi:10.1242/dev.102053

ablation, triple-transgenic *cmlc2:mCherry-N-2A-Fluc*; *Z-CAT* zebrafish were bathed in 0.5 µM tamoxifen in fish water for 16 hours as described previously (Wang et al., 2011). All animal procedures were performed in accordance with Duke University guidelines.

Transgenic *zebraflash* lines

ubi:mCherry-2A-Fluc

The sequences of mCherry, 2A (Kim et al., 2011) and firefly luciferase (Promega) were cloned downstream of the *ubi* promoter (3.5 kb) (Mosimann et al., 2011) by yeast recombinational cloning as described (Oldenburg et al., 1997). The construct was flanked with I-SceI sites to facilitate transgenesis. Purified DNA (30 ng/µl) was injected into one-cell zebrafish embryos after linearization by I-SceI digestion. The full name of this transgenic line is *Tg(ubi:mCherry-2A-Fluc)*^{sd75}.

cryaa:mCherry-2A-Fluc

The sequences of mCherry, 2A and firefly luciferase were cloned downstream of the *cryaa* promoter (0.6 kb) (Kurita et al., 2003) by yeast recombinational cloning. The entire construct was flanked with I-SceI sites to facilitate transgenesis. The full name of this transgenic line is *Tg(cryaa:mCherry-2A-Fluc)*^{sd74}.

cmlc2:mCherry-N-2A-Fluc

The sequences of mCherry-N (mCherry-bacterial nitroreductase fusion) (Grohmann et al., 2009), 2A and firefly luciferase were cloned downstream of the *cmlc2* promoter (1.6 kb) (Huang et al., 2003) by yeast recombinational cloning. The entire construct was flanked with I-SceI sites to facilitate transgenesis. The full name of this transgenic line is *Tg(cmlc2:mCherry-N-2A-Fluc)*^{sd71}. A second line, *Tg(cmlc2:mCherry-N-2A-Fluc)*^{sd72}, was independently selected after transgenesis.

β-actin2:mCherry-2A-Fluc

The sequences of mCherry, 2A and firefly luciferase were cloned downstream of the *β-actin2* promoter (5.8 kb) (Higashijima et al., 1997) by yeast recombinational cloning. The entire construct was flanked with I-SceI sites to facilitate transgenesis. The full name of this transgenic line is *Tg(β-actin2:mCherry-2A-Fluc)*^{sd77}.

cmlc2:EGFP-2A-Fluc transgenic lines

The sequences of EGFP, 2A and firefly luciferase were cloned downstream of the *cmlc2* promoter (1.6 kb) by yeast recombinational cloning. The entire construct was flanked with I-SceI sites to facilitate transgenesis. The full name of this transgenic line is *Tg(cmlc2:EGFP-2A-Fluc)*^{sd73}.

Tagging adult zebrafish for long-term monitoring

To increase the throughput of the imaging and monitor many individual adult zebrafish in the same tank over time, commercially available p-Chips (Gruda et al., 2010) were tested and implanted into the left dorsal trunk muscle (supplementary material Fig. S4A,B). We could follow tagged adult zebrafish over a 4-month period with a 96% success rate (supplementary material Fig. S4C) and with no obvious impact on animal health (supplementary material Fig. S4D).

Transplantation of WKM cells

WKM cells from the *Tg(ubi:mCherry-2A-Fluc)*^{sd75} line were transplanted into irradiated *casper* recipient adult fish by retro-orbital injection as described previously (Traver et al., 2003; Pugach et al., 2009). Recipients were subjected to γ-irradiation using a cesium-137 irradiator at a split dose of 30 gy on day −2 and day −1 prior to transplantation. On the day of transplantation, WKM cells from *ubi:mCherry-2A-Fluc* and non-irradiated *casper* fish were harvested and injected into recipients at doses ranging from 5000 to 100,000 cells per recipient fish. Transplanted fish were kept off-flow for 7 days post-injection in supplemented fish water, as described previously (Pugach et al., 2009).

FACS analysis of WKM cells

WKM cells from *ubi:mCherry-2A-Fluc* fish were harvested and prepared in 0.9× phosphate-buffered saline (PBS) with 5% heat-inactivated fetal bovine serum (FBS). WKM cells were dissociated and filtered prior to FACS analysis. WKM populations were determined using an LSR-II analyzer (BD Biosciences) based on SSC and FSC profiles as previously described (Traver et al., 2003). Flow cytometry data were analyzed using FlowJo software (TreeStar).

Histological analysis

Zebrafish hearts were collected and fixed in 4% paraformaldehyde (PFA) at room temperature for 1 hour or at 4°C overnight. The tissue was then incubated in 30% sucrose overnight at 4°C. All histological analyses were performed using 10 µm cryosections. Immunofluorescence staining was performed as previously described (Lepilina et al., 2006). Antibodies used were: anti-Myosin heavy chain (1:100, F59, mouse monoclonal; Developmental Studies Hybridoma Bank), anti-cardiac troponin T (1:100, mouse monoclonal; Thermo Scientific, MS-295-P1-ABX) and Alexa Fluor 588 goat anti-mouse IgG (H+L; Invitrogen, A-11001). Ventricular muscle surface area was quantified as described using the three largest longitudinal sections from each ventricle (Wang et al., 2011).

In vitro luciferase assays

Zebrafish hearts were collected and snap-frozen in liquid nitrogen. The frozen tissue was ground in 500 µl 1× CCLR (Promega, E1500) in a homogenizer (Tissuelyzer, Qiagen). After a brief centrifugation, the supernatant was assayed for protein concentration (Thermo Scientific Pierce, #23227) and *in vitro* luciferase activity (Promega, E1500).

Imaging

Fluorescence images were acquired using a Leica M205 FA dissecting microscope. For bioluminescence, adult zebrafish harboring a luciferase transgene or transplanted cells expressing luciferase were given 100 mM D-luciferin (Biosynth, L-8240) by bathing in aquarium water or in 10 µl PBS by intraperitoneal (I.P.) injection. I.P. injection is more cost effective, whereas bathing is recommended for small juvenile animals. For bath treatment, animals were allowed to swim in luciferin solution for 15 minutes to reach the plateau phase of bioluminescence. After rinsing in aquarium water, the fish were ready for imaging. For I.P. injection, fish were first anesthetized by tricaine immersion before injection, and then given 3-5 minutes recovery time in aquarium water. We found that bioluminescence immediately reached the plateau phase if luciferin was delivered by I.P. injection. For imaging, adult zebrafish were placed in a low dose of tricaine (0.01 mg/ml) to reduce stress, and placed in an enclosure with a charge-coupled device camera (IVIS Kinetic system, PerkinElmer). Individual adult zebrafish were housed in tissue culture plates with black walls (Molecular Devices, W1155) to avoid light reflection. Exposure times for imaging ranged from 10 seconds to 1 minute per frame, depending upon transgenic lines and the IVIS model used for imaging. Typically, 6-9 fish are imaged at the same time for 20 minutes during the plateau phase. Total photon output was quantified as total photon counts per second (p/s) using Living Image software (PerkinElmer). Ten median values from a total of 20 frames of recorded data were averaged and used for comparison across different fish (Fig. 2A,B). Individually tagged fish were imaged before and after heart injury to monitor their injury levels and regeneration over time. For longitudinal monitoring of the same animal over days or months, a set of control fish (5-8 fish) was repeatedly measured and the mean value of the readout was used to correct day-to-day bias from the imaging system.

Acknowledgements

We thank J. Burris, A. Eastes, P. Williams and N. Blake for zebrafish care; A. Dickson for artwork; G. Palmer for assistance with the luciferase imaging; PharmaSeq for animal tagging chips; and K.D.P. laboratory members for comments on the manuscript.

Competing interests

The authors declare no competing financial interests.

Author contributions

C.-H.C. generated zebrafish lines and performed imaging. E.D. and L.I.Z. designed and performed transplantation experiments and flow cytometry. J.W. generated Z-CAT lines. C.-H.C. and K.D.P. designed the experiments, analyzed the data, and wrote the manuscript. All authors commented on the manuscript.

Funding
K.D.P. was supported by National Institutes of Health grants from The National Institute of General Medical Sciences (NIGMS) [GM074057] and The National Heart, Lung, and Blood Institute (NHLBI) [HL081674]. K.D.P. is a Howard Hughes Medical Institute Early Career Scientist. Deposited in PMC for release after 6 months.

Supplementary material
Supplementary material available online at
http://dev.biologists.org/lookup/suppl/doi:10.1242/dev.102053/-/DC1

References

Andersson, O., Adams, B. A., Yoo, D., Ellis, G. C., Gut, P., Anderson, R. M., German, M. S. and Stainier, D. Y. (2012). Adenosine signaling promotes regeneration of pancreatic β cells in vivo. *Cell Metab.* **15**, 885-894.
Becker, T., Wullimann, M. F., Becker, C. G., Bernhardt, R. R. and Schachner, M. (1997). Axonal regrowth after spinal cord transection in adult zebrafish. *J. Comp. Neurol.* **377**, 577-595.
Bernhardt, R. R., Tongiorgi, E., Anzini, P. and Schachner, M. (1996). Increased expression of specific recognition molecules by retinal ganglion cells and by optic pathway glia accompanies the successful regeneration of retinal axons in adult zebrafish. *J. Comp. Neurol.* **376**, 253-264.
Ceol, C. J., Houvras, Y., Jane-Valbuena, J., Bilodeau, S., Orlando, D. A., Battisti, V., Fritsch, L., Lin, W. M., Hollmann, T. J., Ferré, F. et al. (2011). The histone methyltransferase SETDB1 is recurrently amplified in melanoma and accelerates its onset. *Nature* **471**, 513-517.
Chaudhari, A. J., Darvas, F., Bading, J. R., Moats, R. A., Conti, P. S., Smith, D. J., Cherry, S. R. and Leahy, R. M. (2005). Hyperspectral and multispectral bioluminescence optical tomography for small animal imaging. *Phys. Med. Biol.* **50**, 5421-5441.
Collins, J. W., Meganck, J. A., Kuo, C., Francis, K. P. and Frankel, G. (2013). 4D Multimodality Imaging of Citrobacter rodentium Infections in Mice. *J. Vis. Exp.* **78**. 10.3791/50450
Contag, C. H. and Bachmann, M. H. (2002). Advances in in vivo bioluminescence imaging of gene expression. *Annu. Rev. Biomed. Eng.* **4**, 235-260.
Cronin, M., Akin, A. R., Collins, S. A., Meganck, J., Kim, J. B., Baban, C. K., Joyce, S. A., van Dam, G. M., Zhang, N., van Sinderen, D. et al. (2012). High resolution in vivo bioluminescent imaging for the study of bacterial tumour targeting. *PLoS ONE* **7**, e30940.
Curtis, A., Calabro, K., Galarneau, J. R., Bigio, I. J. and Krucker, T. (2011). Temporal variations of skin pigmentation in C57BL/6 mice affect optical bioluminescence quantitation. *Mol. Imaging Biol.* **13**, 1114-1123.
de Jong, J. L., Burns, C. E., Chen, A. T., Pugach, E., Mayhall, E. A., Smith, A. C., Feldman, H. A., Zhou, Y. and Zon, L. I. (2011). Characterization of immune-matched hematopoietic transplantation in zebrafish. *Blood* **117**, 4234-4242.
Diep, C. Q., Ma, D., Deo, R. C., Holm, T. M., Naylor, R. W., Arora, N., Wingert, R. A., Bollig, F., Djordjevic, G., Lichman, B. et al. (2011). Identification of adult nephron progenitors capable of kidney regeneration in zebrafish. *Nature* **470**, 95-100.
Goldshmit, Y., Sztal, T. E., Jusuf, P. R., Hall, T. E., Nguyen-Chi, M. and Currie, P. D. (2012). Fgf-dependent glial cell bridges facilitate spinal cord regeneration in zebrafish. *J. Neurosci.* **32**, 7477-7492.
González-Rosa, J. M., Martin, V., Peralta, M., Torres, M. and Mercader, N. (2011). Extensive scar formation and regression during heart regeneration after cryoinjury in zebrafish. *Development* **138**, 1663-1674.
Grohmann, M., Paulmann, N., Fleischhauer, S., Vowinckel, J., Priller, J. and Walther, D. J. (2009). A mammalianized synthetic nitroreductase gene for high-level expression. *BMC Cancer* **9**, 301.
Gruda, M. C., Pinto, A., Craelius, A., Davidowitz, H., Kopacka, W. M., Li, J., Qian, J., Rodriguez, E., Kuspiel, E. and Mandecki, W. (2010). A system for implanting laboratory mice with light-activated microtransponders. *J. Am. Assoc. Lab. Anim. Sci.* **49**, 826-831.
Harrison, D. E., Jordan, C. T., Zhong, R. K. and Astle, C. M. (1993). Primitive hemopoietic stem cells: direct assay of most productive populations by competitive repopulation with simple binomial, correlation and covariance calculations. *Exp. Hematol.* **21**, 206-219.
Hess, I., Iwanami, N., Schorpp, M. and Boehm, T. (2013). Zebrafish model for allogeneic hematopoietic cell transplantation not requiring preconditioning. *Proc. Natl. Acad. Sci. USA* **110**, 4327-4332.
Higashijima, S., Okamoto, H., Ueno, N., Hotta, Y. and Eguchi, G. (1997). High-frequency generation of transgenic zebrafish which reliably express GFP in whole muscles or the whole body by using promoters of zebrafish origin. *Dev. Biol.* **192**, 289-299.
Huang, C. J., Tu, C. T., Hsiao, C. D., Hsieh, F. J. and Tsai, H. J. (2003). Germ-line transmission of a myocardium-specific GFP transgene reveals critical regulatory elements in the cardiac myosin light chain 2 promoter of zebrafish. *Dev. Dyn.* **228**, 30-40.
Jacoby, A. S., Busch-Nentwich, E., Bryson-Richardson, R. J., Hall, T. E., Berger, J., Berger, S., Sonntag, C., Sachs, C., Geisler, R., Stemple, D. L. et al. (2009). The zebrafish dystrophic mutant softy maintains muscle fibre viability despite basement membrane rupture and muscle detachment. *Development* **136**, 3367-3376.
Johnson, S. L. and Weston, J. A. (1995). Temperature-sensitive mutations that cause stage-specific defects in Zebrafish fin regeneration. *Genetics* **141**, 1583-1595.
Jopling, C., Sleep, E., Raya, M., Martí, M., Raya, A. and Izpisúa Belmonte, J. C. (2010). Zebrafish heart regeneration occurs by cardiomyocyte dedifferentiation and proliferation. *Nature* **464**, 606-609.
Kikuchi, K., Holdway, J. E., Werdich, A. A., Anderson, R. M., Fang, Y., Egnaczyk, G. F., Evans, T., Macrae, C. A., Stainier, D. Y. and Poss, K. D. (2010). Primary contribution to zebrafish heart regeneration by gata4(+) cardiomyocytes. *Nature* **464**, 601-605.
Kim, J. H., Lee, S. R., Li, L. H., Park, H. J., Park, J. H., Lee, K. Y., Kim, M. K., Shin, B. A. and Choi, S. Y. (2011). High cleavage efficiency of a 2A peptide derived from porcine teschovirus-1 in human cell lines, zebrafish and mice. *PLoS ONE* **6**, e18556.
Kizil, C., Kyritsis, N., Dudczig, S., Kroehne, V., Freudenreich, D., Kaslin, J. and Brand, M. (2012). Regenerative neurogenesis from neural progenitor cells requires injury-induced expression of Gata3. *Dev. Cell* **23**, 1230-1237.
Kurita, R., Sagara, H., Aoki, Y., Link, B. A., Arai, K. and Watanabe, S. (2003). Suppression of lens growth by alphaA-crystallin promoter-driven expression of diphtheria toxin results in disruption of retinal cell organization in zebrafish. *Dev. Biol.* **255**, 113-127.
Lahmann, S., Stiehl, D. P., Honer, M., Dominietto, M., Keist, R., Kotevic, I., Wollenick, K., Ametamey, S., Wenger, R. H. and Rudin, M. (2009). Longitudinal and multimodal in vivo imaging of tumor hypoxia and its downstream molecular events. *Proc. Natl. Acad. Sci. USA* **106**, 14004-14009.
Lepilina, A., Coon, A. N., Kikuchi, K., Holdway, J. E., Roberts, R. W., Burns, C. G. and Poss, K. D. (2006). A dynamic epicardial injury response supports progenitor cell activity during zebrafish heart regeneration. *Cell* **127**, 607-619.
Liang, M. R., Aleström, P. and Collas, P. (2000). Glowing zebrafish: integration, transmission, and expression of a single luciferase transgene promoted by noncovalent DNA-nuclear transport peptide complexes. *Mol. Reprod. Dev.* **55**, 8-13.
Liu, Z., Turkoz, A., Jackson, E. N., Corbo, J. C., Engelbach, J. A., Garbow, J. R., Piwnica-Worms, D. R. and Kopan, R. (2011). Notch1 loss of heterozygosity causes vascular tumors and lethal hemorrhage in mice. *J. Clin. Invest.* **121**, 800-808.
Luker, K. E. and Luker, G. D. (2008). Applications of bioluminescence imaging to antiviral research and therapy: multiple luciferase enzymes and quantitation. *Antiviral Res.* **78**, 179-187.
Ma, E. Y., Rubel, E. W. and Raible, D. W. (2008). Notch signaling regulates the extent of hair cell regeneration in the zebrafish lateral line. *J. Neurosci.* **28**, 2261-2273.
Maguire, K. K., Lim, L., Speedy, S. and Rando, T. A. (2013). Assessment of disease activity in muscular dystrophies by noninvasive imaging. *J. Clin. Invest.* **123**, 2298-2305.
Martinez-Corral, I., Olmeda, D., Diéguez-Hurtado, R., Tammela, T., Alitalo, K. and Ortega, S. (2012). In vivo imaging of lymphatic vessels in development, wound healing, inflammation, and tumor metastasis. *Proc. Natl. Acad. Sci. USA* **109**, 6223-6228.
Mayerhofer, R., Araki, K. and Szalay, A. A. (1995). Monitoring of spatial expression of firefly luciferase in transformed zebrafish. *J. Biolumin. Chemilumin.* **10**, 271-275.
Mosimann, C., Kaufman, C. K., Li, P., Pugach, E. K., Tamplin, O. J. and Zon, L. I. (2011). Ubiquitous transgene expression and Cre-based recombination driven by the ubiquitin promoter in zebrafish. *Development* **138**, 169-177.
Moss, J. B., Koustubhan, P., Greenman, M., Parsons, M. J., Walter, I. and Moss, L. G. (2009). Regeneration of the pancreas in adult zebrafish. *Diabetes* **58**, 1844-1851.
Murayama, E., Kissa, K., Zapata, A., Mordelet, E., Briolat, V., Lin, H. F., Handin, R. I. and Herbomel, P. (2006). Tracing hematopoietic precursor migration to successive hematopoietic organs during zebrafish development. *Immunity* **25**, 963-975.
Niers, J. M., Kerami, M., Pike, L., Lewandrowski, G. and Tannous, B. A. (2011). Multimodal in vivo imaging and blood monitoring of intrinsic and extrinsic apoptosis. *Mol. Ther.* **19**, 1090-1096.
Oldenburg, K. R., Vo, K. T., Michaelis, S. and Paddon, C. (1997). Recombination-mediated PCR-directed plasmid construction in vivo in yeast. *Nucleic Acids Res.* **25**, 451-452.
Paulmurugan, R., Umezawa, Y. and Gambhir, S. S. (2002). Noninvasive imaging of protein-protein interactions in living subjects by using reporter protein complementation and reconstitution strategies. *Proc. Natl. Acad. Sci. USA* **99**, 15608-15613.
Phelan, P. E., Pressley, M. E., Witten, P. E., Mellon, M. T., Blake, S. and Kim, C. H. (2005). Characterization of snakehead rhabdovirus infection in zebrafish (Danio rerio). *J. Virol.* **79**, 1842-1852.
Poss, K. D., Wilson, L. G. and Keating, M. T. (2002). Heart regeneration in zebrafish. *Science* **298**, 2188-2190.
Pugach, E. K., Li, P., White, R. and Zon, L. (2009). Retro-orbital injection in adult zebrafish. *J. Vis. Exp.* **34**, 1645. 10.3791/1645
Rawls, J. F., Mahowald, M. A., Ley, R. E. and Gordon, J. I. (2006). Reciprocal gut microbiota transplants from zebrafish and mice to germ-free recipients reveal host habitat selection. *Cell* **127**, 423-433.
Sacco, A., Doyonnas, R., Kraft, P., Vitorovic, S. and Blau, H. M. (2008). Self-renewal and expansion of single transplanted muscle stem cells. *Nature* **456**, 502-506.
Sadikot, R. T. and Blackwell, T. S. (2008). Bioluminescence: imaging modality for in vitro and in vivo gene expression. *Methods Mol. Biol.* **477**, 383-394.
Sadler, K. C., Krahn, K. N., Gaur, N. A. and Ukomadu, C. (2007). Liver growth in the embryo and during liver regeneration in zebrafish requires the cell cycle regulator, uhrf1. *Proc. Natl. Acad. Sci. USA* **104**, 1570-1575.
Scabini, M., Stellari, F., Cappella, P., Rizzitano, S., Texido, G. and Pesenti, E. (2011). In vivo imaging of early stage apoptosis by measuring real-time caspase-3/7 activation. *Apoptosis* **16**, 198-207.

Stachura, D. L., Svoboda, O., Lau, R. P., Balla, K. M., Zon, L. I., Bartunek, P. and Traver, D. (2011). Clonal analysis of hematopoietic progenitor cells in the zebrafish. *Blood* **118**, 1274-1282.

Tinkum, K. L., Marpegan, L., White, L. S., Sun, J., Herzog, E. D., Piwnica-Worms, D. and Piwnica-Worms, H. (2011). Bioluminescence imaging captures the expression and dynamics of endogenous p21 promoter activity in living mice and intact cells. *Mol. Cell. Biol.* **31**, 3759-3772.

Traver, D., Paw, B. H., Poss, K. D., Penberthy, W. T., Lin, S. and Zon, L. I. (2003). Transplantation and in vivo imaging of multilineage engraftment in zebrafish bloodless mutants. *Nat. Immunol.* **4**, 1238-1246.

Van de Bittner, G. C., Dubikovskaya, E. A., Bertozzi, C. R. and Chang, C. J. (2010). In vivo imaging of hydrogen peroxide production in a murine tumor model with a chemoselective bioluminescent reporter. *Proc. Natl. Acad. Sci. USA* **107**, 21316-21321.

Vihtelic, T. S. and Hyde, D. R. (2000). Light-induced rod and cone cell death and regeneration in the adult albino zebrafish (Danio rerio) retina. *J. Neurobiol.* **44**, 289-307.

Wagers, A. J., Sherwood, R. I., Christensen, J. L. and Weissman, I. L. (2002). Little evidence for developmental plasticity of adult hematopoietic stem cells. *Science* **297**, 2256-2259.

Wang, J., Panáková, D., Kikuchi, K., Holdway, J. E., Gemberling, M., Burris, J. S., Singh, S. P., Dickson, A. L., Lin, Y. F., Sabeh, M. K. et al. (2011). The regenerative capacity of zebrafish reverses cardiac failure caused by genetic cardiomyocyte depletion. *Development* **138**, 3421-3430.

Weger, M., Weger, B. D., Diotel, N., Rastegar, S., Hirota, T., Kay, S. A., Strähle, U. and Dickmeis, T. (2013). Real-time in vivo monitoring of circadian E-box enhancer activity: a robust and sensitive zebrafish reporter line for developmental, chemical and neural biology of the circadian clock. *Dev. Biol.* **380**, 259-273.

White, R. M., Sessa, A., Burke, C., Bowman, T., LeBlanc, J., Ceol, C., Bourque, C., Dovey, M., Goessling, W., Burns, C. E. et al. (2008). Transparent adult zebrafish as a tool for in vivo transplantation analysis. *Cell Stem Cell* **2**, 183-189.

Zinn, K. R., Chaudhuri, T. R., Szafran, A. A., O'Quinn, D., Weaver, C., Dugger, K., Lamar, D., Kesterson, R. A., Wang, X. and Frank, S. J. (2008). Noninvasive bioluminescence imaging in small animals. *ILAR J.* **49**, 103-115.

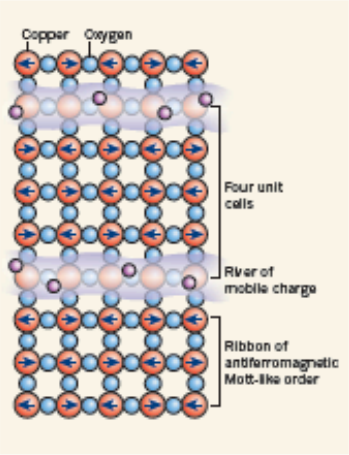

Figure 2 | Stripe-like electronic order in the cuprates. In this form of electronic order, the material's copper oxide planes have ribbons of antiferromagnetic Mott-like order — the spin of each electron (arrowed) is in the opposite direction to those of its neighbours — separated by narrow rivers of mobile charge (purple spheres). The periodicity of the arrangement is four lattice unit cells. Parker and colleagues' results[1] support the hypothesis that fluctuating stripes (more disordered than those shown here) promote superconductivity.

advances in STM technology have enabled the discovery[6] of chequerboard patterns in a magnetic field similar to what would be expected for stripes, and a stripe-like pattern[7] in zero field. However, the main features of these patterns were argued[8,9] to be consistent with a completely different explanation: quasiparticle interference, in which particle-like entities scatter from defects in the material, creating standing waves. Since then, a debate has raged as to whether the features observed in the STM data are fully explainable as quasiparticle interference, or whether stripe-like order must also be present[10,11]. Quantitative tests have been proposed[12] to distinguish between the two classes of effect, and more experiments have been carried out.

Parker *et al.*[1] analysed STM maps at many values of doping and temperature. In addition to the quasiparticle-interference patterns, the authors clearly demonstrated, using tests proposed earlier[12], the existence of a fluctuating stripe order — strongest at 1/8 doping and with a periodicity of four unit cells — at temperature and doping values that are associated with the pseudogap regime. This observation is consistent with the picture of fluctuating microscopic phase separation into ribbons of Mott insulator separated by rivers of charge. They find that the fluctuating stripe order weakens at dopings lower than 1/8, whereas the pseudogap is known to remain strong into the antiferromagnetic phase. This indicates that the pseudogap is necessary for the stripe formation but that the pseudogap and stripe formation are not the same phenomena.

Much more work is needed before the mechanism of superconductivity will be solved or the cuprates have a full microscopic theory, if they ever do. Other points of view and related topics, such as the role of a quantum critical point and the question of whether the pseudogap is a well-defined phase, continue to both incite and inspire. Nevertheless, Parker and colleagues' new data and analysis[1], which show the existence of fluctuating stripe order throughout the pseudogap region of BSCCO, make a convincing case that fluctuating stripes are much more common than previously thought. Although they detect only the charge order and not the spin, and other measurements are needed to create a complete picture, these results increase the plausibility of the hypothesis that fluctuating stripes indeed aid the superconductivity, and will give pause to those who have considered stripes a mere distraction. ■

Kathryn A. Moler *is in the Departments of Applied Physics and of Physics, and the Stanford Institute for Materials and Energy Science, Stanford University, Stanford, California 94305, USA.*
e-mail: kmoler@stanford.edu

1. Parker, C. V. *et al. Nature* **468**, 677–680 (2010).
2. Emery, V. J., Kivelson, S. A. & Zachar, O. *Phys. Rev. B* **56**, 6120–6147 (1997).
3. Tranquada, J. M., Sternlieb, B. J., Axe, J. D., Nakamura, Y. & Uchida, S. *Nature* **375**, 561–563 (1995).
4. Fujita, M., Goka, H., Yamada, K. & Matsuda, M. *Phys. Rev. Lett.* **88**, 167008 (2002).
5. Abbamonte, P. *et al. Nature Phys.* **1**, 155–158 (2005).
6. Hoffman, J. E. *et al. Science* **295**, 466–469 (2002).
7. Howald, C., Eisaki, H., Kaneko, N., Greven, M. & Kapitulnik, A. *Phys. Rev. B* **67**, 014533 (2003).
8. Hoffman, J. E. *et al. Science* **297**, 1148–1151 (2002).
9. McElroy, K. *et al. Nature* **422**, 592–596 (2003).
10. Fang, A., Howald, C., Kaneko, N., Greven, M. & Kapitulnik, A. *Phys. Rev. B* **70**, 214514 (2004).
11. Vershinin, M. *et al. Science* **303**, 1995–1998 (2004).
12. Kivelson, S. A. *et al. Rev. Mod. Phys.* **75**, 1201–1241 (2003).

STEM CELLS

The blood balance

Blood cells are generated from haematopoietic stem cells on demand. The protein Lkb1, which lies at the crossroad of energy metabolism and cell growth, seems to regulate these stem cells' dynamics. SEE ARTICLES P.653, P.659 & LETTER P.701

ELLEN M. DURAND & LEONARD I. ZON

The haematopoietic stem cells (HSCs) give rise to all mature blood cells through the process of haematopoiesis. This rare cell population also maintains the balance of blood cells in response to stress, by fluctuating between quiescent and actively cycling states depending on physiological conditions. Transplantation of HSCs is an effective treatment for cancers, such as lymphoma and leukaemia, as well as for autoimmune diseases and other blood-related conditions[1]. But despite much information about the function and clinical relevance of HSCs, little is known about the energetics and metabolic control of HSC dynamics. Three papers[2–4] in this issue describe a role for the protein Lkb1 in the metabolic regulation of HSCs.

Best known for its functions as a tumour suppressor, Lkb1 is a kinase enzyme that regulates the activity of AMP-activated protein kinase (AMPK) — a master regulator of energetics — and several other AMPK-related enzymes through phosphorylation. When energy and nutrient levels are low, Lkb1 activates AMPK, which in turn causes repression of mTORC (a protein complex that mediates protein synthesis) and a decline in cell proliferation[5] (Fig. 1).

Nakada *et al.*[2] (page 653) set out to determine whether Lkb1 regulates HSC dynamics and function. They used genetically engineered mice (*Mx1-Cre; LKB1*$^{F/F}$), which can be manipulated using a polynucleotide, polyinosine–polycytosine (pIpC), to delete the *Lkb1* gene whenever desired. The authors could thus study the effect of Lkb1 on haematopoiesis, and on the cell-cycle dynamics of not only HSCs, but also the multipotent blood-cell progenitors that arise from HSCs, and whole-bone-marrow (WBM) cells, which include a collection of cells of the haematopoietic system — ranging from HSCs to completely differentiated cells.

Deletion of *Lkb1* resulted in an initial expansion of HSCs and multipotent progenitor cells. With time, however, a depletion of these cell populations and eventually a depletion of all blood cell types (pancytopenia) occurred. *Lkb1* deficiency also led to increased turnover of HSCs and multipotent progenitor cells, but not of WBM cells. This hints that Lkb1 has a role in regulating the cell-cycle dynamics of HSCs and multipotent progenitor cells but not of fully differentiated cells.

Transplantation assays are the gold standard for testing the function of HSCs, as only HSCs can completely restore the haematopoietic

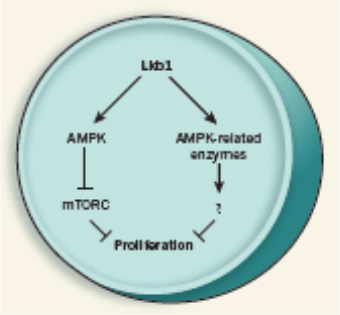

Figure 1 | The regulatory role of Lkb1. Normally, Lkb1 is inactive and so cells can divide. In response to physiological stress, however, Lkb1 signals through the kinase AMPK to suppress mTORC and so decrease cell proliferation. New work[2–4] shows that Lkb1 regulates the function and dynamics of haematopoietic stem cells (HSCs), although these regulatory roles of Lkb1 are not mediated by the AMPK–mTORC pathway. Whether Lkb1 exerts its effects on HSCs through AMPK-related kinases and their as-yet-unknown downstream pathways, remains unclear.

system of the recipient. Nakada *et al.* report that in mice irradiated to deplete their HSCs, Lkb1-deficient WBM cells could not reconstitute the haematopoietic system — an indication that Lkb1 also regulates HSC function. The authors therefore conclude that, compared with more differentiated cells (multipotent progenitor cells and some WBM cells), the survival of HSCs depends more acutely on Lkb1.

Gurumurthy *et al.*[3] (page 659) and Gan *et al.*[4] (page 701) use a different mouse model (*RosaCreERT2; LKB1*$^{L/L}$) to study the effects of *Lkb1* deletion on the haematopoietic system. These authors[3,4] also observe decreased levels of HSCs and multipotent progenitor cells, as well as pancytopenia, albeit at earlier time points following *Lkb1* deletion. Their data are also consistent with those of Nakada *et al.* in showing that, compared with the more differentiated haematopoietic cell types, *Lkb1* deletion particularly affects HSC dynamics, leading to both increased proliferation of these cells and their increased programmed death by the process of apoptosis.

As well as the function and dynamics of HSCs, Lkb1 seems to regulate the function of mitochondria (the cellular powerhouses) in these cells. In cell populations enriched for HSCs, depletion of Lkb1 protein led to a decrease in the expression of PGC-1α and PGC-1β — two transcriptional regulators of mitochondrial biogenesis[4]. Lkb1 depletion also caused a reduction in mitochondrial membrane potential in HSCs[2,3] — a sign of decreased mitochondrial function and integrity. Finally, an increase in mitochondrial mass was associated with the lack of this protein, possibly to compensate for decreased ATP levels in these cells.

Intriguingly, the mechanism by which Lkb1 regulates HSC homeostasis seems to be largely independent of its downstream effectors AMPK and mTORC. Not only was mTORC not activated in Lkb1-deficient HSCs, but the addition of the mTORC inhibitor rapamycin did not overcome HSC defects[2]. Similarly, treatment with the AMPK activators metformin or A-769662 did not reverse any of the cellular or functional defects associated with Lkb1 deletion in HSCs[3,4]. What's more, AMPK-deficient mice did not show a depletion of HSCs — as was seen following Lkb1 depletion — and transplantation of HSCs from these animals into irradiated normal mice allowed long-term multi-lineage reconstitution of blood cells[2].

These findings clearly establish an essential role for Lkb1 in HSC homeostasis, and show that, among blood-lineage cells, the HSC population is particularly sensitive to depletion of this protein. The relatively minor differences in the results of experiments in *Mx1-Cre; LKB1*$^{f/f}$ mice from those in *RosaCreERt2; LKB1*$^{L/L}$ mice could probably be explained by the dose and the source of the pIpC used to trigger *Lkb1* deletion (these factors can cause great variation in the efficiency of conditional gene deletion).

For instance, such differences might account for Gurumurthy and colleagues' observation of an earlier onset of pancytopenia — compared with the findings of Nakada *et al.*[2] — and an increased activity of the enzyme caspase, which mediates apoptosis. As the RosaCreERt2 system is a more reliable and consistent method for targeted gene deletion, the *RosaCreERt2; LKB1*$^{L/L}$ mice may be a more useful model to investigate the extent of defects caused by Lkb1 deficiency, and to ascertain that these effects are truly HSC specific.

Nonetheless, the collective data of all three papers[2–4] provide a framework for understanding the role of Lkb1 in the homeostasis of blood-cell formation and suggest a novel metabolic checkpoint that is active during this process. Whether the AMPK-related kinases mediate the effects of Lkb1 depletion on HSC homeostasis, or whether the mechanism is entirely AMPK independent, remains an intriguing outstanding question. ■

Ellen M. Durand *and* Leonard I. Zon *are at the Children's Hospital Boston, Division of Hematology/Oncology, Boston, Massachusetts 02115, USA.*
e-mails: edurand@fas.harvard.edu; zon@enders.tch.harvard.edu

1. Shizuru, J. A., Negrin, R. S. & Weissman, I. L. *Annu. Rev. Med.* **56**, 509–538 (2005).
2. Nakada, D., Saunders, T. L. & Morrison, S. J. *Nature* **468**, 653–658 (2010).
3. Gurumurthy, S. *et al. Nature* **468**, 659–663 (2010).
4. Gan, B. *et al. Nature* **468**, 701–704 (2010).
5. Shaw, R. J. *Acta Physiol.* **196**, 65–80 (2009).

L.I.Z. declares competing financial interests; see online article for details.

STRUCTURAL BIOLOGY

An alphavirus puzzle solved

Alphaviruses infect their host by binding to cellular receptors and fusing with cell membranes. New studies define the receptor-binding protein of these viruses and its regulation of the membrane-fusion reaction. SEE LETTERS P.705 & P.709

MARGARET KIELIAN

Many viruses are enclosed in an envelope — a membrane that is derived from the infected host cell during virus exit. To infect a new host cell, specialized membrane-fusion proteins on the virus envelope fuse it with a membrane of the host cell, delivering the viral genome into the cell. This fusion activity must be deployed at precisely the right time during virus entry, and must also be silenced during viral assembly and exit. In this issue, Li *et al.*[1] and Voss *et al.*[2] provide structural insights into the regulation of the membrane-fusion proteins of enveloped alphaviruses during the viruses' entry into and exit from the host cell.

Many alphaviruses are medically relevant; chikungunya virus, for example, is an emerging human pathogen responsible for major recent epidemics[3]. There are currently no treatments for alphavirus infections, and detailed information on the structure and life cycle of these viruses is crucial for developing antiviral strategies and vaccines.

But first, a quick glance at what is already known. The membrane-fusion protein of alphaviruses is E1, and its fusion activity is triggered by the mildly acidic pH of intracellular vesicles[4]. Structural studies have defined the architecture of the E1 molecule[5,6], its arrangement on the virus particle[5–8], and conformational changes in it that drive membrane fusion[9]. E1 is tightly associated with another

Cell

Lineage Regulators Direct BMP and Wnt Pathways to Cell-Specific Programs during Differentiation and Regeneration

Eirini Trompouki,[1,10] Teresa V. Bowman,[1,10] Lee N. Lawton,[2] Zi Peng Fan,[2,9] Dai-Chen Wu,[3,4] Anthony DiBiase,[1] Corey S. Martin,[1] Jennifer N. Cech,[1] Anna K. Sessa,[1] Jocelyn L. Leblanc,[1] Pulin Li,[1] Ellen M. Durand,[1] Christian Mosimann,[1] Garrett C. Heffner,[5,6,7,8] George Q. Daley,[5,6,7,8] Robert F. Paulson,[3,4] Richard A. Young,[2] and Leonard I. Zon[1,*]

[1]Stem Cell Program and Division of Hematology/Oncology, Children's Hospital Boston, Harvard Stem Cell Institute, Harvard Medical School and Howard Hughes Medical Institute, Boston, MA 02115, USA
[2]Whitehead Institute for Biomedical Research, Cambridge, MA 02142, USA
[3]Graduate program in Biochemistry, Microbiology, and Molecular Biology
[4]Department of Veterinary and Biomedical Sciences
Pennsylvania State University, University Park, PA 16802, USA
[5]Stem Cell Transplantation Program, Division of Pediatric Hematology/Oncology, Manton Center for Orphan Disease Research, Howard Hughes Medical Institute, Children's Hospital Boston and Dana Farber Cancer Institute, Boston, MA 02115, USA
[6]Division of Hematology, Brigham and Women's Hospital, Boston, MA 02115, USA
[7]Department of Biological Chemistry and Molecular Pharmacology, Harvard Medical School, Boston, MA 02115, USA
[8]Harvard Stem Cell Institute, Boston, MA 02115, USA
[9]Computational and Systems Biology Program, Massachusetts Institute of Technology, Cambridge, MA 02142, USA
[10]These authors contributed equally to this work
*Correspondence: zon@enders.tch.harvard.edu
DOI 10.1016/j.cell.2011.09.044

SUMMARY

BMP and Wnt signaling pathways control essential cellular responses through activation of the transcription factors SMAD (BMP) and TCF (Wnt). Here, we show that regeneration of hematopoietic lineages following acute injury depends on the activation of each of these signaling pathways to induce expression of key blood genes. Both SMAD1 and TCF7L2 co-occupy sites with master regulators adjacent to hematopoietic genes. In addition, both SMAD1 and TCF7L2 follow the binding of the predominant lineage regulator during differentiation from multipotent hematopoietic progenitor cells to erythroid cells. Furthermore, induction of the myeloid lineage regulator C/EBPα in erythroid cells shifts binding of SMAD1 to sites newly occupied by C/EBPα, whereas expression of the erythroid regulator GATA1 directs SMAD1 loss on nonerythroid targets. We conclude that the regenerative response mediated by BMP and Wnt signaling pathways is coupled with the lineage master regulators to control the gene programs defining cellular identity.

INTRODUCTION

Cells sense and respond to their cellular environment through signal transduction pathways, which can deliver information to the genome in the form of activated transcription factors. These factors tend to occupy specific genomic regions and associate with different coactivators and chromatin-remodeling complexes to direct their response. This occurs by either activating or repressing transcription or by changing the chromatin architecture, thus reforming the accessibility of certain genomic loci (Mosimann et al., 2009; Moustakas and Heldin, 2009). This combination of actions allows for the same signaling pathways to be used in multiple cellular environments eliciting different responses.

The BMP and Wnt signaling pathways are two highly conserved signaling pathways that interact during many developmental processes, ultimately through regulation of transcription via SMAD and TCF/LEF transcription factors (Clevers, 2006; Larsson and Karlsson, 2005; Staal and Luis, 2010). Both pathways participate in the formation of the hematopoietic system during development but appear to be expendable during adult steady-state hematopoiesis (Cheng et al., 2008; Goessling et al., 2009; Jeannet et al., 2008; Koch et al., 2008; Lengerke et al., 2008; McReynolds et al., 2007; Nostro et al., 2008; Singbrant et al., 2010; Tran et al., 2010). In both development and regeneration, hematopoietic stem cells (HSCs) divide and differentiate in response to cell-intrinsic and -extrinsic signals to produce all of the hematopoietic lineages. Here we show that the BMP and Wnt signaling pathways are critical for efficient regeneration of the adult hematopoietic system, as they are in development. Additionally, BMP and Wnt have been implicated in differentiation into erythroid and myeloid lineages. Specifically, in culture, BMP treatment can augment erythroid, megakaryocytic, and granulocytic-monocytic output of $CD34^+$

progenitors (Detmer and Walker, 2002; Fuchs et al., 2002; Jeanpierre et al., 2008). Similarly, Wnt3a ligand can regulate the production of erythroid and myeloid cells from embryonic stem cells (ESCs) and myeloid progenitors from adult HSCs (Cheng et al., 2008; Nostro et al., 2008; Staal and Luis, 2010).

The underlying mechanism for BMP and Wnt regulation of regeneration and differentiation resides in the cell-type-specific targets of the SMAD and TCF transcription factors, respectively. Based on previous findings, SMAD and TCF proteins can couple with other transcription factors to regulate a small number of cell-specific genes (Clevers, 2006; Massagué et al., 2005; Mosimann et al., 2009). Signaling-mediated transcription factors have recently begun to be studied in a genome-wide manner, and these studies have revealed that Smad1 and Tcf7l1/Tcf3 can co-occupy target sites with the Oct4/Nanog/Sox2 transcriptional complex on pluripotency target genes in ESCs (Chen et al., 2008; Cole et al., 2008), and TCF7L2 can colocalize with CDX2 in colonic cells (Verzi et al., 2010). This led us to consider the possibility that BMP and Wnt signaling factors couple with distinct transcription factors important for lineage identity during hematopoietic regeneration and differentiation.

To determine how SMAD and TCF transcription factors select their targets in distinct lineages during regeneration and differentiation, we explored their genome-wide DNA binding in various hematopoietic environments across multiple species. Initially, cobinding of Smad1 with Gata2 at individual genes in regenerating progenitors was observed. Genome-wide analysis revealed that SMAD1 and TCF7L2 selectively bind in concert with cell-specific master regulators at lineage-distinctive genes in erythroid and myeloid cell populations. In addition, the expression of a myeloid master regulator in erythroid cells is sufficient to redirect a fraction of Smad1 binding. During differentiation, the binding of signaling factors shifts from genes of multiple hematopoietic lineages in progenitor cells to genes specific for differentiated cells guided by the dominant lineage factor. Together, these data support a mechanism by which lineage regulators direct SMAD and TCF proteins to tissue-specific enhancers. The selective use of these pathways during regeneration suggests that coordinated binding of SMAD1 and TCF7L2 with lineage-restricted regulators is the underlying mechanism for BMP and Wnt effects during hematopoietic differentiation and regeneration.

RESULTS

Wnt and BMP Play Essential Roles in Hematopoietic Regeneration

Wnt and BMP signaling are required during hematopoietic development, but it is unclear whether either pathway is necessary for adult hematopoietic regeneration. A zebrafish model was used to determine whether Wnt or BMP signaling is necessary during this process. Adult zebrafish were sublethally irradiated, and recovery of whole kidney marrow (WKM) cells was monitored by flow cytometry to identify precursor populations that are the first detectable sign of hematopoietic recovery (Traver et al., 2004) (Figure 1A). Stimulation of the Wnt signaling pathway using a heat shock-inducible Wnt8 ligand (Weidinger et al., 2005), or treatment with the GSK3 chemical inhibitor BIO, resulted in an increase in the frequency of precursors (3- and 2-fold, respectively) during regeneration (Figure 1B) (Goessling et al., 2009). In contrast, inhibition of Wnt signaling by heat shock-induced expression of Dkk1 (Stoick-Cooper et al., 2007) led to diminished precursor levels (Figure 1B). Stimulation of the BMP pathway using a heat shock-inducible BMP2 ligand (Rentzsch et al., 2006) enhanced the number of precursors more than 2-fold (Figure 1B), whereas blocking the BMP pathway using either a heat shock-inducible Chordin (Tucker et al., 2008) or the BMP type I receptor chemical inhibitor dorsomorphin (DM) diminished precursor recovery levels to less than half of the wild-type levels (Figure 1B). Murine competitive bone marrow transplantation experiments were used to assess whether the roles for Wnt and BMP in hematopoietic regeneration were conserved and to determine whether the effects were cell-intrinsic (Figure S1A). We found that the ex vivo activation of Wnt signaling led to a greater number of animals with multilineage engraftment (Figure S1B). In contrast, ex vivo inhibition of BMP signaling abrogated engraftment (Figure S1B). These data suggest that Wnt and BMP have a conserved, cell-autonomous role during adult hematopoietic regeneration.

The transcriptional effects of BMP and Wnt signaling were evaluated by studying the expression of hematopoietic genes in zebrafish WKM after irradiation following a 2 hr heat shock induction of BMP2 or Wnt8. Activation of the pathways was confirmed using quantitative PCR (qPCR) for the BMP2 and Wnt8 ligands as well as known downstream targets such as *id1* for BMP and *cyclind1* for Wnt (Figure S1C). Overexpression of BMP increased the levels of the hematopoietic genes *scl, runx1, c-myb*, and *gata2*, whereas Wnt stimulation increased the expression of *scl*, *runx1,* and *gata2* (Figure 1C). These data demonstrate that during in vivo regeneration, BMP and Wnt pathways regulate hematopoietic targets at the level of gene expression, which led us to further investigate whether the signaling-directed transcription factors directly bind to enhancer elements of blood genes.

We next asked whether Smad1, which is a transcription factor activated by BMP signaling, co-occupied hematopoietic genes with the lineage regulator Gata2. In multilineage hematopoietic progenitors, Gata2 is an essential transcription factor that binds to the regulatory elements in genes expressed in progenitors and differentiated lineages (Tsai et al., 1994; Wilson et al., 2010). In order to obtain sufficient cell numbers to perform chromatin immunoprecipitation (ChIP) analysis, a mouse irradiation injury model was used (Hooper et al., 2009). Lineage-negative progenitors were isolated from mice 7 days after a sublethal irradiation, and then ChIP-PCR was performed for known targets of Gata2 (Figure 1D) (Wilson et al., 2010). Smad1 and Gata2 co-occupied hematopoietic genes including *Cd9*, *Il13*, *Meis1*, and *Mapk6* (Figure 1E). Together, these results indicate that BMP and Wnt are required for regeneration and act at least in part by modulating genes bound by the lineage regulator Gata2.

TCF7L2 and SMAD1 Transcription Factors Co-occupy Genomic Sites with GATA Factors in an Erythroid Environment

We next asked whether the transcription factors activated by Wnt and BMP signaling cobind with blood-specific lineage

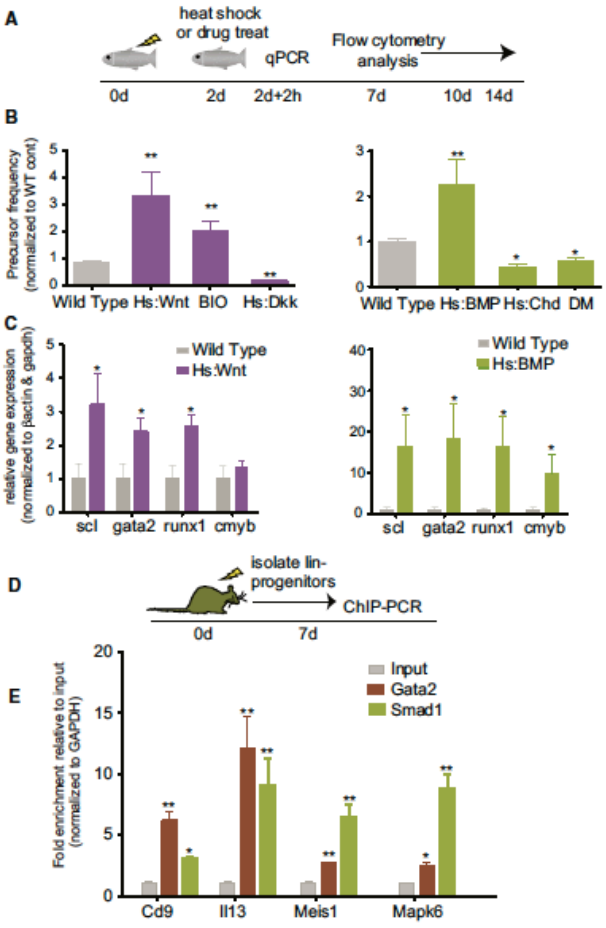

Figure 1. BMP and Wnt Pathways Regulate Hematopoietic Regeneration

(A) Schematic of an irradiation-induced hematopoietic regeneration model. Adult zebrafish are irradiated with 20 Gy γ-irradiation at day 0, treated on day 2, and then WKM cells are dissected and analyzed by flow cytometry or by qPCR.

(B) Activation of the Wnt and BMP pathways enhances regeneration in zebrafish. Graphs depicting the relative frequency ± standard error of the mean (SEM) of precursors in WKM relative to wild-type controls following manipulations to the Wnt (left) and BMP (right) pathways. *$p < 0.05$ and **$p < 0.005$; p values calculated using Student's t test comparing wild-type control treated siblings to treated group.

(C) Activation of the Wnt (left) and BMP (right) pathways leads to upregulation of key hematopoietic genes. qPCR graphs of relative gene expression ± SEM in WKM cells from wild-type, Hs:Wnt, or Hs:BMP 2 days post-irradiation following a 2 hr heat shock induction of Wnt8a or BMP2b transgene expression, respectively. *$p < 0.05$; p values calculated using Student's t test comparing wild-type control treated siblings to treated group.

(D and E) Gata2 colocalizes with Smad1 on hematopoietic targets in murine progenitor cells during regeneration. (D) Schematic of irradiation model. ChIP for Smad1 and Gata2 was performed on lineage-negative progenitors isolated from mice 7 days after a 6.5 Gy irradiation. (E) qPCR of whole-cell extracts (input), Gata2, and Smad1 ChIP. The bars show relative enrichment ± SEM compared to input control. *$p < 0.05$ and **$p < 0.005$; p values calculated using Student's t test comparing ChIP DNA to input control.

See also Figure S1.

regulators genome-wide by performing ChIP-seq for TCF7L2/TCF4 (Wnt pathway) and SMAD1 (BMP pathway) as well as GATA1 and GATA2. ChIP-seq was performed in K562 cells, which are erythroleukemia cells that express GATA1 and GATA2, essential transcription factors for erythroid and progenitor cells, respectively (Cantor, 2005; Tsai et al., 1994; Tsiftsoglou et al., 2009). Cells were treated with BIO to activate the Wnt pathway or BMP4 to activate the BMP pathway. Both TCF7L2 and SMAD1 showed substantial overlap with GATA1 and GATA2 at individual genes and genome-wide (Figures 2A and 2B). To confirm the specificity of the analysis, TCF7L2 and SMAD1 binding at known targets was analyzed (Figure S2A), and we found that inhibition of BMP signaling resulted in considerable loss of SMAD1 binding across the genome (Figure S2B).

If the main targets for TCF7L2 and SMAD1 are the blood genes regulated by GATA factors, then we should see enrichment for red blood cell genes in their targets. Functional classification of the genes occupied by TCF7L2 or SMAD1 in K562 erythroleukemia cells revealed enrichment for genes highly associated with red blood cell development (Figures S2C–S2E). If TCF7L2 and SMAD1 bind to the same sites as GATA1 and GATA2, then there should be enrichment for GATA motifs in the sites bound by TCF7L2 or SMAD1. As expected, the most prominent motif in regions bound by TCF7L2 and SMAD1 was the GATA motif (Figure S2F). Scanning for GATA, SMAD, and TCF motifs across the regions bound by SMAD1, TCF7L2, GATA1, or GATA2 demonstrated enrichment of all three motifs in the bound sites (Figure S2G). Furthermore, Wnt and BMP stimulation did not significantly affect the binding of GATA factors (Figure S3). If GATA factors direct the binding of signaling factors, then the expectation would be to find them interacting with the same genomic sites at the same time. ChIP for SMAD1 was performed followed by ChIP for GATA2, and PCR showed that SMAD1 and GATA2 simultaneously occupied key erythroid genes (Figure 2C). These results are consistent with co-occupancy of TCF7L2 and SMAD1 with GATA1 and GATA2 in K562 cells and demonstrate

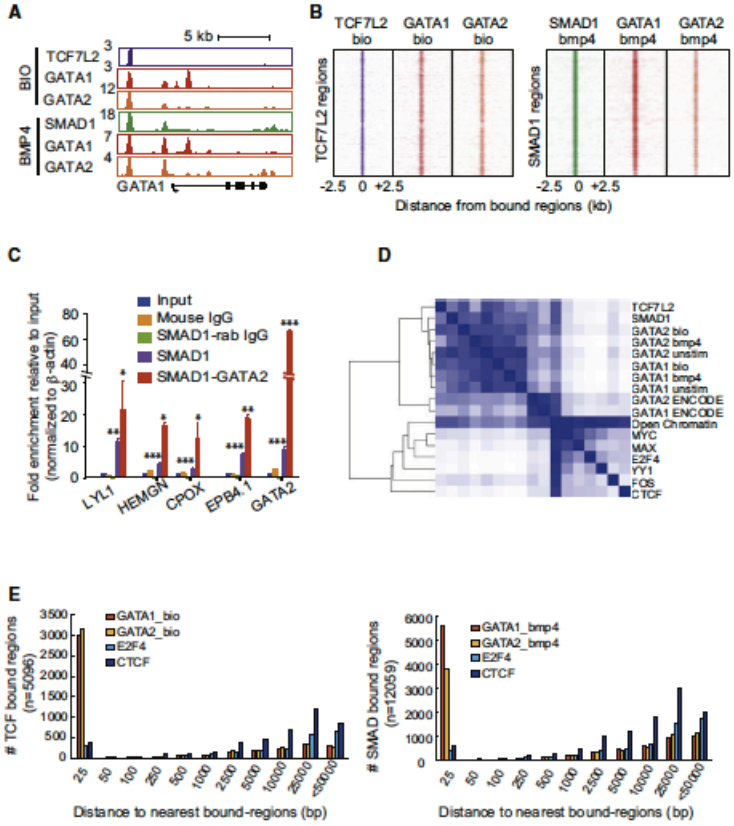

Figure 2. SMAD1 and TCF7L2 Co-occupy the Genome with Key Regulators of the Erythroid Lineage

(A) Gene track of the *GATA1* locus showing TCF7L2 (purple), GATA1 (red), GATA2 (orange), and SMAD1 (green) binding of specific genomic regions along the x axis and the total number of reads per million on the y axis.

(B) SMAD1 and TCF7L2 co-occupy genomic regions with GATA1 and GATA2. Region plots represent the distribution of GATA1- and GATA2-bound regions −2.5 to +2.5 kb relative to all TCF7L2- or SMAD1-bound regions in K562 cells.

(C) qPCR of whole-cell extracts (input), SMAD1 and control mouse IgG, sequential ChIP for GATA2, and control rabbit IgG on the SMAD1 ChIP. The bars show relative enrichment ± SEM compared to input control. *$p < 0.08$ and **$p < 0.04$, ***$p < 0.0005$; p values calculated using Student's t test comparing SMAD1 ChIP to input and SMAD1 ChIP to SMAD1-GATA2 sequential ChIP.

(D) Colocalization of SMAD1 and TCF7L2 is specific to lineage regulators. Heatmap depicting the relative level of colocalization of indicated factors, in K562 cells together with open chromatin data in this cell line.

(E) E2F4 and CTCF binding is not associated with TCF7L2 or SMAD1. The distance from the center of each TCF7L2 site (left) and SMAD1 site (right) to the center of the nearest site bound by the indicated transcription factor was determined. These distances were grouped into bins (x axis). The sum of bound sites in each bin is shown (y axis).

See also Figures S2 and S3.

that Wnt and BMP signaling were directed to genes occupied by GATA factors that specified the red blood cell state.

We next asked whether TCF7L2 or SMAD1 preferentially occupied the genome with GATA1 and GATA2 in K652 cells. Available data were analyzed for other transcription factors in K562 cells (Birney et al., 2007; Raney et al., 2011; Rosenbloom et al., 2010). Both TCF7L2 and SMAD1 tend to bind sites with GATA1 and GATA2 but do not tend to occupy sites with the other tested transcription factors, despite previous reports that SMAD1 could interact with several of these factors in other tissue types (Chen et al., 2002; Kurisaki et al., 2003) (Figure 2D). In addition, the distance from TCF7L2 or SMAD1 sites to the nearest

binding sites for GATA1, GATA2, E2F4, and CTCF was calculated. The majority of TCF or SMAD sites were occupied by the GATA factors but were distant from E2F4 and CTCF sites (Figure 2E). These data indicate that the genome-wide co-occupancy of TCF7L2 and SMAD1 with GATA1 and GATA2 is specific.

Co-occupied Regions Encompass Enhancers

Analysis of TCF7L2 and SMAD1 localization with multiple transcription factors in K562 cells revealed that each of the transcription factors examined occupied "open" chromatin sites as defined by FAIRE-Seq and DNase-Seq, which measure DNA accessibility (Song et al., 2011), indicating that TCF7L2 and SMAD1 do not indiscriminately bind to all open and available DNA sites (Figure 2D). This led us to investigate the class of regulatory elements occupied by BMP and Wnt signaling factors.

Transcriptional regulatory elements fall into well-defined groups that can be defined by position relative to gene, chromatin modification state, and occupancy by known regulators. In order to identify the class of regulatory elements that Wnt and BMP factors co-occupy with master regulators, the enriched regions were mapped to positions relative to RefSeq genes. To assess differences in regions cobound by signaling and lineage regulators versus those bound by a lineage regulator alone, regulatory elements in regions bound by GATA factors and TCF7L2 or SMAD1 were examined and compared to those bound by GATA factors alone. The majority of regions for all groups mapped to introns and intergenic regions, similar to many enhancer elements (Heintzman and Ren, 2009), in contrast to E2F4, which occupies sites adjacent to promoter regions (Figure 3A). This pattern suggests that TCF7L2 and SMAD1 co-occupy distal regulatory elements with GATA1 and GATA2 master regulators.

Mammalian enhancers are associated with the histone modification H3K4me1 (Heintzman et al., 2007, 2009; Rada-Iglesias et al., 2011; Visel et al., 2009). Therefore we asked whether the distinct GATA regions showed differences in these modifications. Although each group was marked by H3K4me1 surrounding the GATA-bound regions, those sites where TCF7L2 or SMAD1 colocalize with GATA factors showed a greater enrichment (Figure 3B). To determine whether these enhancers tend to be associated with actively transcribed genes, the transcriptional activity of genes within 5 kilobases (kb) of the enriched regions was classified into distinct states of active, poised, and silent. Active genes were defined as the RefSeq genes marked by the histone modifications H3K4me3 and H3K36me3. A higher proportion of regions were enriched at active genes (51%–54%) compared to the proportion of all active genes (35%) (Figure S4). Thus, the co-occupied regions of TCF7L2, SMAD1, and GATA factors are predominantly occupying enhancers of actively transcribed genes. Together, these observations predict that the expression level of GATA target genes would be responsive to perturbation of Wnt and BMP signaling.

TCF7L2 and SMAD1 Enhance Transcriptional Activation Mediated by GATA2

TCF7L2 and SMAD1 co-occupy enhancers of active, cell-type-specific genes with GATA factors. To assess the consequences of this co-occupancy on transcriptional output, we examined the effects of each transcription factor alone or in combination on the expression of the hematopoietic gene *LMO2*, which is bound by TCF7L2, SMAD1, GATA1, and GATA2 72 kb upstream of the transcriptional start site (TSS) in K562 cells (Figure 3C) (Landry et al., 2009). Induction of GATA2 alone was sufficient to increase reporter expression, whereas neither SMAD1 nor TCF7L2 alone had any effect (Figure 3D). In contrast, induction of either SMAD1 or TCF7L2 in the presence of GATA2 greatly enhanced reporter activity, indicating that the signaling factors affect transcription of blood-specific enhancer elements in combination with a lineage regulator (Figure 3D).

The observation that an increase in histone modifications is associated with active enhancers bound by TCF7L2, SMAD1, and GATA factors led to the hypothesis that binding of signaling factors could be influencing the chromatin state at these elements to affect transcriptional output. This could occur through recruitment of the histone acetyltransferase p300, with which both TCF/β-catenin and SMAD are known to interact (Hecht and Stemmler, 2003; Nakashima et al., 1999; Pearson et al., 1999). If recruitment of p300 is dependent on the activity of the Wnt and BMP signaling pathways, then perturbations to either Wnt or BMP signaling should affect the localization of p300 to the enhancers of blood-specific genes. As determined by ChIP-PCR, activation of either the Wnt or the BMP pathway in K562 cells did result in an increase of p300 occupancy, whereas inhibition of the pathways diminished p300 occupancy at the enhancer elements of blood genes (Figure 3E). We conclude that TCF7L2 and SMAD1 cooperate with lineage regulators to enhance the transcription of their target genes through co-occupancy of enhancers that are activated through recruitment of p300.

TCF7L2 and SMAD1 Transcription Factors Co-occupy Genomic Sites with C/EBPα in a Myeloid Environment

We next investigated whether TCF7L2 and SMAD1 occupied the genome with a different master regulator in another hematopoietic lineage. ChIP-seq was performed for TCF7L2, SMAD1, and C/EBPα, a known master regulator of the myeloid lineage, in the U937 monocytic leukemia cell line. TCF7L2 and SMAD1 tend to occupy different sites in erythroid (K562) and myeloid (U937) lineages, with only 15% of sites in common (Figure 4A). Furthermore, the sites occupied by TCF7L2 and SMAD1 tend to be the sites occupied by C/EBPα in U937 cells and by GATA in K562 cells (Figures 4B and 4C). In the erythroid environment, TCF7L2, SMAD1, GATA1, and GATA2 were bound within erythroid genes such as *HEMGN*, but those sites were not bound by TCF7L2, SMAD1, or C/EBPα in the myeloid environment (Figures 4B, 4C, S5A, and S5B). Similarly, genes with a stronger association with myeloid cells such as *CXCR4* were bound by TCF7L2, SMAD1, and C/EBPα in the myeloid environments but were not bound by TCF7L2, SMAD1, GATA1, or GATA2 in the erythroid environment (Figures 4B, 4C, S5A, and S5B). Motif scanning of the sequences around TCF7L2-, SMAD1-, or GATA-bound sites in K562 showed enrichment for GATA, SMAD, and TCF motifs and absence of C/EBP motifs, whereas in the myeloid cells C/EBP motifs were present and GATA motifs absent (Figure S5C). Treatment of U937 cells with BIO or BMP4

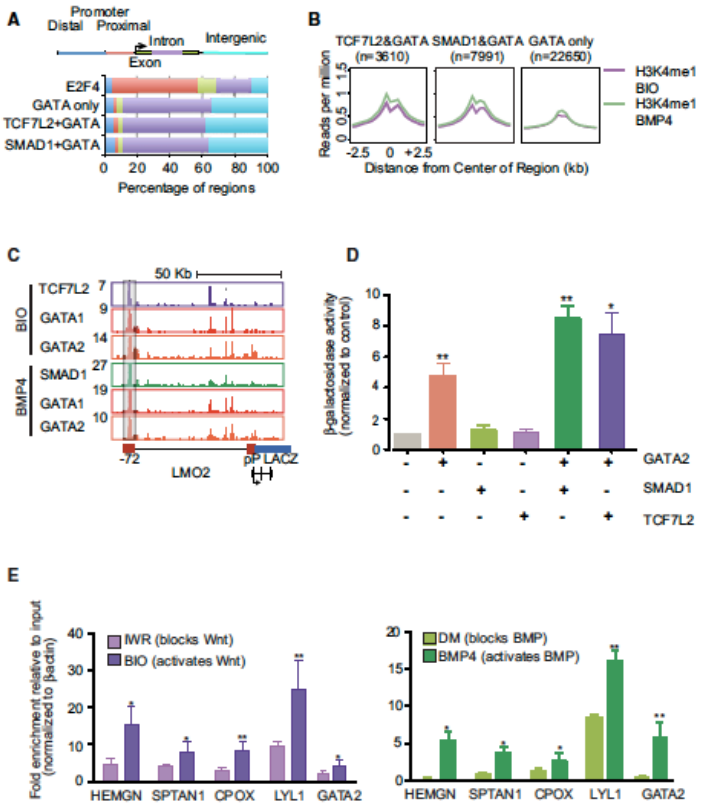

Figure 3. Signaling Factors Cooperate with Lineage Regulators at Distal Enhancers

(A) TCF7L2 and SMAD1 regions colocalize with GATA factors in intronic and intergenic regions. The groups of enriched regions occupied by GATA factors in K562 cells were divided into those occupied by GATA only, TCF7L2 and GATA, or SMAD1 and GATA. E2F4 is shown as a control. Each region was mapped to its closest RefSeq gene: distal promoter (blue), proximal promoter (red), exons (green), introns (purple), and intergenic regions (light blue).

(B) TCF7L2 and SMAD1 regions that colocalize with GATA factors occupy mainly enhancer regions. Composite H3K4me1-BIO (purple) and H3K4me1-BMP4 (green) enrichment profile for TCF7L2 and GATA cobound regions, SMAD1 and GATA cobound regions, or regions occupied only by GATA in K562 cells.

(C) Gene track of the *LMO2* locus. A schematic of the *LMO2* reporter indicating the enhancer and promoter regions included in the construct is shown below.

(D) SMAD1 and TCF7L2 cooperate with GATA2 and enhance transcription of target genes. Graph depicting β-galactosidase activity of the reporter ± SEM following overexpression of the transcription factors listed under each bar. *$p < 0.06$, **$p < 0.01$; p values calculated using Student's t test comparing mock-transfected controls to GATA2 alone and SMAD1/GATA2 or TCF7L2/GATA2 cotransfections to GATA2 alone.

(E) Wnt and BMP signaling enhance p300 recruitment to blood-specific targets. ChIP-PCR graphs showing p300 occupancy after activation or inhibition of the Wnt (left) and the BMP (right) pathways. *$p < 0.06$, **$p < 0.01$; p values calculated using Student's t test comparing inhibitor-treated samples to activator-treated samples. Values are mean ± SEM.

See also Figure S4.

had little influence on C/EBPα binding, showing that activation of the Wnt or BMP signaling pathways does not affect the genomic localization of the myeloid regulator (Figure S5D).

Analysis of bound regions among all the transcription factors analyzed showed a strong cell-type clustering (Figure 4D). TCF7L2- and SMAD1-bound sites in K562 show a stronger correlation with GATA1- and GATA2-occupied regions than TCF7L2- and SMAD1-bound sites in U937. These data suggest that TCF7L2 and SMAD1 show cell-lineage-specific binding at sites co-occupied by master regulators.

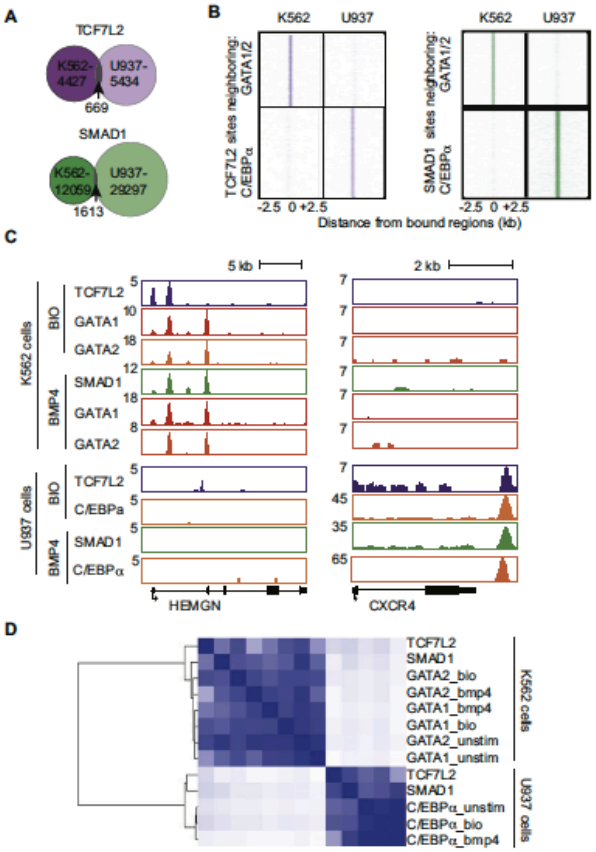

Figure 4. TCF7L2 and SMAD1 Co-occupy Genomic Regions with Cell-Type-Specific Lineage Regulators

(A) Venn diagrams depicting the overlap of regions bound in K562 and U937 cells for TCF7L2 (top) and SMAD1 (bottom). Numbers of regions bound by each factor in each cell line or in the overlap of both are shown.

(B) Region plots comparing the enriched regions of TCF7L2 and SMAD1 in K562 and U937 cells to GATA1 and GATA2 (top) or C/EBPα (bottom) regions.

(C) Gene tracks of *HEMGN* (left) and *CXCR4* (right) showing differential binding of TCF7L2, SMAD1, GATA1, GATA2, and C/EBPα in K562 cells (top) and U937 cells (bottom).

(D) Heatmap depicting the colocalization of GATA1, GATA2, TCF7L2, and SMAD1 in K562 cells and C/EBPα, TCF7L2, and SMAD1 in U937 cells.

See also Figure S5.

C/EBPα Expression Redirects SMAD1 Binding in Erythroid Cells

If lineage-specific transcription factors direct the Wnt and BMP regulators to regulatory elements in distinct lineages, then expression of a master regulator of the myeloid lineage (e.g., C/EBPα) in an erythroid cell type should be capable of redirecting some of the signaling factors to novel sites occupied by the myeloid regulator. In order to test this hypothesis, an estrogen-inducible C/EBPα expressed in K562 cells was used (D'Alo' et al., 2003). Upon estradiol treatment, the C/EBPα estrogen receptor fusion protein translocates into the nucleus. SMAD1 and C/EBPα binding was determined by ChIP-seq in these cells following a 24 hr estradiol induction and a 2 hr BMP4 stimulation (Figure 5A). Expression of C/EBPα directed a fraction of SMAD1 to new sites occupied by C/EBPα (Figure 5B). SMAD1 was retained at GATA targets, such as *SLC6A9*, in C/EBPα-expressing K562 cells, while occupying new sites with C/EBPα exclusive of erythroid regulators (Figure 5C). An example of a newly occupied site lies near two genes, *ALAS2* and *APEX2*. *ALAS2* is expressed in erythroid cells (Sadlon et al., 1999), whereas *APEX2* is important in white blood cells (Ide et al., 2004). The binding of C/EBPα and SMAD1 at this position may result in repression of *ALAS2* in erythroid cells or activation of *APEX2* in white blood cells.

Gata1 Expression Redirects SMAD1 Binding during Differentiation

We next asked whether forced expression of an erythroid master regulator (Gata1) in an erythroblast progenitor cell line could restrict Smad1 binding to only erythroid targets during differentiation. To address this question, the estrogen-inducible Gata1 null erythroblast cell line (G1ER) was used, which was derived from targeted disruption of Gata1 in ESCs. Upon estradiol treatment, the Gata1 estrogen receptor fusion protein translocates into the nucleus and induces the red blood cell differentiation program (Figure 6A) (Cheng et al., 2009; Tsang et al., 1997; Yu et al., 2009). We identified the genome-wide binding of Gata2 and Smad1 in Gata1-deficient (G1E) and Gata1 and Smad1 in Gata1-induced (G1ER) cells following BMP4 stimulation. SMAD and GATA motifs were identified in all samples (Figure S6A). In G1E cells, Smad1 and Gata2 co-occupied genes of multiple hematopoietic lineages (Figures 6B, 6C, S6B, and S6C). During erythroid differentiation, Gata1 replaces Gata2 binding at erythroid genes (Bresnick et al., 2010; Grass et al., 2003). After Gata1 induction, Smad1 binding became more restricted to erythroid genes, and binding to genes expressed in the other lineages was diminished (Figures 6B, 6C, S6B, and S6C). Together the data reveal that induction of lineage-specific regulators alters Smad1 genomic occupancy.

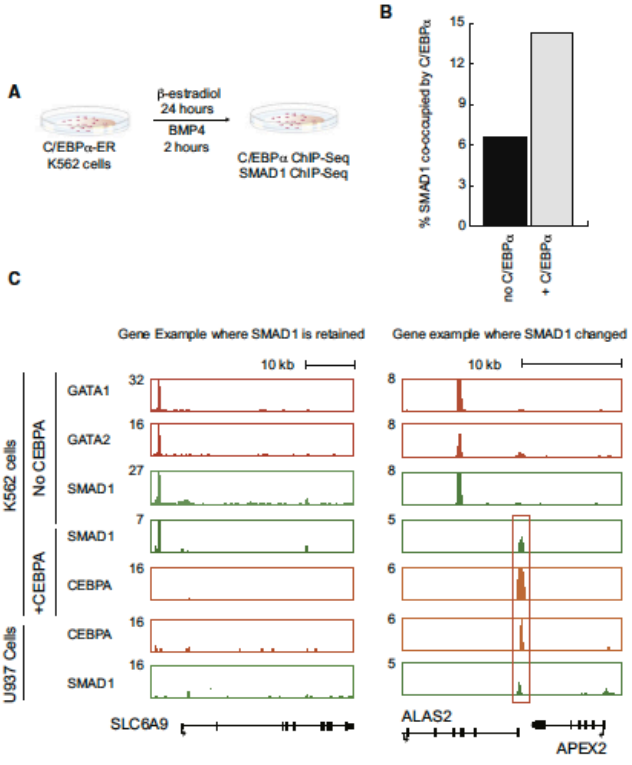

Figure 5. C/EBPα Expression Repositions SMAD1 Binding in K562 Cells

(A) Schematic of C/EBPα-ER K562 experimental model.

(B) The percentage of SMAD1 sites in K562 cells that are co-occupied by C/EBPα (y axis) is shown for K562 cells (no C/EBPα) and those induced by C/EBPα (+C/EBPα). The top 1000 SMAD1-binding sites in each condition were used for this calculation.

(C) Gene tracks of *SLC6A9* (left) and *ALAS2*/*APEX2* (right) showing differential binding of GATA1, GATA2, and SMAD1 in K562 cells (top), SMAD1 and C/EBPα in K562 cells expressing C/EBPα (middle), and U937 cells (bottom).

TCF7L2 and SMAD1 Co-occupancy with Master Regulators Occurs in Primary Hematopoietic Progenitors and Changes during Erythropoiesis

The shifts in SMAD1 occupancy following forced expression of C/EBPα or Gata1 in erythroid environments suggest that during regeneration and differentiation, when there are dynamic changes in the lineage regulators present, signaling factor occupancy will also change according to the cell state. To model a normal differentiation process, analogous to what occurs during regeneration, we examined TCF7L2 and SMAD1 genomic occupancy in primary human progenitor cells following in vitro expansion and differentiation. ChIP-seq was performed for GATA2, TCF7L2, and SMAD1 in mobilized peripheral blood $CD34^+$ progenitor cells (Pro) (Figures 7A and S7A). GATA2 co-occupied more than 75% of TCF7L2- or SMAD1-enriched genes in these hematopoietic progenitor cells (Figures 7B, 7C, and S7B–S7D). In addition to a GATA motif, ETS and RUNX motifs were also enriched in GATA2-, SMAD-, and TCF-bound sequences (Figure S7E). This finding is consistent with recent genome-wide data from murine hematopoietic progenitors that indicate that Gata2 co-occupies sites with multiple regulators, including Runx1 and ETS transcription factors Erg and Fli1, near genes important for multipotent stem cells (Wilson et al., 2010). Together with the binding data, these results imply that TCF7L2 and SMAD1 likely cobind with the entire progenitor transcriptional complex.

To determine how binding changes during differentiation, ChIP-seq for GATA1 and SMAD1 in erythroblast derived from $CD34^+$ progenitors (CD34ery) was performed (Figures 7A and S7A). SMAD1 cobound with GATA1 in CD34-derived erythroblasts (Figures 7B and 7C). The genes bound by SMAD1 were fewer in the erythroid cells compared to the progenitor cells (2683 versus 8094). This change in SMAD1 occupancy suggested refinement of the binding sites from a multilineage to a fully differentiated state (Figures 7B and 7C). The bound genes were enriched for those that are characteristic of the differentiation stage (Figure S7D). In addition to the loss of many bound regions, further binding was acquired at erythroid genes (Figures 7B, 7C, and S7D). These data confirm that cobinding of BMP and Wnt regulators with lineage transcription factors occurs in primary hematopoietic cells in genes that regulate all hematopoietic lineages and shifts upon directed differentiation toward erythroid cells to erythroid-specific genes.

To ascertain whether genes bound by BMP and Wnt transcription factors were regulated by BMP and Wnt signaling, genome-wide expression analysis was performed on $CD34^+$ cells with or without stimulation by BMP4 or BIO, respectively. The expression in unstimulated and stimulated cells was compared 2 hr after the shift to erythroid differentiation conditions. Differentially expressed genes in BMP4-treated groups compared to untreated controls were enriched for genes bound by SMAD1 (32%), and those differentially expressed in BIO-treated samples were enriched for those bound by TCF7L2 (31%) (Table S6). These data suggest that BMP and Wnt signaling coordinate with differentiation signals to alter gene expression via direct binding to common target genes with lineage master regulators.

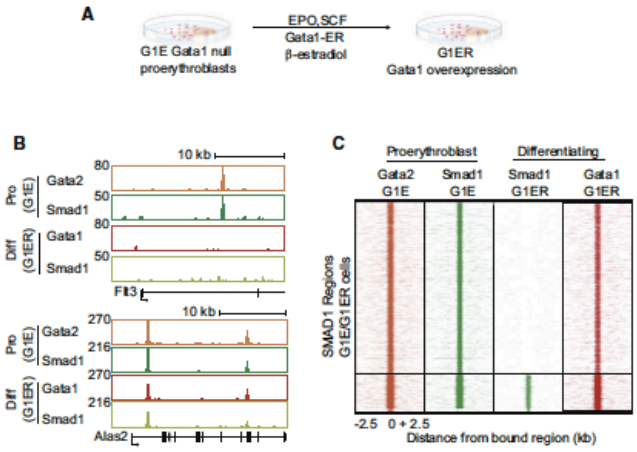

Figure 6. Smad1 Localization Is Directed by Gata1

(A) Schematic of the G1E, G1ER experiment.

(B) Gene tracks of *Flt3* (top) and *Alas2* (bottom) showing differential binding of Gata2 and Smad1 in G1E Gata1 null cells (Proerythroblast) and Gata1 and Smad1 in G1ER erythroid cells (Differentiating).

(C) Overexpression of Gata1 redefines the targets of Smad1. ChIP-seq region plots represent the distribution of regions bound by Smad1 and Gata2 in G1E and Gata1 and Smad1 in G1ER cells −2.5 and +2.5 kb relative to all Smad1-bound sites in G1E and G1ER combined.

See also Figure S6.

DISCUSSION

Here we provide evidence that BMP and Wnt pathways play a dynamic role in hematopoietic regeneration through co-occupancy of regulatory elements with lineage regulators at cell-type-specific genes for each lineage. The co-occupancy of Smad1 and Gata2 was observed on blood targets in hematopoietic progenitors during in vivo regeneration. Lineage-restricted co-occupancy of TCF7L2 or SMAD1 with GATA1 and GATA2 in erythroid cells, C/EBPα in myeloid cells, and GATA2 in progenitors occurs genome-wide. This binding is selective for cell-specific enhancers bound by master regulators. BMP and Wnt signaling cooperate with lineage regulators to enhance transcription of cell-type-specific target genes. Lastly, ectopic expression of a lineage transcription factor was sufficient to direct the genomic localization of signaling-specific factors.

Master regulators direct the site selection of signaling transcription factors in every step during the differentiation process. Recent genome-wide studies have shown that signaling pathway transcription factors localize in binding sites adjacent to ESC master regulators (Chen et al., 2008; Cole et al., 2008; Young, 2011). Our data along with those of Mullen et al. show that this mechanism occurs in many cell types and establishes an order by which the lineage regulators recruit the signaling factors to sites of active genes of biological relevance throughout the whole genome (Mullen et al., 2011). Alterations of the expression and binding of hematopoietic lineage regulators to target genes during regeneration or differentiation can dictate the binding of signaling factors.

Signaling factors selectively colocalize with master regulators, but our studies hint that other factors may help fine-tune signaling factor binding. For example, the transcriptional status of a gene can modify SMAD1 binding. In $CD34^+$ progenitor cells, SMAD1 cobinds with GATA2 on genes expressed in progenitors but is mostly absent from erythroid genes that are not expressed. In erythroid cells, SMAD1 is able to bind these same targets with GATA1, which helps activate these genes (Bresnick et al., 2010; Grass et al., 2003). Additionally, it has been suggested that GATA2 works in different complexes to target progenitor versus erythroid genes (Wilson et al., 2010), and GATA2 is expressed at different levels in these two cell populations. We speculate that it is not only the function of an individual master regulator but also the combinations and the levels of each lineage regulator in a cell along with the transcriptional state of the target that help dictate the genomic location of signaling factors.

Here we provide a model for how this mechanism could be utilized to help orchestrate hematopoietic differentiation during a stress response. During hematopoietic regeneration when these pathways are required, the activation of BMP and Wnt signaling results in the colocalization of SMAD and TCF with the master regulators on genes defining progenitor cell fate. As regeneration continues and progenitor cells begin to differentiate, different master regulators activate the cell-specific genes of more mature hematopoietic lineages and again redefine the binding of signaling transcription factors. Colocalization of lineage and signaling factors has as a result the colocalization of signaling factors themselves. This fact may explain some of the synergistic effects observed between many signaling pathways (Schier and Talbot, 2005). As the BMP and Wnt pathways appear to have a selective function during regeneration, throughout this stress response, coupling transcriptional regulation to the transcription factors expressed highly in a cell lineage explains how BMP and Wnt signaling pathways can have cell-context-dependent effects.

Regeneration is a process of tissue self-renewal. Our data imply that an underlying mechanism of self-renewal is the control of the entire hematopoietic program through the collaboration of master and signaling transcription factors, which is similar to the mechanism by which core self-renewal factors in ESCs perform key roles in ESC fate. Our observation that the BMP and Wnt signaling transcription factors are associated with master regulators of multiple hematopoietic cell types provides insight into the effects of BMP and Wnt signaling that occur during development, regeneration, and disease.

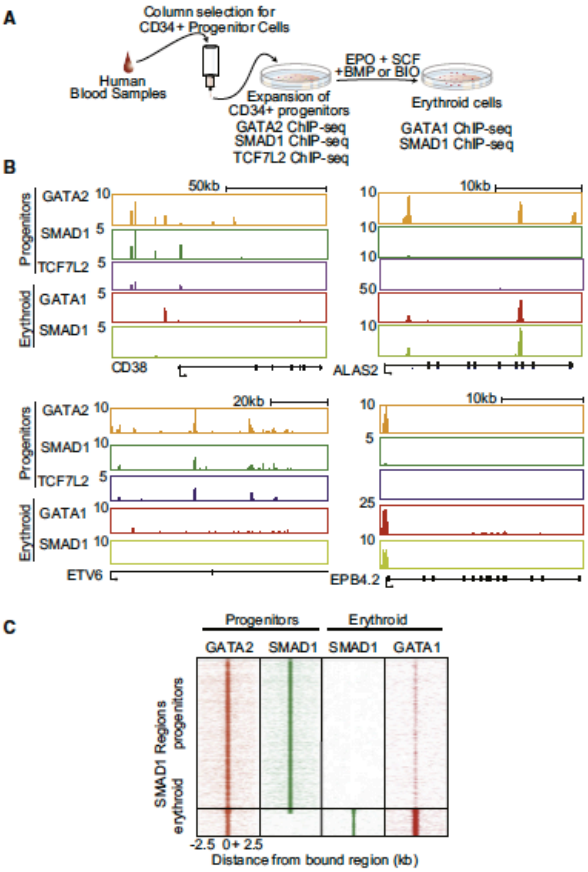

Figure 7. Binding of Signaling Factors Changes during Differentiation

(A) Schematic of CD34$^+$ experiment.

(B) Gene tracks of *CD38*, *ETV6*, *ALAS2*, and *EPB4.2* showing differential binding of GATA2, SMAD1, and TCF7L2 in undifferentiated CD34$^+$ progenitors and GATA1 and SMAD1 in differentiated erythroblasts.

(C) SMAD1 binding becomes restricted to mainly erythroid genes after differentiation of CD34$^+$ hematopoietic cells toward erythrocytes. ChIP-seq region plots represent the distribution of SMAD1-occupied regions in CD34$^+$ progenitors (pro) and in vitro differentiated erythroblasts (ery). GATA2 and SMAD1 in CD34$^+$ progenitors and SMAD1 and GATA1 in erythroid differentiated CD34$^+$ cells −2.5 to +2.5 kb relative to all SMAD1-bound regions in CD34$^+$ progenitors and differentiated erythroblasts are shown.

See also Figure S7.

EXPERIMENTAL PROCEDURES

Zebrafish Irradiation-Induced Regeneration

Zebrafish were maintained as described (Westerfield, 2000). Irradiation-induced regeneration assays were performed as previously described (Burns et al., 2005; Traver et al., 2004). For heat shock treatments, small fish tanks were placed at 37°C for 16 hr. For small-molecule treatments, fish were soaked for 16 hr in fish water containing drug dissolved in DMSO, 2 μM BIO, or 10 μM DM. On days 2, 7, and 14 post-irradiation, WKM cells were analyzed on an LSRII for FSC/SSC parameters. See also Extended Experimental Procedures.

Cell Line Culture Conditions and Stimulation

K562 and U937 cells were maintained in IMDM and RPMI media, respectively, supplemented with fetal calf serum, glutamine, and penicillin/streptomycin. Culture conditions for CEBPα-K562, G1E, G1ER, and human hematopoietic CD34$^+$ cells as well as differentiation media and stimulation conditions are described in Extended Experimental Procedures.

Chromatin Immunoprecipitation

ChIP experiments were performed as previously described (Lee et al., 2006) with slight modifications, which are described in Extended Experimental Procedures. A summary of the bound regions and bound genes determined for all ChIP-seq data is contained within Tables S3, S4, and S5. For ChIP-seq experiments, the following antibodies were used: Smad1 (Santa Cruz sc7965), TCF7L2 (TCF4 Santa Cruz sc8631), C/EBPα (Santa Cruz sc9314), Gata1 (Santa Cruz sc265), Gata2 (Santa Cruz sc9008), p300 (Santa Cruz sc585), and H3K4me1 (Abcam ab8895). Samples were prepared for sequencing using Illumina Genomic DNA kit or TruSeq according to the manufacturer instructions. Also see Extended Experimental Procedures for details on ChIP and ChIP-seq sample preparation and analysis.

ChIP-PCR Analysis of Lineage-Negative Bone Marrow Cells

ChIP in lineage-negative cells isolated from mouse bone marrow was performed as described above. Primers were designed for known Gata2 targets. qPCR reactions were done with iQ SYBR-GREEN Supermix (BIORAD 170-8880), and a CFX-384 Real-Time PCR Detection System (BIORAD) thermal cycler was used. Expression of each gene was normalized to *Gapdh*, and relative levels were calculated using the ΔΔCt method (Applied Biosystems). Quantities are expressed as fold change compared to input controls. Primers are listed in Table S2.

Sequential Chromatin Immunoprecipitation

ChIP analysis was performed, and immunoprecipitated DNA fragments were eluted from the beads by addition of 55 μl 10 mM DTT and incubated at 37°C for 30 min. The supernatant was transferred to a new tube and the material was diluted 30× with sonication buffer and served as the starting material for the second ChIP. ChIP-PCR was performed as described above. See also Extended Experimental Procedures.

Motif Counting

The genomic sequence ±2.5 kb from the center of each enriched region in the dataset indicated was downloaded from the UCSC website with repeats masked with "N." A window of 250 bp was shifted across each sequence at 50 bp intervals, and the number of occurrences of the complete motif sequence or its reverse complement within the window was counted. An

averaged motif occurrence in each scanning window was plotted across the ±2.5 kb regions.

Heatmap Analysis of ChIP-Seq Occupancy

ChIP-seq enrichment for the indicated factor or modification was determined in 100 bp bins (enrichment in the bin as counts per million) centered on the enriched region of a given ChIP-seq dataset. Java Treeview (http://www.jtreeview.sourceforge.net) was used to visualize the data and generate figures shown in this manuscript.

Distance from TCF7L2- or SMAD1-Enriched Regions to Nearest Transcription Factor-Bound Region

The distance (in bp) from each TCF7L2 or SMAD1 site in K562 cells to the nearest site of each transcription factor was calculated. The distance from the boundary of each TCF7L2- or SMAD1-enriched region to the boundary of the nearest site bound by the indicated transcription factor was determined. These distances were grouped into bins (x axis), with the x axis value indicating the upper limit of each bin. The sum of regions in each bin is shown (y axis).

Assignment to Regulatory Regions in K562 Cells

Each enriched region was uniquely assigned into a category of exon, intron, proximal promoter (from 1 kb upstream to the TSS), distal promoter (from 10 kb upstream to 1 kb upstream of the TSS), and intergenic region (more than 10 kb upstream away from body of the gene) according to MySQL access to the UCSC hg18 RefSeq table. When an enriched region could be mapped to more than one regulatory region category because of overlapping genes, it was classified into a regulatory region class in preferential order of exon, intron, proximal promoter, distal promoter, and intergenic region.

Genome-wide Expression Analysis

Affymetrix U133plus2.0 microarrays were used to assess gene expression changes in CD34$^+$ cells with or without Wnt or BMP pathway stimulation. Arrays were done on control, 0.5 μM BIO-treated, or 25 ng/ml rhBMP4-treated cells 2 hr after a shift to erythroid differentiation media. See also Extended Experimental Procedures.

Reporter Assays

K562 cells were transfected using AMAXA nucleofector according to the manufacturer instructions. β-galactosidase activity was measured with the Galacto-Star kit (Applied Biosystems). See also Extended Experimental Procedures.

ACCESSION NUMBERS

Microarray (GSE26351) and ChIP-seq (Superseries—GSE29196, datasets—GSE29193, GSE29194, GSE29195) data were deposited in GEO (http://www.ncbi.nlm.nih.gov/geo/) under the accession numbers indicated.

SUPPLEMENTAL INFORMATION

Supplemental Information includes Extended Experimental Procedures, seven figures, and six tables and can be found with this article online at doi:10.1016/j.cell.2011.09.044.

ACKNOWLEDGMENTS

We would like to acknowledge A. Mullen and D. Orlando for helpful discussions and sharing critical insights prior to publication and G. Frampton for analytical advice and development of the ChIP-seq analysis platform. We thank F. Rentzsch and M. Hammerschmidt for the Hs:BMP zebrafish line, J. Tucker and M. Mullins for the Hs:Chordin zebrafish line, and T. Schlaeger for the GATA2 expression plasmid. We are grateful to X. Bai and R. White for critical reviews of the manuscript and O. Tamplin for computational advice. The Whitehead Genome Technology Core was instrumental in timely data production and analysis support, especially S. Gupta. Microarray studies were performed by the Molecular Genetics Core Facility at Children's Hospital Boston, supported by NIH-P50-NS40828 and NIH-P30-HD18655. This work was supported by NIH #5PO1HL32262-29 and #5R01HL048801-18 (to L.I.Z), NIH 1R01DK080040-01 (to R.F.P.), R01-HG002668 (to R.A.Y.), NIH K01 DK085270-02 (to T.V.B.), NIH U01 HL100001, NIH 1 RC2HL102815, and ROFAR (to G.Q.D.), NIH T32HL007623 (to G.C.H.), HHMI (to L.I.Z. and G.Q.D.), and EMBO fellowship and Jane Coffin Childs Memorial Fund (to E.T.). L.I.Z. is a founder and stock holder of Fate, Inc. and a scientific advisor for Stemgent. G.Q.D. is a member of the Scientific Advisory Boards of MPM Capital, Inc., Epizyme, Inc., and iPierian, Inc.

Received: May 6, 2011
Revised: August 1, 2011
Accepted: September 23, 2011
Published: October 27, 2011

REFERENCES

Birney, E., Stamatoyannopoulos, J.A., Dutta, A., Guigó, R., Gingeras, T.R., Margulies, E.H., Weng, Z., Snyder, M., Dermitzakis, E.T., Thurman, R.E., et al; ENCODE Project Consortium; NISC Comparative Sequencing Program; Baylor College of Medicine Human Genome Sequencing Center; Washington University Genome Sequencing Center; Broad Institute; Children's Hospital Oakland Research Institute. (2007). Identification and analysis of functional elements in 1% of the human genome by the ENCODE pilot project. Nature *447*, 799–816.

Bresnick, E.H., Lee, H.Y., Fujiwara, T., Johnson, K.D., and Keles, S. (2010). GATA switches as developmental drivers. J. Biol. Chem. *285*, 31087–31093.

Burns, C.E., Traver, D., Mayhall, E., Shepard, J.L., and Zon, L.I. (2005). Hematopoietic stem cell fate is established by the Notch-Runx pathway. Genes Dev. *19*, 2331–2342.

Cantor, A.B. (2005). GATA transcription factors in hematologic disease. Int. J. Hematol. *81*, 378–384.

Chen, C.R., Kang, Y., Siegel, P.M., and Massagué, J. (2002). E2F4/5 and p107 as Smad cofactors linking the TGFbeta receptor to c-myc repression. Cell *110*, 19–32.

Chen, X., Xu, H., Yuan, P., Fang, F., Huss, M., Vega, V.B., Wong, E., Orlov, Y.L., Zhang, W., Jiang, J., et al. (2008). Integration of external signaling pathways with the core transcriptional network in embryonic stem cells. Cell *133*, 1106–1117.

Cheng, X., Huber, T.L., Chen, V.C., Gadue, P., and Keller, G.M. (2008). Numb mediates the interaction between Wnt and Notch to modulate primitive erythropoietic specification from the hemangioblast. Development *135*, 3447–3458.

Cheng, Y., Wu, W., Kumar, S.A., Yu, D., Deng, W., Tripic, T., King, D.C., Chen, K.B., Zhang, Y., Drautz, D., et al. (2009). Erythroid GATA1 function revealed by genome-wide analysis of transcription factor occupancy, histone modifications, and mRNA expression. Genome Res. *19*, 2172–2184.

Clevers, H. (2006). Wnt/beta-catenin signaling in development and disease. Cell *127*, 469–480.

Cole, M.F., Johnstone, S.E., Newman, J.J., Kagey, M.H., and Young, R.A. (2008). Tcf3 is an integral component of the core regulatory circuitry of embryonic stem cells. Genes Dev. *22*, 746–755.

D'Alo', F., Johansen, L.M., Nelson, E.A., Radomska, H.S., Evans, E.K., Zhang, P., Nerlov, C., and Tenen, D.G. (2003). The amino terminal and E2F interaction domains are critical for C/EBP alpha-mediated induction of granulopoietic development of hematopoietic cells. Blood *102*, 3163–3171.

Detmer, K., and Walker, A.N. (2002). Bone morphogenetic proteins act synergistically with haematopoietic cytokines in the differentiation of haematopoietic progenitors. Cytokine *17*, 36–42.

Fuchs, O., Simakova, O., Klener, P., Cmejlova, J., Zivny, J., Zavadil, J., and Stopka, T. (2002). Inhibition of Smad5 in human hematopoietic progenitors blocks erythroid differentiation induced by BMP4. Blood Cells Mol. Dis. *28*, 221–233.

Goessling, W., North, T.E., Loewer, S., Lord, A.M., Lee, S., Stoick-Cooper, C.L., Weidinger, G., Puder, M., Daley, G.Q., Moon, R.T., and Zon, L.I. (2009).

Genetic interaction of PGE2 and Wnt signaling regulates developmental specification of stem cells and regeneration. Cell *136*, 1136–1147.

Grass, J.A., Boyer, M.E., Pal, S., Wu, J., Weiss, M.J., and Bresnick, E.H. (2003). GATA-1-dependent transcriptional repression of GATA-2 via disruption of positive autoregulation and domain-wide chromatin remodeling. Proc. Natl. Acad. Sci. USA *100*, 8811–8816.

Hecht, A., and Stemmler, M.P. (2003). Identification of a promoter-specific transcriptional activation domain at the C terminus of the Wnt effector protein T-cell factor 4. J. Biol. Chem. *278*, 3776–3785.

Heintzman, N.D., and Ren, B. (2009). Finding distal regulatory elements in the human genome. Curr. Opin. Genet. Dev. *19*, 541–549.

Heintzman, N.D., Stuart, R.K., Hon, G., Fu, Y., Ching, C.W., Hawkins, R.D., Barrera, L.O., Van Calcar, S., Qu, C., Ching, K.A., et al. (2007). Distinct and predictive chromatin signatures of transcriptional promoters and enhancers in the human genome. Nat. Genet. *39*, 311–318.

Heintzman, N.D., Hon, G.C., Hawkins, R.D., Kheradpour, P., Stark, A., Harp, L.F., Ye, Z., Lee, L.K., Stuart, R.K., Ching, C.W., et al. (2009). Histone modifications at human enhancers reflect global cell-type-specific gene expression. Nature *459*, 108–112.

Hooper, A.T., Butler, J.M., Nolan, D.J., Kranz, A., Iida, K., Kobayashi, M., Kopp, H.G., Shido, K., Petit, I., Yanger, K., et al. (2009). Engraftment and reconstitution of hematopoiesis is dependent on VEGFR2-mediated regeneration of sinusoidal endothelial cells. Cell Stem Cell *4*, 263–274.

Ide, Y., Tsuchimoto, D., Tominaga, Y., Nakashima, M., Watanabe, T., Sakumi, K., Ohno, M., and Nakabeppu, Y. (2004). Growth retardation and dyslymphopoiesis accompanied by G2/M arrest in APEX2-null mice. Blood *104*, 4097–4103.

Jeannet, G., Scheller, M., Scarpellino, L., Duboux, S., Gardiol, N., Back, J., Kuttler, F., Malanchi, I., Birchmeier, W., Leutz, A., et al. (2008). Long-term, multilineage hematopoiesis occurs in the combined absence of beta-catenin and gamma-catenin. Blood *111*, 142–149.

Jeanpierre, S., Nicolini, F.E., Kaniewski, B., Dumontet, C., Rimokh, R., Puisieux, A., and Maguer-Satta, V. (2008). BMP4 regulation of human megakaryocytic differentiation is involved in thrombopoietin signaling. Blood *112*, 3154–3163.

Koch, U., Wilson, A., Cobas, M., Kemler, R., Macdonald, H.R., and Radtke, F. (2008). Simultaneous loss of beta- and gamma-catenin does not perturb hematopoiesis or lymphopoiesis. Blood *111*, 160–164.

Kurisaki, K., Kurisaki, A., Valcourt, U., Terentiev, A.A., Pardali, K., Ten Dijke, P., Heldin, C.H., Ericsson, J., and Moustakas, A. (2003). Nuclear factor YY1 inhibits transforming growth factor beta- and bone morphogenetic protein-induced cell differentiation. Mol. Cell. Biol. *23*, 4494–4510.

Landry, J.R., Bonadies, N., Kinston, S., Knezevic, K., Wilson, N.K., Oram, S.H., Janes, M., Piltz, S., Hammett, M., Carter, J., et al. (2009). Expression of the leukemia oncogene Lmo2 is controlled by an array of tissue-specific elements dispersed over 100 kb and bound by Tal1/Lmo2, Ets, and Gata factors. Blood *113*, 5783–5792.

Larsson, J., and Karlsson, S. (2005). The role of Smad signaling in hematopoiesis. Oncogene *24*, 5676–5692.

Lee, T.I., Johnstone, S.E., and Young, R.A. (2006). Chromatin immunoprecipitation and microarray-based analysis of protein location. Nat. Protoc. *1*, 729–748.

Lengerke, C., Schmitt, S., Bowman, T.V., Jang, I.H., Maouche-Chretien, L., McKinney-Freeman, S., Davidson, A.J., Hammerschmidt, M., Rentzsch, F., Green, J.B., et al. (2008). BMP and Wnt specify hematopoietic fate by activation of the Cdx-Hox pathway. Cell Stem Cell *2*, 72–82.

Massagué, J., Seoane, J., and Wotton, D. (2005). Smad transcription factors. Genes Dev. *19*, 2783–2810.

McReynolds, L.J., Gupta, S., Figueroa, M.E., Mullins, M.C., and Evans, T. (2007). Smad1 and Smad5 differentially regulate embryonic hematopoiesis. Blood *110*, 3881–3890.

Mosimann, C., Hausmann, G., and Basler, K. (2009). Beta-catenin hits chromatin: regulation of Wnt target gene activation. Nat. Rev. Mol. Cell Biol. *10*, 276–286.

Moustakas, A., and Heldin, C.H. (2009). The regulation of TGFbeta signal transduction. Development *136*, 3699–3714.

Mullen, A.C., Orlando, D.A., Newman, J.J., Loven, J., Kumar, R.M., Bilodeau, S., Reddy, J., Guenther, M.G., DeKoter, R., and Young, R.A. (2011). Master transcription factors determine cell-type-specific responses to TGF-β signaling. Cell *147*, this issue, 565–576.

Nakashima, K., Yanagisawa, M., Arakawa, H., Kimura, N., Hisatsune, T., Kawabata, M., Miyazono, K., and Taga, T. (1999). Synergistic signaling in fetal brain by STAT3-Smad1 complex bridged by p300. Science *284*, 479–482.

Nostro, M.C., Cheng, X., Keller, G.M., and Gadue, P. (2008). Wnt, activin, and BMP signaling regulate distinct stages in the developmental pathway from embryonic stem cells to blood. Cell Stem Cell *2*, 60–71.

Pearson, K.L., Hunter, T., and Janknecht, R. (1999). Activation of Smad1-mediated transcription by p300/CBP. Biochim. Biophys. Acta *1489*, 354–364.

Rada-Iglesias, A., Bajpai, R., Swigut, T., Brugmann, S.A., Flynn, R.A., and Wysocka, J. (2011). A unique chromatin signature uncovers early developmental enhancers in humans. Nature *470*, 279–283.

Raney, B.J., Cline, M.S., Rosenbloom, K.R., Dreszer, T.R., Learned, K., Barber, G.P., Meyer, L.R., Sloan, C.A., Malladi, V.S., Roskin, K.M., et al. (2011). ENCODE whole-genome data in the UCSC genome browser (2011 update). Nucleic Acids Res. *39*(Database issue), D871–D875.

Rentzsch, F., Zhang, J., Kramer, C., Sebald, W., and Hammerschmidt, M. (2006). Crossveinless 2 is an essential positive feedback regulator of Bmp signaling during zebrafish gastrulation. Development *133*, 801–811.

Rosenbloom, K.R., Dreszer, T.R., Pheasant, M., Barber, G.P., Meyer, L.R., Pohl, A., Raney, B.J., Wang, T., Hinrichs, A.S., Zweig, A.S., et al. (2010). ENCODE whole-genome data in the UCSC Genome Browser. Nucleic Acids Res. *38*(Database issue), D620–D625.

Sadlon, T.J., Dell'Oso, T., Surinya, K.H., and May, B.K. (1999). Regulation of erythroid 5-aminolevulinate synthase expression during erythropoiesis. Int. J. Biochem. Cell Biol. *31*, 1153–1167.

Schier, A.F., and Talbot, W.S. (2005). Molecular genetics of axis formation in zebrafish. Annu. Rev. Genet. *39*, 561–613.

Singbrant, S., Karlsson, G., Ehinger, M., Olsson, K., Jaako, P., Miharada, K., Stadtfeld, M., Graf, T., and Karlsson, S. (2010). Canonical BMP signaling is dispensable for hematopoietic stem cell function in both adult and fetal liver hematopoiesis, but essential to preserve colon architecture. Blood *115*, 4689–4698.

Song, L., Zhang, Z., Grasfeder, L.L., Boyle, A.P., Giresi, P.G., Lee, B.K., Sheffield, N.C., Gräf, S., Huss, M., Keefe, D., et al. (2011). Open chromatin defined by DNaseI and FAIRE identifies regulatory elements that shape cell-type identity. Genome Res. *21*, 1757–1767.

Staal, F.J., and Luis, T.C. (2010). Wnt signaling in hematopoiesis: crucial factors for self-renewal, proliferation, and cell fate decisions. J. Cell. Biochem. *109*, 844–849.

Stoick-Cooper, C.L., Weidinger, G., Riehle, K.J., Hubbert, C., Major, M.B., Fausto, N., and Moon, R.T. (2007). Distinct Wnt signaling pathways have opposing roles in appendage regeneration. Development *134*, 479–489.

Tran, H.T., Sekkali, B., Van Imschoot, G., Janssens, S., and Vleminckx, K. (2010). Wnt/beta-catenin signaling is involved in the induction and maintenance of primitive hematopoiesis in the vertebrate embryo. Proc. Natl. Acad. Sci. USA *107*, 16160–16165.

Traver, D., Winzeler, A., Stern, H.M., Mayhall, E.A., Langenau, D.M., Kutok, J.L., Look, A.T., and Zon, L.I. (2004). Effects of lethal irradiation in zebrafish and rescue by hematopoietic cell transplantation. Blood *104*, 1298–1305.

Tsai, F.Y., Keller, G., Kuo, F.C., Weiss, M., Chen, J., Rosenblatt, M., Alt, F.W., and Orkin, S.H. (1994). An early haematopoietic defect in mice lacking the transcription factor GATA-2. Nature *371*, 221–226.

Tsang, A.P., Visvader, J.E., Turner, C.A., Fujiwara, Y., Yu, C., Weiss, M.J., Crossley, M., and Orkin, S.H. (1997). FOG, a multitype zinc finger protein,

acts as a cofactor for transcription factor GATA-1 in erythroid and megakaryocytic differentiation. Cell *90*, 109–119.

Tsiftsoglou, A.S., Vizirianakis, I.S., and Strouboulis, J. (2009). Erythropoiesis: model systems, molecular regulators, and developmental programs. IUBMB Life *61*, 800–830.

Tucker, J.A., Mintzer, K.A., and Mullins, M.C. (2008). The BMP signaling gradient patterns dorsoventral tissues in a temporally progressive manner along the anteroposterior axis. Dev. Cell *14*, 108–119.

Verzi, M.P., Hatzis, P., Sulahian, R., Philips, J., Schuijers, J., Shin, H., Freed, E., Lynch, J.P., Dang, D.T., Brown, M., et al. (2010). TCF4 and CDX2, major transcription factors for intestinal function, converge on the same cis-regulatory regions. Proc. Natl. Acad. Sci. USA *107*, 15157–15162.

Visel, A., Blow, M.J., Li, Z., Zhang, T., Akiyama, J.A., Holt, A., Plajzer-Frick, I., Shoukry, M., Wright, C., Chen, F., et al. (2009). ChIP-seq accurately predicts tissue-specific activity of enhancers. Nature *457*, 854–858.

Weidinger, G., Thorpe, C.J., Wuennenberg-Stapleton, K., Ngai, J., and Moon, R.T. (2005). The Sp1-related transcription factors sp5 and sp5-like act downstream of Wnt/beta-catenin signaling in mesoderm and neuroectoderm patterning. Curr. Biol. *15*, 489–500.

Westerfield, M. (2000). The Zebrafish Book: A Guide for the Laboratory Use of Zebrafish (Danio rerio), 4th edn (Eugene, OR: M. Westerfield), pp. 1–35.

Wilson, N.K., Foster, S.D., Wang, X., Knezevic, K., Schütte, J., Kaimakis, P., Chilarska, P.M., Kinston, S., Ouwehand, W.H., Dzierzak, E., et al. (2010). Combinatorial transcriptional control in blood stem/progenitor cells: genome-wide analysis of ten major transcriptional regulators. Cell Stem Cell *7*, 532–544.

Young, R.A. (2011). Control of the embryonic stem cell state. Cell *144*, 940–954.

Yu, M., Riva, L., Xie, H., Schindler, Y., Moran, T.B., Cheng, Y., Yu, D., Hardison, R., Weiss, M.J., Orkin, S.H., et al. (2009). Insights into GATA-1-mediated gene activation versus repression via genome-wide chromatin occupancy analysis. Mol. Cell *36*, 682–695.